Control of telomeric homology-directed repair by poly(ADP-ribose) metabolism

by

My Song Hoang

B.S., Union College, 2015

B.A., Union College, 2015

Submitted to the Graduate Faculty of the

School of Medicine in partial fulfillment

of the requirements for the degree of

Doctor of Philosophy

University of Pittsburgh

2019

UNIVERSITY OF PITTSBURGH

SCHOOL OF MEDICINE

This dissertation was presented

by

My Song Hoang

It was defended on

December 4, 2019

and approved by

Bennett Van Houten, Professor, Department of Pharmacology & Chemical Biology

Kara A. Bernstein, Associate Professor, Department of Microbiology & Molecular Genetics

Andrea J. Berman, Associate Professor, Department of Biological Sciences

Patricia L. Opresko, Professor, Department of Environmental & Occupational Health

Dissertation Director: Roderick J. O'Sullivan, Assistant Professor, Department of Pharmacology & Chemical Biology

Control of telomeric homology-directed repair by poly(ADP-ribose) metabolism

My Song Hoang, PhD

University of Pittsburgh, 2019

Immediately after single-stranded break (SSB) and double-stranded break (DSB) formation, the synthesis of poly(ADP-ribose) (PAR) reconfigures the local chromatin environment and initiates recruitment of DNA repair proteins. The degradation of PAR chains by poly(ADP-ribose) glycohydrolase (PARG) is essential for DNA repair progression. Here, we show that pharmacological interference of PAR metabolism disrupts the homology-directed repair (HDR) mechanisms that mediate alternative lengthening of telomeres (ALT). Using a proteomics strategy, we uncovered PAR-regulated telomere-associated proteins that coordinate the early stages of the ALT mechanism. These distinct factors exhibit PAR dependency for localization to ALT telomeres in order to orchestrate diverse functions, such as RNA stabilization, actin nucleation, and chromatin remodeling. Most significantly, we identified a key function for PARylation in recruiting the HIRA histone chaperone complex to ALT telomeres, where it is required for deposition of histone H3.3 specifically during G2 Break-Induced Replication (G2-BIR). We propose that HIRA acts to compensate for the loss of a functional ATRX-DAXX complex in ALT cancers and therefore adopts elevated importance in sustaining ALT+ cell viability.

Table of Contents

List of Tables

List of Figures

Preface

I would like to extend my deepest gratitude and appreciation to the people who have helped me bring this project to fruition. First and foremost, I would like to thank my advisor, Dr. Roderick O'Sullivan, for his guidance, expertise, and encouragement throughout this project. You have fostered my strengths and equipped me with the skills to be the best version of myself. You continually motivate me to be a better scientist with your keen questions and high, yet reasonable expectations. You have pushed me farther than I thought I could go. The most valuable lesson you have taught me is the importance of following through on all my tasks and commitments. You have been an incredible mentor during my graduate training – from inception to completion.

I would like to acknowledge my exceptional committee members, each of whom has provided invaluable advice and guidance throughout my research process. Dr. Ben Van Houten: You never stopped challenging me. In doing so, you helped me develop a meticulous scientific approach. Dr. Kara Bernstein: Your unwavering support helped me overcome several scientific hurdles. Dr. Patricia Opresko: Your knowledge and expertise helped move my project forward. Dr. Andrea Berman: Your keen questions and feedback helped me become more inquisitive about my research.

I also appreciated the tremendous support from the Molecular Pharmacology program at the University of Pittsburgh School of Medicine. The academic training that I received here has been pivotal to my accomplishments. I would like to specifically mention Dr. Bruce Freeman, Dr. Patrick Pagano, Dr. Guillermo Romero, Dr. Tija Jacobs, and Dr. Jonathan Beckel, who have contributed to creating a training program that fosters collaboration and innovation.

I am indebted to my former mentors who were instrumental in shaping my love of learning. My highschool teachers at the United Nations International School of Hanoi, Mr. Wayne Hodgkinson, Mr. Jeremy Thompson, Mrs. Julie Shaw, and Mr. Steve Powers, encouraged me to keep an open-mind. My English and Biology professors at Union College, Dr. Robert Lauzon, Dr. Jill Salvo, Dr. Quynh Chu-LaGraff, and Dr. Hugh Jenkins, showed me the importance of an interdisciplinary approach to solving problems. Dr. Larry Karnitz, my advisor during a summer research fellowship at the Mayo Clinic, instilled in me the confidence to ask questions and the curiosity to pursue scientific questions.

Last, but not least, I am extremely grateful for my tremendous support system. My mom and dad: You are my ultimate role models. You came to the United States to lead a better life for our family. Your courage and sacrifices have given me bountiful opportunities to fulfill my dreams. Your love and guidance encouraged me to pursue my passions. My brother, James: I am extremely thankful that we are close siblings – from the early childhood days when we shared a RuneScape account to currently, as we explore the atypical food scene together.

Additionally, I have to give a huge thanks to my friends who have dealt with my weirdness and have kept me positive during difficult times. The current and past O'Sullivan lab members, Nicole Kaminski, Michelle Lynskey, Jonathan Barroso-Gonzalez, Ragini Bhargava, Laura Garcia-Exposito, Justin Roncaioli, and Marco De Vitas: Each of you has contributed to such a great lab environment that is conducive to high-quality science with a side of fun and laughter. Alex Layden: You have been incredibly supportive of my aspirations in and out of the lab. Our peculiar Pittsburgh adventures have kept me sane! Ethan Bassin, Manoj Chelvanambi, and Daniel Zuppo: The Stack'd 9PM crew lasted for so many years. Braulio Bonilla: I always enjoy our reagent exchanges. Alp Asan: Over the years, we have become close friends, beyond Molecular

Pharmacology buddies! Sam Herron: Our Sunday brunches has led to many insightful discussions on science and random things. Chris Chuckran: I am glad we became close friends after our awkward encounter during the summer Microscopy class. Matt Wu: Our update phone calls always cheer up my day.

Everyone in my life has directly or indirectly helped me reach my aspirations. I am excited for what the future holds for me. I look forward to seeing where my curiosity takes me next!

1.0 Introduction

Telomeres are specialized nucleoprotein structures that protect the ends of chromosomes from degradation and fusion. Telomeric DNA sequences are tandem arrays of the 5'-TTAGGG-3' hexanucleotide (1). Telomeres consist of a 3' G-rich overhang that folds back and anneals to the double-stranded hexameric repeats, forming a lariat-like structure termed the t-loop (2–4). The six-member protein complex, Shelterin (TRF1, TRF2, POT1, RAP1, TPP1, and TIN2), associates at telomeres and stabilizes the t-loop (5). TRF1 (Telomere Repeat Binding Factor 1) and TRF2 (Telomere Repeat Binding Factor 2) bind to the double-stranded TTAGGG region. RAP1 (Repressor/Activator Protein 1) associates with and stabilizes TRF2. POT1 (Protection of Telomere 1) binds to the single-stranded telomeric overhang. TPP1 (Adrenocortical Dysplasia Homolog (ACD)) is a binding partner of POT1. TIN2 (TRF1-and TRF2-Interacting Nuclear Protein 2) tethers the TPP1/POT1 complex to TRF1 and TRF2, which bridges the single-stranded and double-stranded regions of the telomere (5). These properties are integral to chromosome end-protection and act as a safeguard to shield exposed chromosome ends from being recognized as double-stranded breaks (DSBs) by the DNA repair machinery (6).

In normal somatic human cells, telomeres shorten overtime after each cell division due to the end replication problem, which arises from incomplete replication of the lagging strand (7). Progressive and irreversible loss of telomeres eventually reaches a critical point when cellular senescence is triggered to prevent genomic instability (8). To bypass this barrier, cells containing inactivating mutations in p53 and Rb pathways gain proliferative activity (9–11). However, eventually chromosome ends can become too short and unprotected, which generates end-to-end fusions and dicentric chromosomes (12). Telomere crisis results in an array of genomic

aberrations, including chromosome deletions, amplifications, translocations, chromothripsis, kataegis, and polyploidization (12,13). As a consequence, these cells are eliminated by autophagic cell death and apoptosis (13).

Cancer cells circumvent telomere dysfunction by adopting telomere maintenance mechanisms to achieve replicative immortality (14). Approximately 85% of cancers reactivate the specialized reverse transcriptase telomerase to synthesize *de novo* telomeric DNA (15). Two components of telomerase, the non-coding telomerase template RNA (hTR) and dyskerin, are constitutively expressed. The *TERT* promoter region is enriched with binding motifs for a range of transcription factors, including the MYC oncogene, but lacks TATA and CAAT boxes (16). Notably, the *TERT* promoter is unmethylated in normal somatic cells, which is thought to favor repressor-binding (17). Together, the silencing of the promoter and low basal transcription rate limit the number of molecules of the key catalytic subunit *TERT* (18). To counteract this, acquisition of TERT promoter mutations and upstream genomic rearrangements elevate *TERT* mRNA expression and telomerase activity. Genomic rearrangements in regions proximal to the *TERT* gene locus (5p15.33) can introduce enhancers that increase *TERT* expression (17). Hotspot mutations in the promoter of *TERT*, the catalytic subunit of telomerase, leads to telomerase activation (19–21). In familial and sporadic melanomas, two common non-coding mutations are located at -124 and -146 nucleotides upstream from ATG within the *TERT* promoter region (22). The prevalence of *TERT* promoter mutations varies according to cancer type and histology (23).

However, *TERT* expression is permanently repressed in 10-15% of cancers, which are largely derived from the mesenchymal-adrenergic lineage (24). These cancers engage in the recombination-mediated pathway termed Alternative Lengthening of Telomeres (ALT) (25). ALT telomeres display a permissive chromatin state, stochastic DNA damage, replication stress, as well

as inactivation of type I interferon response – all of which contribute to a favorable environment for homology-directed repair (HDR) pathways that mediate telomere maintenance and aberrant tumor growth (26–30). Understanding how ALT cancers hijack HDR mechanisms is the primary focus of this dissertation, as discussed in detail below.

1.1 The Physiological Basis of ALT

1.1.1 Clinical Relevance of ALT

10%-15% of all cancers activate the ALT pathway for telomere maintenance (25,31–33). While ALT is not commonly detected in tumors of epithelial origin (carcinomas), it is prevalent in tumors of mesenchymal (osteosarcomas and soft tissue sarcomas) and neuroepithelial (astrocytomas) origins (24,34,35). In addition, it is detected in highly aggressive tumor types such as pancreatic neuroendocrine (PanNETs), glioblastoma multiforme, and neuroblastoma. It still remains elusive as to why these cancers rely on the ALT pathway. However, it has been proposed that tumors of mesenchymal origin may have greater barriers to upregulation of telomerase activity, which force cells to favor the emergence of ALT (36,37). It is speculated that these cell types have altered control of senescence and crisis, which lead to stochastic telomeric damage and replication stress. Another possibility is that varying tissue types may have differential regulation of recombination and chromatin remodeling pathways (33,37,38). Interestingly, hybrids of ALT and telomerase-positive (TEL+) cells continue to exhibit immortalization, but with suppressed ALT phenotypes (37,39,40). This suggests that there is the existence of an ALT repressor in

telomerase-positive cells. Nevertheless, it is unknown whether loss of such repressor occurs in cancer cells of mesenchymal lineage.

1.1.2 Phenotypic Characteristics of ALT cancers

Loss of function mutations and deletions in ATRX/DAXX: One of the signature markers associated with ALT is the loss of expression of alpha-thalassemia/mental retardation syndrome, X-linked (ATRX) and death domain associated protein (DAXX) (41). Missense mutations and exon deletions that produce a non-functional or truncated ATRX protein, respectively, are identified in whole genome sequencing (WGS) of a wide range of tumor types that invariably become classified as ALT positive (42). Additionally, 70%-80% ALT cell lines have ATRX/DAXX mutations. Similarly, inactivating mutations in DAXX are also detected, particularly *in vivo*, with some ALT+ cell lines harboring a chimeric fusion protein formed between DAXX and kinesin motor protein KIFC3 (43). Clinical observations of PanNETs have identified loss of ATRX/DAXX protein expression and the manifestation of ALT as late events in tumor evolution, linked with metastatic disease (44). This late origin of ALT is consistent with numerous *in vitro* studies when the transient depletion or disruption of ATRX or DAXX is not sufficient to initiate ALT (42,45). The supposition is that additional genetic and/or epigenetic alterations in p53 or the acquisition of other passenger mutations may be mitigating factors for ALT initiation (46). Indeed, recurrent mutations in Isocitrate Dehydrogenase (IDH1) are more prevalent in gliomas and can promote ALT initiation in cells lacking ATRX *in vitro* (47,48). IDH1 is a metabolic factor that catalyzes decarboxylation of isocitrate to α-ketoglutarate (α-KG). IDH1 regulates the demethylation of histones and DNA.

ALT-associated PML bodies (APBs): APBs are structural complexes enriched in promyelocytic leukemia (PML) bodies, telomeric DNA, telomere associated proteins, and DNA repair proteins (49). PML bodies are matrix-associated domains in the nucleus that recruit proteins with diverse cellular functions. Specifically, APBs are only observed within a small subset, approximately 5-10%, of asynchronously dividing ALT-positive cell populations (50). Immunofluorescence-Fluorescence *in situ* Hybridization (IF-FISH), based on colocalization of PML and telomeres, is used to detect APBs in ALT+ immortal cell lines and archived formalin-fixed paraffin-embedded tumors (34,51). It has been reported that APBs are enriched in the G2/M phase and are decreased in frequency in cells exiting mitosis and re-entering the G1 phase. This suggests that the formation of APBs is a dynamic process and is coordinated with the cell cycle (52).

APBs structurally comprise of PML/SP-100 that form a 0.01-1μm diameter shell enclosing telomeric DNA, telomere specific proteins (Shelterin components TRF1 and TRF2), as well as DNA damage response and repair factors (such as gamma-H2A Histone Family Member X (γH2AX), ATP-binding Cassette-ATPase (Rad50)/Meiotic Recombination 11 Homolog 1 (Mre11)/Nijmegen Breakage Syndrome Protein 1 (NBS1), and Structural Maintenance of Chromosomes Protein 5/6 (SMC5/6)) (53–55). Several lines of evidence indicate that APB formation is driven by SUMOylation events mediated by SUMO E3 Ligase MMS21, a component of the SMC5/6 complex (55,56). SUMOylation is a post-translational modification that covalently conjugates small ubiquitin-like modifiers (SUMO) to an array of cellular proteins in a similar manner to ubiquitylation (57). To initiate APB formation, MMS21 SUMOylates telomere binding-proteins, TRF1 and TRF2, to assemble PML/SP100 at telomeres through interactions between SUMO and SUMO-interacting motifs (SIM) (58). These SUMOylation events facilitate the

formation of liquid-liquid demixing condensates that can dynamically alter the scaffold-protein interaction (59). A positive SUMOylation feedback loop is established, leading to the recruitment of repair and recombination factors that promote telomere elongation (55,58). Additionally, NBS1, which is a vital component of the Mre11-Rad50-Nbs1 (MRN) repair and recombination complex, is essential for assembly of functional APBs (60,61)

Although the function of APBs is not well-defined, there is strong evidence arguing that the presence of APBs promotes ALT activity. The presence of APBs have been used to identify most ALT+ tumors while the repression of ALT is accompanied by a decrease in APBs (34,62). It has been shown that PML bodies in ALT cells directly associate with chromosome ends, allowing for telomere clustering and recombination (63). In addition, a recent study proposed that ALT telomere DNA synthesis is exclusively detected in APBs during G2 (64). However, DNA synthesis could not be differentiated between a single telomere, multiple telomeres, or extrachromosomal circles. APBs likely serve as a recombinogenic platform to enrich proteins that enhance replication and homologous recombination. By sequestering these proteins to telomeres, APBs provide the prime environment for telomere recombination and extension in ALT. Understanding the exact mechanisms of APB formation will lead to improved assessment of ALT tumors.

Extrachromosomal Telomeric Repeats (ECTRs): Although ECTRs are present in ALT cells, their function is not well-characterized (65–68). There are two common types of ECTRs that are linked with ALT. Firstly, partially single-stranded C-rich circles (c-circles) are abundant in ALT+ cancers, but not in TEL+ cancers (69–71). An established PCR-based method is used to measure c-circle levels in cancer cell lines and human blood samples (72). The abundance of c-circles can be quantified using a modified rolling circle amplification (RCA) assay that relies on ϕ29 DNA polymerase. Thus, c-circles are widely used as a specific and quantitative biomarker for

ALT activation (69,72). Secondly, heterogenous double-stranded telomeric circles (t-circles) are also commonly found in ALT (65,70,73). However, t-circles are neither ALT nor cancer specific; they can be the result of telomere trimming in normal germline cells and in cells with overexpression of telomerase components, both of which have extensively long telomeres (74,75). Although ALT+ and TEL+ cells are able to produce t-circles, only ALT+ cells contain c-circles, which suggests that c-circles may arise from an undetermined mechanism of altered telomerase activity (71).

Telomere Sister Chromatid Exchanges (T-SCEs): ALT cancers display hyper-recombination, which manifests as elevated frequency of telomere-sister chromatid exchanges (T-SCEs) (76–80). These events can be detected using telomere specific chromosome-orientation fluorescent *in situ* hybridization (CO-FISH), which utilizes specific telomere probes for the G-rich lagging and C-rich leading strands (50). The exchange between two sister chromatids is visualized as a double signal at one telomere. Although T-SCEs are a marker of ALT, it is not indicative of telomere extension (81). Additionally, it is speculated that crossover events can also arise from recombination with non-sister telomeres or ECTR elements (78).

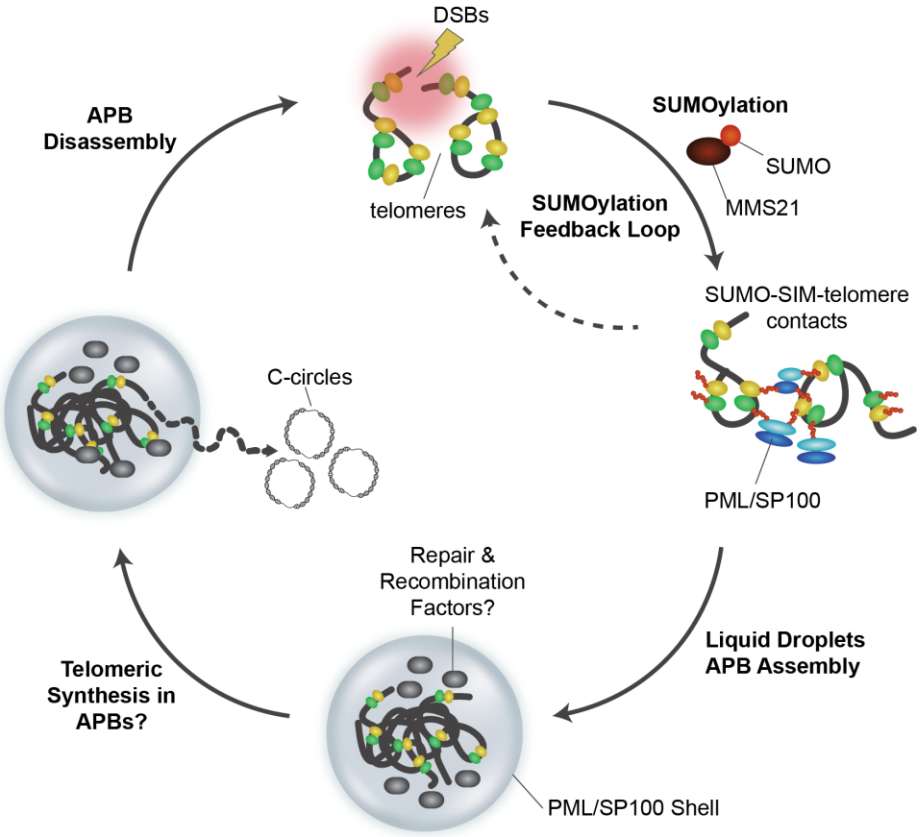

Figure 1. Schematic of ALT-associated HDR mechanisms occuring in APBs. SUMOylation of Shelterin components, TRF1 and TRF2, recruits PML/SP100 via SUMO-SIM interactions. SUMOylation-induced APB condensates lead to clustering of telomeres and DNA repair factors within the PML/SP-100 shell. A positive SUMOylation feedback loop enhances APB formation. APBs act as a platform to concentrate repair and recombination factors to facilitate telomeric DNA synthesis, particularly of extra-chromosomal C-circles. APBs are disassembled as a result of deSUMOylation events.

1.1.3 Telomerase-Independent Lengthening of Yeast Telomeres

Budding yeast cells lacking a functional *est1* gene, which encodes yeast telomerase, exhibit progressive shortening of the terminal $G_{1\text{-}3}T$ telomeric repeats (82). While the majority of cultured yeast cells in an *est1*$^{-}$ culture die, a minor subpopulation of survivors regains the ability to divide and maintain telomere length. Thus, when the primary pathway for telomere maintenance is defective, an alternative pathway emerges to bypass senescence and cell death. These survivors consist of two types: Type I utilizes Rad51-dependent recombination while Type II engages in a Rad51-indpendent mechanism that is mediated by break-induced replication (BIR) (60,83). While POLD32, homolog of POLD3, is dispensable for replication and gene conversion, it is required for BIR to establish a full replication fork by recombination in the absence of an origin of replication (84). Type I survivors have tandem duplication of the Y' element, a highly polymorphic repetitive sequence present in the subtelomeric regions of many yeast telomeres (83,85,86). These show amplification of the Y' elements, but have very short $G_{1\text{-}3}T$ telomeric repeats. Meanwhile, Type II survivors exhibit rearrangement and/or tandem duplication of the distal portion of the Y' element. Type II survivors demonstrate highly heterogeneous long tracts of $G_{1\text{-}3}T$, resembling telomeres present in ALT cancers. These studies suggest that Type II survivors in budding yeast and the mammalian ALT pathway may share mechanistic similarities.

1.2 Homology-directed Repair Mechanisms in ALT

Through imaging of individual proteins and unbiased proteomics profiling of ALT telomere composition, an undoubted constitutive and selective association of HR factors with ALT

telomeres has been determined (87–90). They include the central recombinase RAD51, single-stranded DNA binding Replication Protein A (RPA), the DNA resection MRN complex, Bloom helicase (BLM) and several HR accessory factors Breast Cancer Gene 1 (BRCA1), Breast Cancer Gene 2 (BRCA2), RAD51-associated Protein 1 (RAD51AP1) and RAD52 (27,28,64,91–94). These are frequently sequestered together with clusters of telomeres and Shelterin subunits in APBs, which are characteristic markers of recombination-mediated repair and extension of telomeres in ALT cancer cells (49). Recombination and extension are two independent, potentially competing HDR mechanisms that underpin ALT, both of which utilizes exposed DNA ends at stochastic telomere or stalled replication forks as primers (Figure 2). RAD51-dependent homologous recombination facilitates error-free repair of telomeres (95,96). Later in G2/M phase, a pathway that is dependent on RAD52, Proliferating Cellular Nuclear Antigen (PCNA), Replication Factor C 1-5 complex (RFC), and DNA polymerase δ (PolD3) mediates conservative DNA synthesis and extends telomere length (93,97,98). Recent studies have shed light on the complex regulation of these HDR mechanisms.

The intrinsic difficulty of replicating long tracts of GC rich telomeric sequences has been implicated as the basis for constitutive HDR activity at ALT telomeres (Figure 2). Stalling of replication forks pose a threat to genome stability. This can arise due to polymerase collision with DNA nicks, DNA gaps or polymerase barriers like G-quadruplexes that can readily form within ALT telomeres (99,100). These replisome collisions are detected by the DNA damage sensor kinase, Ataxia-Telangiectasia and Rad-3 related (ATR) (98). The ATR signaling cascade initiates the processing of stalled forks and downstream signaling to attenuate telomere replication (101–103). Subsequently, repair and restart of these stalled forks involves dedicated remodeling enzymes like SWI/SNF-related, matrix associated, actin-dependent regulator of chromatin,

subfamily A-like 1 (SMARCAL1), an ATP-dependent strand annealing helicase, and/or Fanconi anemia complementation group M (FANCM), a DNA-dependent ATPase/Translocase subunit of the Fanconi Anemia (FA) core complex (29,30,104). FANCM also works with RNaseH1 to dissolve aberrant R-Loops that form between the TERRA lncRNA and telomeric DNA sequences, which can accumulate and destabilize replication forks and HR intermediates within ALT telomeres (105). The activity of these proteins is essential for mediating replication fork reversal and repair. Preventing fork remodeling, by depletion of SMARCAL1 or disruption of FANCM, unleashes staggering increases in APB frequency and size (27,29,30). These cells exhibit elevated RAD51-dependent clustering of telomeres, chromosomal abnormalities, and DNA damage signaling that is consistent with rampant, uncontrolled recombination. ALT cell lines that are deficient in these proteins, particularly FANCM, display acute cell death. Thus, this initial response by SMARCAL1 and FANCM represents a critical mechanism to salvage stalled forks at ALT telomeres (12,13,69). It also acts as a front-line tolerance mechanism that limits excessive telomere recombination and damage to preserve ALT cancer cell survival and proliferation.

Once stabilized and repaired, an active fork can be restored by RAD51-dependent HR (Figure 2). RAD51 presynaptic filaments explore nuclear space, probing for identical telomeric sequences that provide the template for error-free repair (96). At genomic DSBs, RAD51-dependent homology search involves the consumption of ATP and polymerization of nuclear F-actin filaments that propel homologous DNA sequences into proximity of each other (106). Though yet to be determined, the same processes are likely to stimulate telomere clustering in ALT. As with HR at genomic DSBs, homology search during ALT is co-regulated and stimulated by HR accessory factors such as BRCA1, BRCA2, RAD51AP1 and the SMC5/6 heterodimer (28,55,91). However, ALT is distinct from conventional HR due to the involvement of the

Homologous Pairing Protein 2-Meiotic Nuclear Division Protein 1 (HOP2-MND1) heterodimer that is normally associated with meiotic HR (98). The involvement of HOP2-MND1 at telomeres could assist in overcoming reduced homology search and capture kinetics at G-C rich regions, such as those at telomeres. It was also proposed that HOP2-MND1's role in gametogenesis is a remnant of a primordial meiotic origin of ALT that is reactivated in telomerase deficient cancer cells (96). However, the basis of meiotic factors like HOP2 involvement in ALT remains unclear.

Once homologous telomeric sequences have been captured, the presynaptic filament invades, aligns and combines with the double-stranded partner DNA, forming the synaptic complex (Figure 2). This action displaces a strand of DNA, forming the Displacement Loop (D-Loop). At the terminal 3'hydroxyl group, PCNA is loaded by RFC to prime and initiate semi-conservative DNA synthesis. Given the high GC-rich content at telomeres, the translesion DNA polymerase, Pol η, might be employed to initiate DNA synthesis before Pol δ takes over (87). During DNA synthesis that emanates from stalled forks, the translocase activity of FANCM works in unison with the DNA unwinding and decatenation activities of the BLM-TOP3A-RMI1-2 (BTR) complex to promote branch migration and eventual dissolution of D-loops and Holliday Junctions (HJs) (81,107,108). The dissolution activity of the BTR complex is crucial as it facilitates Pol δ -dependent telomere extension and suppresses telomere sister chromatid exchange (t-SCE) events, thereby preserving the original orientation of telomeric DNA strands (81).

In addition to HJ resolution, BLM has also been shown to alleviate persistent telomere replicative stress at forks that escape reversal (Figure 2). Here, BLM's helicase activity can facilitate EXO1-DNA2 dependent resection that potentially sets the stage for repair by an alternate RAD51-independent HDR pathway (93). RAD52 could be recruited and initially stabilize these HR intermediates, perhaps to limit resection. Then, utilizing its single-strand annealing (SSA)

activities, RAD52 subsequently facilitates intra-chromosomal pairing of telomeric DNA sequences located on proximal sister chromatids and D-loop formation (64,94). This process primes break induced replication (BIR)-related DNA synthesis at ALT telomeres. In fact, recent evidence has implicated several BIR-like pathways that are essential aspects of ALT telomere maintenance (98). These conservative DNA synthesis pathways take place beyond the confines of S-phase, function in G2 and M-phases, share independence from RAD51-dependent HDR, and universally adopt the specialized PCNA-RFC-Polδ replisome. The predominant pathway, called G2-BIR, relies on RAD52-mediated restoration of stalled replication during G2 mentioned above since cells lacking any of RAD52 or the POLD3-POLD4 subunits of Pol δ display attenuated DNA synthesis and extensive telomere shortening (64,94,98). RAD52 is also crucial for a spontaneous form of DNA synthesis during the early stages of mitosis, termed Mitotic DNA synthesis, or spontaneous mitotic DNA synthesis (MiDAS), which can occur at chromosome arms and at telomeres (109–111). The predominance of the RAD52-dependent pathway over its RAD51-mediated counterpart has been attributed to each protein's distinct binding kinetics (94,98). Also, the individual substrate requirements of RAD51 and RAD52, as well as the mechanisms of HR intermediate processing, will likely dictate commitment to either pathway.

Stalled forks that escape or are incompatible with repair using the mechanisms outlined above must be salvaged before mitosis (Figure 2). These can be subjected to endonucleolytic resolution by a complex comprised of SLX1-SLX4, MUS81-EME1, XPF-ERCC1 (SMX). The SMX complex cleaves or resolves each junction of the intermediate structure (112). The SMX complex associates with telomeres, irrespective of whether telomerase or ALT is active (113,114). It acts as an all-purpose responder to detrimental telomere damage, where it dismantles complex HR entanglements. This generates large deletions of telomeric DNA at these intermediates.

RAD52 also stimulates MiDAS at intermediates that are resolved by SMX (110). However, unlike RAD52-dependent DNA synthesis during G2, MiDAS that is stimulated by SLX4 appears to be abortive or non-productive. This is corroborated by SLX4-deficient cells that display a net loss in overall telomere length in ALT cells.

In ALT cells, the SMX complex appears to fulfill a greater role in antagonizing the HJ dissolution of the BTR complex, which seems to be essential for telomere length homeostasis (81) (Figure 2). In the absence of functional BTR, the promiscuous resolvase activity of SMX becomes uncontrolled and promotes unwarranted recombination, yielding excessive t-SCEs and diminished DNA synthesis. In contrast, disrupting SMX-mediated resolution promotes unrestrained BLM-mediated dissolution and DNA synthesis at telomeres. Interestingly, an auxiliary constituent of the SMX complex, SLX4IP, was shown to directly bind and potentially antagonize BLM's dissolution activity (112). ALT cells lacking both SLX4 and SLX4IP exhibit staggering increases in recombination, mitotic anomalies and a severe synthetic lethal phenotype that was fully rescued by depletion of BLM. Thus, the BTR dissolution and SMX resolvase activities are subject to exquisite molecular and temporal regulation that is vital in maintaining what has been termed productive ALT.

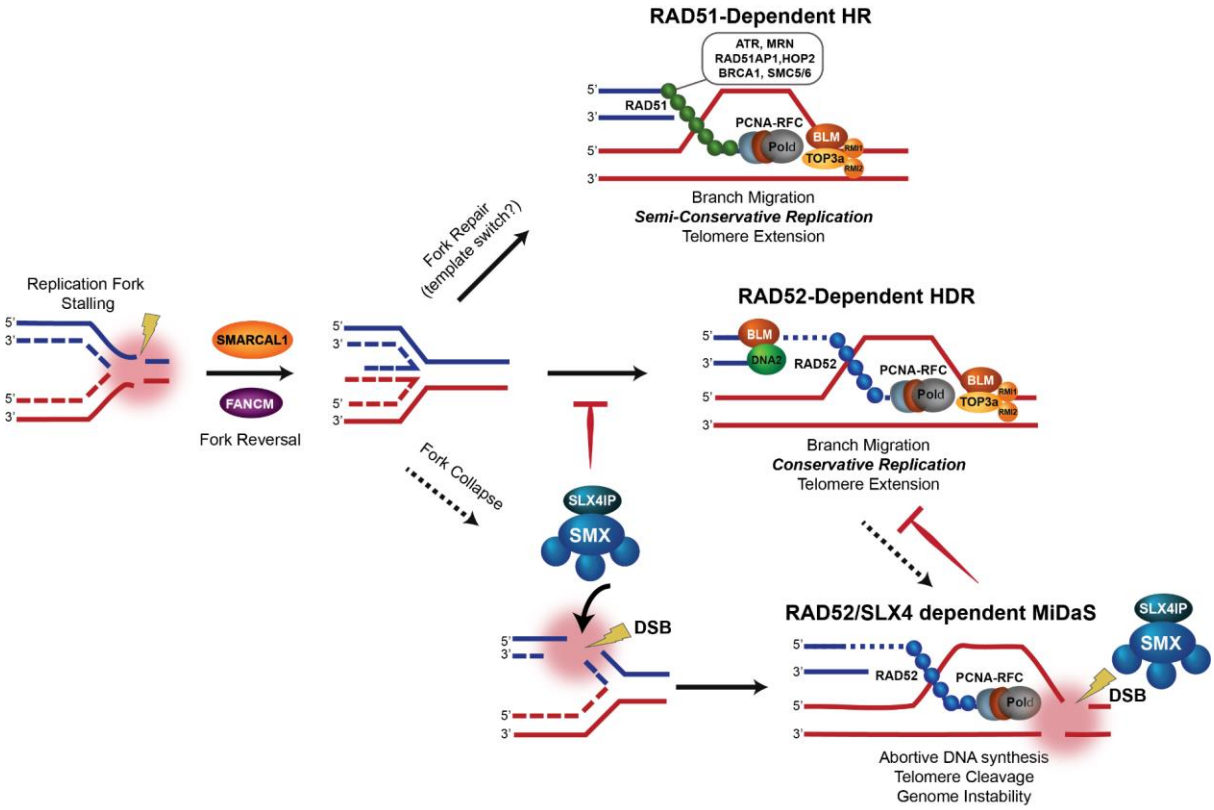

Figure 2. HDR mechanisms of ALT. Telomeres pose a challenge for the replication machinery, leading to replication fork stalling. There are various pathways to resolve this impediment in ALT, which are RAD51-dependent HR, RAD52-dependent HDR, and RAD52/SLX4-dependent MiDAS.

1.3 Chromatin Remodeling in ALT

It is speculated that remodeling of telomere architecture plays a key role in the emergence and maintenance of ALT. Through a sequencing approach, it was recently discovered that variant repeats (TCAGGG, TGAGGG, and TTGGGG) are interspersed throughout the telomeres of ALT cells (115). The C-type (TCAGGG) variant repeat is predominantly enriched within the canonical repeat arrays and provides a high affinity binding site for the nuclear receptors COUP-TRF2 and TRF4 (116). The binding of nuclear receptors to telomeres leads to the engagement with ZNF827,

a zinc-finger protein that recruits the nucleosome modeling and histone deacetylation (NuRD) complex. The result is decreased shelterin binding, destabilization of the telomere architecture, and an elevated recombinogenic telomeric state. This disequilibrium primes a positive feedback loop for further spreading of variant repeats from the proximal region of telomeres, which has profound implications for ALT telomere structure and function (115,117).

Intriguingly, ATRX/DAXX-associated mutations functionally converge through their effects in reconfiguring chromatin structure. DAXX and ATRX form a multifunctional chromatin-remodeling histone chaperone complex that is responsible for the replication independent deposition of histone H3.3 (118). In the absence of functional ATRX-DAXX, failure to assemble chromatin with histone H3.3 can have pleiotropic effects on transcription and single-stranded DNA (ssDNA) repair mechanisms such as nucleotide excision repair (NER), while also negatively impacting chromatin compaction and integrity (119). ATRX deficiency has also been implicated in alterations in sub-telomeric DNA methylation on the basis that it interacts with DNA methyltransferase 1 (DNMT1) (120). Remarkably, heterozygous mutations in histones H3.1 and H3.3 at or adjacent to key lysine residues, K27M and G34R/G34R, which are targeted by lysine methyltransferases complexes Enhancer of Zeste 2 (EZH2) and SET domain containing 2 (SETD2), respectively, have also been identified in ALT-positive glioma (121,122). Thus, it appears that at singular or multiple distinct points during ALT cancer cell evolution, telomeric chromatin undergoes considerable modification and expansion, losing its DNA repair refractory state and becoming more accessible and permissive for HDR mechanisms that sustain telomere length in ALT cancers (26,117).

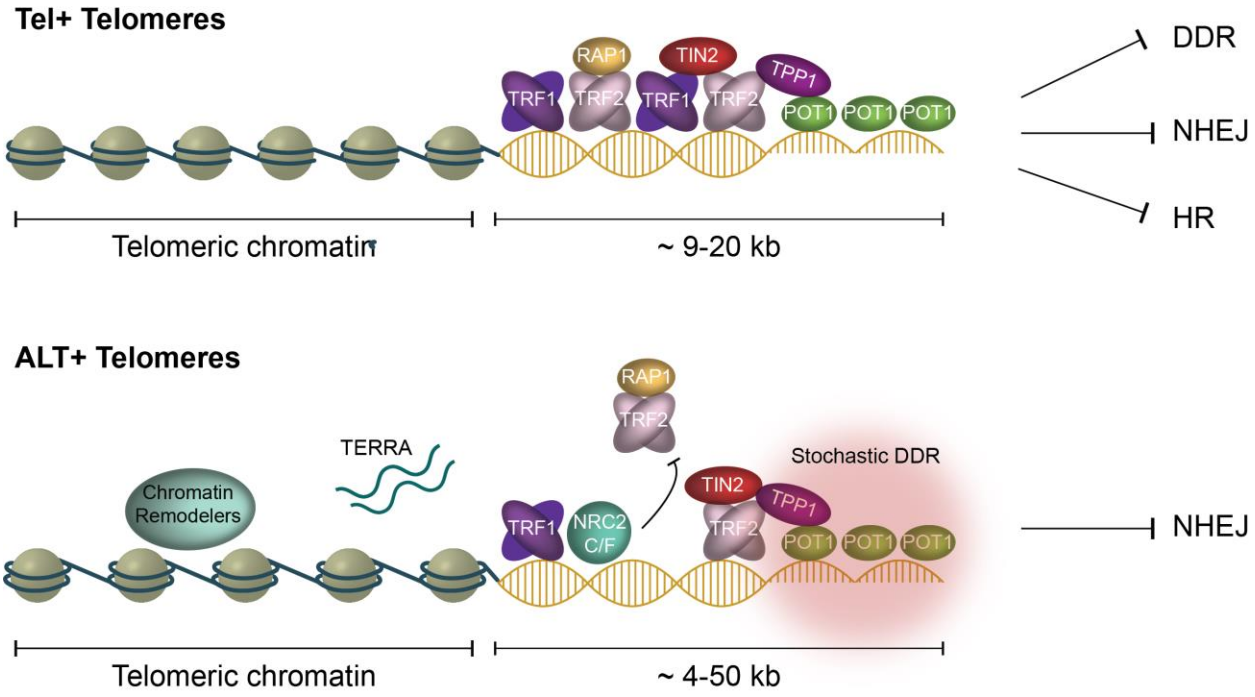

Figure 3. Distinct chromatin landscape of ALT facilitates HR. While TEL+ telomeres have a more closed chromatin structure, ALT+ telomeres are more accessible to facilitate a favorable environment for HDR. ALT telomeres exhibit stochastic DNA damage and replication stress, all of which contribute to a permissive telomeric state for ALT mechanisms.

1.4 Poly(ADP-ribosyl)ation

1.4.1 Poly(ADP-ribose) Polymerase (PARP) Family

ADP(ribosyl)ation is a reversible post-translational modification that covalently attaches ADP-ribose (ADPr) onto Glu, Lys, or Asp residues of acceptor proteins by using nicotinamide adenine dinucleotide (NAD+) as a substrate (123). While mono(ADP-ribosyl)ation (MARylation) adds a single ADPr unit, poly(ADP-ribosyl)ation (PARylation) can add up to 200 ADPr units via

linear and branched glycosidic linkages (124). This modification is catalyzed by diverse members of the poly(ADP-ribose) polymerase (PARP)/ADP(ribosyl)transferase (ADPRT) family (123). In humans, there are 17 members in the PARP family, which belong to five subfamilies based on functional domains in regions outside of the PARP domain. These include: 1) DNA-dependent PARPs, 2) tankyrases, 3) CCCH zinc finger PARPs, 4) macro PARPs, and 5) unclassified PARPs (123,125–127). The DNA-dependent PARPs (PARP1, PARP2, and PARP3) are the only members of the PARP family that are expressed in the nucleus (128–130). These PARPs, along with PARP4-6, share a conserved His-Try-Glu (H-Y-E) triad in their catalytic domains (131). PARP1 recognizes different lesions, including SSBs, DNA crosslinks, stalled replication forks, and DSBs (132). On the other hand, PARP2 binds less efficiently to SSBs and has been proposed to recognize gaps and flap structures that correspond to advanced repair intermediates (133,134). PARP3 has been shown to play a role in the cellular response to DSBs during classical non-homologous end-joining (c-NHEJ) and mitotic progression (135,136). Tankyrase 1 (TNKS1) and Tankyrase 2 (TNKS2) have redundant functions to regulate telomere maintenance via PARylation of TRF1, oncogenic pathways, as well as spindle pole formation in mitosis (137,138). The CCCH-type PARPs (PARP7, PARP12, and PARP13) and the macroPARPs (PARP9, PARP14, and PARP15) have been documented to regulate transcription and the viral response (123,139–143).

1.4.2 Poly(ADP-ribose) Polymerase 1 (PARP1)

The focus of this dissertation is on PARP1, the most abundant and ubiquitous member of the PARP family (144). PARP1 is a 116-kDa protein that comprises of an N-terminal DNA-binding domain, central automodification domain, and C-terminal catalytic domain (127). Amino acid acceptors of PARylation include Lys, Arg, Glu, Asp, Cys, Ser, and Thr (131). There are

several paradigms that propose the stoichiometry of PARP1 peptides involved in auto-PARylation (131). There is compelling evidence for the bimolecular model that argues asymmetric PARP1 dimerization (145–147). Here, one DNA-bound PARP1 molecule functions as the catalyst while the second PARP1 molecule is inactive, but serves as the PAR acceptor. In addition, it is proposed that both PARP1 molecules can act as catalysts and acceptors simultaneously if the PARP1 binding sites on DNA are closely adjacent to each other (145–147) Despite the convincing argument for the bimolecular model, it has been speculated that PARP1 functions as a monomer to modify itself intramolecularly *in cis*. The structural model of PARP1 bound to DNA nicks and hydrogen/deuterium exchange-mass spectrometry data suggest that the BRCT-WGR linker is flexible enough to reach the active site of PARP1 when the monomer is bound to DNA nicks. Thus, one PARP1 molecule is sufficient to serve as both the catalyst and acceptor of PAR (148,149). Using atomic force microscopy (AFM), PARP1 has been shown to bind nicks, ends, and abasic sites in DNA as a monomer. PARP1 changes from three-dimensional DNA damage searching to one-dimensional diffusion after auto-PARylation or in the presence of APE1 (150).

PARP1 plays a prominent role in DNA repair, chromatin remodeling and transcription, which will be discussed in detail in the below sections (132,151,152). There are hundreds of proteins that directly or indirectly interact with PAR (153). This leads to a diverse array of biological outcomes that are involved in genotoxic, oxidative, oncogenic, and inflammatory stress responses (144). These proteins bind PAR through distinct PAR-binding modules, such as: basic PAR-binding motif (PBM), PAR-binding zinc finger (PBZ), Macrodomains, WWE domains, FHA and BRCT domains, RNA and DNA binding motifs, RNA recognition motif (RRM), SR repeats and KR-rich motifs, OB-fold, PIN domains, and RGG motifs (154). Due to the many facets of PAR in the DSB response, deficiencies in PARP1 and PARP2 have profound consequences for

genome stability (155). Studies have shown that there is a functional interaction between PARP1 and PARP2 in regulating chromosomal stability and embryonic development in mice (155–157). Both can homo- and heterodimerize, and are involved in the base excision repair (BER) pathway. While *Parp1*$^{-/-}$ mice exhibit higher sensitivity to high-dose ionizing radiation and alkylating agents, *Parp2*$^{-/-}$ mice demonstrate hyper-radiosensitivity to low-dose radiation. *Parp1*$^{-/-}$ *Parp2*$^{-/-}$ double mutant mice are not viable and die at the onset of gastrulation. These studies indicate that PARP1 and PARP2 have distinct roles in the DNA damage response, but play a redundant role with regard to cell survival.

1.4.3 Poly(ADP-Ribose) Glycohydrolase (PARG)

Although extensive and rapid PARylation is necessary to elicit recruitment of the DNA damage machinery to DNA lesions, hyper-PARylation is detrimental to cells and is resolved by poly(ADP-ribose) glycohydrolase (PARG) (158). Excessive PARylation may trap DNA damage repair factors at the damaged site, blocking access to downstream processes. In addition, this leads to PARthanatos, a process in which PAR acts as a cell death effector (159). Excessive PAR migrates from the nuclei to cytosol, which leads to apoptosis inducing factor (AIF) translocation from the mitochondria to the nucleus (159–161). In addition, PARP1 overactivation may deplete cellular energy through NAD+ consumption, triggering the release of AIF and ultimately, cell death (159,162,163). Thus, the timely and orderly degradation of PAR is important to maintain efficient repair and cellular processes.

To date, PARG is the only enzyme that can hydrolyze the O-glycosidic linkages of PAR polymers, thereby generating free ADPr (164). PARG catalyzes PAR chain degradation through endo- and exoglycolytic activities, but still leaves a terminal ADPr moiety attached to the acceptor

amino acid residue from its substrate (165). There are five other dePARylation enzymes that have been identified, including ARH3 (ADP(ribosyl)hydrolase 3), TARG1 (Terminal ADP-ribose protein glycohydrolase), NUDT9 (Nudix Hydrolase 9), NUDT16 (Nudix Hydrolase 16) , and ENPP (Ectonucleotide pyrophosphatase/phosphodiesterase) (166). Although ARH3 contains exo-glycohydrolysis activity to release free ADPr, its activity is much lower than that of PARG (167). TARG1 does not hydrolyze PAR to ADPr and can only remove whole PAR chains from glutamate residues of acceptor proteins (168). NUDT9 and NUDT16 only cleaves pyrophosphate bonds to release iso-ADP-ribose and AMP from PAR chains or MARylated proteins (169,170).

There are five isoforms of PARG that have been described – the nuclear, full-length PARG protein (110 kDa), two splice variants that lack exon 1 (102 kDa) or exons 1 and 2 (99 kDa), and two mitochondrial isoforms (60 kDa and 55 kDa) (125,171–173). Nuclear, full-length PARG comprises of an N-terminal regulatory region, PCNA binding motif, nuclear export signal, mitochondrial export sequence, a highly structured B-domain, and essential catalytic macrodomain (164). The crystal structure of PARG was resolved from the bacterium *Thermomonospora curvata* by Slade et al. (174). This revealed that the catalytic domain of PARG belongs to a distant member of the ubiquitous ADPr-binding macrodomain family (175,176). They proposed a model for PAR binding and catalysis by modelling the PARG complex with ADP-ribose and the PARG inhibitor ADP-HPD as well as complementing with biochemical studies. The diphosphate-binding loop that flanks one side of the ADPr binding cavity is highly conserved between PARG and other macrodomain structures. However, the other side of the cavity is lined with the PARG-specific signature sequence (GGG-X_{6-8}-QEE), which is inserted into the macrodomain fold to allow for the Glu115 side chain to protrude into the PARG active site. This PARG-specific loop differentiates PARG from the other macrodomain proteins and enables the ability for PAR hydrolysis (174).

Nuclear PARG exhibits a dual recruitment mode to damaged lesions, which involves its dependency on PARP1, PAR, and PCNA binding. PARP1 and PAR provide access to the damaged lesions by relaxing the chromatin structure and serving as a docking site for PARG recruitment. PARG then interacts with PCNA through a non-canonical PIP box-domain located within the disordered regulatory region (177). Specifically, the acetylation site K409 permits stabilization of the PCNA-PARG interface via hydrophobic and electrostatic interactions. This interaction enhances PARG residency at damaged lesions. Since PCNA displays slow and constant accumulation at damaged lesions, PARG's interaction with PCNA could potentially keep PAR levels at a lower, steady-state for later steps of repair (178). In fact, PARG is recruited to replication forks through PCNA where it hydrolyzes PAR that accumulates at unligated Okazaki fragments (179).

As PARG is the primary enzyme to degrade PAR, it plays a fundamental role in embryonic development and maintenance of genome stability (180). Loss of the *PARG* gene results in early embryonic lethality at the gastrulation stage (embryonic day 6.5), which phenocopies *Parp1*$^{-/-}$ *Parp2*$^{-/-}$ double mutant mice (156). This deleterious consequence affirms that the regulation of PAR levels is essential for cell survival and that there is a lack of a compensatory mechanism for PARG. In addition, proper PAR catabolism is essential for the completion of efficient repair in response to genotoxic stress. Depletion of the nuclear isoform of PARG, $PARG_{110,}$ leads to compromised repair of DNA damage caused by various genotoxic agents (171,181). $PARG_{110}^{-/-}$ cells display elevated genome instability, as seen by high frequency of sister chromatid exchanges, micronuclei formation, and chromosomal aberrations. PARG activity is dispensable for DNA replication in unperturbed conditions and recovery from transiently stalled replication forks (171,181). However, PARG is crucial during prolonged replication stress to prevent massive PAR

production, which leads to replication fork collapse and DSBs. Another study showed that PARG depletion leads to perturbed fork progression and accumulation of abnormal DNA replication (182). PARG-defective cells also exhibit ataxia-telangiectasia-mutated (ATM) and ataxia-Rad3-related (ATR) activation, as well as downstream DSB repair factors, such as p53-binding Protein 1 (53BP1) and RAD51. Thus, PARG is essential to sustain cellular energy supplies and ensure the faithful stepwise transitions during DNA repair and replication. This collectively affirms that tight regulation of PAR metabolism is critical to maintain cellular homeostasis.

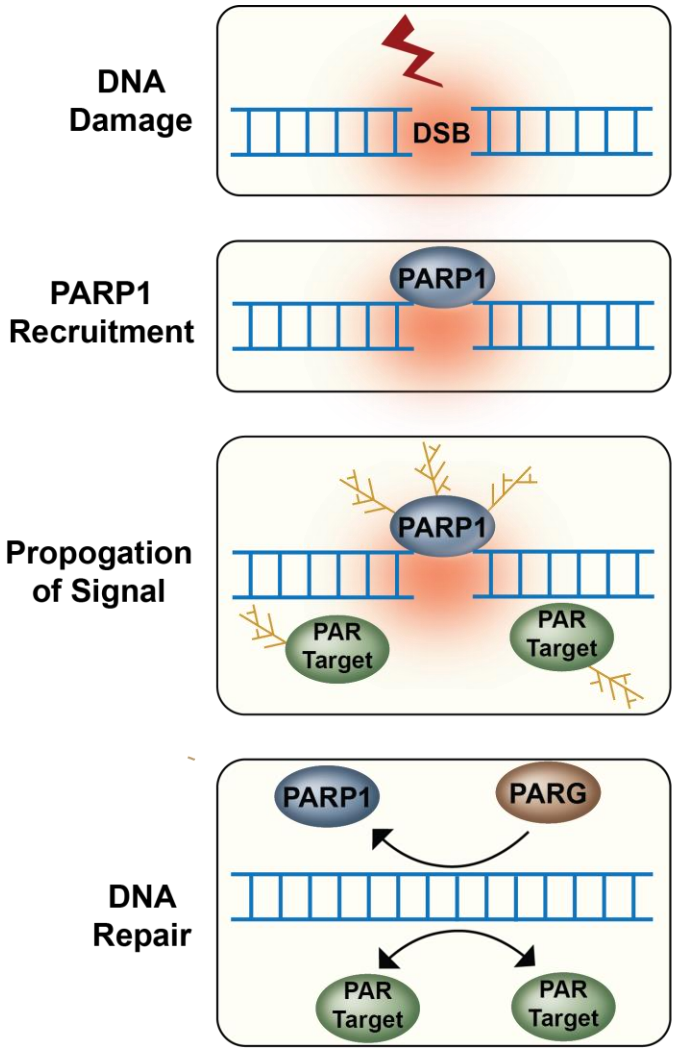

Figure 4. PARylation is an apical signal of DNA damage. A damaged DNA lesion, such as a DSB, recruits PARP1 to the site of damage to propagate the DNA damage signal for various cellular events. The completion of repair is marked by PARG-mediated PAR hydrolysis.

1.4.4 Role of PARylation in DSB Repair

DSBs are repaired through HR or NHEJ depending on the cell cycle and chromatin state. PARP1 is required for a robust DSB response, as it is an apical sensor that is recruited to the damaged lesion within seconds of DSB formation (183). Initial DSB responders, such as ATM

and Mre11 contain PAR-binding domains and have been shown to interact with PAR *in vitro*. PARP1-stimulated recruitment of the MRN complex could favor pathway choice for repair of DSBs towards HR (184–186). PARP1 also regulates the early recruitment of other HR factors, including BRCA1. PARP1 may indirectly enhance BRCA1 localization through its interaction with BRCA1-associated RING domain protein 1 (BARD1), which facilitates BRCA1's role in end resection and loading of RAD51 onto DNA (187). However, BRCA1 is only partially dependent on PARP1 since it can still be recruited to DSBs by ubiquitylation (188). This indicates that there are compensatory mechanisms for the initial DSB response because PARP1 depletion does not completely abolish the recruitment of these HR factors and only delays their recruitment. However, it is well-established that loss or inhibition of PARP1 leads to a hyper-recombinogenic phenotype (189,190). An explanation for this phenotype involves PARP1-mediated stabilization of BRCA1 and receptor-associated protein 80 (RAP80), which restricts HR by blocking strand invasion. Another possibility is that PARP1 deficiency leads to processing of SSBs into DSBs, which would enhance reliance on HR. This is supported by the synthetic lethality that results from loss of BRCA1 and BRCA2 in combination with PARP inhibitors (191,192).

PARP1 competes with Ku70/80 for pathway choice in G1 and S/G2-phase. PARP1 and the Ku70/80 complex are recruited to DSBs at similar kinetics (183). While the Ku70/80 complex occupies DSBs specifically in the G2-phase, PARP1 can PARylate the Ku70/80 complex and displace it during S/G2-phase. This prevents Ku70/80 complex-mediated c-NHEJ during S/G2-phase, leading to PARP1 regulation of alt-NHEJ during this phase. Alt-NHEJ involves minimally resected ends that are joined through microhomology. The gap is then filled by Pol θ and ligated by LIG3 (193). Alt-NHEJ is considered a backup pathway for c-NHEJ (194). Intriguingly, telomere-internal DSBs are also repaired by both HR and PARP1/LIG3-dependent end-joining

(195). The inability of the Shelterin complex to repress alt-NHEJ and HR at telomere internal DSBs poses a confounding question regarding the unique telomeric environment that is permissive to these repair mechanisms.

1.4.5 Role of PARylation in Replication

PARP1 plays a pivotal role in regulating replication fork progression during replication stress. Impediments to replication can generate unrepaired single-strand breaks at DNA replication forks, which cause fork stalling until the lesion is fully repaired. Persistent fork stalling leads to fork collapse, resulting in one-ended DSBs that become substrates for HR (196). It has been established that RecQ1 helicase interacts with PARylated PARP1, which restrains its fork restoration activity to prevent premature restart of regressed forks after camptothecin (CPT) treatment (197). Inhibition of PARP1 allows for untimely restart of reversed forks, which ultimately primes replication run-off and increased DSB formation. This affirms the importance of PARP1 as a mediator of the stabilization of replication forks through regulation of fork reversal.

Interestingly, Maya-Mendoza et al. showed that inhibition of PARP1 accelerates fork progression, but does not increase fork stalling, which is in contrast with the previously described accepted model by Berti et al (197,198). DNA fiber analysis revealed aberrant acceleration of fork progression by 60% above the normal speed without affecting fork symmetry (198). The authors proposed that PARylation acts as a sensor for replication stress and can signal fork arrest. PARP1 also induces p53-mediated accumulation of p21, which further prevents defective forks from progression. PARP1 inhibition exceeds the threshold for fork speed and triggers DDR in cells. Increased fork speed may lead to bypass of DNA lesions as well as reduced fidelity of DNA polymerases, which further contribute to genomic instability (198). Overall, both viewpoints agree

that controlled regulation of fork progression via PARP1 is crucial for preservation of genome integrity.

1.4.6 Role of PARylation in Chromatin Remodeling

Cells rely on reorganization of chromatin structure to increase the accessibility of the DNA repair machinery to damaged lesions. PARP1 modulates chromatin architecture through direct PARylation of histones and chromatin remodelers (128,199). Early studies showed that PARylation of nucleosomes leads to chromatin decondensation *in vitro* (200). Later evidence proposed a more intricate interplay between PARylation and the histone core of nucleosomes (H2A, H2B, H3, and H4) as well as the linker histone H1 (201). Biochemical tools and mass spectrometry revealed that PARP1 covalently modifies the lysine residues of the core histone tails (K13 of H2A, K30 of H2B, K27 and K37 of H3, and K16 of H4). It is speculated that the accumulation of negatively charged PAR polymers neutralizes the positive charge from the amino acid side chain of the histone core and can act as a repellant to DNA. PARylation of the histone tails may also interfere with other post-translational modifications that rely on the same residue. Therefore, PARylation likely has a global impact on histone dynamics, histone degradation, and histone incorporation (201).

Chromatin relaxation and nucleosome eviction from the DNA facilitates recruitment of chromatin remodelers for the unfolding and spatial expansion of chromatin regions. One of the well-characterized chromatin remodeling enzymes is Amplified in Liver Cancer 1 (ALC1), which becomes active upon release by PARP1's product, PAR (202,203). The ALC1 macrodomain regulates auto-inhibition to ensure that chromatin relaxation is dependent on DNA damage. When DDR is activated, PAR serves as an allosteric activator and triggers ALC1-mediated chromatin

expansion. Furthermore, the chromatin remodeler chromodomain helicase DNA-binding protein 2 (CHD2) is recruited to DSBs in a PARP1-dependent manner (204). PARP1 recruitment of CHD2 permits chromatin expansion and deposition of histone variant H3.3 at sites of DNA damage, which function to promote NHEJ. In addition, the SWI/SNF-related matrix-associated actin-dependent regulator of chromatin subfamily A member 5 (SMARCA5) likely binds to PAR chains on the E3 ubiquitin ligase RNF168 upon DNA damage (205). This PARP-mediated signaling cascade that links SMARCA5 to RNF168 also drives DSB repair by NHEJ.

1.4.7 PARP Inhibitors

PARP inhibition exploits the vulnerabilities in cancers that have a deficiency in homologous recombination (HR). There has been dramatic advancement towards the development of PARP inhibitors for treatment of tumors with BRCA1/2 mutations. Germline BRCA1/2 mutations are linked to inherited breast and ovarian cancers (206). These tumors are selectively targeted due to synthetic lethality. PARP inhibitors lead to persistent SSBs that convert to DSBs upon fork collapse. Thus, tumors that harbor HR defects are particularly vulnerable to PARP inhibitors because they cannot repair these DSBs and eventually undergo cell death.

PARP inhibitors drive cytotoxicity through differential inhibition of PARP catalytic activity and PARP trapping, in which trapped PARP1-DNA complexes interfere with DNA replication and repair (207). Four PARP inhibitors have FDA-approval for treatment in women with an inherited BRCA1/2 mutation who have ovarian cancer – Talazoparib (Talzenna), Olaparib (Lynparza), Rucaparib (Rubraca), and Niraparib (Zejula). The relative trapping capacity of these inhibitors is: Talazoparib > Niraparib > Olaparib > Rucaparib (208–210). This dissertation

specifically uses Olaparib (Kd~1 μM), which was first approved in 2014 and is currently the first-line maintenance therapy in BRCA-mutated advanced ovarian cancer.

1.4.8 PARG Inhibitors

There is currently no PARG inhibitor that is approved by the FDA, which highlights the fact that PARG inhibitors are much more underdeveloped than PARP inhibitors. PARG inhibition is a promising approach to exploit vulnerabilities in cancers with an altered DDR pathway. There is no known close homolog of PARG, which limits the possibility of redundant pathways to arise upon PARG inhibition. PARG inhibitors have been grouped into three major categories: DNA intercalators, tannins, and ADPr analogues. DNA intercalators and tannins were not ideal candidates because they lack specificity and elicit severe toxicity (211). Adenosine diphosphate (hydroxymethyl)pyrrolidinediol (ADP-HPD), an analogue of ADPr, became a more promising PARG inhibitor due to its higher potency and selectivity (IC_{50} = 120 nM) (212,213). In addition, rhodamine-based small molecules were developed and showed selectivity since they did not inhibit ARH3 or PARP1 (214). However, none of these inhibitors were cell-permeable and only biochemical assays were performed with them (214). Although Mono-galloyl glucose derivatives and modified salicylanilides were discovered as an attempt to overcome lack of cell permeability, they also inhibited PARP1 and had lower potency (215,216). Thus, the lack of selective, cell-permeable PARG inhibitors have hampered the study of PARG inhibition in the biological context.

James et al. discovered the first selective, potent PARG inhibitor from a high throughput screen (HTS) of 1.4M compounds in 2016 (217). They were able to detect PAR accumulation in murine cells and a variety of human cancer cells in response to DNA damage and treatment with the PARG inhibitor. Only in the presence of DNA damage did the PARG inhibitor lead to dose-

dependent increase in nuclear PAR chain signal. Upon optimization of the lead compound, they managed to improve the EC_{50} to 0.040 μM. Thus, their compound (PDD00017273) became commercially available on Tocris. PDD00017273, termed PARGi in this dissertation, is used for all experiments (218).

Pharmacological inhibitors of PARP and PARG are used in this thesis dissertation to elucidate the role of PAR metabolism in ALT telomere maintenance. Olaparib is an FDA-approved inhibitor of PARP1. Its mechanism of action is two-fold (219). First, its structure is a nicotinamide moiety that competes with NAD^+, which is the substrate to generate ADP-ribose. Second, Olaparib traps PARP onto the DNA and interferes with DNA repair. Many studies reveal that PARP1 trapping drives the cytotoxicity of Olaparib in HR-deficient cancers (207,220,221). PARP1 trapping leads to elevated collisions at the replication fork, which eventually generates DSBs that cannot be repaired. Thus, there is an important distinction between PARP1 inhibition and PARP1 depletion. On the other hand, there are no PARG inhibitors in the clinic. However, the lab acquired a cell-permeable competitive PARG, as an well as an inactive analog (218). These inhibitors enabled the study of how telomere dynamics shift due to disrupted PAR metabolism.

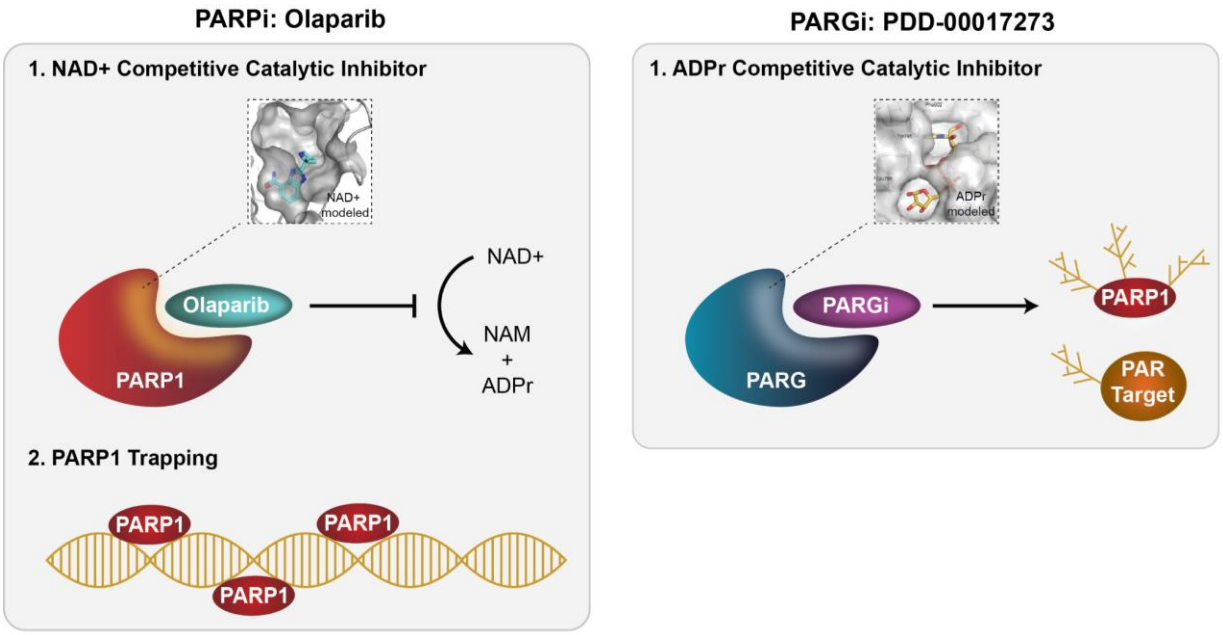

Figure 5. Mechanism of PARP and PARG inhibitors. Olaparib inhibits PARP1 activity by competing with NAD+ as well as traps PARP1 onto the DNA, which interferes with DNA repair. PDD-00017273 (PARGi) is the first cell-permeable competitive inhibitor of PARG. Adapted from Shen et al., ASPET, 2015 (219) (http://jpet.aspetjournals.org/content/353/3/446) and Tucker et al., Plos One, 2012 (222) (https://journals.plos.org/plosone/article?id=10.1371/journal.pone.0050889).

1.5 Major Hypotheses

There are several outstanding questions in the field regarding the exact stimulus that activates ALT, as well how multiple DNA repair pathways are coordinated in ALT telomere maintenance. There are three hypotheses in this thesis dissertation. 1) If the tight regulation of PAR turnover is necessary to control the dynamic state of telomeres in ALT, then pharmacological inhibition of PARP1 and PARG will have consequences on ALT activity. 2) If we identify PARylated telomeric proteins in ALT, then this will give us a snapshot into the apical events that promote ALT activity. 3) If we determine the importance of PAR-regulation in the function of

early ALT regulators, then we can target these vulnerabilities to kill ALT cancers. Specifically, in ALT cancers that predominantly have loss of function mutations in ATRX/DAXX, PAR-mediated regulation of HIRA-mediated chromatin assembly is potentially a compensatory pathway at ALT telomeres. Each hypothesis is discussed in detail below with a summary of the pertinent background information that supports the hypothesis.

1.5.1 PAR metabolism is an important regulator of the recombinogenic potential of telomeres in ALT cancer cells

To date, the implications of deregulated PAR turnover at ALT telomeres have not been described. PARylation likely holds an elevated importance in ALT cancers since they rely on maintaining the balance between DNA damage signaling and genomic stability. One evidently critical outcome of the reconfiguration of chromatin is that telomere integrity is challenged and subject to recurrent replicative stress and stochastic DNA double strand breaks (27,29). It is generally accepted that recurrent cycles of DNA damage provide the trigger and DNA substrates for ALT-associated HDR. However, prolonged DNA damage signaling and genomic instability may lead to anti-proliferative signaling that induces apoptosis or cell cycle arrest. ALT cellular phenotypes, such as APB formation, presence of ECTR DNA, and increased T-SCEs, highlight the recombinogenic potential of ALT telomeres (34,58,63,65). The enrichment and activity of SMARCAL1 and FANCM at ALT telomeres affirms the prevalence of replication stress and how resolution of this replication stress is crucial for ALT telomere maintenance (29,30,104). It was also recently proposed that FANCM unwinds telomeric R-loops formed by TERRA, which normally enhances replicative stress at ALT telomeres (30). Depletion of SMARCAL1 and

FANCM suppresses ALT activity, indicating the importance of reversing and remodeling stalled replication forks to overcome replication impediments (29,30,104).

These lines of evidence suggest that ALT cells have adopted a dynamic interplay between telomeric damage and genomic stability. The role of PARylation is of particular interest in ALT because of its expansive function in regulation of DDR. As PARylation is an apical event in DDR, it can potentially be a driver for fine-tune control of telomeric damage to maintain a specific threshold for telomere elongation and cell viability. PARP inhibition leads to bypass of damaged lesions and fork acceleration, which triggers replication stress (198). Additionally, PARylated PARP1 directly limits the restart capacity of RecQ1 in order to stabilize forks in the regressed state until the damage is repaired (197). This leads to the hypothesis that perturbing PAR metabolism would alter replication stress levels at ALT telomeres and ultimately disrupt ALT telomere maintenance. PARP inhibition likely causes saturation of the DDR machinery, leading to unresolved intermediates that convert to DSBs. These DSBs would prime fragile telomeric regions for recombination. On the other hand, PARG inhibition likely results in unscheduled recruitment, retention and repulsion of DDR factors, which culminate in impaired HDR and ALT activity. The data supporting this hypothesis is presented in chapter 2.

1.5.2 PAR-regulated telomere-associated proteins coordinate the early steps of ALT telomere maintenance

PARylation is a critical sensor that detects damaged lesions generated by endogenous and exogenous toxic stresses. PARylation is involved in an array of DDR pathways, yet only recently were the molecular targets of PARylation characterized. Jungmichel et al. identified a differential impact of various types of genotoxic stress on protein PARylation by using a sensitive proteomics

approach based on high-accuracy quantitative mass spectrometry (223). Analysis of the genotoxic-stress PARylome revealed proteins enriched in DNA repair, DNA replication, chromosome organization, transcription, RNA processing, and RNA splicing. Interestingly, more than 60% of their diverse protein network contained nucleic-acid binding activity. This proteomics approach was adapted in this dissertation to characterize the PARylome at ALT telomeres. The identification of a PAR-regulated protein network at ALT telomeres would be beneficial to pinpoint the key factors that are essential in ALT initiation and maintenance.

The first wave of proteins that respond to telomeric DNA damage may rely on PARylation to aggregate at ALT telomeres. Jungmichel et al. identified that the enrichment of RNA-binding proteins, such as the FET proteins (FUS, EWS1, TAF15), was 2-fold greater than the total number of RNA binding proteins in the entire genome (223). RNA-binding proteins typically harbor low-complexity domains (LCDs) and have been shown to undergo PAR-seeded liquid demixing to orchestrate the earliest cellular response to DNA damage (224). In addition, it is thought that APB assembly is mediated by liquid phase separation, via SUMO-SIM interactions, to coalesce DNA repair factors for ALT telomere synthesis (225). The proteomics approach employed in this dissertation allows for the capture of these early ALT mediators, which would otherwise be transient as they undergo PAR hydrolysis. Chapter 3 of this dissertation provides support for the hypothesis that sustained PAR at telomeres, through PARG inhibition, would dramatically reconfigure the telomeric proteome and abrogate ALT activity.

1.5.3 HIRA adopts elevated importance in ALT due to loss of a functional ATRX-DAXX complex

Chapter 3 of the dissertation identifies the HIRA chaperone complex and all of its components, Histone Regulator A (HIRA), Calcineurin Binding Protein 1 (CABIN1) and Ubinuclein 1 (UBN1), to be PAR-regulated and associate at ALT telomeres. The HIRA complex plays a key role in the repair of UV-C lesions (226,227). HIRA depletion was reported to disrupt transcription recovery after DNA repair. HIRA also collaborates with histone binding protein ASF1a to deposit histone H3.3 onto chromatin in a DNA replication-independent manner (226,227). This is an important feature, since loss of function mutations in ATRX/DAXX, which deposits H3.3 during replication, are pervasive in ALT cancers. In fact, re-expressing ATRX in an ALT-cell line reverses the ALT phenotype (228). ATRX mitigates aberrant secondary structures, such as G-quadruplexes, that arise during telomeric replication. ATRX can also sequester MRN, which prevents HR from being initiated at telomeres. Thus, the lack of ATRX activity in ALT cancers leads to unresolved replicative impediments and enhanced HR.

It is plausible that due to lack of ATRX activity, HIRA is potentially the sole functional H3.3 histone chaperone in many ALT+ cancers. HIRA's elevated importance in ALT is supported by data from Project Achilles, which identified ALT cell lines, such as U2OS, SAOS2, and CAL72, to have greater gene dependency on HIRA. With this line of reasoning, it is hypothesized that HIRA does not fully compensate for ATRX's ability to alleviate replication stress at ALT telomeres. These secondary structures become unresolved or directly cleaved by MRN, which results in fork collapse that generates DSBs. This ultimately triggers HDR and potentiates the ALT phenotype. PARylation of HIRA is the early signal that recruits it to sites of telomeric damage to deposit H3.3 for chromatin remodeling during DNA synthesis in G2-BIR. Thus, HIRA enables the

basal level of stochastic DNA damage and replication stress that promotes ALT. Upon PARG inhibition, HIRA is retained at telomeres, which abrogates ALT telomere maintenance by impairing chromatin remodeling and uncoupling it from efficient repair by G2-BIR. This is the focus of chapter 4 in this dissertation.

2.0 Disrupted PAR metabolism alters recombinogenic activity at ALT telomeres

2.1 Introduction

There are several lines of evidence that strongly supports ALT as an HR-mediated DNA synthesis mechanism that arises from inherent replication stress and stochastic DNA damage at ALT telomeres. Double-stranded breaks (DSBs) at internal telomeric regions and telomeric replication forks act as substrates for homology-directed repair (HDR) in ALT (195). In S-phase, telomeres pose a challenge for the replication machinery, leading to replication fork stalling. The stalled replication fork can undergo fork reversal and restart by the FANCM-BTR complex (104). Replication stress is relieved at telomeres and ALT activity is restrained. However, unresolved replication stress leads to fork collapse, which provides direct DSB substrates for ALT-mediated telomere synthesis and recombination by RAD51-dependent mechanisms (96,98). The SMX complex (SLX1-SLX4, MUS81-EME1, and XPF-ERCC1) and BTR complex (BLM-TOP3A-RMI) maintains the balance between telomeric recombination and extension (81). The SMX complex promotes resolution of telomeric recombination intermediates in the absence of telomere extension. This is counteracted by the BTR complex, which initiates telomere dissolution for long-tract ALT-mediated telomere synthesis. Intra-telomeric strand invasion and persistence of collapsed forks in G2 activates PCNA-RFC-POLD3-mediated DNA synthesis. However, SLX4IP can antagonize the BTR complex to favor SMX-dependent resolution (112).

Although the molecular events involved in ALT are well-studied, the stimulus of HDR pathway choice and the regulation of such events to maintain the equilibrium between DNA damage and cell viability still remains elusive. PARylation is a promising candidate because it is

an apical molecular response to DNA breaks and replicative stress. Published data in the O'Sullivan lab characterized the telomeric proteome in the ALT+ U2OS cell line using proximity-dependent biotinylation (BioID) (87). This work revealed a greater enrichment of PARP1 at ALT+ telomeres compared to TEL+ telomeres. The exposed termini of chromosomes represent natural triggers of PARP activity (229). Indeed, PARPs including PARP1, PARP2 and Tankyrase, reside at telomeres in human cell lines (230). TRF1 and TRF2 are core constituents of the Shelterin complex that shield telomeres from DNA damage sensors, including any unwarranted PARP activity (231). However, upon telomere dysfunction through loss or genetic disruption of Shelterin and the canonical Ligase IV dependent non-homologous end joining mechanism (cNHEJ), PARP1-XRCC1-Ligase III can promote telomere fusions by alternative non-homologous end joining (alt-NHEJ) (232). In contrast, internal telomeric DSBs appear to be preferentially repaired by similar PARP1-dependent alt-NHEJ, which resembles HDR (195). Recent findings have identified a role for PARylation in response to replication fork destabilization when the Regulator of Telomere Elongation (RTEL) helicase is non-functional (233). Thus, PARylation or the synthesis of PAR by PARPs is a crucial factor in the management of damaged telomeres.

The breakdown of PAR chains occurs via enzymatic hydrolysis by the essential enzyme PARG (174). PARG-mediated hydrolysis of PAR salvages NAD+ that is recycled and transferred to mitochondria to eventually generate essential metabolites, including adenosine triphosphate (ATP). Unhydrolyzed PAR sequesters cellular NAD^+ that cannot be replenished without PARG, leading to catastrophic energy failure (180). Another consequence of PARG depletion is that failure to hydrolyze PAR chains compromises DNA repair, leading to the accumulation of unrepaired DNA lesions and DSBs (182,234). In fact, PARG is recruited to replication forks through PCNA where it hydrolyzes PAR that accumulates at unligated Okazaki fragments (179).

Therefore, PARG is essential to sustain cellular energy supplies and ensure the faithful stepwise transitions during DNA repair and replication.

Here, we show that pharmacological interference of PAR metabolism disrupts the HDR mechanisms that mediate ALT. PARP and PARG inhibition have opposing effects on ALT activity. While PARP inhibition (PARPi) exacerbates ALT features, such as APBs, T-SCEs, and C-Circles, PARG inhibition (PARGi) diminishes these ALT phenotypes. Intriguingly, prolonged PARG treatment leads to dramatic telomere shortening in ALT+ cells. To further understand how alterations in PAR turnover affects ALT activity, we used an established system where an inducible U2OS cell line expresses the FokI endonuclease fused to TRF1. This introduces DSBs specifically at telomeres, which serve as substrates for HDR mechanisms in ALT. PARG inhibition leads to decrease in telomere clustering, mobility, and replication, which indicates that both HR and G2-BIR are impaired as a consequence of PAR accumulation. Together, our work establishes the importance of PAR catabolism for mediating efficient HDR in ALT.

2.2 Results

2.2.1 Effectiveness of the PARP inhibitor (Olaparib) and PARG inhibitor (PDD00017273)

The availability of highly specific and effective compounds (e.g. Olaparib) enabled the phenotypic assessment of PARP inhibition in a wide range of cellular contexts, including the synthetic lethal elimination of BRCA1/2 deficient breast and ovarian cancer cells (191,192). Following the resolution of the crystal structure of PARG, specific small molecules that block the active site of PARG have been developed (214). We verified the effectiveness of one of these,

PDD00017273 (PARGi), by monitoring the accumulation of PAR in hydroxyurea treated U2OS cells by western blot using a specific anti-PAR (10H) antibody (Figure 6A). PARylation is a reversible, transient modification, which means that the suppression of PARG is necessary to prevent PAR degradation. In addition, other studies have also used exposure to DNA-damaging agents to enhance DNA damage-dependent PARylation (166). Thus, PAR accumulation is only observed in cells treated with the combination of HU and PARGi, which confirms the effectiveness of the inhibitor. We also examined PARGi's specificity by treating cells with an inactive analog ($PARGi^{Me}$), which contains an additional methyl group that blocks the inhibitor's catalytic activity. Indeed, damaged cells treated with $PARGi^{Me}$ did not retain PAR. In addition, the same pattern was seen in cells where PARP1 and PARG were depleted using shRNA knockdown (Figure 6B). The effectiveness of PARPi was confirmed through the abolishment of PAR accumulation in cells with PARG shrRNA knockdown. After proven effectiveness and specificity, we decided to utilize these inhibitors for our subsequent studies.

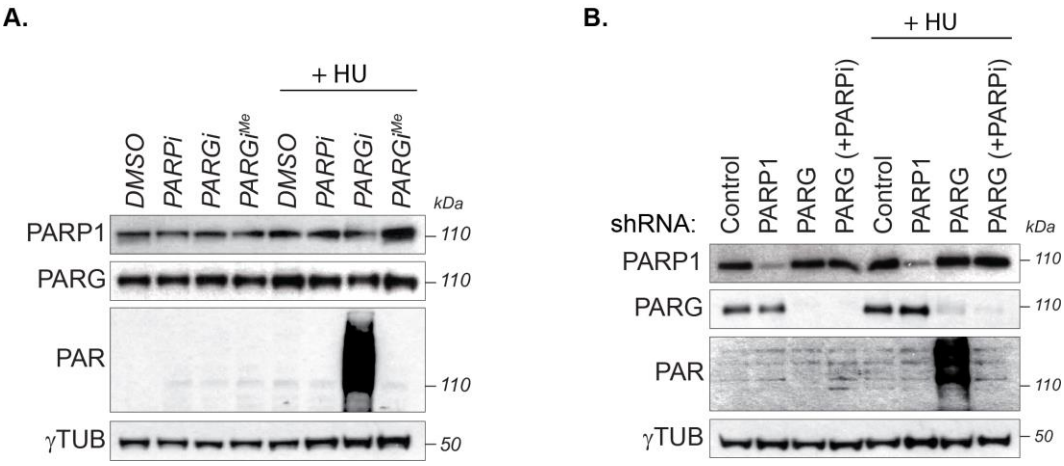

Figure 6. Western blot analysis of PAR induction. A) Western blot analysis of PARP1, PARG, and PAR expression in U2OS cells treated with DMSO, PARPi, PARGi or inactive PARGi^{Me} (all 5μM). Cells were untreated or treated with 2mM hydroxyurea (HU) for 4hrs to control for PARylation induction. B) Western blot validation of PARP1 and PARG knockdown and PAR accumulation in U2OS cells expressing non-targeting scrambled shControl, shPARP1 or shPARG. Cells were untreated or treated with hydroxyurea (HU) to control for PAR induction.

2.2.2 PARP and PARG inhibition have opposing effects on ALT activity

We next assessed the effect of PARP and PARG inhibition on telomeres that are maintained by the ALT pathway. ALT-positive (ALT+) cancer cell lines are typified by the presence of a low but consistent percentage of cells containing telomeres that localize to PML bodies forming unique sub-nuclear structures known as ALT-associated PML bodies (APBs). These are thought to represent centers of telomeric HR. Quantification of their numbers by immunofluorescence combined with fluorescence *in situ* hybridization (IF-FISH) is routinely used as a first line measurement of ALT activity. We found that a 72hr treatment using standard 5μM doses of Olaparib (PARPi) or PARGi elicited the opposite effect on APB levels in several independent ALT cell lines including U2OS and Saos2 (Figure 7A and 7B). Whereas PARPi

increased their frequency, PARGi significantly decreased the percentage of APB positive (APB+) U2OS and Saos2 cells. Interestingly, we found that PARP inhibition led to *de novo* formation of APBs in a HeLa LT cell line that maintains its hyper-extended telomere length through telomerase mediated TTAGGG repeat addition (Figure 7B). This is consistent with previous findings that PARP inhibition can provoke ALT-like features at telomeres. To control for possible off-target effects, we treated cells with an inactive PARGi analog, PDD00031704, ($PARGi^{-Me}$) which cannot engage PARGs active site (Figure 7B). Treatment with this small molecule had no effect on APB levels. Experiments using lower doses of 100nM-1μM of PARGi for prolonged periods (Figure 7C), as well as shRNA depletion of PARP1 and PARG in U2OS, Saos2 and HeLa LT (Figure 7D and Figure 42), produced results similar to inhibitor treatments. Notably, the reduction of APBs was reversed to normal levels when PARPi was added to PARG depleted U2OS cells. These data showed that the observed responses were truly due to diminished PARP1 and PARG activity.

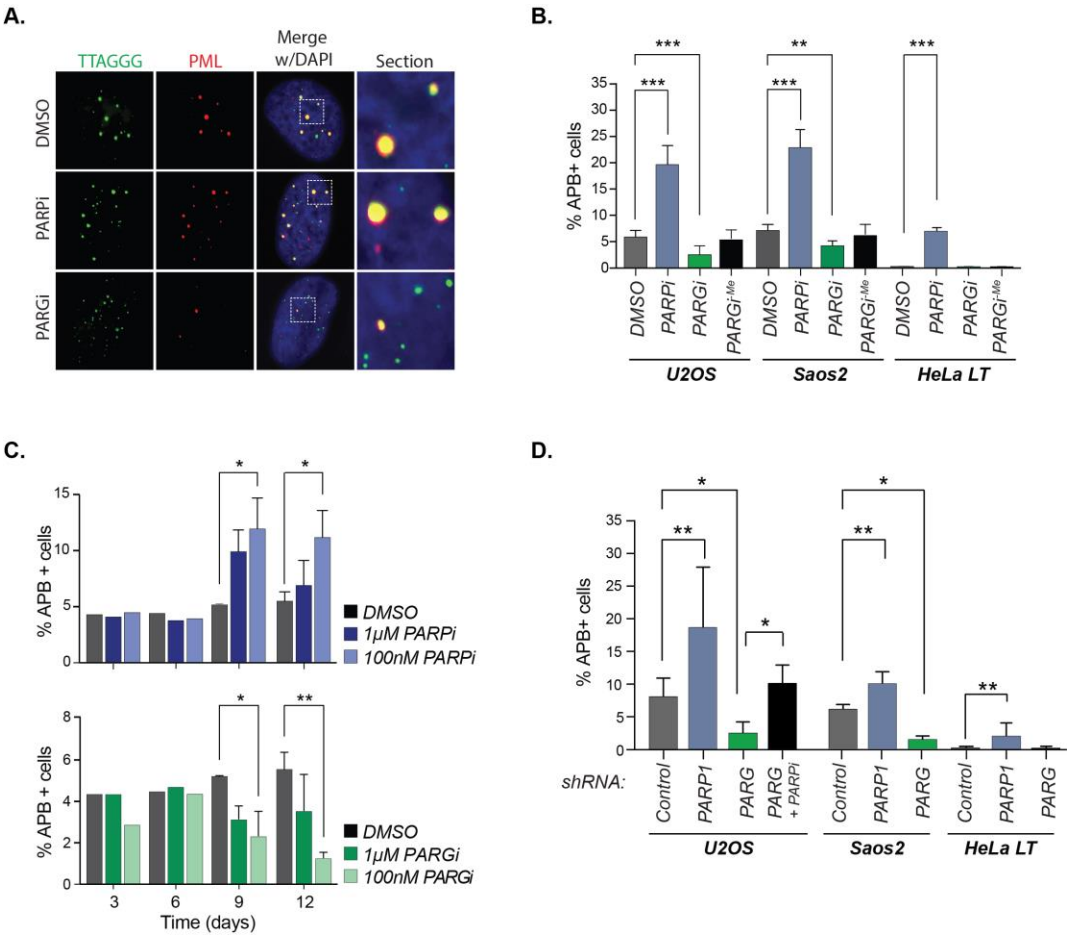

Figure 7. PARP and PARG inhibition have opposing effects on APBs. A) Representative images of APBs (PML-TTAGGG colocalization) in U2OS cells treated with indicated inhibitors. B) Quantification of APBs (%) in U2OS, Saos2, and Hela LT after the indicated treatments. C) APBs (%) in U2OS cells treated with lower doses of PARPi or PARGi (100nM and 1mM) over 3, 6, 9 and 12 days. D) Quantification of APBs (% positive cells) in U2OS, Saos2 and HeLa LT cells expressing shControl, shPARP1 or shPARG. All graphed data in the figure are mean ± SEM, n=1200 cells. Statistical significance was determined using one-way ANOVA. *P≤ 0.05, **P≤ 0.001, ***P≤ 0.001, ****P< 0.001.

We next assessed whether PARP and PARG inhibition impacted the frequency of telomere sister chromatid exchanges (T-SCEs), that are commonly studied as a surrogate of telomere recombination, using the chromosome orientation FISH (COFISH) assay. Metaphase spread chromosomes were prepared from DMSO, PARPi and PARGi-treated U2OS, Saos2 and HeLa LT

cells (Figure 8A). This revealed that PARPi significantly increased T-SCEs in the ALT+ U2OS and Saos2 cells, but also in HeLa LT cells where this recombination associated activity is normally restrained. As seen previously with the inhibitor data, the same trend was evident in cells where PARP1 or PARG were depleted by shRNA knockdown (Figure 8B).

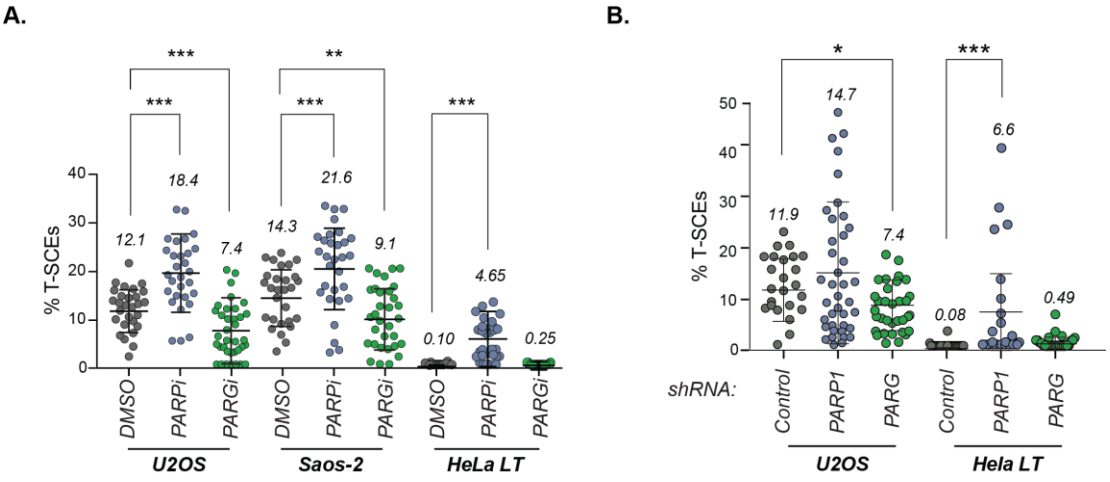

Figure 8. PARP and PARG impact frequency of T-SCEs. A) Telomere sister chromatid exchanges (T-SCEs) in U2OS, 12 days after PARPi (1μM) or PARGi (1μM) treatment. B) Quantification of T-SCEs (% per metaphase) in U2OS, Saos2 and HeLa LT cells expressing shControl, shPARP1 or shPARG. All graphed data in the figure are mean ± SEM, n=45 metaphases. Statistical significance was determined using one-way ANOVA. *P≤ 0.05, **P≤ 0.001, ***P≤ 0.001, ****P< 0.001.

The robust opposing effects observed in inhibitor-treated cells raised the question of whether telomere length might be altered in ALT+ cells that are chronically deprived of PARP or PARG activity. We subjected ALT+ U2OS and TEL+ HeLa LT cells to prolonged treatments with lower doses of PARPi (1 μM) and PARGi (1 μM) for ~30PDs and assessed telomere length by pulsed field gel electrophoresis (PFGE) (Figure 9). This showed that PARPi in U2OS cells greatly reduced the overall signal of telomeric DNA while not overtly affecting the mean telomere length. In contrast, PARG inhibition profoundly reduced telomere length in U2OS cells and another

independent ALT+ cell line, VA13, with lengths now ranging from 2kb-25kb and a mean length of ~10kb (Figure 9 and Figure 43). Parallel treatment of HeLa LT with PARPi and PARGi did not change telomere length (Figure 9). We also found that PARPi inhibition significantly enhanced the levels of extra-chromosomal C-circles in U2OS cells and provoked their *de novo* formation in HeLa LT cells. In contrast, PARG inhibition had no effect on C-circle levels in ALT cells. These results suggest that the changes in telomere length were due to telomere shortening and not the accumulation of extra-chromosomal telomeric DNA species. Overall, this comprehensive analysis demonstrates that the equilibrium between the anabolism and catabolism of PAR is a determinant of the recombinogenic potential of telomeres that sustains telomere length in ALT cancer cells.

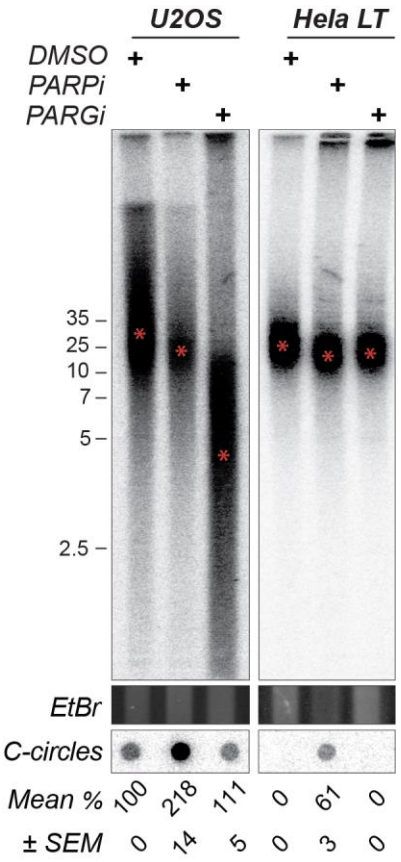

Figure 9. PARGi leads to telomere shortening in ALT+ cells. PFGE of DMSO, PARPi (1μM) or PARGi (1μM) treated U2OS cells. The mean telomere length (kb) was calculated using TeloTool and is indicated by the red dot.

2.2.3 ALT cancer cells exhibit modest sensitivity to PARG inhibition

To assess whether ALT cells display greater susceptibility to PARP and PARG inhibition, we conducted clonogenic survival assays of ALT+ (U2OS, Saos2, LM216J) and TEL+ (HOS, SJSA1, LM216T) cells that were exposed to the same doses (1 μM) that elicited alterations in ALT recombination and telomere length maintenance (Figure 10). It should be noted that LM216J and LM216T cells are isogenic cell lines Whereas the ALT+ and TEL+ cell lines were all sensitive to d PARP inhibition, ALT+ cell lines were indeed more sensitive to PARGi. However, the differential sensitivity of ALT+ cells compared to TEL+ cells was modest for PARGi treatment.

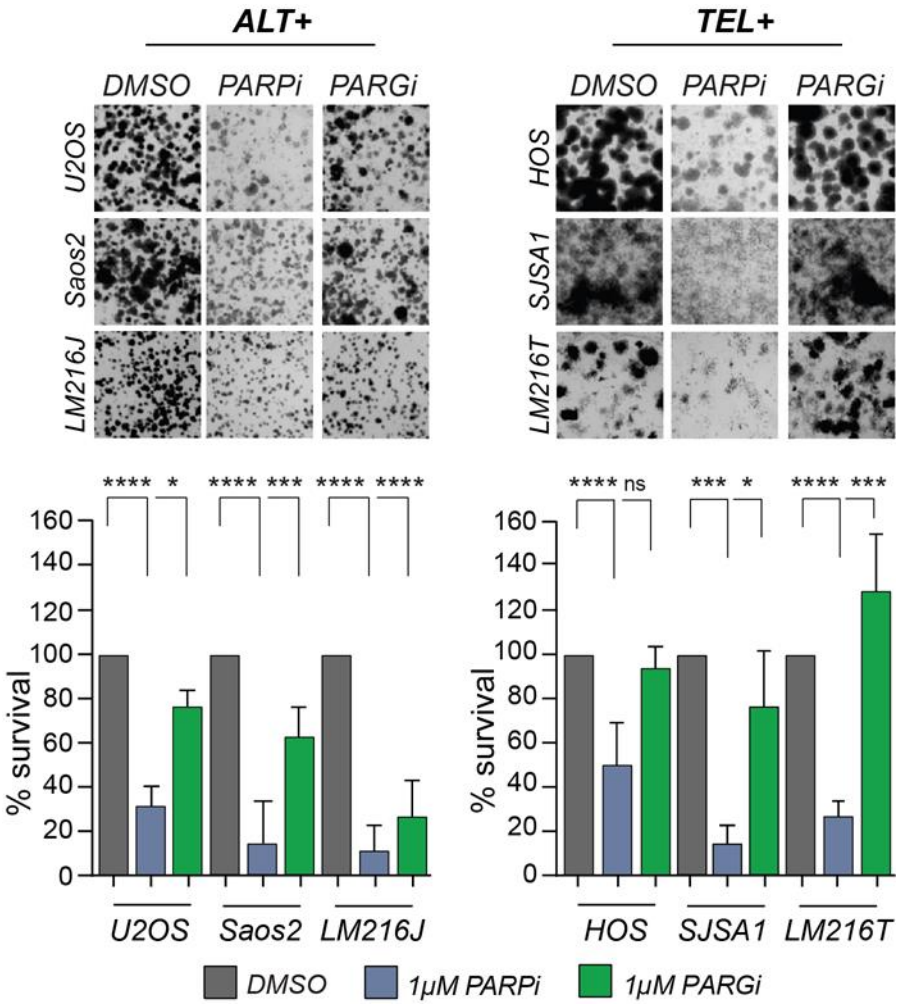

Figure 10. ALT+ cells display modest sensitivity to PARGi. Representative images and quantification from clonogenic survival assays with ALT+ and TEL+ cells treated with DMSO, PARPi (1μM) or PARGi (1μM) for 7 days. All graphed data in the figure are mean ± SEM, n=3. Statistical significance was determined using student t-test. *P≤ 0.05, **P≤ 0.001, ***P≤ 0.001, ****P< 0.001.

2.2.4 PAR metabolism is required to sustain the key steps of the ALT mechanism

To understand how disrupting PAR metabolism affects ALT telomere maintenance, we took advantage of U2OS cells that express the Doxycycline/4-OHT/Shield inducible (WT) or

catalytically inactive (DA) c-terminal of FokI endonuclease fused to TRF1. FokI is a type IIS restriction endonuclease that recognizes the non-palindromic recognition site (5'GGATG) and cleaves 9 to 13 nucleotides downstream of it (235). In solution, FokI exists as a monomer with two domains: N-terminal DNA-binding domain that associates with the entire recognition site and C-terminal catalytic domain with one active site (236). FokI must dimerize to cleave both strands of DNA or it can nick DNA and block replication fork progression (237). Our TRF1-FokI system induces the DSB cleavage of telomeric DNA to trigger HR and G2-BIR (Figure 11). This results in larger telomeric foci that can be visualized and quantified by immunofluorescence (IF). This accentuates the presence of these ALT-associated processes that are otherwise relatively difficult to study in unperturbed ALT cells.

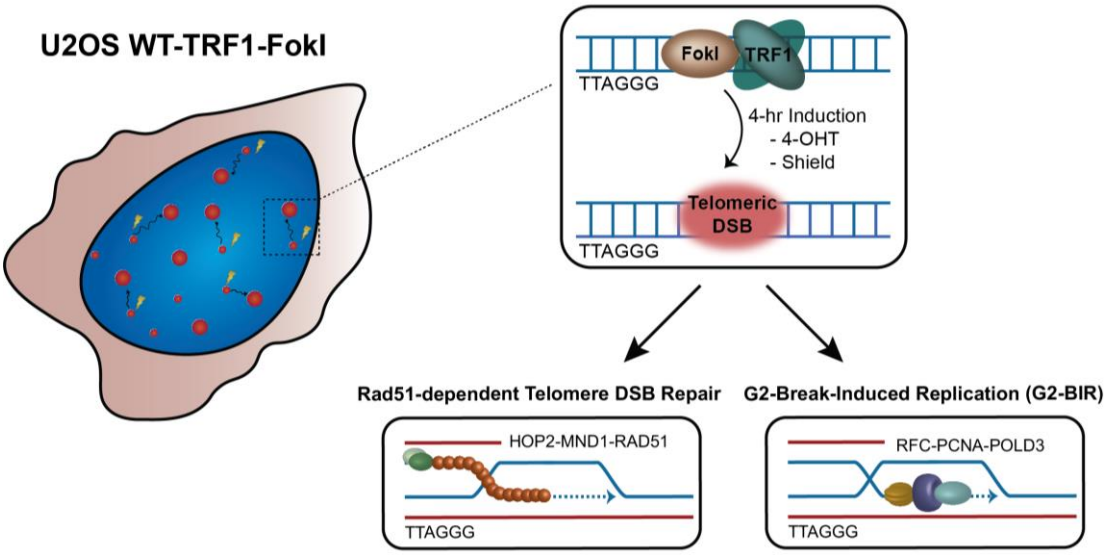

Figure 11. TRF1-FokI schematic. Targeted introduction of DNA nicks and DSBs at telomeres through FokI endonuclease fused to TRF1 activate HDR responses. Long-range homology search is performed through a RAD51-dependent mechanism that involves the RAD51-HOP2-MND1 complex. DNA synthesis in ALT cancer cells is RAD51-independent and largely restricted to G2 and M-phases. In G2-BIR, RAD52-PCNA-RFC-mediated loading of Polδ is essential for conservative synthesis of both leading and lagging DNA strand.

We first asked whether TRF1-FokI-induced DSBs provoked the accumulation of PAR directly at telomeres (Figure 12). Immediately following induction of wildtype (WT) or inactive (DA) TRF1-FokI, DMSO, PARPi, PARGi, or the inactive PARGi^{-Me} analog, was added to induced U2OS cell cultures. PAR accumulation was only detected by western blot using the 10H anti-PAR antibody in extracts from WT TRF1-FokI cells that were treated with PARGi (Figure 12). As previously shown, U2OS cells expressing WT TRF1-FokI exhibited elevated levels of Histone H2AX Serine 139 (γH2AX) and CHK2-Threonine 68 (CHK2-T68) phosphorylation. Acute treatment with PARPi enhanced these markers of DNA damage in WT TRF1-FokI cells and was sufficient to generate DNA damage response signaling in DA TRF1-FokI. In contrast, acute

PARGi treatment did not alter the initial or downstream TRF1-FokI-induced DNA damage response signaling.

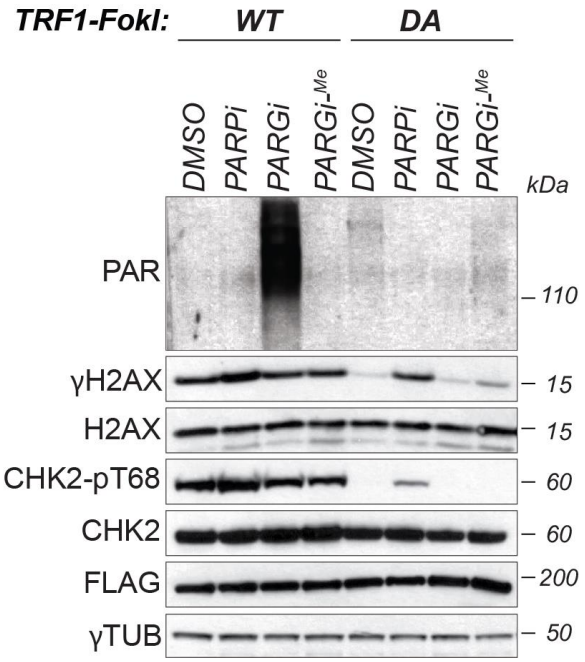

Figure 12. WT TRF1-FokI induces telomeric DNA damage. Comparison of PAR levels and DSB responses in WT TRF1-FokI and DA TRF1-FokI cells with DMSO, PARPi (5μM) or PARGi (5μM) TRF1-FokI expression is similar across all samples, as indicated by FLAG western.

IF revealed a focal enrichment of PAR specifically at telomeres only in WT TRF1-FokI cells treated with PARGi, and not DA TRF1-FokI cells, indicative of the DNA damage dependency of this response (Figure 13A-B). TRF1-FokI-induced DSBs are mostly processed by HDR-based mechanisms, though perhaps not entirely, with alt-NHEJ also fulfilling a role at repair of internal telomeric DSBs (195). During HDR, loading of the HR presynaptic filaments with RAD51 stimulates the search for homologous DNA sequences with which to pair and recombine. In the context of TRF1-FokI, this can be optically visualized as the clustering of telomeres into large foci (96,98). This has the effect of increasing the size and reducing the overall number of telomeric or TRF1-FokI foci as detectable by IF (Figure 13C). This dynamic was readily observed

following quantification of telomere size and number in DMSO treated WT TRF1-FokI-induced cells Although PARPi did not enhance clustering events in WT TRF1-FokI cells, such events were observed in DA TRF1-FokI cells. This is consistent with earlier observations that PARPi is sufficient to induce ALT like phenotypes in non-ALT cells. Strikingly, when PARGi was added to WT TRF1-FokI cells, the number and size of individual telomeres remained close to levels observed in DA TRF1-FokI cells. The same outcome was observed in PARGi-treated VA13 ALT+ cells, but not in TEL+ HeLa LT cells, reflecting a specific perturbation of ALT-associated telomere dynamics when PAR turnover is blocked (Figure 44).

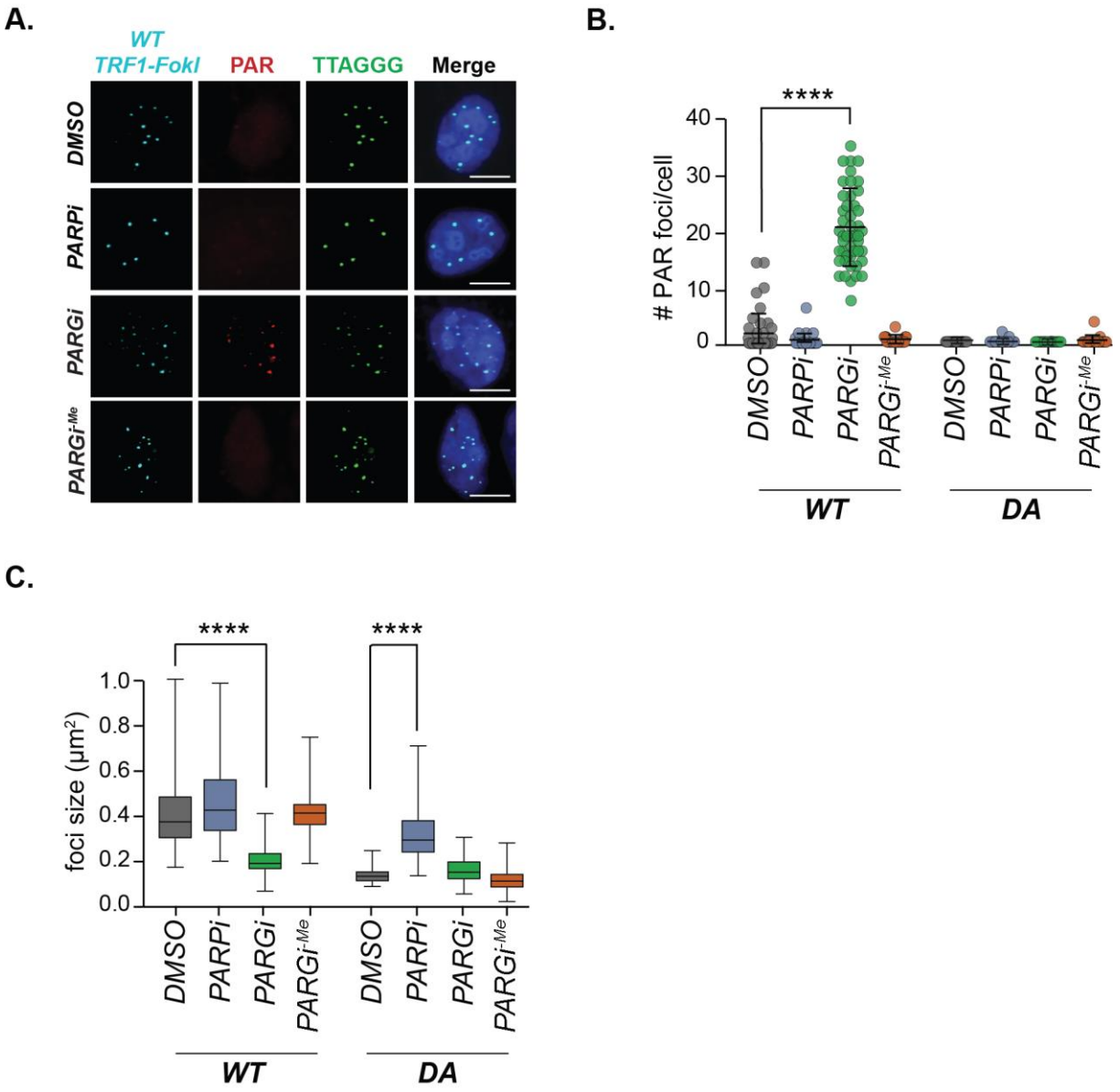

Figure 13. PARGi abolishes TRF1-FokI -telomere clustering. A) Representative IF-FISH images showing PAR localization at telomeric foci in WT TRF1-FokI cells. B) Quantification of PAR foci colocalization with TRF1-FokI telomeric foci. C) TRF1-FokI telomeric foci number and size in WT and DA cells for each experimental condition. All graphed data in the figure are mean ± SEM, n=75 cells. All graphed data in the figure are mean ± SEM, n=45 metaphases. Statistical significance was determined using one-way ANOVA. *P≤ 0.05, **P≤ 0.001, ***P≤ 0.001, ****P< 0.001. All scale bars, 5µm.

This PAR accumulation was abolished upon co-treatment with both PARGi and PARPi, but not with XAV939, an inhibitor of the specialized PARP, Tankyrase (Figure 14A). We also determined that PARG localizes directly to WT TRF1-FokI DSBs. This was dependent on its PCNA interaction peptides (PIPs) and PARP1 activity (Figure 14B). Therefore, PARP1-mediated PARylation, and its hydrolysis by PARG, represent direct mediators of the response to DSB formation at telomeres.

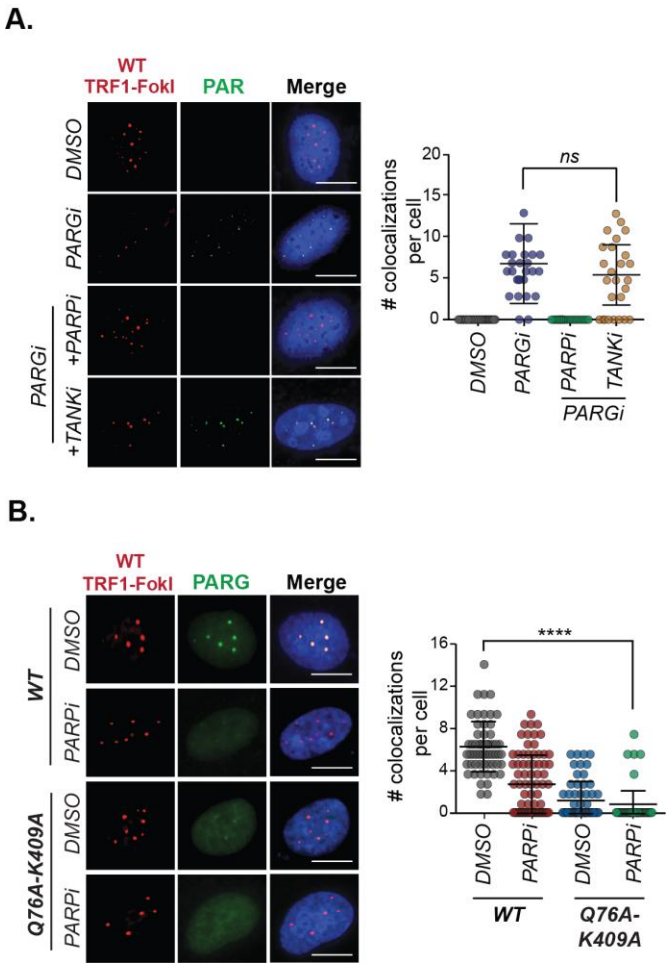

Figure 14. PARylation is an early and direct mediator of TRF1-FokI DSB formation. A) Representative IF images and graph displaying PAR localization to TRF1-FokI telomeres in response to PARPi (5μM) and TANKi (XAV939) (10μM). B) Representative IF images and graph showing PARG localization in WT TRF1-FokI cells transfected with GFP-PARG-FL and GFP-PARG Q76A-K409A. All graphed data in the figure are mean ± SEM, n=25 cells. All graphed data in the figure are mean ± SEM, n= 50 cells. Statistical significance was determined using one-way ANOVA. *P≤ 0.05, **P≤ 0.001, ***P≤ 0.001, ****P< 0.001.

We also tested whether PARylation affects telomere mobility independently of TRF1-FokI-induced DSBs, in typical ALT+ cells. Optical visualization and tracking of telomeres can be achieved using fluorescently tagged TRF1 fusion protein. The mobility of individual or groups of eGFP-TRF1 molecules, representing telomeres, is empirically calculated as a function of mean

squared displacement (MSD). Undamaged telomeres in normal and TEL+ cancer cells exhibit patterns of nuclear mobility that are consistent with random diffusion. In contrast, ALT+ telomeres display trajectories that are consistent with directed motion as part of homology search and pairing of telomeres during HR (96). Using U2OS cells that stably express eGFP-tagged TRF1 (eGFP-TRF1), we captured the three-dimensional telomere motion in x, y and z planes at 2-minute intervals for 2hrs following acute treatment with DMSO, PARPi and PARGi (Figure 15). Uninterrupted telomere motion was tracked, analyzed and quantified as a function of MSD. While PARP inhibition significantly increased the cumulative MSD from ~8μm/hr to ~12.45 μm/hr, PARG inhibited U2OS cells were clearly constrained, having an MSD of ~6.9 μm/hr. Cumulatively, these data independently show that PARylation influences the long-range, directional motion of telomere. Ultimately, this impacts telomere contacts that are an intrinsic and essential aspect of telomeric HR.

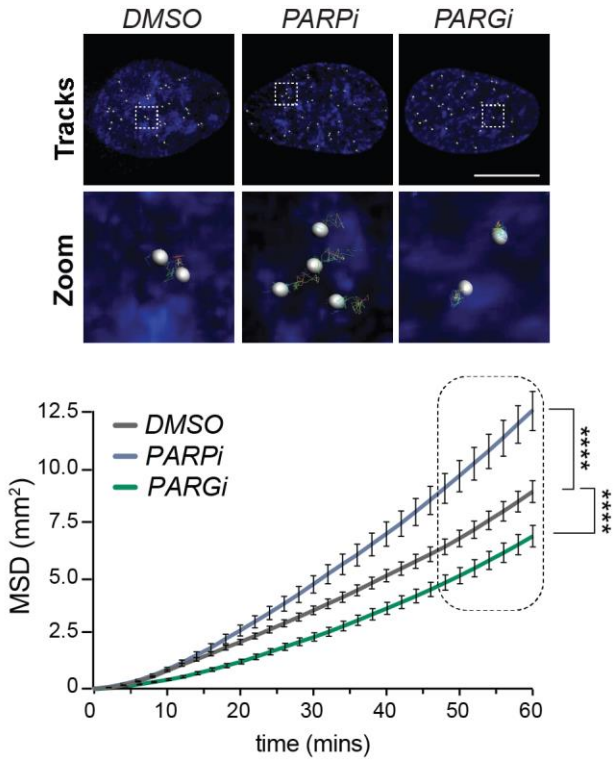

Figure 15. PARylation perturbs long-range telomere movement in ALT cells. Representative movie stills of tracked telomere (eGFP-TRF1) movement in U2OS cells treated with DMSO, PARPi (5μM) or PARGi (5μM). Graph displays the cumulative Mean Squared Displacement (MSD) of telomeres imaged and analyzed, n=100 telomeres. Statistical significance was determined using student t-test. *P≤ 0.05, **P≤ 0.001, ***P≤ 0.001, ****P< 0.001.

2.2.5 PARG inhibition impairs G2-Break Induced Replication (G2-BIR)

During G2-BIR, nascent DNA synthesized at the break can be labeled with BrdU, immunoprecipitated with anti-BrdU antibodies, and then quantified by telomere southern blot. The addition of PARPi to WT TRF1-FokI-induced cells did not enhance overall nascent telomere synthesis (Figure 16A). Notably, cells treated with PARGi showed a 50% decrease in BrdU incorporation, indicating a perturbation in break-induced telomere DNA synthesis. One possibility is that the localization of key mediators of DNA synthesis to telomeres is altered. In agreement

with this hypothesis, the accumulation of essential G2-BIR replisome constituents, PCNA and POLD3, following TRF1-FokI induction was diminished when PARGi was present (Figure 16B).

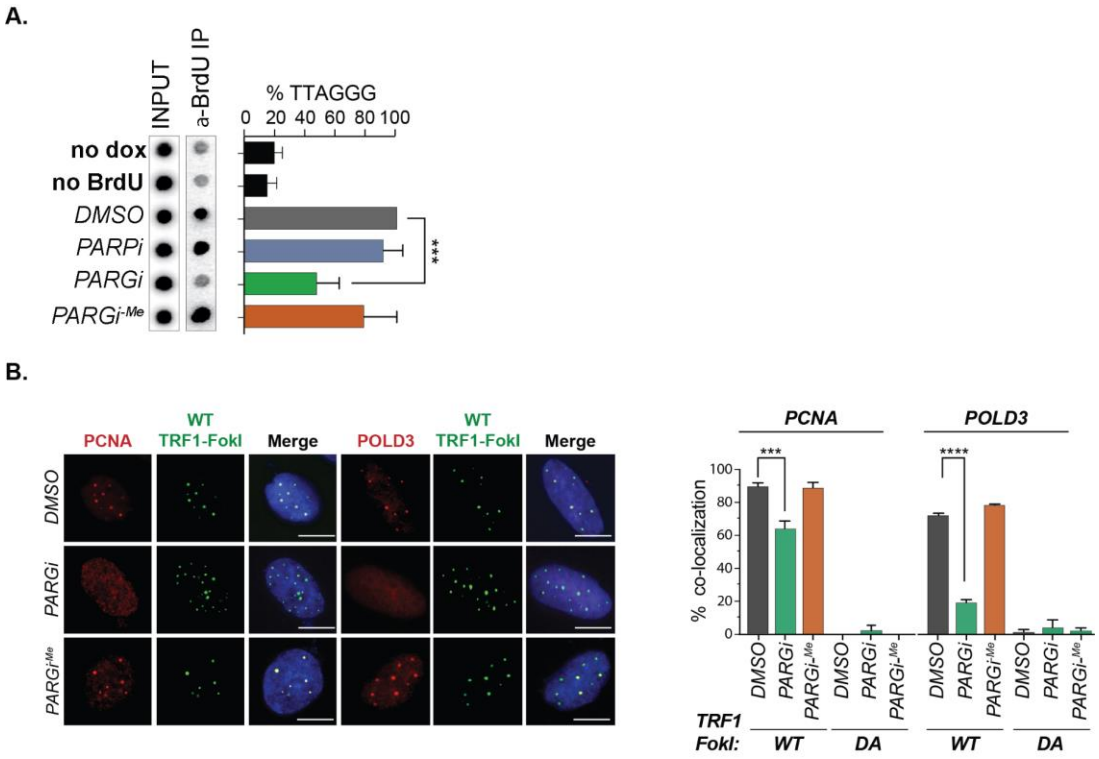

Figure 16. PARGi impairs G2-BIR. A) TRF1-FokI-mediated break-induced synthesis assay to measure nascent DNA synthesis during G2-phase. B) Representative images and graph displaying PCNA or POLD3 localization at WT TRF1-FokI and DA TRF1-FokI telomeres. All graphed data in the figure are mean ± SEM. A) n=3 and B) n=75 cells. Statistical significance was determined using one-way ANOVA. *P≤ 0.05, **P≤ 0.001, ***P≤ 0.001, ****P< 0.001.

We next employed a modified DNA combing technique in combination with telomere FISH to investigate individual telomeric replication events following deregulation of PAR metabolism. After 3hrs of induction, WT TRF1-FokI U2OS cells were sequentially pulsed for 20 minutes with nucleotide analogs, Chlorodeoxyuridine (CldU) and Iododeoxyuridine (IdU). PARP and PARG inhibitors were added at induction. DNA fibers that contained CldU, IdU and telomeric FISH signals were then imaged and analyzed (Figure 17A). In agreement with previous studies, in

control DMSO-treated cells, we observed nascent telomere DNA fibers averaging 9.224 μm in length, from which we calculated a mean DNA synthesis rate of 0.9kb per minute (Figure 17B). Fibers from PARPi and PARGi-treated cells averaged 11.13μm and 7.228μm, respectively. We then calculated the average rates of DNA synthesis of 1.1kb/min and 0.7kb/min, respectively. The former is consistent with evidence that PARP inhibition accelerates replisome velocity (198). We then plotted the individual IdU and CldU tract lengths to determine progression of DNA synthesis between pulses. Whereas IdU-CldU tracts from DMSO treated cells were approximately equal, having a high degree of linearity (Pearson coefficient $r^2=0.9524$), those from both PARPi and PARGi-treated cells differed significantly – irrespective of the large differences in track length (Figure 17C). This reflects the perturbation of replication fork restart and elongation upon deregulation of PAR metabolism.

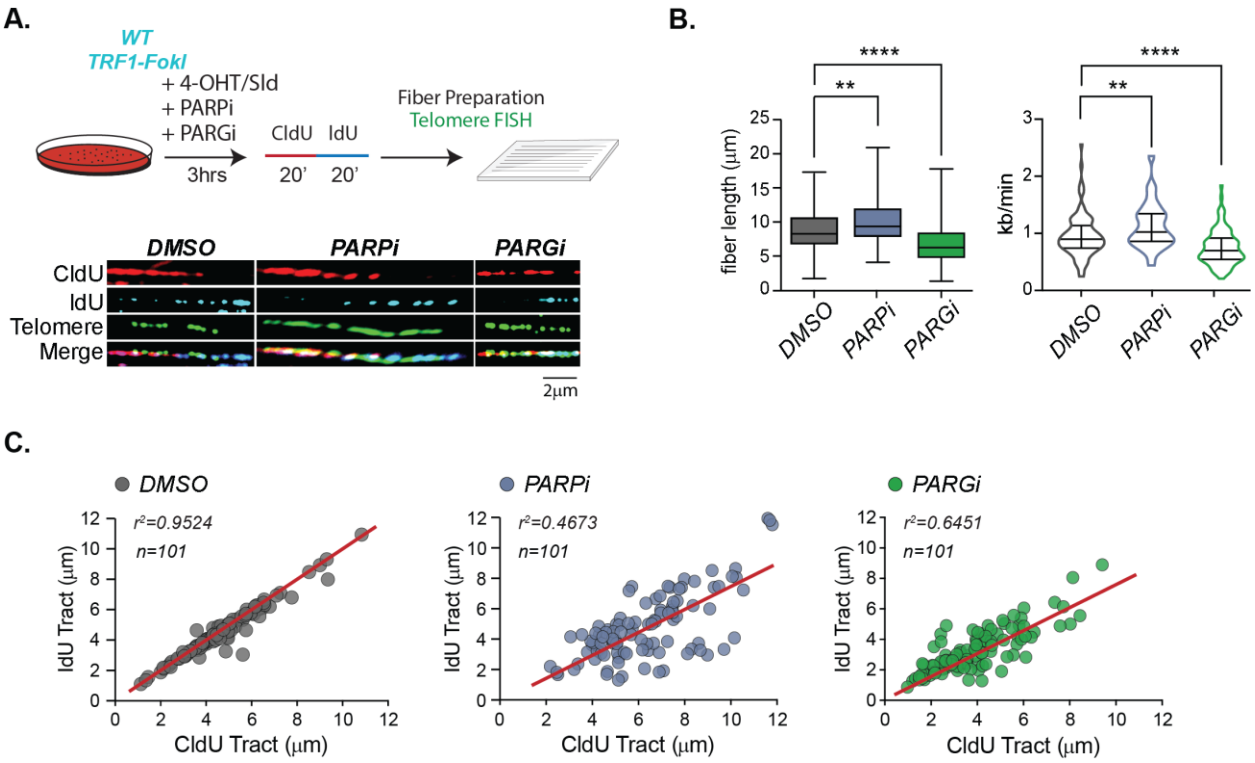

Figure 17. Disrupted PAR metabolism interferes with telomeric replication. A) Schematic of DNA combing in WT TRF1-FokI cells treated with DMSO, PARPi or PARGi, as above. Representative images of telomeres (green) with CldU (red) and IdU (blue) for indicated conditions. B) Quantification of telomeric fiber length of combined pulses. Left: Length of telomere fibers was measured by NIS-element software. Right: Violin plot analysis of fork velocity calculated based on the conversion of 0.26 micron to 1kb DNA over the combined 40 min CldU/IdU pulse. C) Graph of telomeric tract length distribution in each experimental condition by plotting CldU telomeric tract length with IdU telomeric tract length for 100 telomeric fibers. Statistical significance was determined using one-way ANOVA. *P≤ 0.05, **P≤ 0.001, ***P≤ 0.001, ****P< 0.001.

Overall, these results demonstrate that PARG inhibition prevents the localization of constituents of the G2-BIR replisome to ALT telomeres, providing a rationale for the observed deficiency in telomeric DNA synthesis. Overall, the data suggest that the fine-tuned control of PAR catabolism by PARG maintains efficient HDR at ALT telomeres. This implicates PAR-dependent processes in regulating telomere recombination and G2-BIR. This also indicates a

biphasic activation of PARP and PARG at early stages of these processes in S and G2 cell cycle phases, with the inhibition of PARG presumably having major ramifications on the progression of HDR.

2.3 Discussion

In this chapter, we report that the equilibrium of PAR synthesis by PARP and hydrolysis by PARG are critical aspects of telomere maintenance by the ALT pathway. Whereas inhibition of PARP1 stimulates telomere recombination, we found that inhibition of PARG and subsequent retention of PAR perturbs HDR mechanisms that mediate ALT. PARP inhibitors are the first cancer therapy designed to exploit synthetic lethality (238). PARP inhibitors trap PARP on the DNA, which can impede replication fork progression (207). In ovarian and breast cancers with BRCA1/2 mutations, persistence of SSBs from fork collapse leads to DSBs that cannot be repaired due a defect in HR (192). In addition, PARP inhibition allows untimely RECQ1-catalyzed fork restart upon DNA damage, which leads to replication run-off and increased DSBs (197). However, in ALT cancers whose telomeres are predisposed to initiate HDR, PARPi-generated DSBs become substrates to further prime HDR mechanisms. This model explains how PARPi promotes ALT hallmarks, such as increased T-SCEs, c-circles, and APBs. Notably, PARPi is sufficient to induce ALT-like phenotypes in the TEL+ Hela LT cell line. A possible explanation for this is that Hela LT cells have long telomeres with disrupted telomere homeostasis that predispose them for ALT upon a DDR stimulus. This is corroborated by previous studies showing that telomere extension beyond normal levels provokes telomere-trimming, leading to generation of ECTRs and T-SCEs (74,239).

Our data shows that PARPi enhances HR and G2-BIR in U2OS DA TRF1-FokI cells. This is seen by the increase in T-SCEs and APBs, as well as telomere clustering in DA TRF1-FokI cells. A reasonable interpretation for the telomere clustering results is that the number of DSBs generated by the TRF1-FokI system already saturates the HR machinery. In this case, PARPi would not further potentiate the maximum threshold for ALT reliance on HDR mechanisms. However, PARPi still perturbs replication at these telomeres and enhances the progression past damaged lesions, which is consistent with a previous study (198). Thus, PARPi still contributes to the chronic replication stress and spontaneous DNA damage that is already observed at ALT telomeres. It is already known that the G-rich, repetitive regions of telomeres impinge on replication efficiency and are considered common fragile sites (240,241). This can be heightened in ALT due to non-canonical variant sequences that can disrupt binding of TRF1 and TRF2 (115). Nucleosome assembly defects and decondensation of chromatin at ALT telomeres also contribute to a permissive landscape for HDR-mediated DNA synthesis (41,242). In addition, loss of ASF1, which mediates H3.3 histone eviction and deposition, leads to the induction of ALT (243). In this context, PARPi simply tips the balance in favor of an environment that is conducive to recombination.

PARGi has opposing consequence on ALT telomere maintenance and cell viability. At a fundamental level, negatively charged PAR imposes a biophysical reconfiguration of chromatin known as PAR-seeded liquid phase separation that sets the stage for DNA repair (224). This is consistent with evidence that PAR-regulated phase separators have key functions in sensing DSBs, including those at telomeres (224). Liquid phase transitions can promote RAD52 assembly and BITS during G2-phase (244). This involves BLM-dependent DNA resection and synergistic interactions between SUMOylated peptides and SUMO-interaction motifs (SIMs). However,

emerging evidence indicates PARP activity can stimulate SUMOylation of HDR factors (245). Thus, a parsimonious model to explain the observed effects of PARG inhibition on ALT-associated HDR could be that while PAR is initially synthesized at the DSBs or ssDNA gaps by PARP, PARG inhibition prevents the hydrolysis of PAR, recycling of NAD+ cofactor and downstream target modification. This would block PAR-regulated phase separation – in essence paralyzing the repair process at its early or intermediate stages, providing a means to tune repair with the cellular metabolism.

2.4 Methods

2.4.1 Statistics

GraphPad Prism was used to calculate statistical significance for one-way ANOVA or student t-test. Statistical tests, number of cells scored, and biological replicates are indicated in the figure legends. *P≤ 0.05, **P≤ 0.001, ***P≤ 0.001, ****P< 0.001.

2.4.2 Cell Culture

U2OS, Saos2, Hela LT, HOS, SJSA1 cell lines were obtained from ATCC. VA13, LM216T/J and WT/DA TRF1-FokI U2OS cell lines were obtained from Roger Greenberg (University of Pennsylvania). Each cell line was cultured in DMEM +Glutamax (Life Technologies) supplemented with 10% bovine growth serum or 10% fetal bovine serum. Cells

were cultured at 20% O_2 and 7.5% CO_2. U2OS, HeLa LT and 293FT cell lines were validated by STR profiling and confirmed mycoplasma free by ATCC cell line authentication services.

2.4.3 PARP and PARG Inhibitors

The active (PDD00017272) PARG inhibitor and its inactive analogue (PDD00031704) used in this study were developed and generously provided by the Drug Discovery Unit at Cancer Research UK (Manchester). The pharmacokinetics and selectively of these molecules towards PARG have been described. Olaparib (KU-0059436, AZD2281) used to inhibit PARP1 and PARP2 was purchased from Selleck Chem. 5 μMσ of PARPi and PARGi were used in short term experiments (less than 3 days). 100 nM and 1 μM of PARPi and PARGi were used in long term experiments, (greater than 4 days).

2.4.4 Western Blotting

Cells were harvested with trypsin, quickly washed in PBS, counted with Cellometer Auto T4 (Nexcelom Bioscience) and directly lysed in 4X LDS sample buffer at 10^4 cells per μl. Proteins were gently homogenized using universal nuclease (Pierce/ThermoFisher), denatured for 10mins at 68°C and resolved by SDS-Page electrophoresis, transferred to nitrocellulose membranes, blocked in 5% milk or BSA and 0.1 % Tween for 30mins and probed with primary antibodies. For secondary antibodies, HRP-linked anti-rabbit or mouse (Amersham) was used, and the HPR signal was visualized with SuperSignal ECL substrate (Pierce) as per the manufacturer's instructions.

2.4.5 Direct Immunofluorescence (IF)

Cells on glass coverslips were washed twice in PBS and fixed with 2% PFA for 10mins. Cells were permeabilized with 0.1% (w/v) sodium citrate and 0.1 % (v/v) Triton X-100 for 5mins and incubated with fresh blocking solution (1 mg/mL BSA, 10% normal goat serum, 0.1% Tween) for at least 30mins. Primary antibodies were diluted in blocking solution and added to cells for 1hr at RT or overnight at 4°C. Next, cells were washed in 3 times with PBS for 5mins and incubated with Alexa coupled secondary antibodies (488nm, 568nm, 647nm) (Life Technologies) for 1hr at RT. Then, cells were washed 3 times with PBS and mounted on slides with Prolong Gold Anti-fade reagent with DAPI (Life Technologies). Once the Prolong Anti-fade has polymerized and cured for ~24hrs cells were visualized by conventional florescence with 40X and/or 63X Plan λ objective (1.4 oil) using a Nikon 90i or Nikon A1R Spectral confocal microscope.

2.4.6 IF-FISH

After secondary antibody incubation, cells were washed as above but then the IF staining was fixed with 2% paraformaldehyde (PFA) for 10mins. PFA was washed off with PBS and coverslips dehydrated with successive washes in 70%, 95% and 100% EtOH for 3mins were allowed to air dry completely. Next, the coverslips were mounted on glass slides with 15μl per coverslip of hybridization mix (70 % deionized Formamide, 1mg/ml of Blocking Reagent [Roche], 10mM Tris-HCl pH 7.4) containing Alexa 488-$(CCCTAA)_4$ PNA probe (PNA Bio). DNA was denatured by setting the slides on a heating block set to 72°C for 10mins and then incubating for at least 4hrs or overnight at RT in the dark. The coverslips were then washed twice for 15mins with Wash Solution A (70% deionized formamide and 10mM Tris-HCl pH7.2) and three times

with Solution B (0.1M Tris-HCl pH7.2, 0.15M NaCl and 0.08% Tween) for 5mins at RT. EtOH dehydration was repeated as above and finally the samples were mounted and analyzed as mentioned above.

2.4.7 ALT-Associated PML Bodies (APBs) Quantification

Anti-PML antibody was used in conjunction with telomere-FISH to identify APBs. Cells were visualized by conventional florescence with 40X objective (1.4 oil) using a Nikon 90i microscope. Large image scans of 3x3 fields were taken. Colocalization of PML and telomeres were analyzed using a macro in the NIS Elements software. APB+ cells were scored if there was one colocalization event per cell.

2.4.8 Chromatin Orientation Fluorescent *In Situ* Hybridization (CO-FISH)

CO-FISH was performed as described with the variation that cells were incubated with BrdU and BrdC simultaneously for ~12hrs, and hybridization was performed with Alexa 488-$(CCCTAA)_4$ and Alexa 568-$(TTAGGG)_4$ PNA probes. In brief, cell cultures were incubated with 7.5mM BrdU and 2.5mM BrdC for ~12hrs. After removal of nucleotide analogs, colcemid (Gibco) was added for ~2hrs, cells were harvested by trypsinization, swelled in 75mM KCl and fixed in 70% Methanol: 30% Acetic Acid. Samples are stored at -20°C for days. Metaphase chromosomes were spread by dropping onto washed slides, then RNase A (0.5 mg/ml) and pepsin treated. Slides were incubated in 2×SSC containing 0.5 mg/ml Hoechst 33258 for 15mins in the dark and irradiated for 40mins (5.4×10^5 J/m2, energy 5400) at in a UV Stratalinker 2400 (Stratagene). The nicked BrdU/C substituted DNA strands are degraded by Exonuclease III digestion. The slides

were then washed in PBS, dehydrated by EtOH washes and allowed to air dry completely. The remaining strands were hybridized with fluorescence labeled DNA probes of different colors, specific either for the positive telomere strand $(TTAGGG)_4$ (polymerized by lagging strand synthesis) (Alexa-488, green color), or the negative telomere strand $(CCCTAA)_4$, (polymerized by leading strand synthesis) (Alexa-568, red color). Prior to hybridization of the first PNA, DNA is denatured by heating at 72°C for 10mins, as in IF-FISH, and then incubated for 2hrs at RT. Slides were washed for 15mins with Wash Solution A (see IF-FISH), dried and then incubated with the second PNA for 2hrs at RT. The slides were then washed again twice for 15mins with Wash Solution A and 3 times with Wash Solution B (see IF-FISH) for 5mins at RT. The second wash contained DAPI (0.5μg/mL). Finally, cells were dehydrated in EtOH as above and mounted (Vectashield). The resulting chromosomes show dual staining and allow distinction between leading and lagging strands. Metaphase chromosomes were visualized by conventional florescence microscope with a 63X Plan λ objective (1.4 oil) on a Nikon 90i microscope.

2.4.9 C-Circle Assay

CC assay was performed as described previously. Genomic DNA was purified, digested with *Alu*I and *Mbo*I and cleaned up by phenol-chloroform extraction and precipitation. DNA was diluted in ultraclean water and concentrations were exhaustively measured to the indicated quantity (30, 15, 7.5ng) using a Nanodrop (ThermoFisher). Samples (10μl) were combined with 10μl BSA (NEB; 0.2 mg/ml), 0.1 % Tween, 0.2mM each dATP, dGTP, dTTP and 1× Φ29 Buffer (NEB) in the presence or absence of 7.5U ΦDNA polymerase (NEB). Samples were incubated at 30°C for 8hrs and then at 65°C for 20mins. Reaction products were diluted to 100μl with 2×SSC and dot-blotted onto a 2×SSC-soaked nylon membrane. DNA was UV cross-linked onto the

membrane and hybridized with a P^{32} end-labeled $(CCCTAA)_4$ oligo probe to detect C-circle amplification products. All blots were washed, exposed to PhosphoImager screens, scanned using a Typhoon 9400 PhosphoImager (GE Healthcare) and quantified with Image J. In all reactions, when Φ29 was omitted as a negative control, DNA was used.

2.4.10 Pulse Field Gel Electrophoresis

Telomere gels were performed using telomere restriction fragment (TRF) analysis. Genomic DNA was digested using *AluI* and *MboI* (NEB). 4–10 μg of DNA was run on a 1% PFGE agarose gel (Bio-Rad) in 0.5×TBE buffer using the CHEF-DRII system (Bio-Rad) at 6V cm−1; initial switch time 1 second, final switch time 6 seconds, for 17hrs at 14°C. The gel was then dried for 2hrs at 60°C, denatured in a 0.5M NaOH/1.5M NaCl solution, and neutralized. Gel was hybridized with ^{32}P-labelled $(TTAGGG)_4$ oligonucleotides in Church buffer overnight at 55°C. The next day, the membrane was washed three times in 2×SSC buffer and once in 2x SSC 0.5% SDS, exposed onto a storage phosphor screen and scanned using Typhoon 9400 PhosphoImager (GE Healthcare). Telomere length was determined using TeloTool software

2.4.11 Clonogenic Assay

1000 cells were seeded in 6 well plates in duplicate and cultured for 7 days before fixation and staining in a 1% crystal violet solution. Plates were scanned and analyzed with ImageJ, which was used to count positive stained colonies and calculate total cell coverage per well. 1 mM of PARPi and PARGi were diluted in media and replaced every 3 days.

2.4.12 Live Cell Imaging

As a surrogate for telomeres eGFP-TRF1 foci were tracked in a 3-dimensional volume after imaging with a Nikon A1RS point scanning confocal microscope. Fields were imaged with a 60x 1.40 NA objective using 405nm and 488nm excitation laser lines at 500nm steps in Z. Nuclear volumes were corrected for gross displacement in X & Y due to cell migration using NIS Elements software. Images were deconvolved again using NIS Elements to account warping due to spherical aberration. The nuclear volumes and relative foci positions were then corrected for nuclear rotation by defining the medial axis of a z-projected nucleus, and determining its angular displacement relative to the field. The volumetric data was rotated to correct for angular displacement relative to the previous time point. Telomere (eGFP-TRF1) foci positioning and tracks were defined with Imaris analysis software. Fine X, Y, and Z-axial displacement were corrected by defining a centroid point for each nuclear volume and correcting individual foci positions. Each telomere focus position was corrected relative to the centroid displacement from the previous time point in the X, Y and Z-axis. This fine correction accounts for slight nuclear drift concentrated in the Z-axis, as slight upward and downward motion of the nucleus can drastically skew the displacement of individual telomere foci. Telomere movement from a minimum of 30 cells per condition was captured. The complete motion of >100 telomeres over 60 mins analyzed using the methods previously described, with the adjustments for motion in z. Telomeres whose motion could not be tracked for a complete hour were omitted from analysis.

A Euclidian model was used to calculate the vector displacement for the nuclear centroid and telomere foci over time.

$$\boldsymbol{d}_{t_n} = \sqrt{(\boldsymbol{x}_{t_n} - \boldsymbol{x}_{t_{n-1}})^2 + (\boldsymbol{y}_{t_n} - \boldsymbol{y}_{t_{n-1}})^2 + (\boldsymbol{z}_{t_n} - \boldsymbol{z}_{t_{n-1}})^2}\,.$$

The same vector displacement model was used in determining the mean squared displacement for foci over time

2.4.13 TRF1-FokI Telomere Clustering

mCherry-DD-ER-WT/DA TRF1-FokI cells were induced by adding 40ng/mL Doxycycline for ~24hrs followed by 4-OHT (1μM) and Shield1 ligand (1μM). Inhibitors were added at the start of induction. Cells were processed for immunofluorescence and telomere number and size were quantified using NIS-Elements Advanced Research software (Nikon).

2.4.14 BrdU Pulldown Dot Blot

BrdU-IP was performed as described with minor modifications. Briefly, TRF1-FokI-inducible cells were induced by adding 40ng/mL Doxycycline for ~24hrs followed by 4-OHT (1□M) and Shield1 ligand (1μM). Cells were pulsed with 100μM BrdU (Sigma) for 2hrs before collection. Extracted genomic DNA was sheared by sonication into 100–300 bp fragments. Sheared gDNA was denatured for 10mins at 95°C and cooled in an ice-water bath. Denatured gDNA was incubated with 2μg anti-IgG (Sigma) or anti-BrdU antibody (BD) diluted in immunoprecipitation buffer (0.0625 % (v/v) Triton X-100 in PBS) rotating overnight at 4°C. The next day, samples were incubated with 30μl Protein A/G agarose beads (Santa Cruz) pre-bound to a bridging antibody (Active Motif) for 1h rotating at 4°C. Beads were then washed three times with immunoprecipitation buffer and once with TE buffer. Beads were then incubated twice in elution buffer (1% (w/v) SDS in TE) for 15mins at 65°C. Pooled eluates were purified with ChIP DNA Clean & Concentrator kit (Zymo). Samples were diluted into 2×SSC buffer, treated at 95°C

for 5mins, and dot-blotted onto an Amersham Hybond-N+ nylon membrane (GE). The membrane was then denatured in a 0.5N NaOH/1.5M NaCl solution, neutralized, and ultraviolet crosslinked. The membrane was hybridized with ^{32}P-labelled $(TTAGGG)_4$ oligonucleotides in Church Buffer overnight at 55°C. The next day, the membrane was washed four times in 2X SSC buffer and once in 2X SSC/0.5% SDS, exposed onto a storage phosphor screen (GE Healthcare), scanned and analyzed with ImageJ.

2.4.15 DNA Fiber Combing Combined with Telomere FISH

350,000 WT TRF1-FokI cells were seeded in a 60mm dish and were induced by adding 40ng/mL Doxycycline for ~24hrs followed by 4-OHT (1μM) and Shield1 ligand (1μM) for 3hrs. PARPi (5μM) or PARGi (5μM) were added to the media upon induction. Cells were subsequently labelled by incubating with 25μM CldU for 20mins followed by 250μM IdU for 20mins. Cells were harvested with trypsin and resuspended in ice-cold PBS at 1.2 x 10^6 cells/ml. 2μL of the cell suspension was pipetted onto a slide. 10μL of lysis solution (1M Tris-Cl (pH 7.4), 500mM EDTA (pH 8), and 10% SDS) was gently added to the cell suspension and slides were incubated for 5mins. Slides were tilted at a 15º angle to allow the drop to travel the length of the slide. Slides were then dried for 7-8mins and fixed with MeOH and Acetic Acid (3:1) for 7-8mins. Slides were kept in 70% EtOH until denaturation for a maximum of 7 days. For denaturation, slides were initially incubated in MeOH/0.1% βME for 5 min and then incubated in denaturation buffer (0.1M NaOH, 70% EtOH, and 0.1% βME) for either 12mins. Subsequently, slides were incubated in fixation buffer (0.5% Glutaraldehyde in denaturation buffer) for 5mins. Slides were rinsed sequentially with 70%, 95%, and 100% EtOH and left to dry for 30mins-1hr. DNA fibers were hybridized

overnight with biotin-OO-$(CCCTAA)_4$ locked nucleic acid (LNA) probe (Exiqon) at 37ºC. The LNA probe was visualized using the Alexa Fluor 488-conjugated streptavidin antibody (Life Technologies) followed by incubation with the biotinylated anti-avidin antibody (Vector) and sequential addition of the Alexa Fluor 488-conjugated streptavidin antibody (Life Technologies). IdU and CldU were detected using mouse anti-IdU (BD) and rat anti-CldU (Abcam) monoclonal antibodies followed by Alexa Fluor 647-goat anti-mouse (Life Technologies) and Alexa Fluor 555-goat anti-rat (Life Technologies) secondary antibodies. Images were acquired using the Nikon 90i microscope equipped with a 63X Plan λ objective (1.4 oil). The line measurement tool on the NIS-element software (Nikon) was used to calculate the length of replication tracts and telomeres. For conversion of microns to kilobases, 0.26 micron corresponded to 1kb of DNA.

3.0 Proteomic interrogation of the ALT-associated PARylome

3.1 Introduction

ALT telomeres exist in a dynamic state to facilitate HR events that drives telomere elongation. This behavior was initially described in a study that artificially inserted a tag sequence near the telomeric repeats to probe for telomere length (95,246). ALT+ telomeres demonstrate rapid elongation and shortening during cell division, which is not seen in TEL+ telomeres. In fact, this tag sequence can be duplicated from one chromosome to other chromosome ends in ALT+ cells. Time-lapse imaging also reveals that a subfraction of telomeres associate with and disassociate from telomere clusters at relatively immobile PML bodies (247). These telomere clusters are not stable structures, but are transient in nature to promote spatial movement for recombination. In addition, the telomeric DSB response at ALT telomeres triggers inter-telomere associations that are mediated by the RAD51-HOP2-MND1 machinery (96). This implicates a specialized homology search mechanism that requires surveillance of nuclear space to enable telomere synapsis and recombination.

Although it is established that the molecular events in ALT are intimately connected to telomere dynamics, the intricate interplay between these diverse factors are not fully characterized. The exact stimulus that drives these processes have yet to be determined. Our previous results link PARylation to ALT telomere maintenance. PARylation is considered a reversible, dynamic post-translational modification that is an early sensor of diverse processes, including HR (223). It is possible that PARylation modulates early processes in ALT, which can be a determinant for cell fate. Therefore, characterization of the PAR-regulated ALT proteome would be useful to fully

explore the exquisite control of PARylation during HR and G2-BIR. To date, there has been studies that identify the ALT-associated proteome as well as the PARylated proteome in response to genotoxic agents (87,223). However, the PARylome in ALT has not been characterized and will be discussed in further detail in this chapter.

The ALT proteome has already been established by published work from the O'Sullivan lab. Garcia-Exposito et al. isolated and compared the telomeric protein composition of ALT+ and TEL+ cells using BioID (87). Mutant BirA is fused to TRF1, which binds exclusively and constitutively at telomeres. Upon addition of biotin, BirA promiscuously biotinylates proximal proteins to the telomeres, which can either be through direct or indirect interactions. They identified a total of 454 proteins, of which 139 are exclusively associated at ALT telomeres. As a proof of concept, all six components of the Shelterin complex are recovered in the pulldown for ALT+ and TEL+ telomeres. Several Shelterin accessory factors, such as MRE11a, APOLLO, FEN1, PARP1, BLM, and Tankyrase 1, are also retrieved in both cell lines. Known factors that are unique to ALT are only captured at ALT+ telomeres. These factors include: PML, SLX4, ERCC1, NR2C1, NR2C2, and ZNF827. Proteins that only associate at ALT+ telomeres are involved in DDR, including those responsible for chromatin remodeling, DNA replication, HR, mismatch repair, single-strand annealing, and translesion DNA synthesis. Although these factors have defined roles in DDR, their convergence at ALT telomeres still remains elusive. This study was able to use proteomics as a starting point to identify a non-canonical role of Polη to ameliorate replicative stress and sustain HDR mechanisms at ALT telomeres (87). Thus, this distinct telomeric landscape lends the opportunity to explore non-canonical, distinctive regulators of ALT-associated proteins.

Mass spectrometry-based studies have established that the PAR-regulated proteome is extensive and that diverse protein groups are modified depending on the particular lesion or genotoxic stress. These strategies have involved immunoprecipitation of PARylated proteins using a PAR specific antibody (10H) and/or a PAR-binding module, often in combination with metabolic or chemical labeling (248). A well characterized ADP-Ribose binding module used for proteomic studies is the *Archeoglobus fulgidus* macrodomain, Af152. Af1521 is a wide-spread and conserved 190-residue domain that is found in approximately 300 proteins (249). A high degree of sequence conservation is seen at the Af1521 ligand binding pocket (176). Specifically, hydrophobic residues that line the adenine and ribose binding pockets are generally conserved to retain the correct fold. spectrometry (BioID) using BirA fused to TRF1 (BirA-TRF1) (87). This provided a broad annotation of proteins that constitutively Thus, Af1521 selectivity towards ADPr relies on its recognition of this distal ribose. Af1521 recognizes both mono ADP-Ribose and the terminal ADP-Ribose of PAR chains with high affinity (Kd=0.13μM) as well as selectivity for covalently modified proteins. The latter property of Af1521 is important as it confers specificity for proteins that are PARylated over proteins that contain motifs such as PBZ (PAR binding Zinc finger) or WWE domains that bind PAR *in cis* (250). Additional specificity in determining true PARylated proteins is provided by the use of a mutant Af1521 (G42E) that is defective in PAR binding. These studies reveal a myriad of proteins involved in RNA and DNA metabolism that provides an additional layer of crosstalk between different machineries in DDR (176,223,251). Overall, it is plausible that there are also functional intersections between PAR and ALT-associated factors due to the basal levels of replication stress and stochastic DNA damage at ALT telomeres.

This chapter highlights our employed proteomics strategy to isolate and assess the PARylated proteome at ALT telomeres. This technique allows for the capture of early regulators

of ALT that are transient and dynamic at steady-state conditions. Sustained PARylation dramatically reconfigures the ALT proteome. Specifically, PAR-regulated mediators of the ALT pathway belong to diverse functional groups, such as DNA repair, RNA-binding, chromatin remodeling, chromatin assembly, and F-Actin nucleation. These PAR-regulated factors only localize to ALT telomeres upon PARG inhibition, which validate their dependency on PAR. Our mass spectrometry hits also display a functional relevance in ALT cancers since their depletion leads to diminished ALT activity. Collectively, these results reveal the importance of PARylation in the fine-tune control of ALT telomere maintenance.

3.2 Results

3.2.1 Identification of the telomeric protein targets of PARG inhibition

We hypothesized that the phenotypes observed with PARGi are due to the inability of PARG to hydrolyze PAR on its target proteins, whose dynamics and functions are likely to be altered as a consequence. We chose to employ wildtype *(wt)* and mutant *(mut)* Af1521 macrodomain PAR binding modules to determine the ALT telomere-associated PARylome that is induced by WT TRF1-FokI in U2OS cells. We also performed Af1521 pulldowns from DA TRF1-FokI expressing cells to discriminate proteins that are PARylated due to endonucleolytic cleavage of telomeric DNA (Figure 18A). WT/DA TRF1-FokI were induced for 4hrs before cells were harvested. A mainstay in previous PARylation studies has been the requirement to deplete cells of PARG by RNAi to prevent PAR hydrolysis. In this case, PARGi was added to preserve cellular PAR following the induction of WT/DA TRF1-FokI. PARG and PARP1 activity that can be

stimulated by DNA shearing and oxidation were inhibited in solution by the addition of PARGi and PARPi in lysis and dilution buffers during sample processing.

After initial processing, each sample was split into two for subsequent pulldown with *wt* and *mut*-Af1521 macrodomains and western blot for PAR detection using the validated 10H anti-PAR antibody, as well as some known PARylated proteins (Figure 18B). The expected accumulation of PAR chains was observed in pulldowns using *wt*-Af1521 from WT TRF1-FokI-induced cells that harbor telomere specific DSBs. Most of the accumulation of PAR represents auto-PARylation of PARP1 protein that was also enriched in *wt*-Af1521 pulldowns from WT TRF1-FokI-induced cells. We also probed for PARylation of known DNA damage-induced PARP-targeted proteins such as ALC1 (also known as CHD1L) and RECQ1 (202,223). Both were readily detected using specific antibodies. We also confirmed PARylation of TRF1 and TRF2, which has been previously reported (229). We did not detect PARylation of the p65 subunit of NFκB, a negative control previously used in similar studies (223). Following this successful initial optimization, we were confident that the approach would allow for proteomic identification of the telomere-associated PARylome induced by TRF1-FokI DSBs.

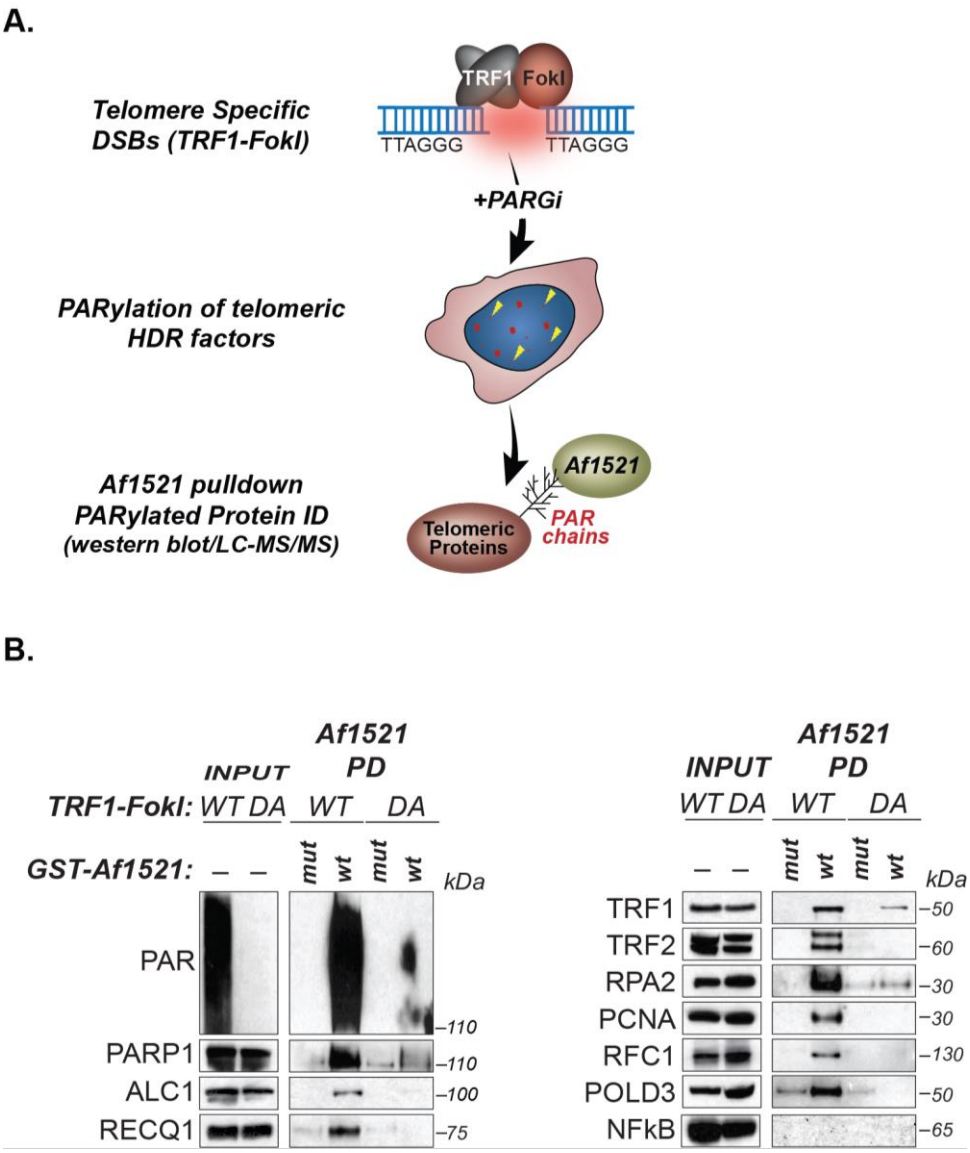

Figure 18. Proteomics approach to characterize the ALT PARylome. A) Schematic representation of TRF1-FokI-Af1521 proteomic strategy to identify ALT PAR-modulated telomeric proteins. B) PAR-modulated proteins from WT TRF1-FokI and DA TRF1-FokI U2OS cells were pulled down with GST-Af1521_wt and GST-Af1521_mut beads. Western blotting was performed with the indicated antibodies to detect PAR and enriched PARylated proteins. NF-κB antibody was used as a negative control.

3.2.2 Characterization of the ALT telomeric PARylome

In total, six samples prepared from *wt*/*mut*-Af1521 experiments using WT TRF1-FokI U2OS cells were subjected to protein identification by LC/MS mass spectrometry. Two negative control *wt/mut*-Af1521 samples prepared from DA TRF1-FokI U2OS cells were also analyzed. The final dataset was parsed using SAINT and CRAPOME proteomic databases (see Methods) producing a list of 117 proteins reliably detected in Af1521 pulldowns (Figure 19). We previously conducted an assessment of telomere composition in ALT+ U2OS cells by proximity dependent protein biotinylation mass spectrometry (BioID) using BirA fused to TRF1 (BirA-TRF1) (87). This provided a broad annotation of proteins that constitutively reside at, and transiently associate with, ALT telomeres. . A possible explanation is that the distinct telomeric landscape allows for certain DSB repair pathways to be more preferable

We re-analyzed this BirA-TRF1 dataset in tandem with the Af1521 data by using the same statistical and protein annotation software (19). This produced a list of 280 protein constituents of U2OS telomeres. Strikingly, when we assessed the overlap between the two datasets, a mere 13 proteins were present in both datasets (Figure 19). This reflects how fundamentally reconfigured ALT telomeres become following PARG inhibition. Given the evidence that PARylation is among the earliest modifications at sites of DNA damage, yet must be rapidly hydrolyzed by PARG, PARG inhibition likely facilitates the detection of PAR-regulated DSB associated proteins that are difficult to detect under steady-state conditions (252). In other words, these proteins likely represent the first responders to DSBs and early initiators of repair by HDR – providing a window into the apical events that promote ALT telomere maintenance.

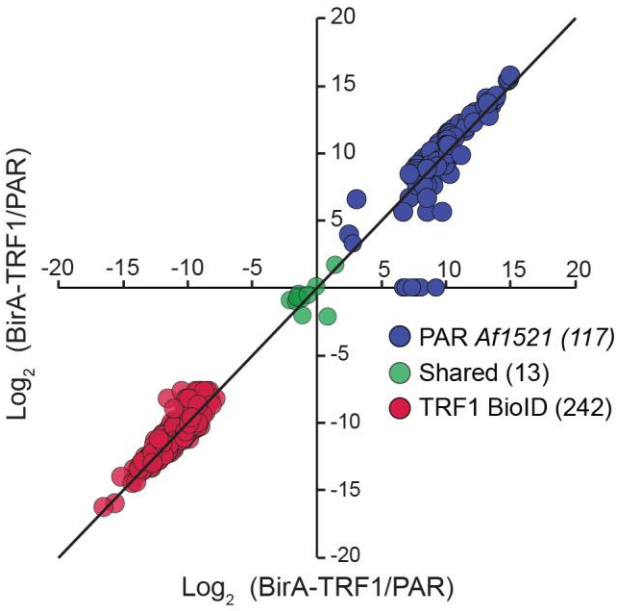

Figure 19. Distinct reconfiguration of ALT landscape upon PARGi. Comparison between telomere composition of ALT+ U2OS cells to factors identified by Af1521-PAR proteomics.

3.2.3 PAR-regulated mediators of the ALT phenotype

Functional annotation revealed an equal number of nuclear (59/117) and cytoplasmic proteins (58/117) (Figure 20A). The cohort included protein binding (88/117), DNA binding (25/117), poly-A RNA binding (22/117) and an unexpected number of actin binding (13/117) proteins (Figure 20A). Parsing the data for gene ontology (GO) classification determined that the protein hits most associated with chromatin structure modification, lagging strand replication, DNA and RNA metabolism and DNA Repair. For the latter, PARP1's obligate partners XRCC1 and LIGIII were identified by *wt*-Af1521 mass spectrometry confirming a role for alternative end joining in repair of TRF1-FokI-induced DSBs (Figure 20B).

Among the chromatin regulators ALC1, Scaffold Attachment Factor B1 (SAFB1) and Vasolin-containing Protein (VCP/p97) were found to localize to DSBs to mediate the relaxation

and remobilization of DSB vicinal chromatin (202,253–255) (Figure 20 and Figure 45A) Several RNA binding proteins present in this dataset included heterogeneous nuclear RNA binding proteins; heterogenous nuclear ribonucleoprotein A1 (hnRNPA1), heterogenous nuclear ribonucleoprotein U-like 1 (hnRNPUL1) and RNA-Binding Motif Protein X-Linked (RBMX) that have also been linked with maintaining telomere integrity and DNA repair by HDR (Figure 21B) (256–258). Other RNA binding proteins present included the FET (FUS; fused in liposarcoma/EWS; Ewing sarcoma/TAF15; TATA-box binding protein associated factor 15) proteins that have been implicated in initiating the PARP-mediated DNA damage response by promoting DNA repair complex assembly via liquid phase de-mixing (224) (Figure 20 and Figure 45A)**.** Interestingly, several factors involved in actin nucleation, such as Actin-related proteins 2 and 3 (ARP2-3), ARP2/3 complex subunits 2 and 3 (ARPC2-3), were enriched in the *wt*-Af1521 mass spectrometry (Figure 20 and Figure 45A)**.** The ARP2/3 complex promotes nuclear actin-dependent clustering of DSBs during homology directed repair (106). We confirmed that the ARP2/3 complex is responsible for telomere clustering since its inhibition impaired telomere clustering (Figure 47A-B). Inhibition of ARP2/3 also led to constrained telomere motion, similar to levels seen with PARG initiation (Figure 47C).

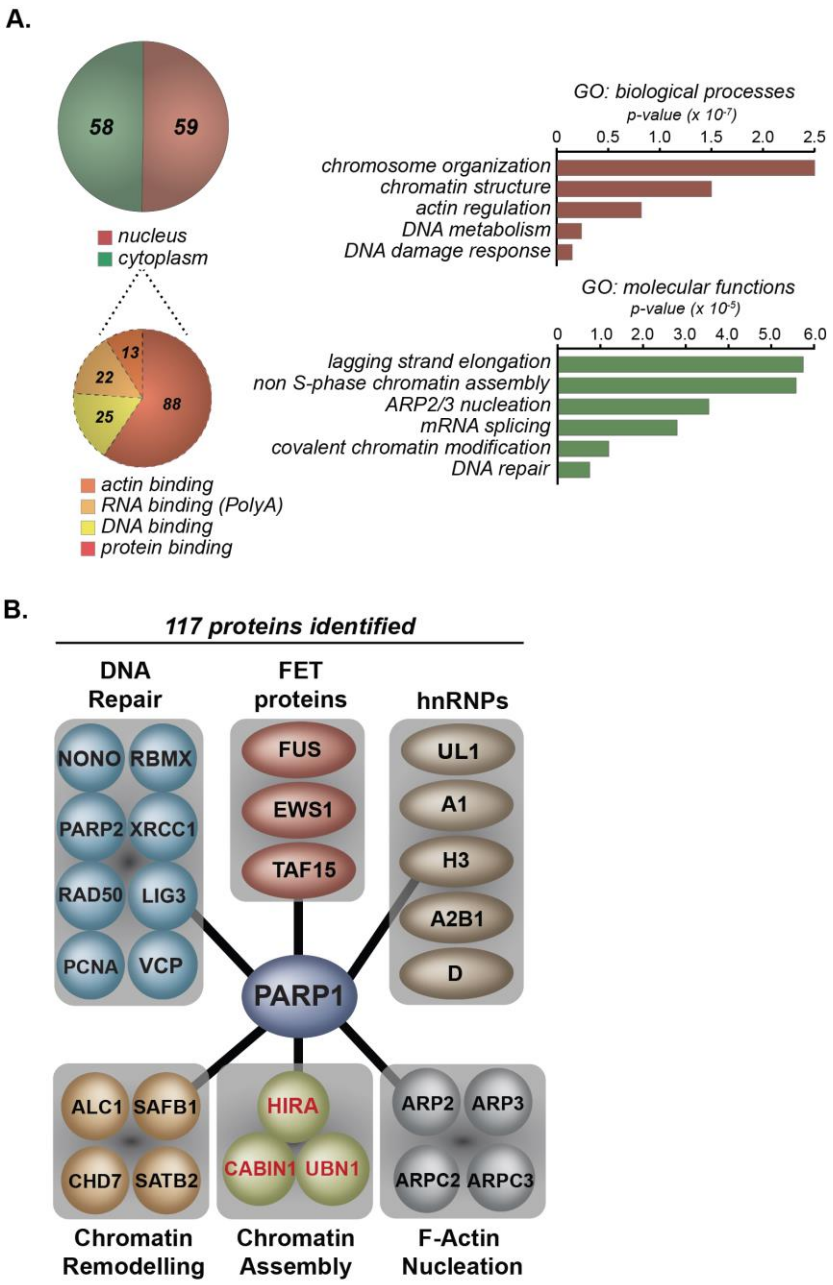

Figure 20. Distinct functional groups of PAR-regulated ALT telomeric proteins. A) Left: Functional annotation of the cellular distribution and ribonucleoprotein associations of enriched proteins identified by Af1521-PAR proteomics. Right: GO term annotation and ranking of enriched proteins by biological processes and molecular functions. Ranking was determined by statistical significance using DAVID (https://david.ncifcrf.gov/). B) Clustering of distinct functional protein groups identified by Af1521-PAR proteomics.

We examined whether any factors from these groups localize to TRF1-FokI-induced DSBs by transient expression in WT and DA cells (Figure 21A-B, Figure 45B, and Figure 46). None of the transiently expressed eGFP-tagged versions of SAFB1, RBMX, hnRNPUL1, FUS, VCP/p97 or ARP3 localized to WT TRF1-FokI-induced U2OS cells. (Figure 21B). However, when induced cells were also treated with PARGi, the specific accumulation of these proteins within TRF1-FokI foci was readily observed and quantified. In each case, this localization pattern was abolished upon addition of PARPi, highlighting the PAR-dependent nature of their association with ALT telomere DSBs. We confirmed that RBMX, FUS and ARP3 are directly PARylated by *in vivo* PARylation assay in response to WT TRF1-FokI DSBs (Figure 21C).

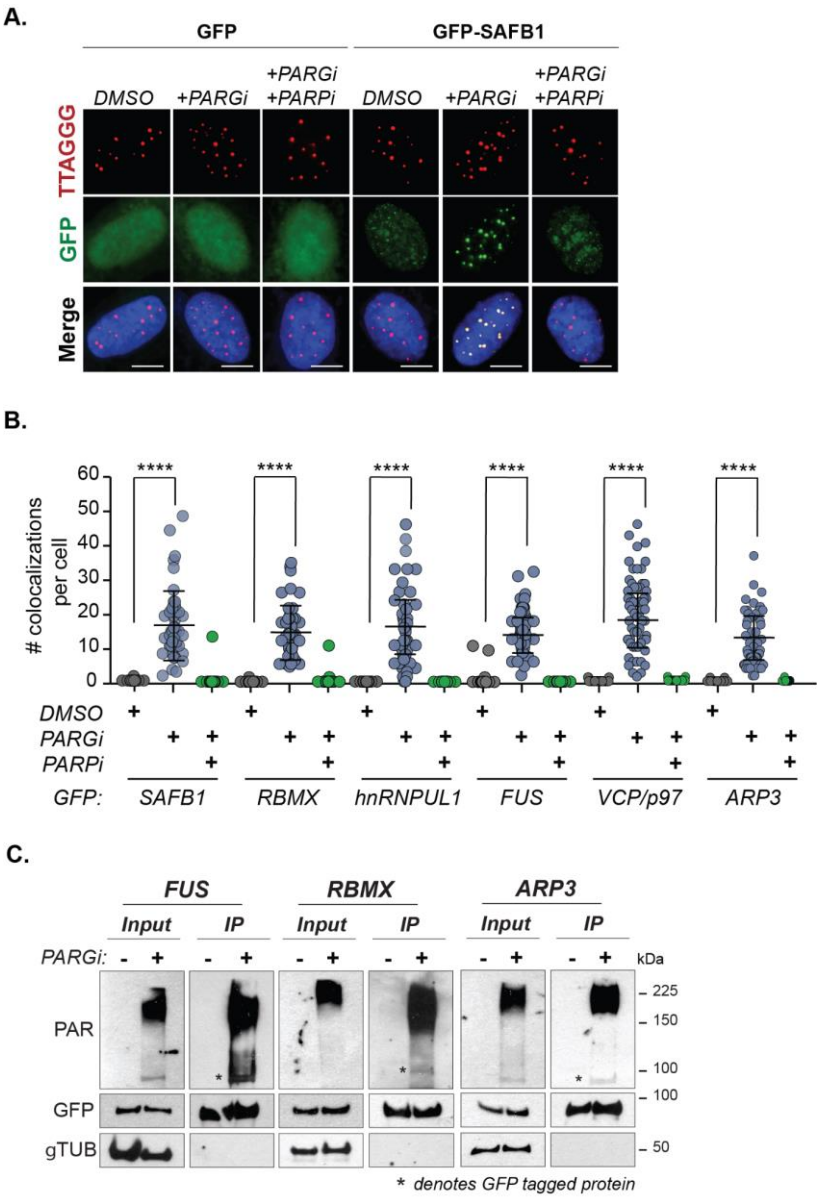

Figure 21. PAR-regulated factors associate with ALT telomeres. A) Representative IF images showing the localization of one of the PAR-regulated hits, GFP-SAFB1, in WT TRF1-FokI U2OS cells following treatment with DMSO, PARPi (5μM) and combined PARGi/PARPi (both 5μM). B) Validation of telomere association of GFP-fusion proteins from Figure 20. WT TRF1-FokI cells were transfected with the indicated GFP-tagged proteins. C) *In vivo* PARylation assay with GFP-tagged FUS, RBMX and ARP3. * indicates the band corresponding to the PARylated GFP-tagged target protein. All graphed data in the figure are mean ± SEM, n=75 cells. Statistical significance was determined using one-way ANOVA. *P≤ 0.05, **P≤ 0.001, ***P≤ 0.001, ****P< 0.001. All scale bars, 5μm.

We next asked if these factors (SAFB1, RBMX, hnRNPUL1, FUS, VCP/p97, and ARP3), are required to sustain ALT activity. Using siRNA knockdown, we depleted U2OS and VA13 ALT+ cell lines of these factors and examined effects on APB levels after 72hrs (Figure 22A-B). In each case, the number of APB+ cells within the observed population was reduced by ≥50%. We also assessed the effects of depleting these factors on WT TRF1-FokI-induced telomere clustering, as before. As was the case with PARG inhibition, the depletion of SAFB1, RBMX, hnRNPUL1, VCP/p97, FUS and ARP2-3 strongly reduced telomere clustering when compared to cells transfected with control non-targeting siRNAs. Based on this analysis, we find that targeting PAR-regulated factors for knockdown impairs telomere dynamics in multiple and diverse ways; possibly by limiting PAR-seeded liquid phase separation, repair-associated RNA remobilization, chromatin remodeling and even by perturbing actin nucleation. The net result is that critical aspects of the ALT mechanism and response to DSBs are systematically perturbed. In addition, these data provide strong validation of the proteomic approach taken here, in that we have several identified early regulators of ALT telomere maintenance whose activity relies on the timely and efficient metabolism of PAR.

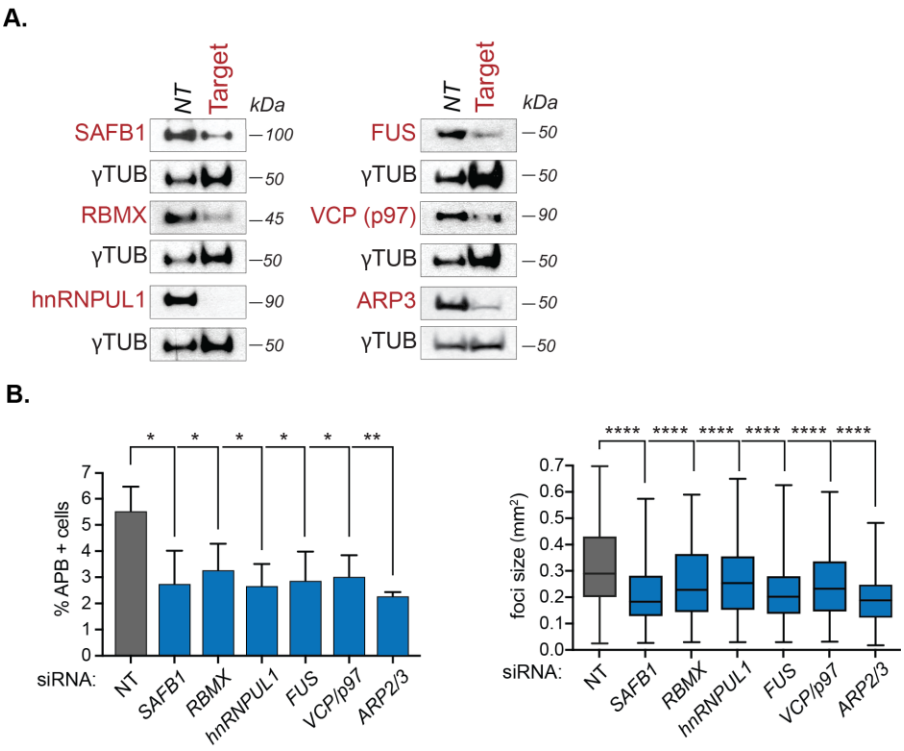

Figure 22. siRNA knockdown of PAR-regulated factors impairs ALT actiivity. A) Western blotting performed with antibodies to validate siRNA knockdown of protein hits from Af1521-PAR proteomics in U2OS cells. All scale bars, 5μm. B) Left: Quantification of APBs (%) and right: TRF1-FokI-mediated telomere clustering in U2OS cells transfected with indicated siRNA. All graphed data in the figure are mean ± SEM, n=75 cells. Statistical significance was determined using one-way ANOVA. *P≤ 0.05, **P≤ 0.001, ***P≤ 0.001, ****P< 0.001.

3.3 Discussion

By combining telomere specific proteomics and PARG inhibition, we uncovered factors that we propose to constitute the first wave of proteins that respond to telomeric DNA damage in ALT. The enrichment of chromatin remodelers, such as ACL1, SAFB1, and VCP/p9, corroborate that chromatin plasticity promotes ALT (202,253,254). PAR has been shown to recruit ALC1 to damaged lesions and enhance its enzymatic activity (202). Additionally, there is modular allostery

of ALC1 via its ATPase domain and macrodomain (203). PARP1 activation releases ALC1 from autoinhibition and ensures that it only promotes chromatin relaxation in response to DNA acetylation to promote efficient γH2AX spreading. The AAA-ATPase VCP/p97 is recruited to DSBs in an RNF8- and ubiquitin-dependent manner (253). VCP/p97 displaces L3MBTL1, a Polycomb-group protein that binds the same H4K20Me2 modification as 53BP1. Therefore, exposed H4K20Me2 enhances spreading of 53BP1 at DSBs. This example reveals how ubiquitylation orchestrates the recognition of methylated histones to promote chromatin accessibility; it particularly emphasizes the importance of the exquisite crosstalk between various post-translational modifications to maintain genome integrity.

Chromatin reorganization in response to DNA damage must be robust and tightly coordinated to maintain efficient DNA repair. There is an intricate molecular network of chromatin modifications with significant crosstalk and redundancies (259). Signal propagation across large, specialized chromatin domains provides accessibility for DDR factors. Signal amplification not only exists within one pathway, but can occur through the interplay between multiple pathways. Notably, there is a functional crosstalk between PARylation and SUMOylation. SUMOylation conjugates small ubiquitin-like modifiers (SUMO) onto target proteins. PARylation cooperates with SUMOylation to stabilize trapped topoisomerase I (TOP1) cleavage complexes at DNA damage sites (260). Together, they also recruit SLX4 nuclease scaffold complex to damaged lesions (245). Other studies reinforce how PARylation positively feeds into the ubiquitylation pathway (261). SUMO E3 ligases PIAS1 and PIAS4 mediate chromatin ubiquitylation at DSBs, which leads to accrual of BRCA1, 53BP1, and E3 Ligase RNF4 (262–264). On the other hand, PARylation recruits the repressive Polycomb and NuRD complexes to sites of damage. This stimulates RNF8/RNF168-mediated histone ubiquitylation and the ubiquitin-dependent

accumulation of RNF168 and BRCA1 (265,266). Ultimately, this promotes DSB repair and checkpoint activation in response to genotoxic stress.

However, there are physiological barriers imposed by the chromatin architecture that safeguards against unwarranted and excessive DNA damage signaling. PTMS such as PARylation and SUMOylation are extremely transient to ensure faithful termination upon completion of repair (261). This is critical to prevent saturation of repair factors, which would be counterproductive and lead to uncoupling of downstream events. It was proposed that an abundance of rate-limiting chromatin modifiers could dictate pathway choice and chromatin spatial and temporal dynamics (259). For example, the absence of TRIP12 and UBR4, which are regulators of the RNF168 nuclear pool, leads to supraphysiological levels of RNF168 and excessive spreading of chromatin ubiquitylation. This is followed by deregulated accumulation of ubiquitin-regulated genome caretakers involved in NHEJ and HR, such as 53BP1 and BRCA1 (267).

In the ALT context, the interplay between PTMs and regulators of chromatin assembly become more pertinent since chronic replication stress at telomeres generates high levels of DSBs. In ALT, disrupted regulation of chromatin modifications would permit continuous hyperactivation of chromatin remodeling at the precise threshold for HDR that does not trigger cell death. An outstanding question is whether there is an ALT-specific chromatin barcode that would differentiate the ALT telomeric landscape from other genomic regions. More specifically, is there differential regulation of PAR-dependent chromatin remodelers at ALT telomeres? If PARylation is the initial signal that sets chromatin modeling in motion, when are these events disengaged to prevent non-productive, sequestered cellular pools of genome caretakers? To resolve this conundrum, it is necessary to further understand the intricate role that PARylation plays in the hierarchy of signaling at ALT telomeres.

RNA-binding proteins are another group of PAR-mediated factors that associate at ALT telomeres. These include proteins such as FET proteins (FUS-EWS1-TAF15) and multiple hnRNPs, whose low-complexity domains (LCD) sense and compartmentalize damaged DNA within phase separated liquid condensates (224). The capacity to detect these factors likely reflects their prolonged retention, as the dissolution of these LCD aggregates is usually very rapid and requires that they undergo PAR hydrolysis (268). The FET proteins are linked to pathological protein aggregation, exhibit frequent gene translocations in cancers, and are prototype intrinsically disordered proteins (IDPs) that contain prion-like SYQG-rich amino-terminal LCD and an extended RGG-rich carboxyl-terminal LCD-containing 18-22 RGG repeats (224,269). hnRNPUL1 is implicated in PARP1-dependent stimulation of DNA end resection in response to DSB repair (257,270). Steady-state PARG and the transient nature of DNA damage allows for the reversibility and dissolution of these compartments. Although liquid-liquid demixing events prime the initial recruitment of DNA repair factors to damaged sites, these proteins can independently form higher-order structures that become irreversible aggregates. The additional mechanisms to resolve such irreversible events are not known.

Liquid phase separation is particularly relevant to the assembly of APBs, which are thought to be centers of recombination in ALT. Zhang et al. stimulated *de novo* formation of APBs in live cells and showed that APB assembly relies on liquid demixing that is driven by SUMO-SIM interactions (225). They confirmed that APB condensates contain PML as the scaffold component while DNA repair factors, such as 53BP1, PCNA, and POLD3, were recruited in a manner that is independent of condensation. Based on these studies and dissertation work, it is plausible that APB nucleation via phase separation events is mediated by a crosstalk between SUMOylation and PARylation. This PAR-SUMO switch would accommodate the rapid perturbations in ALT

telomere dynamics, in which rapid APB assembly and disassembly is critical for extensively short and long telomeres. However, the exact molecular details of this interplay and how it functions in the spatial and temporal regulation of APB nucleation still needs to be elucidated.

Both HR (RAD50 and PCNA) and alt-NHEJ (LIG3 and XRCC1) factors were captured in the mass spectrometry results. It has already been established that RAD51 and the HR machinery mediates directional ALT telomere movement and clustering. It is not surprising that RAD50, which is part of the MRN complex (MRE11-RAD50-NBS1), is found at ALT telomeres to facilitate end-resection in HR (96). In addition, PCNA is part of the G2-BIR replisome (RFC-PCNA-POLD3), which underlies nascent telomeric synthesis during G2 in ALT (98). Interestingly, alt-NHEJ has been implicated in the repair of telomere-internal DSBs and is dependent on PARP1 and LIG3. Alt-NHEJ is considered a mutagenic DSB repair pathway that utilizes 1-16 nucleotides of homology flanking the DSB for end joining (271). It is often associated with deletions, insertions, and chromosome translocations. Generally, alt-NHEJ is a backup pathway for abrogated HR and c-NHEJ. However, alt-NHEJ may occur at telomeres because telomeric short tandem repeats are conducive for minimal resection and end joining. Overall, this represents how ALT telomeres elicit multifaceted repair pathways to preserve the balance between telomere dysfunction and telomere maintenance.

The depletion of select PAR-regulated factors from our proteomics study leads to impaired APB formation and DSB-induced telomere clustering. This underscores the importance of PARylation in varying stages of ALT telomere maintenance. PARG inhibition allows for the retention and capture of factors that dynamically associate at ALT telomeres. Those involved in chromatin remodeling and liquid phase separation represent first-wave responders in the ALT

pathway. Thus, perturbing PAR regulation will have huge ramifications for the maintenance of repair mechanisms at tolerable levels in ALT cancers.

3.4 Methods

3.4.1 Statistics

GraphPad Prism was used to calculate statistical significance for one-way ANOVA or student t-test. Statistical tests, number of cells scored, and biological replicates are indicated in the figure legends. *P≤ 0.05, **P≤ 0.001, ***P≤ 0.001, ****P< 0.001.

3.4.2 Cell Culture

U2OS cell line was obtained from ATCC. VA13 and WT/DA TRF1-FokI U2OS cell lines were obtained from Roger Greenberg (University of Pennsylvania). Each cell line was cultured in DMEM +Glutamax (Life Technologies) supplemented with 10% bovine growth serum. Cells were cultured at 20% O_2 and 7.5% CO_2. U2OS cell line was validated by STR profiling and confirmed mycoplasma free by ATCC cell line authentication services.

3.4.3 Af1521 Pulldown

The *Af1521* pulldown protocol was adapted from Jungmichel et al. Briefly, 4 x10^7 WT TRF1-FokI and DA TRF1-FokI cells were induced as usual. PARGi (5μM) was added during the

4-hour induction period. Cells were lysed using ice-cold modified RIPA buffer (50mM Tris-HCl (pH 7.5), 400mM NaCl, 1mM EDTA, 1% NP-40, and 0.1% Na-deoxycholate). PARPi and PARGi were added to lysis buffers to block *in vitro* PARP and PARG activity. Equal protein amounts were incubated with *wt* or *mut* GST-*Af1521* (Tulip Biolabs, PA) in modified RIPA buffer (without NaCl) for 2hrs at 4ºC. Beads were washed with modified RIPA buffer (150mM NaCl). Bound complexes were eluted in 4X LDS buffer.

3.4.4 Mass Spectrometry

Mass spectrometry was conducted at MS Bioworks (Ann Arbor, MI.). Immuno-precipitated samples stored in 4X LDS buffer were separated ~1.5cm on a 10% Bis-Tris Novex mini-gel (Invitrogen) using the MES buffer system. The gel was stained with coomassie and each lane was excised into ten equally sized segments. Gel pieces were processed using a robot (ProGest, DigiLab) as follow: First washes were with 25mM ammonium bicarbonate followed by acetonitrile. Then, reduced with 10mM dithiothreitol at 60°C followed by alkylation with 50mM iodoacetamide at RT. Samples were digested with trypsin (Promega) at 37°C for 4hrs, and then quenched with formic acid. Samples supernatants were analyzed directly without further processing using a nano LC/MS/MS with a Waters NanoAcquity HPLC system interfaced to a ThermoFisher Q Exactive. Peptides were loaded on a trapping column and eluted over a 75μm analytical column at 350nL/min; both columns were packed with Jupiter Proteo resin (Phenomenex). The mass spectrometer was operated in data-dependent mode, with MS and MS/MS performed in the Orbitrap at 70,000 FWHM resolution and 17,500 FWHM resolution, respectively. The fifteen most abundant ions were selected for MS/MS.

3.4.5 Proteomic Analysis

Raw mass spectrometry files were converted into open mzML format using msconvert utility of Proteowizard software suite. MS/MS spectra were searched using the MSFragger database search tool (version 20180316) against a UniProt/SwissProt Homo sapiens protein sequence database downloaded in May 21, 2019, appended with TRF1_FokI and Y1521_ARCFU fusion proteins and its respective mutated versions. MS/MS spectra were searched using a precursor-ion mass tolerance of 20 p.p.m., fragment mass tolerance of 20 p.p.m., and allowing C12/C13 isotope errors (-1/0/1/2/3). Cysteine carbamylation (+57.0215) was specified as fixed modifications, and Methionine oxidation (+15.9949), N-terminal protein acetylation (+42.0106) were specified as variable modifications. The search was restricted to fully tryptic peptides, allowing up to two missed cleavage sites. The search results were further processed using the Philosopher toolkit (https://philosopher.nesvilab.org/) as follows. MSFragger output files (in pepXML format) were processed using PeptideProphet (with the high–mass accuracy binning and semi-parametric mixture modeling options) to compute the posterior probability of correct identification for each peptide to spectrum match (PSM). ProteinProphet was executed on all resulting pepXML files from PeptideProphet resulting in a list of proteins groups (in protXML format). This combined protXML file, as well as the pepXML for each individual experiment, were then processed using Philosopher's filter and abacus functions to generate a combined spectral count matrix. The combined protXML file was filtered using the Philosopher filter function to 1% protein-level False Discovery Rate (FDR) using the target-decoy strategy. The PSM lists in each experiment were filtered using a sequential FDR strategy, keeping only PSMs passing 1% PSM-level FDR and mapped to proteins that also passed the global 1% protein-level FDR filter. Each peptide was assigned either as a unique peptide to a particular protein or (if

shared) assigned as a razor peptide to a single protein that had the most peptide evidence. The combined filtered protein list, as well as the filtered PSM lists for each individual experiment, were then processed using Philosopher's abacus function to generate a combined spectral count matrix. Each row in the resulting table represented a protein (with a single accession number selected among indistinguishable protein entries) and its abundance (unique plus razor PSM counts) across all experiments. The resulting quantification matrix was loaded into reprint-apms.org online resource to calculate abundance Fold Change (FC) scores comparing WT vs MUT experiment. A final cut-off of FC≥2 was arbitrarily set. This produced a final listing of 117 proteins that was used for *in silico* functional annotation in DAVID (Database for Annotation, Visualization, and Integrated Discovery) (https://david.ncifcrf.gov/) and downstream functional validation by experimentation.

3.4.6 Transient Transfection

U2OS and WT TRF1-FokI U2OS cell lines were seeded to obtain 70-80% cell density on day of transfection. Transfection mixture contained a 3:1 ratio of Lipofectamine 2000 to GFP construct. Specifically, for transfection of WT TRF1-FokI U2OS cells, 40 ng/mL of Doxycycline was added 2 hours prior to transfection for WT TRF1-FokI U2OS cells. Inhibitors and Doxycycline was added to media when media was changed 6 hours after the transfection. 4-OHT and Shield was added 24 hours later for 4hrs and cells were harvested for collection.

3.4.7 *In Vivo* PARylation Assay

GFP-immunoprecipitation was performed with GFP-TRAP®_A agarose beads (Chromotek). Briefly, 1 x 10^6 WT TRF1-FokI cells were seeded in a 10cm dish. ~24hrs later, cells were transfected with GFP-constructs using Lipofectamine 2000 (Invitrogen) as per manufacturer's instructions and 40ng/mL Doxycycline was added to the media as before. Cells were later induced with 4-OHT (1μM) and Shield1 ligand (1μM) for 4hrs with the addition of PARGi (5μM). Cells were harvested using ice-cold PBS, scraped from the dish and transferred to pre-cooled tubes. Cell pellets were resuspended in 200μL ice-cold RIPA buffer (10mM Tris-HCl (pH 7.5), 150mM NaCl, 0.5mM EDTA, 0.5% NP-40, 0.09% Na-Azide) with 1mM PMSF, 2.5mM $MgCl_2$, 1mg/ml DNase (Pierce) and protease inhibitor cocktail (Sigma). To extract HIRA proteins, modified RIPA buffer (500mM NaCl) was used as before. Tubes were placed on ice for 30mins with extensive pipetting every 10mins. Tubes were centrifuged at 20,000x g for 10 min at 4ºC and lysates were transferred to pre-cooled tubes. 300μL ice-cold dilution/wash buffer (10mM Tris-HCl (pH 7.5), 150mM NaCl, 0.5mM EDTA, 0.018% Na-Azide) with 1mM PMSF, 2.5mM $MgCl_2$, and protease inhibitor cocktail (Sigma) was added to tubes. 50μL of lysate was resuspended in 50μL 4X LDS buffer to save as 10% input samples. GFP-TRAP®_MA magnetic beads were equilibrated in dilution/wash buffer. 25μL of the bead slurry was added to each tube and rotated for 1hr at 4ºC. Beads were magnetically separated and washed twice with wash/dilution buffer. Beads were resuspended in 100μL 4X LDS buffer and boiled for 10mins at 95ºC. Beads were magnetically separated and SDS-PAGE was performed with the supernatant. PARylated proteins were detected using specific anti-PAR (10H) antibody.

3.4.8 siRNA Knockdown

For siRNA knockdown the *On-Target Plus (OTP)* siRNA SMARTpools from Dharmacon (GE) were used. 400,000 cells were seeded per well of a 6-well plate containing growth medium without antibiotics. 4hrs later cells were transfected. siRNAs and Dharmafect were diluted in OptiMEM (Life Technologies). A working siRNA concentration of 20nM was used. We used 2.5 μL Dharmafect transfection reagent per well. The transfection reagent mixture was added dropwise to one well in 1.8 mL of media without antibiotics. The next day, cells were transferred to 10-cm plates with coverslips. Transfection medium was replaced with complete culture media. Cells were harvested at 72hrs post-transfection. Inhibitors were added 24 hours prior to collection.

3.4.9 APBs Quantification

After 72 hours of siRNA knockdown, coverslips from 10-cm plates were collected for APB analysis. Anti-PML antibody was used in conjunction with telomere-FISH to identify APBs. Cells were visualized by conventional florescence with 40X objective (1.4 oil) using a Nikon 90i microscope. Large image scans of 3x3 fields were taken. Colocalization of PML and telomeres were analyzed using a macro in the NIS Elements software. APB+ cells were scored if there was one colocalization event per cell.

3.4.10 TRF1-FokI Telomere Clustering

After 48 hours of siRNA knockdown, WT TRF1-FokI U2OS cells were induced by adding 40ng/mL Doxycycline. After an additional 24 hours, 4-OHT (1μM) and Shield1 ligand (1μM)

were added to the media for 4 hours. Inhibitors were added at the start of induction. Cells were processed for immunofluorescence and telomere number and size were quantified using NIS-Elements Advanced Research software (Nikon).

4.0 Regulation of HIRA-mediated chromatin assembly at ALT telomeres by PARylation

4.1 Introduction

A salient feature of ALT cancers are inactivating mutations in ATRX/DAXX/H3.3. ATRX belongs to the Snf2-family of ATP-dependent chromatin remodelers. Snf2 proteins are DNA translocases that remodel nucleosomes by placing an ATP-dependent torsional strain on DNA (272). Several studies have implicated mammalian ATRX in the deposition of histone variant H3.3, which differs from the core H3 (H3.1/H3.2) by 4-5 amino acids (273,274). While core H3 is only incorporated during S-phase, variant H3.3 is expressed throughout the cell cycle and acts in a replication-independent manner. CHIP-Seq analyses reveal that H3.3 is enriched in transcriptionally active chromatin at transcription start sites, enhancers, and promoters (275–277). Interestingly, the ATRX/DAXX complex is critical for H3.3 incorporation at pericentric heterochromatin and at telomeres (278–280). ATRX/DAXX binds to G-rich tandem repeats that are prevalent in telomeres. Telomeric regions have predisposition to form G-quadruplex (G4) structures, which destabilize the genome. Thus, ATRX/DAXX resolves G4 structures at telomeres by remodeling and incorporation of H3.3 (120).

This is particularly relevant for ALT tumors since loss of chromatinization may potentiate HDR processes. Re-introduction of ectopic ATRX in U2OS cells reverses the ALT phenotype (228). ATRX expression reduces replication fork stalling by cooperating with DAXX to decrease the presence of telomeric G4. Thus, ATRX prevents fork collapse and subsequent restart by HDR in ALT. In addition, ATRX sequesters the MRN complex away from telomeric DNA and APBs, which halts end resection of DSBs and subsequent strand invasion. Notably, G4 structures are

favorable substrates for the MRN complex (281). It is likely that MRN cleaves G4 structures at ALT telomeres during DNA replication, which generates persistent DSBs followed by HDR-mediated DNA synthesis. This model supports the mounting evidence that HR-mediated repair of collapsed forks is a key determinant of ALT telomere maintenance.

Despite the importance of ATRX/DAXX at telomeres, transient depletion or disruption of ATRX is not sufficient to induce ALT (42). This implies that there are either additional alterations that trigger ALT or there are mitigating factors in TEL+ cancers that suppress the ALT pathway. It was recently reported that ATRX promotes HR at genomic regions in TEL+ cells. ATRX/DAXX incorporates H3.3 at sites of extended DNA synthesis to overcome any topological constraints at the moving D-loop (282). These findings are surprising since loss of ATRX/DAXX is frequently seen in ALT tumors that rely on HDR mechanisms. A possible explanation is that the distinct telomeric landscape allows for certain DSB repair pathways to be more preferable. In ALT, loss of ATRX/DAXX elevates the frequency of secondary structures at telomeric repeats, such as G4s and RNA/DNA hybrids, which may be driving events for the ALT pathway. ATRX has been shown to bind to G4 structures and ATRX deficiency leads to increased levels of G4s (120,283).

ALT cells need to adapt a mechanism that allows for the tolerance of chronic replication stress and coordination of timely chromatin deposition to provide topological stability during HDR. The HIRA histone chaperone complex is a promising candidate that could potentially compensate for loss of ATRX/DAXX function in ALT tumors. The HIRA chaperone complex comprises of HIRA, UBN1, CABIN1, and it collaborates with Anti-Silencing Function 1A Histone Chaperone (ASF1a) to deposit H3.3 in a replication-independent manner (88,284). HIRA is the central scaffold for the assembly of the complex subunits. The stability of the complex is dependent on the presence of all three components, since knockdown or removal results in reduction of

protein expression. The N-terminal WD40 repeat domain in HIRA associates with a weakly conserved domain slightly N-terminal to the Hpc2-related domain (HRD) in UBN1 (285). UBN1 is critical for H3.3 incorporation onto chromatin (88). HIRA interacts with CABIN1 through residues 736-963 of the C-terminal domain. While CABIN1 is dispensable for H3.3 incorporation, it contributes to maintaining the structural integrity of the complex (284). The HIRA B-domain, which spans residues 439-475, makes contact with the ASF1a N-terminal core (286). ASF1a contacts HIRA to deliver H3.3 histones to the HIRA complex for deposition onto chromatin. It is proposed that UBN1 can reject the ASF1a/H3.1 complex because it has greater binding affinity to H3.3. This ensures that only H3.3 is deposited by the HIRA complex (287,288). Homotrimerization of HIRA is crucial for its 3:2 interaction with CABIN1 as well as enrichment and activity at UV damaged sites (227,287).

HIRA-mediated H3.3 deposition underpins diverse biological functions. HIRA plays a role in DNA repair, cell senescence, sperm nucleus decondensation after fertilization, embryo development, and anti-viral immunity (226,275,289–298). It has been reported that HIRA promotes transcription restart after UVC irradiation (226). HIRA enhances *de novo* deposition of H3.3 at the damaged chromatin. This is critical for the bookmarking of damaged chromatin and subsequent priming for later transcription once the damage lesion is repaired. In addition, the HIRA complex can bind to regions of naked DNA without any sequence specificity to incorporate H3.3 by a nucleosome gap filling mechanism (291). This occurs at regions with transient naked DNA, such as sperm reprogramming or post-replication. RNA Pol II also associates with HIRA for additional targeting to promoters, coding regions, and a subset of cis-regulatory elements. This salvage pathway ensures that there are no nucleosome-free regions that would lead to chromatin defects. ChIP-seq and gene expression analyses demonstrate that most HIRA-binding sites

colocalize with UBN1, ASF1a, and H3.3 at the three main regulatory elements: promoters of active genes, active, and weak/poised enhancers (290). Overall, HIRA is involved in an intricate network of biological processes that could converge at ALT telomeres.

In this chapter, we show that the HIRA histone chaperone complex associates at ALT telomeres. HIRA is likely the sole histone chaperone for H3.3 deposition during HDR. HIRA-mediated chromatinization permits restrained replication stress that results in productive ALT telomere maintenance. PARylation targets HIRA to damaged ALT telomeres for rapid and faithful restoration of DSBs. However, PARG inhibition keeps HIRA at these lesions and perturbs incorporation of H3.3. Thus, HIRA retention at ALT telomeres has deleterious consequences on downstream HDR-mediated DNA synthesis and ultimately, cell survival.

4.2 Results

4.2.1 Enrichment of HIRA-UBN1-CABIN1 complex at ALT telomeres

Of the many potentially PAR-regulated factors identified by *wt*-Af1521 mass spectrometry, it was striking that peptides corresponding to constituents of the HIRA histone H3.3 chaperone complex (HIRA-UBN1-CABIN1) were highly enriched. This was in contrast with the histone H3.1/H3.2 chaperone complex Chromatin Assembly Factor (CAF1) complex consisting of three subunits CAF1a (p150), CAF1b (p60) and Retinoblastoma binding protein 4 (RBBP4) (Figure 23). The CAF1 complex differs from the HIRA complex because it only deposits newly synthesized H3/H4 in a replication-dependent manner (299). Meanwhile, H3.3/H4 can be incorporated during and outside of S-phase. In fact, the ATRX/DAXX complex deposits H3.3/H4

at pericentric heterochromatin and telomeres (279). Missense mutations in ATRX and DAXX are pervasive in ALT+ cancers, with one or both proteins not expressed in most ALT+ tumors or cancer cell lines (41,42). Consequently, HIRA may be the sole functional H3.3 histone chaperone complex for nucleosome assembly during G2/M in many ALT+ cancer cells. Therefore, it seemed plausible that HIRA, and its PARylation, could contribute to HDR repair associated activities at ALT telomeres, neither of which has previously been determined.

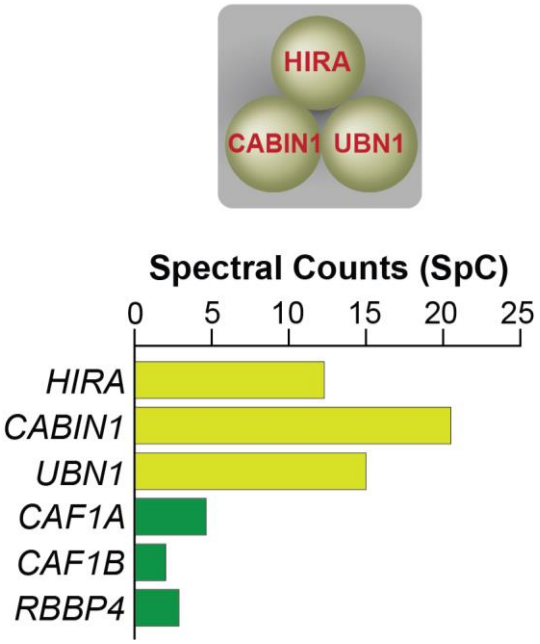

Figure 23. The HIRA complex is enriched at ALT telomeres. Spectral counts of the HIRA (HIRA-UBN1-CABIN1) and CAF1 (CAF1A-CAF1B-RBBP4) complexes Af1521-PAR proteomics. The CAF1 complex (green) is not enriched at ALT telomeres.

4.2.2 Depletion of HIRA complex abrogates HDR in ALT

HIRA is the molecular scaffold in the HIRA-CABIN-UBN1 chromatin assembly complex, in which knockdown of HIRA also co-depletes CABIN1 and UBN1, as was previously shown (291) (Figure 24A) Depletion of each protein abrogated APB levels and TRF1-FokI-induced

telomere clustering in U2OS and VA13 cells. HIRA depletion elicited the strongest effects (Figure 24B). By BrdU-IP we found that HIRA depletion strongly impaired G2-BIR (Figure 24C).

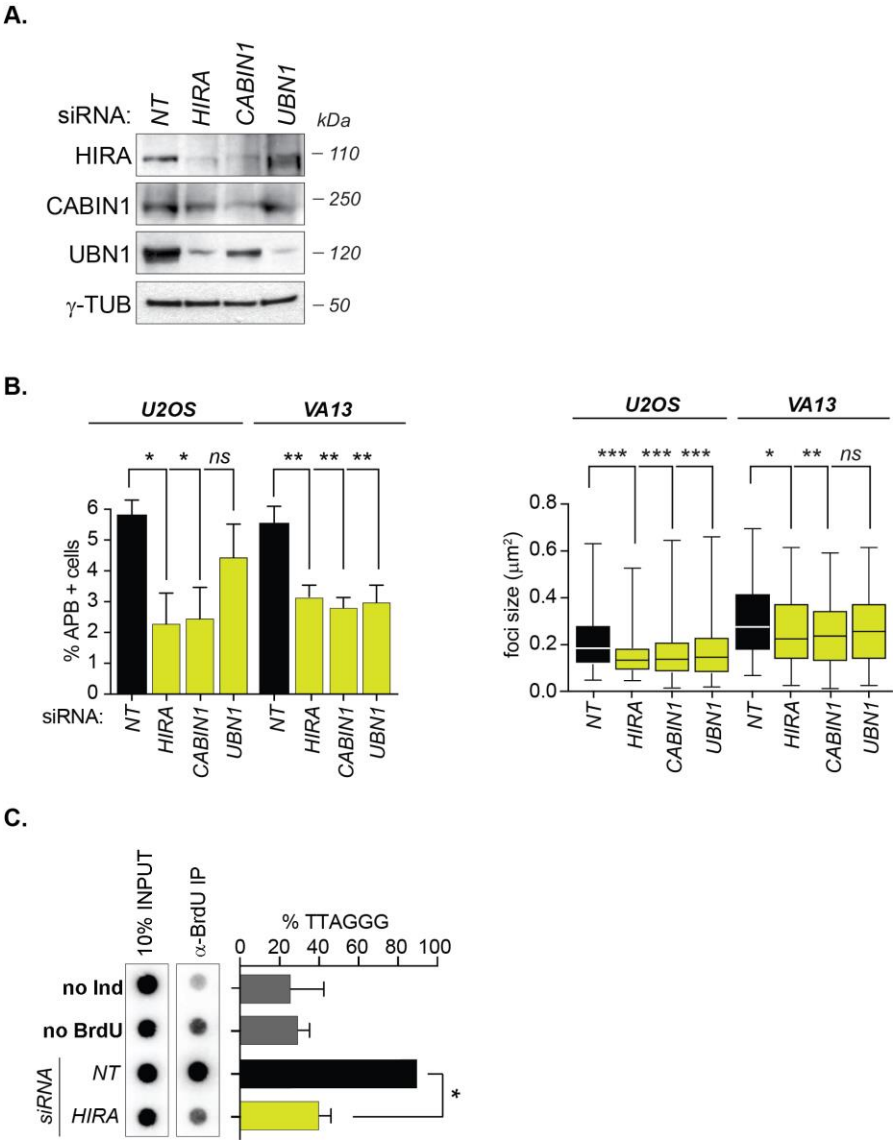

Figure 24. Depletion of HIRA impairs ALT telomere maintenance. A) Western blot validation of HIRA, CABIN1 and UBN1 knockdown. B) *Left:* Quantification of APBs and *right:* TRF1-FokI-induced clustering in U2OS cells following transfection with the indicated siRNAs. C) TRF1-FokI-mediated break-induced synthesis assay following transfection with non-targeting (NT) and HIRA siRNAs. B) *left:* n=1200 cells, *right:*150 cells and C) n=3. Statistical significance was determined using one-way ANOVA. *P≤ 0.05, **P≤ 0.001, ***P≤ 0.001, ****P< 0.001.

4.2.3 HIRA is responsible for H3.3 deposition at ALT telomeres

We reasoned that the phenotype observed with HIRA depletion is linked with deficiencies in histone H3.3 deposition at sites of G2-BIR. We confirmed this by combining transient ectopic expression of GFP-tagged histone H3.3 and HIRA depletion in G2-synchronized U2OS cells and WT TRF1-FokI cells, both of which allow for G2-BIR to occur. Here, we observed punctate foci corresponding to GFP-H3.3 that co-localized with telomeres in U2OS cells that were arrested in G2 with the cyclin-dependent kinase (CDK) inhibitor, RO-3306, and WT TRF1-FokI-induced U2OS cells (Figure 25A-B). However, these GFP-H3.3 foci were completely abolished upon depletion of HIRA.

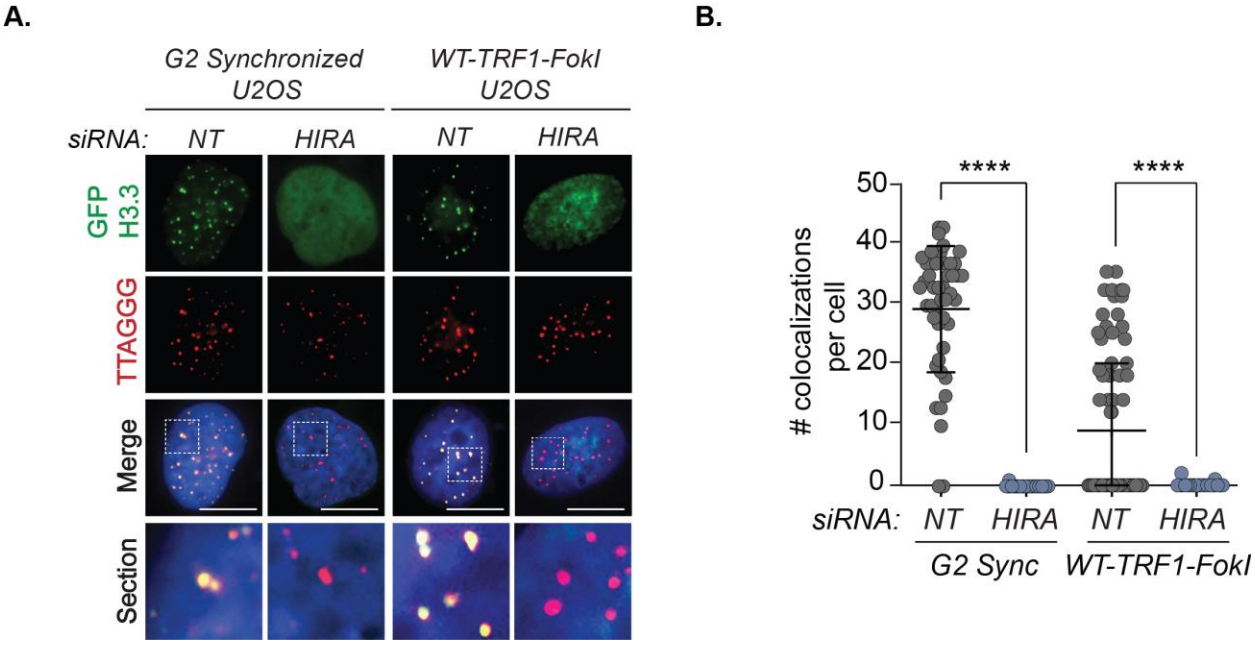

Figure 25. HIRA mediates H3.3 localization at ALT telomeres. A) Representative IF images of GFP-Histone H3.3 localization to telomeres in G2-synchronized and WT TRF1-FokI-induced U2OS cells. B) Quantification of colocalization between GFP-Histone H3.3 and telomeres in the conditions shown in A. All graphed data in the figure are mean ± SEM, n=75 cells. Statistical significance was determined using one-way ANOVA. *P≤ 0.05, **P≤ 0.001, ***P≤ 0.001, ****P< 0.001. All scale bars, 5μm.

The localization of transiently expressed YFP-HIRA to telomeres was not readily apparent in asynchronous U2OS cells, even though some vicinal associations were observed (Figure 26A). However, the telomeric accumulation of YFP-HIRA was readily evident and was accentuated by PARGi (Figure 26A-B). A small number of YFP-HIRA telomere associations were observed in cells expressing WT TRF1-FokI. PARGi markedly changed this with YFP-HIRA forming clear foci at telomeres harboring WT TRF1-FokI-induced DSBs. Telomeric YFP-HIRA foci were reduced in the presence of PARPi, indicative of a PARP1 dependency. In agreement with previous findings, we found that YFP-HIRA readily formed foci shortly after irradiation of U2OS cells with UV-C (Figure 48A-B). Although YFP-HIRA foci were also observed after exposure to ionizing radiation (γIR), their frequency was substantially lower. In these instances of DNA damage, the dependency on PARG inhibition was not as clear as what was observed in the context of YFP-HIRA accumulation at ALT telomeres. These set of experiments indicate that PAR-mediated HIRA assembly at ALT telomeres is responsible for H3.3 deposition during and outside of S-phase in ALT+ cancer cells.

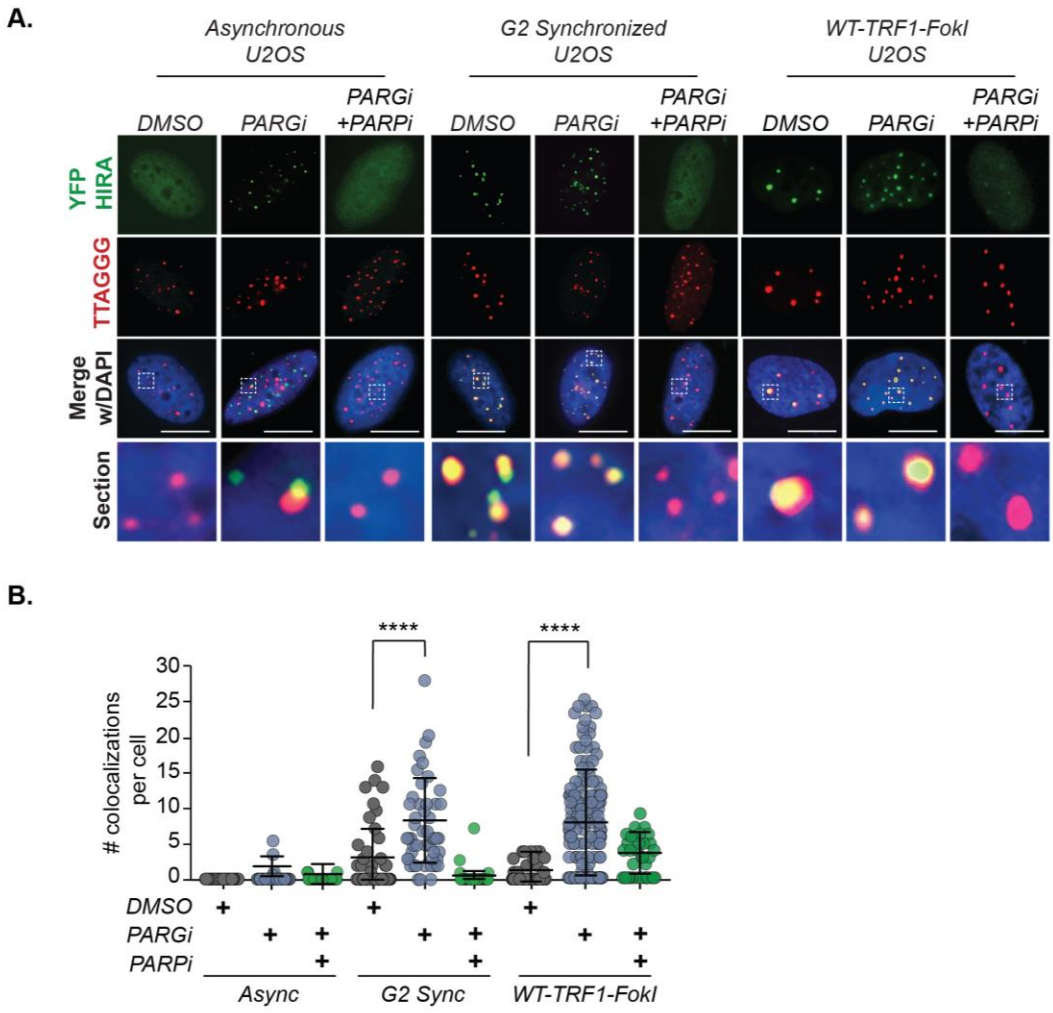

Figure 26. PAR-dependent localization of HIRA to ALT telomeres. A) Representative IF images of YFP-HIRA localization to telomeres in asynchronous, G2-synchronized and WT TRF1-FokI-induced U2OS cells treated with DMSO, PARGi or co-treated with PARGi and PARPi (all 5μM). B) Quantification of colocalization between YFP-HIRA and telomeres in the conditions shown in a. All graphed data in the figure are mean ± SEM, n=75 cells. Statistical significance was determined using one-way ANOVA. *P≤ 0.05, **P≤ 0.001, ***P≤ 0.001, ****P< 0.001. All scale bars, 5μm.

4.2.4 Identification of a PAR-modulated HIRA region

The requirement for PAR in recruitment of HIRA to ALT telomeres prompted us to determine whether HIRA was itself directly modified by *in vivo* PARylation assay. Indeed, the signature PAR smear corresponding to YFP-HIRA protein was detected only in WT TRF1-FokI cells, confirming that HIRA is PAR-modulated following telomeric DSB formation (Figure 27A). To determine the requirements for PAR modulation of HIRA, we used a series of mutants that disrupt HIRA complex formation via homotrimerization (W799A-D800A), HIRA binding to ASF1a (I461D), as well as Δ427-472 (also termed ΔB-domain) (227,286). By *in vivo* PARylation assay, we found that loss of the B-domain, and preventing homotrimerization, abolished YFP-HIRA PAR-modulation (Figure 27B).

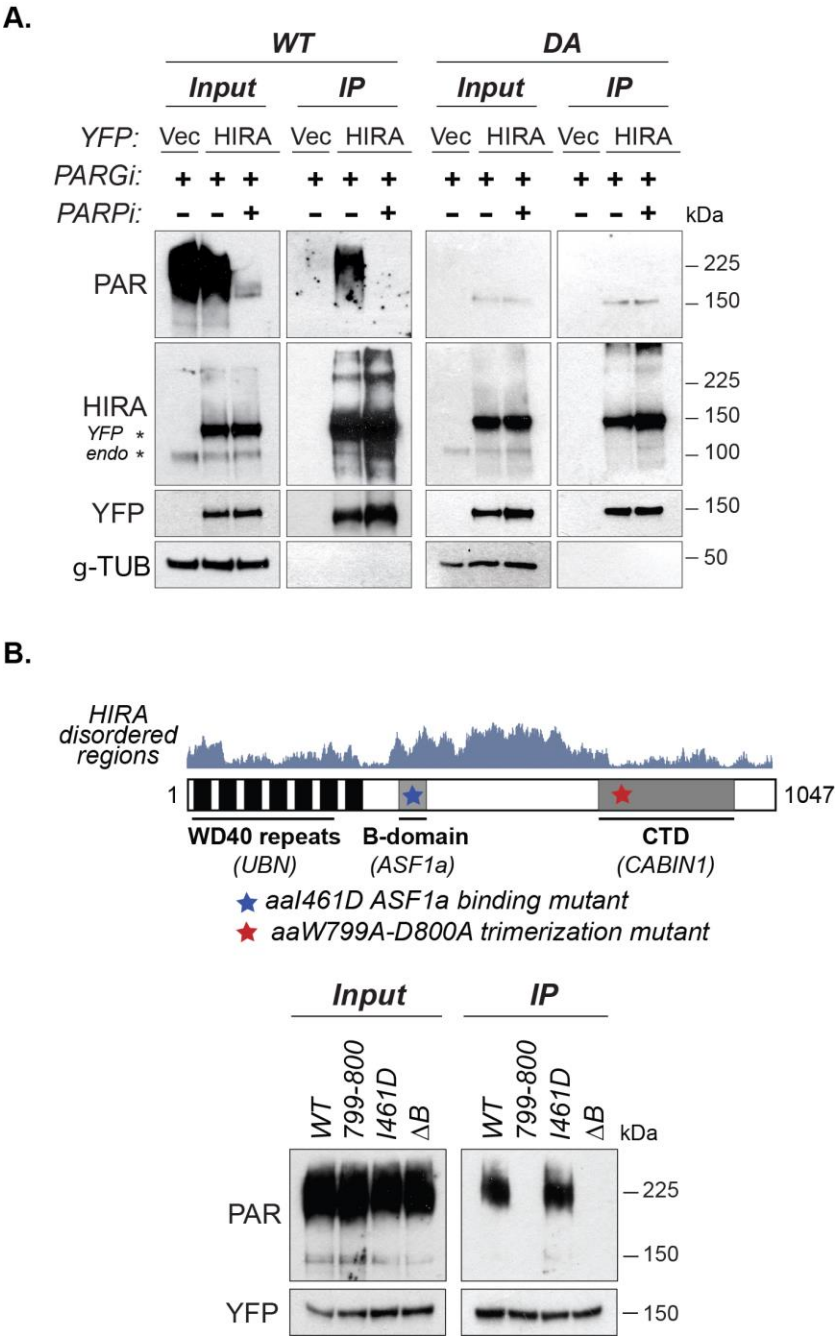

Figure 27. HIRA exhibits direct PAR-modulation. A) *In vivo* PARylation assay. YFP alone (Vec) or YFP tagged HIRA were transfected into WT/DA TRF1-FokI U2OS cells containing PARGi, or a combination of PARGi and PARPi to test for PARP1 dependency. Captured GFP proteins were subjected to western analysis and blotted with anti-GFP and anti-PAR (10H) antibodies. (B) *Top:* Schematic of HIRA domain structure. Mutated regions are shown in red and blue stars. *Below: In vivo* PARylation assay of WT, homo-trimerization (W799A-D800A) I461D mutants and ΔB domain truncated YFP-HIRA in WT TRF1-FokI U2OS cells.

4.2.5 PAR modulation of HIRA is critical for its role in ALT

We next determined whether loss of PARylation at these mutants is critical for the localization of HIRA to ALT telomeres (Figure 28A-B). The homotrimerization and B-domain mutants abrogated YFP-HIRA localization to TRF1-FokI DSBs (Figure 28B). Interestingly, the ASF1a interaction point mutant I461D could be PAR-modulated and retained the ability to localize to telomeric DSBs. However, deletion of the complete B-domain, which also encompasses the ASF1a binding I461 residue, abolished both PAR modulation and localization of YFP-HIRA to TRF1-FokI-induced DSBs.

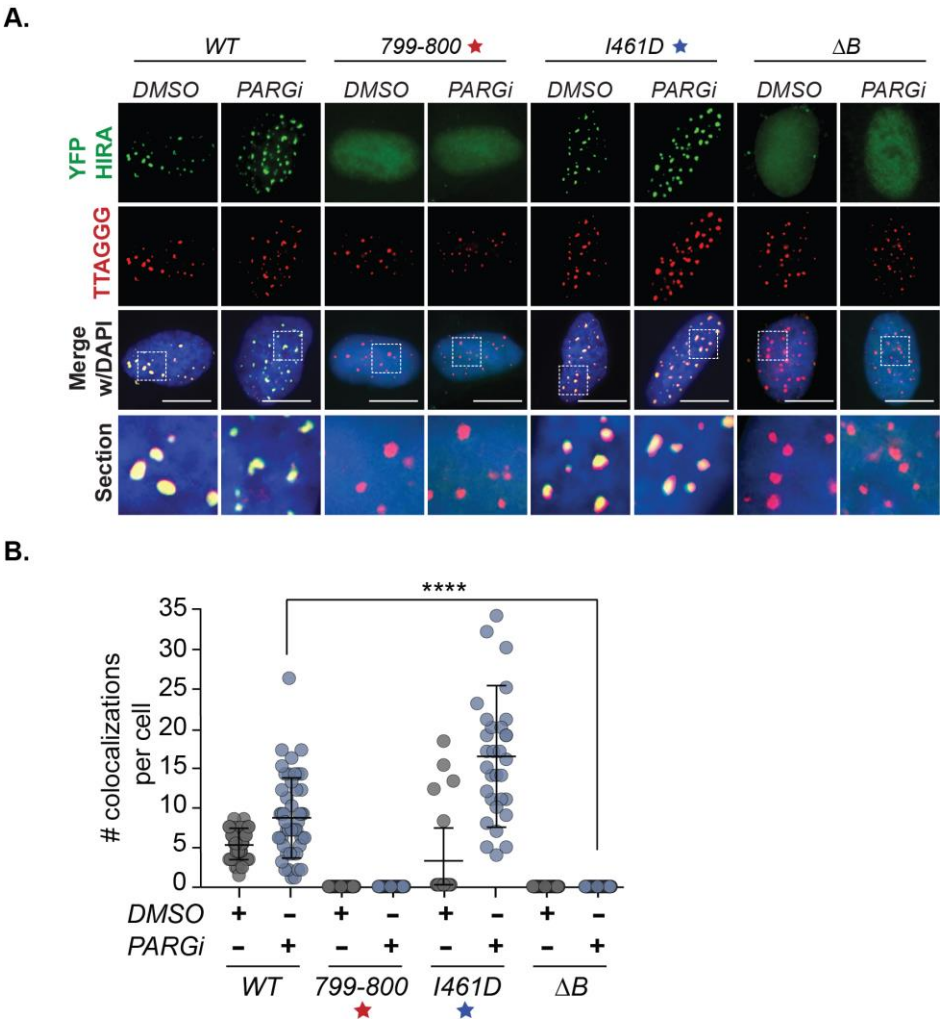

Figure 28. PAR-modulation of HIRA B-domain recruits HIRA to ALT telomeres. A) Representative IF images. B) Quantification of WT, W799A-D800A, I461D, and ΔB domain truncated mutants YFP-HIRA localization to WT TRF1-FokI telomeres. All graphed data in the figure are mean ± SEM, n=75 cells. Statistical significance was determined using one-way ANOVA. *P≤ 0.05, **P≤ 0.001, ***P≤ 0.001, ****P< 0.001. All scale bars, 5μm.

To determine if PAR modulation of HIRA might affect ALT, we examined whether ectopic expression of wildtype or mutants of HIRA could rescue the phenotypes of HIRA knockdown (Figure 29A). We found that PAR-modulated WT and ASF1a I461D mutants, but not non-PAR-modulated homotrimerization or ΔB-domain mutants, fully restored APBs and telomere clustering (Figure 29B). These observations indicated that the HIRA complex and PAR-regulation of the B-

domain in HIRA are critical for its recruitment and residency at telomeric breaks that are repaired by HDR during G2-phase. Taken together, this analysis reveals that HIRA is directly recruited to telomeric chromatin by PAR-dependent mechanisms during G2-phase. PAR-modulated HIRA mediates deposition of histone H3.3 at telomeric DSBs undergoing HDR in order to compensate for the loss of ATRX-DAXX.

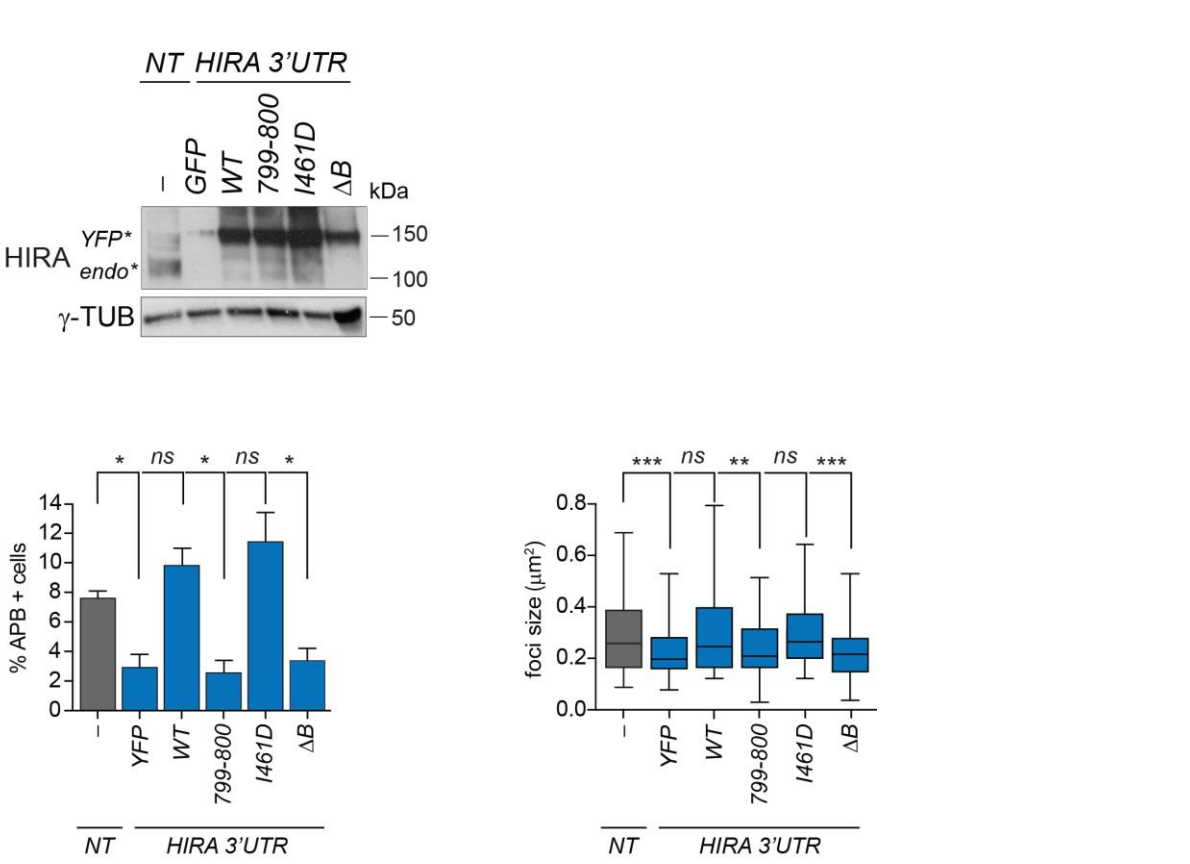

Figure 29. PAR-modulation of HIRA is essential for its function in ALT. A) Western blot showing depletion of endogenous HIRA and complementation with the indicated HIRA constructs in U2OS cells. B) *Left:* Quantification of APBs (%) in U2OS cells and *right:* TRF1-FokI-induced clustering in U2OS cells. All graphed data in the figure are mean ± SEM. B) *left*: n=1200 cells and *right*: n=150 cells. Statistical significance was determined using one-way ANOVA. *P≤ 0.05, **P≤ 0.001, ***P≤ 0.001, ****P< 0.001.

4.2.6 HIRA compensates for loss of ATRX/DAXX function in ALT cells

Due to the absence of functional ATRX-DAXX complex in ALT cells, HIRA is likely to be solely responsible for histone H3.3 deposition at ALT telomeres. To assess whether it usurps ATRX's role at telomeres, we reconstituted ATRX in U2OS cells using a previously characterized U2OS cell line, U2OS^{ATRX}, where ATRX expression can be induced with Doxycycline. Indeed, following induction of ATRX in these cells, transiently transfected YFP-HIRA was largely absent from WT TRF1-FokI DSBs after PARGi. Instead, a clear focal accumulation of ATRX was observed at telomeric DSBs (Figure 30A-B). This implied that HIRA fulfills an elevated role in ALT cancer cells and its prolonged depletion could be cytotoxic.

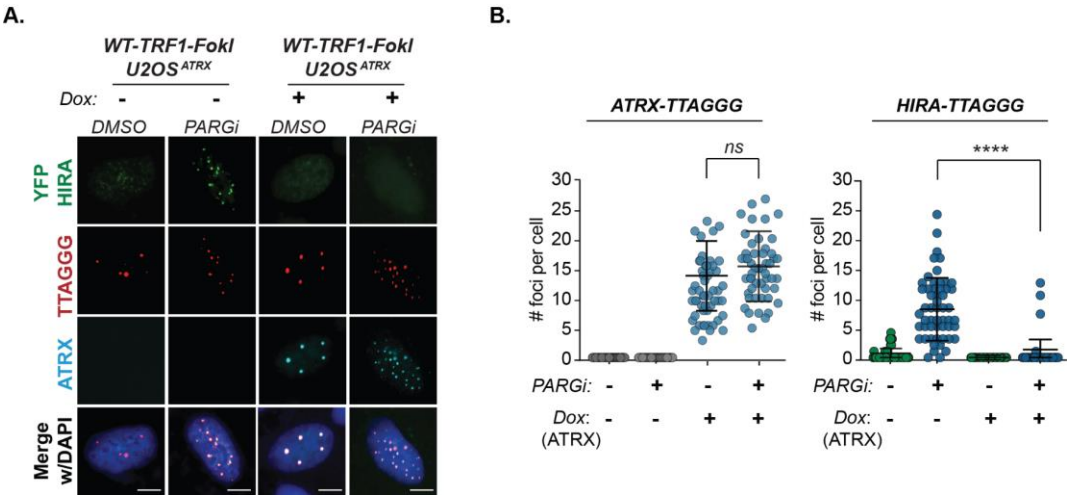

Figure 30. HIRA localization to ALT telomeres relies on loss of ATRX. A) Representative IF images of YFP-HIRA localization in U2OS cells expressing WT-ATRX following addition of Doxycycline (40ng/ml). B) Quantification of ATRX-TTAGGG and (YFP-HIRA)-TTAGGG foci in U2OS^{ATRX} cells ± (40µg/µl) for 5 days. All graphed data in the figure are mean ± SEM, n=150 cells. Statistical significance was determined using one-way ANOVA. *P≤ 0.05, **P≤ 0.001, ***P≤ 0.001, ****P< 0.001.

Notably, we found that stable depletion of HIRA using independent lentiviral expressed short hairpin RNAs elicited a more potent cytotoxic effect in ALT+ U2OS, Saos2, LM216J cells than in TEL+ HOS, SJSA1, LM216T counterparts (Figure 31 and Figure 49). Thus, HIRA gains an elevated importance in ALT+ cancer cells – perhaps as an adaptation to the loss of functional ATRX and DAXX. This implicates HIRA as a target for a novel epigenetic synthetic lethal interaction with ATRX deficiency that could specifically target ALT+ cancers.

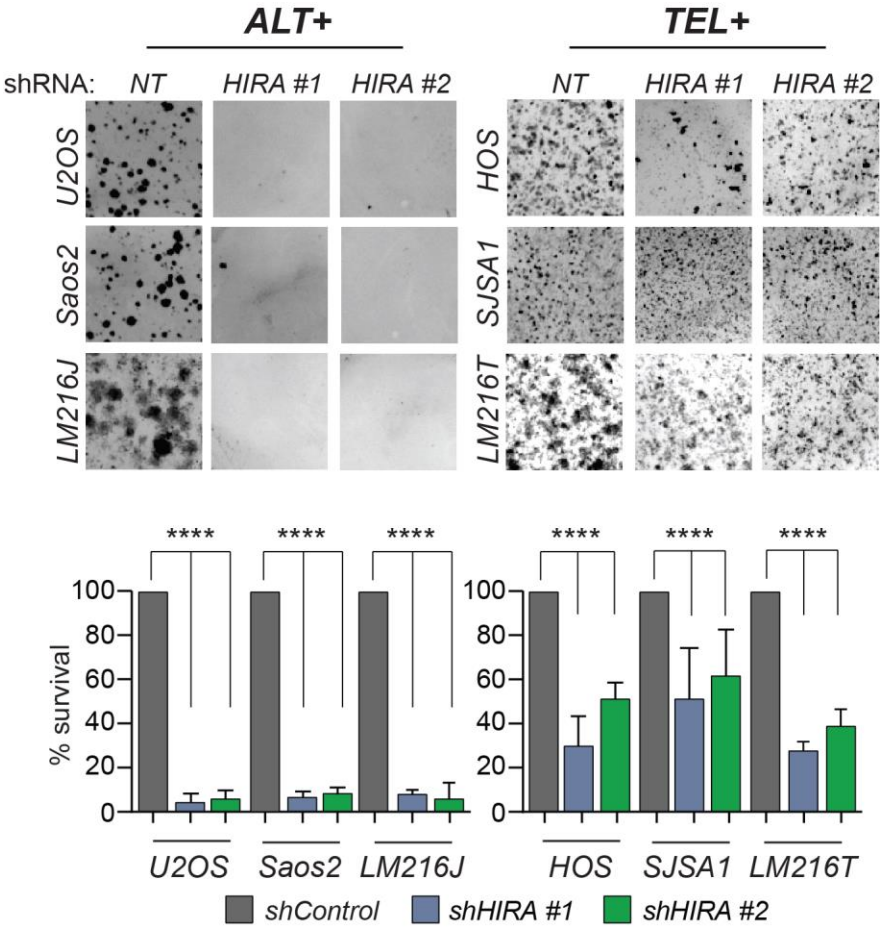

Figure 31. Loss of HIRA induces greater cytotoxicity in ALT cancers. Representative images and quantification of proliferation assays by crystal violet staining with the indicated ALT+ and TEL+ cell lines stably expressing scrambled non-targeting (*NT*) and HIRA shRNAs (#1 and #2) for 5 days. All graphed data in the figure are mean ± SEM, n=3. Statistical significance was determined using student t-test. *P≤ 0.05, **P≤ 0.001, ***P≤ 0.001, ****P< 0.001.

4.3 Discussion

Chromatin reorganization is necessary to coordinate the accessibility of damaged ALT telomeres for repair factors that mediate HDR processes. As described in chapter 2, one facet of disrupted PAR metabolism is the alteration of protein dynamics during complex assembly and compartmentalization of damaged telomeres. In addition, the perturbation of HDR observed upon PARG inhibition can also arise from aberrations in DNA synthesis and resulting ssDNA gaps. It has been established that PAR accumulates at replication intermediates to prevent untimely processing (179). This is also consistent with studies demonstrating a role for PARP1 and PARG in replication fork stabilization (197,198). However, ssDNA gaps can also accumulate due to defects in chromatin assembly and provoke replicative stress, which are recurrent factors in initiating and sustaining the mechanisms of the ALT pathway (300). When present, ATRX and DAXX form a multifunctional complex that not only functions as the default telomeric histone H3.3 chaperone complex, but also fulfills additional roles to alleviate replicative stress and DNA damage at telomeres (228). For instance, due to the intrinsic inefficiency of repair-coupled DNA synthesis during G2-phase, it was proposed that ATRX physically associates with PCNA and Polδ to maximize the efficiency of DNA synthesis coupled histone H3.3 deposition by resolving replicative barriers like G4-structures (282). It thus seems logical that the restoration of chromatin at ALT telomeres takes on greater urgency due to the loss of functional ATRX and DAXX.

Our data indicates that the HIRA complex plays a critical role at ALT telomeres since depletion of HIRA and the complex subunits abrogates HDR processes that mediate ALT. As seen in previous studies, depletion of HIRA severely decreases protein expression for CABIN1 and UBN1, which confirms that HIRA serves as the molecular scaffold for the stable assembly of the complex (284,285). Depletion of UBN1 and CABIN1 also results in decreased HIRA expression,

showing that each subunit contributes to the stability of the HIRA complex. Decreased levels of UBN1 leads to diminished incorporation of H3.3 onto chromatin. On the other hand, depletion of CABIN1 was shown to be dispensable for H3.3 deposition (88,284,287).

We propose that HIRA recruitment represents a fail-safe to prevent inadequate chromatinization of ALT telomeres and that PARylation plays a major role in enabling this adaptation. This is in line with a role for HIRA to preserve chromatin integrity that would be modulated by PARylation. Previous studies have shown that HIRA associates transiently to UV-C damaged chromatin prior to repair (226). As above, the greater detection of HIRA at telomeres upon PARG inhibition likely reflect its impaired dissociation from initial binding sites at telomeric DSBs. Due to the immobilization of HIRA, chromatin restoration could be uncoupled from G2-BIR since chromatin imposed topological barriers can block replisome progression. Immobilization of HIRA could also impinge on chromatin expansion from the DSB site by altering localized histone modification patterns, histone H4 lysine 16 acetylation for example, that contribute to chromatin expansion at break sites (296).

However, in G2 and TRF1-FokI cells, few HIRA foci still persist at ALT telomeres without PARG inhibition, suggesting that HIRA can be partially recruited by other PAR-independent mechanisms. In fact, Zhang et al. showed that RPA1 directly recruits HIRA to regulatory elements and regulates H3.3 deposition in the G1 phase of the cell cycle (301). RNA transcripts at promoters and enhancers may generate R-loop structures, which contain a DNA-RNA hybrid and displaced ssDNA, to which RPA can bind to. Similarly, ALT cancers contain telomeric repeat-containing RNA (TERRA), which are a class of long noncoding RNAs transcribed at telomeres. These can also form R-loops and render ALT telomeres recombinogenic. It is possible that HIRA can localize to RPA-bound R-loops to alleviate replication stress in ALT. However, this likely does not occur

in parallel with PARylation since our unpublished data and data from Illuzzi et al. show that PAR accumulation displaces RPA from telomeric DNA and chromatin, respectively (302). In addition, UBN1 harbors a lysine-rich middle domain that binds to DNA without sequence specificity (288). It also binds to free H3.3, but not nucleosomes or tetrasomes. It is speculated that UBN1 can target HIRA to chromatin or stretches of nucleosome-free DNA. UBN1-mediated targeting has been reported on HIRA's role in a gap-filling mechanism. Further studies need to be completed to further elucidate the interplay between different factors that mediate HIRA localization to ALT telomeres.

Blocking PARylation of HIRA interferes with its recruitment to ALT telomeres, with ensuing defects in HDR that largely phenocopied HIRA depletion. Thus, we sought to determine the region of HIRA that was PARylated in order to observe whether this could result in the uncoupling of chromatin restoration from DNA synthesis. The homotrimerization (W799A-D800A) mutant does not form a HIRA complex and is not enriched at damaged sites upon UV irradiation (227). Similarly, the absence of complex formation could hinder its ability to become PARylated and localize to damaged lesions in ALT. The ASF1a binding mutant (I461D) localizes to ALT telomeres and rescues the suppression of ALT that is seen with HIRA depletion. The I461D mutant is sufficient to abolish HIRA binding to ASF1a (227). On the other hand, the B-domain mutant (Δ427-472), which contains the I461 residue, cannot be recruited to ALT telomeres and does not restore HIRA function. This suggests that PARylation of HIRA proceeds ASF1a binding and is key for HIRA enrichment at ALT telomeres.

It seems significant that the PARylation of HIRA occurs within its B-domain. Its location within the disordered region of HIRA is consistent with the preferential targeting of PARylation to low complexity (LC) or disordered protein regions that are important conduits of adaptive

protein interactions (224). Though the precise functional contribution of the B-domain to HIRA function remains to be fully elucidated, this region makes contacts with ASF1a, suggestive of a pivotal role in histone H3.3 transfer and deposition (286). In addition to ASF1a, histone deposition at DSBs was shown to involve PARylation of constituents of the Nucleosome Remodeling/Deacetylase (NuRD) complex, some of which have previously been implicated in telomeric HDR (116,204). It would be of interest to determine whether PARylation of HIRA influences the recruitment of other PAR-regulated histone deposition factors. This could provide insights as to how the sequestration of HIRA to ALT telomeres and telomeric DSBs is distinct from mechanisms that recruit it to transcriptional units and sites of UV-C damage.

Finally, it should be noted that even though HIRA efficiently reconstitutes chromatin with histone H3.3, it does not fulfill ATRXs other roles in mitigating replicative stress (228,279,282,303). Aberrant secondary structures (e.g. G4s, ssDNA loops) that would otherwise be dealt with could remain and impair chromatin assembly. Shelterin would also not bind such structures. In this way, HIRA's inability to fully compensate for ATRX-DAXX would contribute to basal replicative stress and stochastic DNA damage that is observed in ALT cells lacking ATRX and DAXX. However, it also provides a rationale for the greater dependency on HIRA that was exhibited by the subset of ALT cells used in this study. Investigations into the outcomes of HIRA deficiency on ALT cancer cell viability and the mechanisms by which cells succumb to this vulnerability could be expanded in precise detail. If proven that HIRA expression and function at telomeres is a determinant of ALT cancer cell survival, inhibitors of HIRA expression or HIRA protein regulation could provide an attractive opportunity for anti-ALT therapy development. This strategy will capitalize on the nearly ubiquitous absence of ATRX and/or DAXX in ALT+ cancer cells.

4.4 Methods

4.4.1 Statistics

GraphPad Prism was used to calculate statistical significance for one-way ANOVA or student t-test. Statistical tests, number of cells scored, and biological replicates are indicated in the figure legends. *P≤ 0.05, **P≤ 0.001, ***P≤ 0.001, ****P< 0.001.

4.4.2 Cell Culture

U2OS, Saos2, Hela LT, HOS, SJSA1 cell lines were obtained from ATCC. VA13, LM216T/J and WT/DA TRF1-FokI U2OS cell lines were obtained from Roger Greenberg (University of Pennsylvania). U2OS^{ATRX} cell line was acquired from David Clynes (University of Oxford). Each cell line was cultured in DMEM +Glutamax (Life Technologies) supplemented with 10% bovine growth serum or 10% fetal bovine serum. U2OS^{ATRX} cells were specifically grown in tetracycline-free FBS (Takara). Cells were cultured at 20% O_2 and 7.5% CO_2. U2OS, HeLa LT and 293FT cell lines were validated by STR profiling and confirmed mycoplasma free by ATCC cell line authentication services.

4.4.3 siRNA knockdown

For siRNA knockdown the *On-Target Plus (OTP)* siRNA SMARTpools from Dharmacon (GE) were used. To deplete endogenous HIRA for rescue experiments siRNA targeting the 3'UTR of HIRA mRNA (see Supplementary Table S1) synthesized and purchased from Dharmacon (GE).

400,000 cells were seeded per well of a 6-well plate containing growth medium without antibiotics. 4hrs later cells were transfected. siRNAs and Dharmafect were diluted in OptiMEM (Life Technologies). A working siRNA concentration of 20nM was used. We used 2.5 μL Dharmafect transfection reagent per well. The transfection reagent mixture was added dropwise to one well in 1.8 mL of media without antibiotics. The next day, cells were transferred to 10-cm plates with coverslips. Transfection medium was replaced with complete culture media. Cells were harvested at 72hrs post transfection. Inhibitors were added 24 hours prior to collection.

4.4.4 Lentiviral production and infection

pLKO-based lentivirus was produced in 293FT cells by co-transfecting pLKO constructs containing either control or shRNAs against HIRA together with psPAX2 (#12260) and pMD2.G (#12259) packing plasmids (Addgene) to produce lentivirus. 48hrs after transfection, filtered supernatants were used to infect cell lines. Cells were selected with puromycin for 2 days and protein knockdown was analyzed by western blot.

4.4.5 APB Quantification

After 72 hours of siRNA knockdown, coverslips from 10-cm plates were collected for APB analysis. Anti-PML antibody was used in conjunction with telomere-FISH to identify APBs. Cells were visualized by conventional florescence with 40X objective (1.4 oil) using a Nikon 90i microscope. Large image scans of 3x3 fields were taken. Colocalization of PML and telomeres were analyzed using a macro in the NIS Elements software (Nikon). APB+ cells were scored if there was at least one colocalization event per cell.

4.4.6 TRF1-FokI Telomere Clustering

After 48 hours of siRNA knockdown, mcherry-DD-ER-WT TRF1-FokI U2OS cells were induced by adding 40ng/mL Doxycycline. After additional 24 hours, 4-OHT (1μM) and Shield1 ligand (1μM) were added to the media for 4 hours. Inhibitors were added at the start of induction. Cells were processed for immunofluorescence and telomere number and size were quantified using NIS-Elements software (Nikon).

4.4.7 BrdU Pulldown Dot Blot

The BrdU pulldown was performed after 72 hours of siRNA knockdown of HIRA in WT TRF-FokI U2OS cells. 48 hours post siRNA transfection, 40ng/mL Doxycycline was added to the media. 24 hours later, 4-OH (1μM) and Shield1 ligand (1μM) were added for a total of 4 hrs. The last 2 hrs, cells were pulsed with 100μM BrdU (Sigma) before collection. Extracted genomic DNA was sheared by sonication into 100–300 bp fragments. Sheared gDNA was denatured for 10mins at 95°C and cooled in an ice-water bath. Denatured gDNA was incubated with 2μg anti-IgG (Sigma) or anti-BrdU antibody (BD) diluted in immunoprecipitation buffer (0.0625 % (v/v) Triton X-100 in PBS) rotating overnight at 4°C. The next day, samples were incubated with 30μl Protein A/G agarose beads (Santa Cruz) pre-bound to a bridging antibody (Active Motif) for 1h rotating at 4°C. Beads were then washed three times with immunoprecipitation buffer and once with TE buffer. Beads were then incubated twice in elution buffer (1% (w/v) SDS in TE) for 15mins at 65°C. Pooled eluates were purified with ChIP DNA Clean & Concentrator kit (Zymo). Samples were diluted into 2×SSC buffer, treated at 95°C for 5mins, and dot-blotted onto an Amersham Hybond-N+ nylon membrane (GE). The membrane was then denatured in a 0.5N NaOH/1.5M

NaCl solution, neutralized, and ultraviolet crosslinked. The membrane was hybridized with ^{32}P-labelled $(TTAGGG)_4$ oligonucleotides in Church Buffer overnight at 55°C. The next day, the membrane was washed four times in 2×SSC buffer and once in 2xSSC/0.5% SDS, exposed onto a storage phosphor screen (GE Healthcare), scanned and analyzed with ImageJ.

4.4.8 H3.3 and HIRA IF

GFP-H3.3 and HIRA-YFP were transiently transfected into U2OS or WT TRF1-FokI U2OS cell lines. U2OS cells were arrested in G2 by adding 1 μM of RO-3306 at 24 hours post transfection. 40 ng/mL of Doxycycline was added to WT TRF1-FokI U2OS cells. Inhibitors were also added at this time point. 24 hours later, WT TRF1-FokI U2OS cells were induced with 4-OHT and Shield Ligand. Cells were pre-extracted for 5 minutes at RT using pre-extraction buffer (0.06M EGTA, 0.5 PIPES, 0.5M $MGSO_4$, 3M KCl, and 0.5% Triton-X). Cells were then fixed in 4% PFA at 4^{o}C. IF proceeded normally after this step.

4.4.9 *In Vivo* PARylation Assay

GFP-immunoprecipitation was performed with GFP-TRAP®_A agarose beads (Chromotek). Briefly, 1 x 10^6 WT TRF1-FokI cells were seeded in a 10cm dish. ~24hrs later, cells were transfected with GFP-constructs using Lipofectamine 2000 (Invitrogen) as per manufacturer's instructions and 40ng/mL Doxycycline was added to the media as before. Cells were later induced with 4-OHT (1μM) and Shield1 ligand (1μM) for 4hrs with the addition of PARGi (5μM). Cells were harvested using ice-cold PBS, scraped from the dish and transferred to pre-cooled tubes. Cell pellets were resuspended in 200μL ice-cold RIPA buffer (10mM Tris-HCl

(pH 7.5), 150mM NaCl, 0.5mM EDTA, 0.5% NP-40, 0.09% Na-Azide) with 1mM PMSF, 2.5mM $MgCl_2$, 1mg/ml DNase (Pierce) and protease inhibitor cocktail (Sigma). To extract HIRA proteins, modified RIPA buffer (500mM NaCl) was used as before. Tubes were placed on ice for 30mins with extensive pipetting every 10mins. Tubes were centrifuged at 20,000x g for 10 min at 4ºC and lysates were transferred to pre-cooled tubes. 300µL ice-cold dilution/wash buffer (10mM Tris-HCl (pH 7.5), 150mM NaCl, 0.5mM EDTA, 0.018% Na-Azide) with 1mM PMSF, 2.5mM $MgCl_2$, and protease inhibitor cocktail (Sigma) was added to tubes. 50µL of lysate was resuspended in 50µL 4X LDS buffer to save as 10% input samples. GFP-TRAP®_MA magnetic beads were equilibrated in dilution/wash buffer. 25µL of the bead slurry was added to each tube and rotated for 1hr at 4ºC. Beads were magnetically separated and washed twice with wash/dilution buffer. Beads were resuspended in 100µL 4X LDS buffer and boiled for 10mins at 95ºC. Beads were magnetically separated and SDS-PAGE was performed with the supernatant. PARylated proteins were detected using specific anti-PAR (10H) antibody.

4.4.10 ATRX re-expression

ATRX cDNA was cloned into the Tet-on 3G Inducible Expression System (Clontech) and transfected into using Xfect transfection reagent (Clontech), to generate the U2OS^{ATRX} stable cell line. This was acquired from David Clynes (University of Oxford). 100 ng/mL of Doxycycline was added onto cells for 5 days. WB analysis was performed to ensure re-expression of ATRX in U2OS cell lines that were treated with Doxycycline. All experiments were performed after U2OS^{ATRX} cells have been treated with Doxycycline for 5 days.

4.4.11 Clonogenic Assay

Clonogenic assays were started after cells were infected with lentivirus carrying control or shRNAs against HIRA. 2 days post infection, 2000 cells were seeded in 6 well plates in duplicate and cultured for 7 days with 1μg/mL of puromycin selection. Plates were then fixed and stained in a 1% crystal violet solution. Plates were scanned and analyzed with ImageJ, which was used to count positive stained colonies and calculate total cell coverage per well.

5.0 Future Directions

This thesis highlights the importance of controlled ALT activity to limit the toxicity of rampant DNA damage. Disrupted PAR metabolism tips the delicate balance between pro- and anti-recombinogenic signals for productive ALT activity. Our data shows that PAR-regulated HIRA fulfills a protective function at ALT telomeres. HIRA exhibits elevated importance in ALT+ cancers to compensate for the loss of ATRX/DAXX. This body of work has given rise to several future directions that would provide greater insight into the molecular events that drive ALT telomere maintenance. Taken together, these proposed experiments provide a stepping stone to the development of anti-ALT therapeutic agents.

5.1 Does Disrupted PAR Metabolism Have Direct Effects on ALT Telomere Maintenance?

Perturbations in PAR metabolism alter ALT activity. While PARPi substantiates ALT phenotypes and HDR processes, PARGi holds the opposing effect and leads to substantial loss of telomere length. Additionally, ALT cancers exhibit modest sensitivity to prolonged exposure to PARGi. Although it is undisputed that PARGi elicits a negative impact on ALT activity, it will be important to test if the effects are due to direct effects of PARGi on ALT-mediated mechanisms or indirect effects due to PARP1 and PAR accumulation at damaged sites. PARP1 overactivation leads to massive consumption of NAD+ and consequential depletion of cellular ATP pools (304). Prolonged PARP1 activation decreases the half-life of NAD+ in a dose-dependent manner. In fact, mammalian cells exposed to a high dosage of genotoxic stress display 20% reduction in NAD+

within 5-15 minutes. This depletion of cellular NAD+ pools also affects other metabolic processes that rely on NAD+ as a cofactor to generate ATP, such as glycolysis and tricarboxylic acid cycle (TCA cycle) (305–307). Additionally, accumulation of PAR polymers is detrimental to cells and leads to a cellular process known as PARthanatos, which harnesses cytological and morphological features of apoptosis and necrosis (159,160). Cellular toxicity is dependent on the length and complexity of PAR polymers. Direct delivery of PAR polymers that consisted of greater than 60 ADPr units are toxic to neurons and Hela cells (159,161). Toxicity is observed at 20 nM of PAR and cell death induced at 80 nM of PAR.

NAD+ and ATP measurements can be performed to test the indirect effects of cellular energy consumption. There are several NAD/NADH and ATP/ADP quantification kits that are commercially available (308). The NAD/NADH kit is based on an enzymatic cycling reaction that reduces NAD+ to NADH. NADH then reacts with a colorimetric probe that can be measured at 450 nm. The ATP/ADP assay works through the reaction of released cellular ATP with the substrate (D-luciferin) to produce light. ADP is also converted to ATP, which then reacts with D-luciferin as in the first step. As a result, this measures the total ADP and ATP levels as well as ATP concentration in cells. We can measure NAD+ and ATP levels in TEL+ and ALT+ cells that are subjected to acute or prolonged exposure to PARGi, as reported in chapter 2.

These experiments would likely show that NAD+ and ATP levels drop in both ALT+ and TEL+ cell lines because PARGi prevents PAR metabolism, which leads to excessive consumption of NAD+ as a substrate to generate PAR. This is probably more evident during extended PARGi treatment due to gradual depletion of a limited NAD+ pool. Thus, we can determine the appropriate dosage and timing of PARGi that elicits direct effects as oppose to toxicity from PAR accumulation. In particular, ALT+ cells may either exhibit greater energy depletion or higher

sensitivity due to the burden of telomeric damage. To further elaborate on this, we can rescue energy depletion by administering dihydronicotinamide riboside (NRH), which is a potent NAD+ concentration enhancer both *in vitro* and *in vivo* (309). NRH structurally resembles NAD+ precursors and can be converted by cellular ATP-dependent kinase activity. NRH-treated cells are resistant to cell death induced by hydrogen peroxide and methylmethane sulfonate. Likewise, the phenotypes observed with PARGi in ALT+ cells may be attenuated. However, if ALT+ cells are not fully restored upon addition of NRH, then this would imply a specific and direct mechanism of PARGi at ALT telomeres.

5.2 How does PAR Modulation Contribute to HDR Pathway Choice?

One of the outstanding questions in the field is what determines telomere synthesis via RAD51-dependent or RAD51-independent mechanisms at ALT telomeres. Several studies have identified the unique molecular machinery involved in each HDR pathway. First, telomeric DSBs undergo resection that is mediated by the MRN complex, BLM-EXO1-DNA2, or WRN-DNA2 (54,244). Subsequently, ATR activation leads to RPA/RAD51/HOP2-MND1-mediated homology searches and inter-telomeric recombination that occur primarily in S-phase (60,96). There are two RAD51-independent pathways that have been reported: spontaneous mitotic DNA synthesis (MiDAS) and G2-BIR in G2/M (93,98). These processes are optimal during the narrow window of late G2 and mitosis when there is not sufficient time for RAD51-driven homology searches. MiDAS is RAD52-dependent and engages in MMBIR (less than 1-6 nucleotide required homology) for template switching (109–111). Min et al. proposed that ALT cells exhibit more telomeric replication defects that lead to engagement of MiDAS (93). However, MiDAS is

restricted to prometaphase and occurs at a low frequency, which likely means that it is not the primary mode of DNA synthesis in ALT cancers (94). On the other hand, G2-BIR can persist in mitosis (interphase, prometaphase, and metaphase) and does not rely on RAD52 and SLX4-MUS81. Ultimately, these RAD51-independent pathways converge on a noncanonical replisome that comprises of PCNA-RFC-POLD3 for DNA synthesis (94,98).

ALT telomeres engage in these distinct HDR pathways depending on the initial telomere lesion and cell cycle phase. However, the differential contribution of cellular factors and initial stimulus of each pathway in ALT still remains poorly understood. Chapter 2 demonstrated that PARGi disrupted both canonical and non-canonical HDR, resulting in negative consequences for ALT telomere maintenance. Chapter 3 revealed that the molecular machineries involved in these diverse repair pathways are regulated by PARylation. A reasonable explanation could be that PARylation perturbs cell-cycle distribution and increases the probability of specific HDR processes to occur during a particular cell cycle phase. PARGi-treated ALT cells display modest perturbations in cell cycle progression, with some cells accumulating in S-phase. (Hoang et al. unpublished data). In addition, a similar cell cycle is observed in shControl and shPARG Hela LT cells in unstressed conditions and after short HU treatment (302). PARG-deficient cells haven been shown to exhibit impaired S-phase progression upon prolong exposure of HU. This suggests that the basal level of replication stress in ALT cells mimics that of short HU exposure as ALT telomeres undergo recurrent cycles of stochastic DNA damage.

Another avenue to explore is whether PARGi favors canonical or non-canonical HDR. A simple approach would be to parse our Af1521 mass spectrometry data, as discussed in chapter 3, to see whether PARylated factors at telomeric DSBs belong to either RAD51-dependent or -independent pathways. We could perform the Af1521 pulldown in isogenic cell lines LM216J

(ALT+) and LM216T (TEL+) WT TRF1-FokI cell lines that are synchronized at specific cell cycle phases. This experiment is under the premise that these are competing HDR mechanisms and do not occur in parallel with each other. The expectation would be that the PARylome changes depending on cell-cycle progression since distinct HDR pathways are employed at either S and G2-phases or early and late mitosis. The resulting PARylomes of ALT+ and TEL+ cancers will likely be fundamentally different since ALT+ cells have characteristic features that prime them for increased recombination. This is supported by the distinct telomeric composition of unperturbed U2OS and Hela LT cells, in which 139 proteins were specific to ALT+ cancers (87). Additionally, we could expand our *in vivo* PARylation assay to include known factors of RAD51-dependent and -independent factors using the same conditions described above. Together, this would yield useful insights into the diverse contributions of PARylation at different time points in the regulation of ALT activity.

Proteomics has its limitations though and cell-based studies need to be performed to validate the fine-tune control of HDR mechanisms by PARylation. In our proteomics strategy, it is likely that some key mediators will not be accounted for in the mass spectrometry data due to their low abundance, poor sequence coverage, or loss during the Af1521 pulldown. Alternatively, the mode of replication can be indicative of HDR pathway choice. RAD51-dependent mechanisms will undergo semi-conservative replication while RAD51-independent mechanisms engage in conservative replication that is mediated by break-induced replication processes. We can utilize a triple-FISH method to differentiate between telomeric semi-conservative and conservative replication (Figure 32). Previous studies have used Cyclin E overexpression to induce DNA replication stress at U2OS cells to trigger repair by BIR. Cyclin E-potentiated fork collapse leads to elevated conservative synthesis (97).

Thus, we would use U2OS WT TRF1-FokI that are treated with PARGi to see if this alters the preference in an HDR mechanism. Metaphase chromosomes that are treated with BrdU and BrdC for one cell-cycle will be subjected to three consecutive strand-specific FISH staining steps (97) (Figure 32). First, metaphases are stained using telomere strand-specific dual color FISH under denaturing conditions. This marks both telomeric strands for reference in subsequent staining steps. Second, after destaining, metaphases are labelled by non-denaturing, telomere strand-specific, dual color CO-FISH. Newly synthesized DNA strands are degraded and only parental strands that have been replicated in a semi-conservative manner can hybridize with the telomeric probes. Conservatively replicated telomeres would result in one sister chromatid with both nascent strands degraded while the other sister chromatid would comprise of parental strands that cannot hybridize with the probe. Both outcomes lead to no signal at chromosome ends. The final step is destaining, followed by telomere strand-specific, dual color FISH under denaturing conditions. At semi-conservatively replicated telomeres, the labelling pattern will remain the same. In contrast, conservatively replicated telomeres have two annealed parental strands that will hybridize with the telomeric probes. This third step further confirms that the absence of a signal in conservatively replicated telomeres during the second step was not due to technical errors. Additionally, triple-FISH can provide valuable information on partial semi-conservatively and conservatively replicated telomeres, which can occur at telomeric replication fork collapse that is repaired by BIR or if these HDR processes are occurring simultaneously in ALT. Overall, this would be highly informative as to whether PARGi is sufficient to shift the balance in HDR processes that regulate ALT.

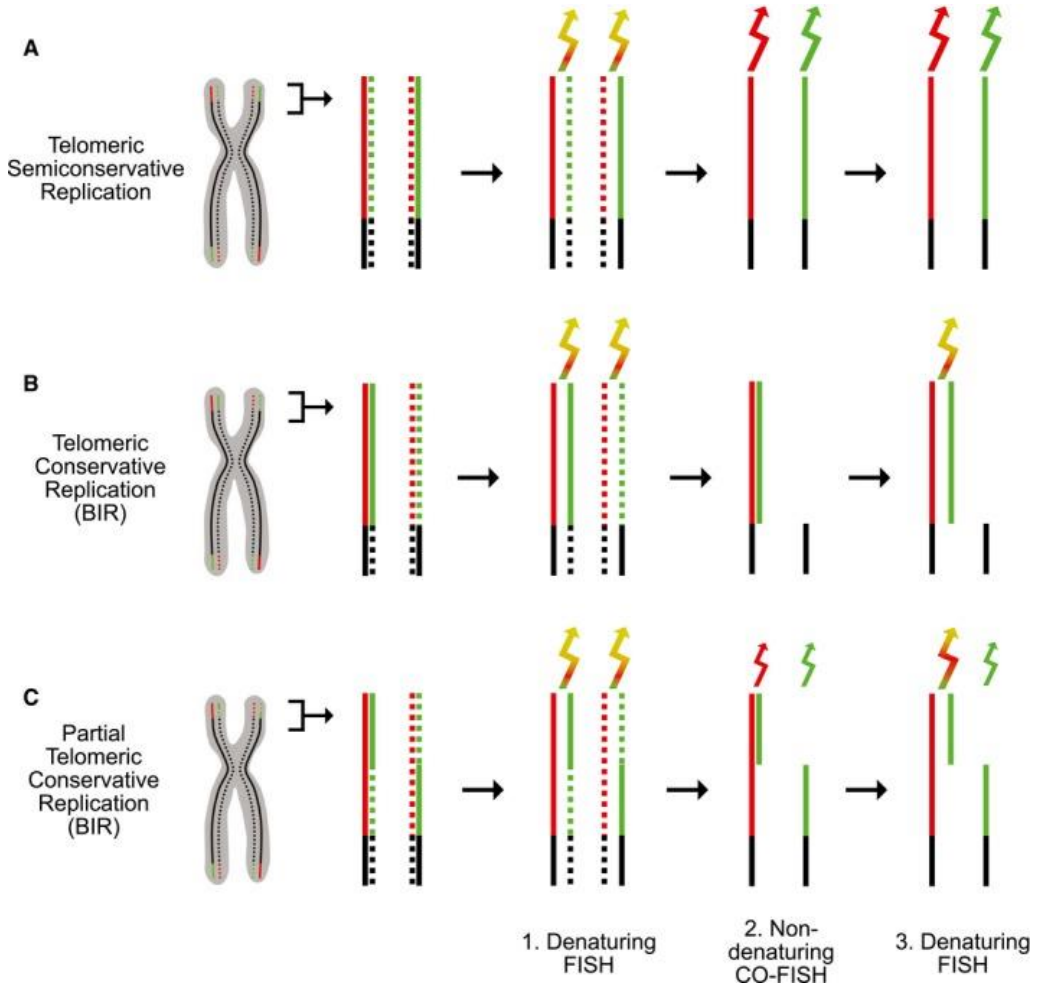

Figure 32. Triple-FISH schematic to quantify BIR. Semiconservative replication results in non-overlapping signals at both strands. B) Conservative replication leads to an overlapping yellow signal on one strand. C) Partial conservative and semi-conservative replication lead to staining patterns that incorporate A and B. Adapted from Roumelioti FM et al., EMBO Rep, 2016 (97) (https://www.embopress.org/doi/full/10.15252/embr.201643169).

Our current Af1521 data in chapter 3 provides valuable insight into PAR-regulated early responders of ALT, which could be key to determining what is the initial stimulus of HDR pathway choice. Interestingly, we found ARP2/3, a component of the actin polymerization machinery, to be enriched at ALT telomeres. Schrank et al. showed that ARP2/3 binds to DSBs and mediates HDR instead of NHEJ. ARP2/3 enhances the movement of sites of DSBs resection. This actin-

driven clustering also promotes processing and resolution of DSBs that are undergoing HDR. These two results show that there is a positive feedback loop between DSB mobility and end resection, resulting in propagation of repair factors at the site of damage (106). We show that ARP2/3 is directly PARylated. Additionally, we determined that inhibition of ARP2/3 using CK-666 (ARP2/3i) hinders telomere clustering and telomeric mobility to levels seen with PARGi (Figure 47). This implicates ARP2/3 in orchestrating the early decision for long-range HDR in the hierarchy of signaling. The link between PARylation and the organization of the cytoskeleton in mammalian cells have been enigmatic. However, there are studies in other organisms that reveal the importance of ADP-ribosylation in modulating actin polymerization. For example, overexpression of PARP in the *Drosophila* developing eye causes disorganization of cytoskeletal filamentous actin (F-actin) and disrupts tissue polarity (310). The authors posited that excessive MAR or PAR interacts with actin and prevents F-actin formation. In addition, the bacterium *Photorhabdus luminescens* utilizes TccC3 and TccC5, adenosine diphosphate ADP(ribosyl)transferases, to ADP(ribosyl)ate actin to initiate actin polymerization (311). These studies suggest a possibly conserved mechanism of ADP(ribosyl)ation in modulating biological processes that rely on actin organization.

Therefore, it is promising to understand the function of PAR-mediated ARP2/3 actin nucleation in the homology search mechanism at ALT telomeres. To determine whether PARylation disrupts ARP2/3 function, we could transfect nuclear-actin-chromobody-tag-GFP in U2OS eRFP-TRF1 cells and U2OS mCherry-WT TRF1-FokI cells treated with PARGi or ARP2/3i (106). We would measure the colocalization of actin structures resembling foci (actin-cb foci) with eRFP-TRF1 or mCherry-TRF1-FokI. WT TRF1-FokI cells will exhibit more and larger actin-cb foci at ALT telomeres since it is known that telomeric damage initiates long-range

homology search through the RAD51-dependent pathway (96). It has already been proven that adding ARP2/3i abolishes these actin-cb-foci, confirming that these structures are sites of ARP2/3-dependent nucleation. It is likely that PARGi will elicit similar effects if it inhibits the downstream activity of ARP2/3. It would also be informative to arrest cells in G2/M phase, where long-range homology is dispensable for BIR-related processes. It is likely that ARP2/3i may not play a large role in G2/M. The observed phenotype would be smaller actin-cb-foci or the absence of actin-cb-foci. Moreover, Schrank B.R et al. only shows the enrichment of ARP2/3 at damaged chromatin, but does not look at whether ARP2/3 directly binds to DNA (106). It would be valuable to determine whether ARP2/3 binds to telomeric DNA and if that association is disrupted upon PAR accumulation. Biotinylated telomeric ssDNA oligos can be preincubated with purified ARP2/3. Then, increasing concentrations of PAR polymers can be added to assess displacement of ARP2/3 from telomeric DNA. Additionally, we can identify potential PAR-binding or PARylatable regions in ARP2/3 and test mutants using the *in vitro* and *in vivo* PAR-binding and PARylation assays. Together, these experiments would directly implicate PARylation or PAR-binding of ARP2/3 as a driver of HDR in S-phase.

Another interesting notion to follow is the role of PARylation in the repression of alt-NHEJ, which also uses DSBs as substrates for repair. Normally, alt-NHEJ is a backup for defective HR and c-NHEJ (194) . PARP1 is a key component of alt-NHEJ and is in direct competition for binding of DSBs with Ku70/80, which is a determinant of c-NHEJ pathway selection (312). Alt-NHEJ is also implicated in the repair of telomere-internal DSBs (195). In the context of ALT, PARP1 loading onto resected DNA would initiate alt-NHEJ. However, ALT cells favor other HDR mechanisms because alt-NHEJ is mutagenic and pushes genome instability beyond tolerable levels. It is possible that ALT cells activate alt-NHEJ to counteract abrogation of HDR processes

and c-NHEJ due to PARGi. Indeed, we found several alt-NHEJ factors, such as LIG3 and XRCC1, enriched at ALT telomeres upon PARGi.

This raises the question of whether the PARylation of several alt-NHEJ factors contributes to the inhibitory effects of ALT. We can deplete alt-NHEJ factors in conjunction with HR factors in U2OS cells, followed by quantification of ALT phenotypes, such as APBs, T-SCEs, and c-circles. Depletion of alt-NHEJ factors in ALT+ cells likely would not repress ALT because the preferred HDR mechanisms are still present. However, depletion of alt-NHEJ with HR factors, such as RAD51 or POLD3, might lead to greater ALT suppression compared to depletion of the HR factors by themselves. This would help determine if alt-NHEJ arises as the ultimate backup in ALT cells. To tackle the role of PARylation, we can observe the recruitment of endogenous and GFP-tagged alt-NHEJ factors, such as LIG3 and XRCC1, at ALT telomeres in U2OS WT TRF1-FokI cells treated with PARGi. We expect alt-NHEJ factors to localize to ALT telomeres in the presence of PARGi since important HR factors, such as PCNA, POLD3, and RPA2 are displaced. In fact, loss of RPA has been shown to stabilize annealed intermediates that promote alt-NHEJ (271). These experiments would provide a convincing argument that the tight regulation of PAR metabolism is imperative in maintaining the competition for DSB repair at ALT telomeres (Figure 33).

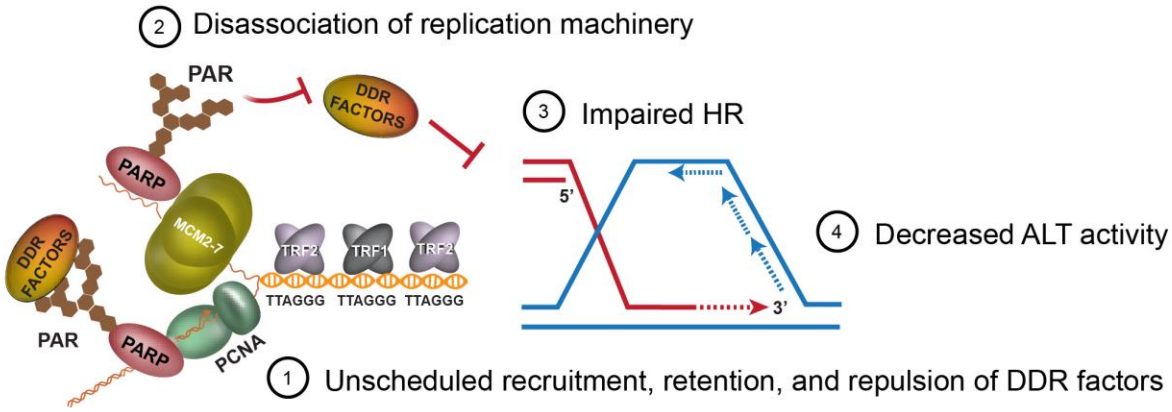

Figure 33. PARGi uncouples HDR proccesses at ALT telomeres. PARGi leads to retention of PARylated and PAR-binding DDR factors, as well as negatively charged PAR polymers at telomeres. This abrogates the efficiency of ALT-mediated pathways and impairs ALT activity.

5.3 What is the Prospect of PARG Inhibitor Use in the Clinic?

There have not been many studies that have elucidated the efficacy of PARG inhibitors in the clinic. Loss of PARG is a major resistance mechanism to PARPi in HR-deficient cancers, such as ovarian and triple-negative breast cancers. Gogola et al. show that PARG inhibition rescues PARP1 signaling and reduces toxic accumulation of PARP1-DNA complexes (313). Although PARG inhibition deters PARPi treatment, it exposes therapeutic vulnerabilities that could be used to target resistant tumors. This is supported by a study that demonstrates radiosensitization of BRCA1/2-deficient cancers upon treatment with PARGi (314). Additionally, PARG inhibition in ovarian cancers renders them sensitive to persistent replication stress and replication catastrophe (315). PARGi is synthetic lethal with inactivation of several DNA replication factors, such as TIMELESS, HUS1, and RFC2. Pharmacological induction of replication stress through CHK1 inhibition sensitizes cancer cells to PARGi. Notably, PARGi toxicity is enhanced by WEE1 kinase

inhibition and forces arrested cells into mitotic catastrophe. This sensitization to replication stress provides merit for potential combination therapies with PARGi.

ALT is more reliant on replication stress for telomere maintenance, which creates the opportunity to exploit the vulnerabilities in disrupted DDR for therapy (Figure 34). In our survival assays, ALT cells appear to have a modest decrease in growth upon PARGi treatment. It is possible that PARGi leads to cell death in ALT+ cells because the replication stress levels surpass the normal levels required to maintain telomeric integrity. There have been several instances, where inhibition or depletion of HDR factors disrupts the ALT mechanism and provokes death of ALT cancer cells. Indeed, ALT cell lines were reported to exhibit acute sensitivity to inhibition of ATR kinase, an apical sensor of replicative stress and mediator of the repair response (316,317). Similarly, depletion of FANCM and TOP3A induces a potent acute apoptotic phenotype in ALT cancer cell lines (30). In addition, chemical stabilization of G4 quadruplexes that require dissolution by BLM could also be harnessed to elicit a cytotoxic response (318). Thus, targeting the FANCM-BTR complex represents a potentially viable option for therapy development. The key may lie in determining combinations that induce ALT-specific synthetic lethality through either restricting HDR pathway switches or inducing catastrophic recombination, as implied by the systemic death of cells lacking SLXIP and SLX4 (112).

It is not unreasonable to assume, based on the striking correlation with ALT, that the absence of functional ATRX-DAXX complex affords the opportunity to determine synthetic lethal interactions that eliminate ALT cancer cells. Identifying and targeting factors that functionally compensate for ATRX loss in remediation of replicative stress might yield some benefits for exploitation of ALT-specific vulnerabilities. CRISPR-based or small compound library screens to identify synthetic lethal partners of ATRX deficiency are yet to be reported. Mitigating factors

might be the heterogeneity of available standard ALT cells lines in terms of tissue of origin, ploidy and somatic mutation burden. However, one interesting example of synthetic lethality with ATRX inactivation was reported in which the specific killing of ALT cancer cells was induced following infection with mutant Herpes Simplex Virus-1 (HSV-1) (319). This was directly attributed to repression and proteasomal degradation of PML protein isoforms upon loss of ATRX and demonstrated the potential utility of viral-based therapy to kill ATRX-deficient ALT cancer cells.

Like ATRX inactivation, PML proteins hold unique importance in the biology of ALT cells. Shuttling of telomeres to PML bodies by SUMOylation driven liquid phase separation is a signature event in ALT (55,225). Conventionally, this is linked with productive DNA synthesis at telomeres. However, it was recently shown that the sequestration of telomeres within APBs could be a poison pill. POT1 – an ssDNA binding constituent of Shelterin that is essential for chromosome end protection and telomere replication is targeted for Ubiquitin specific protease-7 (USP7)-dependent proteolysis (320). Yet, this detrimental event that could unleash ATR-dependent DNA damage signaling is prevented by a newly identified ALT specific factor, Testis-Specific Y-encoded Like Protein (TSPYL5). TSPYL5 counteracts the destabilizing activity of USP7. In doing so, TSPYL5 fulfills a key role in sustaining ALT cell viability since its depletion elicits rampant apoptosis due to compromised telomere function. This remarkable finding shows that disrupting APBs, or more specifically, APB-resident factors that confer protection against PML-USP7-dependent proteolysis could be a silver bullet for ALT-based cancers.

Interfering with the processing of DNA intermediates of telomere recombination has typically provoked acute cytotoxicity and apoptotic cell death. In those contexts, telomere shortening is often not observed. Rather, there seems to be a complete systems failure. This contrasts with chronic, progressive telomere shortening and DNA damage accumulation due to

disruption of key mediators of HDR like RAD52 that culminate in a senescence-like growth arrest (55,64). However, in one surprising case, the perturbation of telomere maintenance in ALT cells lacking RAD51AP1, a co-regulator of RAD51, provoked a cytoprotective autophagic phenotype (28). As with autophagy during crisis, telomere dysfunction and Cyclin GMP-AMP Synthase (cGAS)-dependent sensing of telomeric DNA fragments appears to mediate autophagy in ALT cells (321,322). However, in contrast to autophagy during cellular crisis, this autophagic pathway conferred cell survival (28). Only when autophagy was inactivated did the ALT cells succumb by apoptosis. The absence of Stimulator of Interferon Genes (STING) seems to be a prime culprit for this distinction since it is required for telomere dysfunction-induced autophagy during crisis and repressed in ALT cells (321). Other factors are likely to dictate outcomes such as the particular burden of telomere damage. For instance, autophagy in crisis responds to overwhelming and catastrophic telomere deprotection during mitosis. In contrast, the RAD51AP1 KO ALT cells displayed a relatively modest chronic telomere damage phenotype (28). If ALT cancer cells rely on autophagy for survival, this could represent a new vulnerability in ALT cells that presents an opportunity for therapeutic evaluation. These implicate novel and somewhat unexpected means by which ALT cancers could be targeted.

This rationale aligns with the potential for exploiting elevated replication stress at ALT telomeres. We can interrogate the gene expression of proteins involved in resolution of replication stress to see if this drives vulnerability in ALT cancers (323). A comparison of the gene profile in ALT+ and TEL+ cancers would allow us to determine differential upregulation and downregulation of replication stress-related genes that are specifically involved in ALT+ cancers. We could also cross reference this to a previous BioID analysis that identified a unique network of 139 proteins that converge at ALT telomeres (87). We can then select genes that are upregulated

specifically in ALT+ cancers and conduct synthetic lethal screens with PARGi in a wide array of ALT+ cells, using TEL+ cell lines as controls. ALT telomeres exist in an atypical chromatin and genomic configuration that act in concert to manage genomic instability. Thus, deregulation of factors involved in relieving replicative stress in conjunction with PARGi may tip this delicate balance towards cell death. This screen could be invaluable in identifying replication stress enrichment biomarkers that would be informative to develop effective combinatorial therapies that exploit the vulnerabilities of ALT cancers (Figure 34).

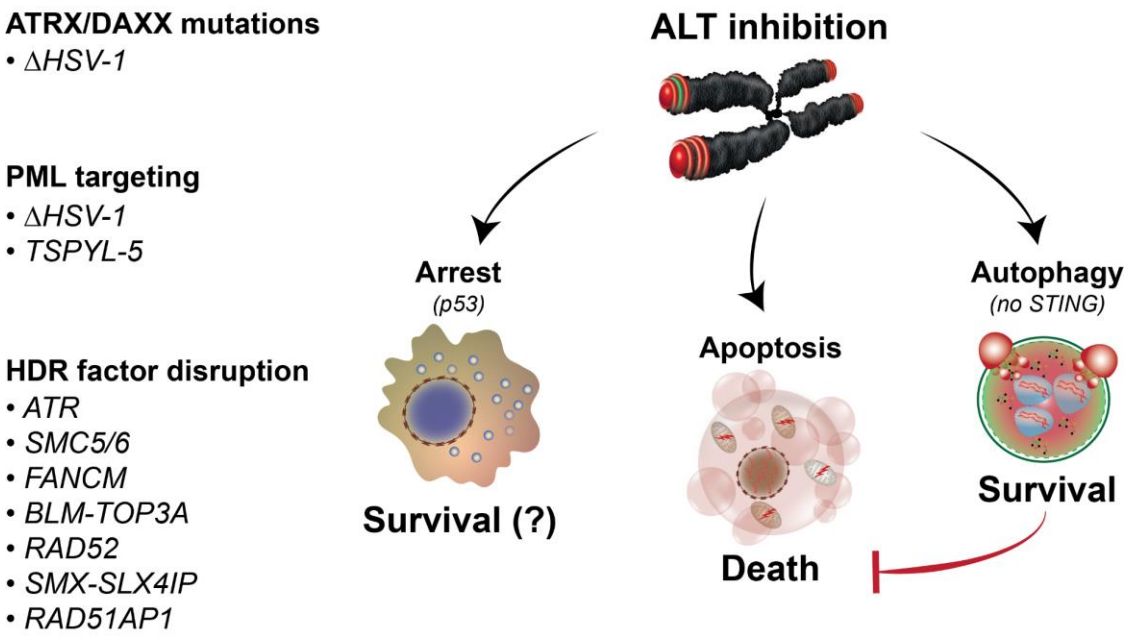

Figure 34. The fate of ALT-inhibited cancer cells. ALT cancers exist in an equilibrium between beneficial HDR and telomere dysfunction. A shift from this equilibrium poses a therapeutic vulnerability that can be exploited for selective killing of ALT cancers. Synthetic lethality with ATRX/DAXX is a promising target since ATRX/DAXX loss of function mutations are prevalent in ALT cancers. Similarly, ALT-associated PML bodies (APBs) is an attractive target for therapy since APBs are unique to ALT cancers and are implicated in telomere metabolism of ALT cells. Disruption of APBs with infection of Herpes Simplex Virus-1 (HSV-1) or depletion of TSPYL5 have been shown to elicit cytotoxicity. In addition, several lines of evidence report that inhibition of HDR factors perturbs ALT activity and provokes to cell death. Intriguingly, the absence of STING in ALT cancers enables activation of the pro-survival autophagic pathway. This reliance on autophagy may present a unique opportunity in ALT cancers to tip the balance in favor of apoptotic cell death.

5.4 Is HIRA Directly PAR-modulated?

In chapter 4, we demonstrate that HIRA is directly PARylated through our mass spectrometry analysis and *in vivo* PARylation assay. Jungmichel et al. have confirmed that these

methodologies yield covalent modification of target proteins through validation in both *in vivo* and *in vitro* PARylation approaches (223). However, protein activity and subcellular localization can be influenced by either direct covalent modifications by PARP1 or free PAR that can bind to proteins in a non-covalent manner (166). Thus, it would be instrumental to confirm that HIRA activity is modulated by direct PARylation of the protein. It would be useful to initially inspect the HIRA protein sequence for potential PAR-binding modules. These can include PAR-binding consensus motifs (PBMs), PAR-binding zinc finger motifs (PBZs), macrodomain folds, WWE domains, and RGG repeats (154). PBMs have been identified in over 800 proteins and comprise of approximately 20 amino acids with a cluster of hydrophobic amino acids spaced by basic residues. PBZs contain a consensus sequence of less than 30 amino acids. Only two proteins in the human proteome contain high-affinity PBZ motifs ($K_d \sim 10^{-3}M$). 11 human proteins have macrodomains, which are large regions containing 130-190 amino acids. The WWE domain is found in 12 human proteins and contains the conserved amino acids tryptophan (W) and glutamate (E). The RGG motif are regions that are rich in arginine (R) and glycine (G). Over 1000 diverse human proteins comprise of RGG motifs.

We can analyze the amino acid sequence of HIRA through protein domain databases to predict potential PAR-binding modules. Several protein domain and alignment databases can be used, such as SMART (Simple Modular Architecture Research Tool), NCBI CDD (Conserved Domain Database), UniProt (Universal Protein Resource), MUSCLE (Multiple Sequence Alignment), and LALIGN (FASTA Package of Sequence Analysis Program). This reveals that HIRA does not contain the previously described PAR-binding modules. To further support this, HIRA is not found in a study that characterized the PAR-binding interactome through large-scale mass spectrometry-based proteome analysis (153). In fact, using Peptide 2.0, the HIRA amino acid

composition is found to be 41.6% hydrophobic, 13.37% basic, 10.52% acidic, and 34.41% neutral. As mentioned in chapter 4, HIRA's hydrophobic cleft is important for its association with ASF1a. There are also clusters of salt bridges that form between the basic residues of HIRA and the acidic residues of ASF1a. Intriguingly, these basic residues lie within the B-domain of HIRA and are interspersed throughout small patches of hydrophobic residues. We can envision that this can act similar to PBMs and can potentially facilitate PAR binding to HIRA. However, these basic residues can also serve as sites for covalent conjugation of PAR onto HIRA. Taken together, further experimental studies need to be performed to eliminate the potential for indirect PAR accumulation to prevent HIRA localization and function.

Interestingly, our results indicate that the mutant HIRA construct that lacked the B-domain cannot localize to ALT telomeres and be PAR-modulated. The 36 amino acids that span the B-domain are within a highly disordered region of HIRA. Regions of structural low complexity are preferentially targeted for PAR-seeded liquid de-mixing (224). Additionally, the B-domain contains the critical I461 residue for ASF1a binding (286). The interface between HIRA's B-Domain and ASF1a is mediated through B-sheet, salt bridge and van der Waals interactions. Downstream of I461 are three arginine residues (458-460), which can be acceptors of PAR and are required for ASF1a binding. A potential explanation is that negatively charged PAR at these basic residues can disrupt the B-sheet and repel ASF1a through electrostatic forces. Thus, the B-domain in HIRA could be PAR-regulated to prevent histone exchange from ASF1a. The next step to confirm the importance of these arginine residues would be to generate HIRA mutant constructs that contained individual point mutations of residues 458-460 or a HIRA mutant construct with all three residues mutated to alanine. These constructs would be tested in the same experiments as

reported in chapter 4. It is expected that the RRR mutant constructs would generate similar results to that of the B-domain if it is the region that directly engages with PAR.

To further confirm that HIRA is covalently PARylated, we can perform an *in vitro* PARylation assay with purified, recombinant human HIRA, full length human His-PARP1, [^{32}P]-NAD^+, and double-stranded DNA oligomer. HIRA can be separated using an SDS-gel and detected using autoradiography. The caveat of this assay is that HIRA is the same size as automodified PARP1, which would not allow for differentiation on the SDS-gel. To overcome this, we would need to optimize a method to remove PARP1 from the end reaction. Unfortunately, automodified PARP1 is abundant and likely to be challenging for a full cleanup of the reaction. We would need to purify His-PARP1 with a mutated BRCT domain to prevent automodification. Although it has been shown that the binding of PAR to the BRCT domain recruits other DDR factors to sites of damage, perhaps it would not be necessary for an *in vitro* PARylation assay where HIRA and PARP1 are in the same vicinity. Alternatively, we can attempt to IP HIRA after these reactions. In addition, HIRA may not be stable without the presence of the other complex subunits. Ray-Gallet et al. determined that the HIRA subunit forms a homotrimer and binds two CABIN1 subunits *in vitro* (227). It is possible that we need to complement the *in vitro* PARylation assay with recombinant CABIN1 and UBN1 to maintain the complex stability required for its PARylation. If these practical limitations are overcome, then this approach will confirm that PARP1 can covalently target HIRA for PARylation.

In addition, we can carry out an *in vitro* PAR binding assay where we immunoprecipitate YFP-HIRA or YFP-HIRA mutant constructs and then detect the binding or not of biotinylated PAR. YFP-PARP1 would be used as a positive control. YFP constructs will be separated on an SDS-PAGE denaturing gel and transferred to a nitrocellulose membrane. The membrane will be

incubated with biotinylated PAR polymers. The membrane can then be probed for streptavidin-HRP and re-probed for YFP to detect the HIRA constructs as well as PARP1. If HIRA contains PAR-binding modules, then we should only detect PAR-binding in the YFP-HIRA and YFP-I461D constructs. These constructs have been previously shown to localize to ALT telomeres, be PARylated in our *in vivo* PARylation assay, and are able to rescue the phenotypes seen with depletion of HIRA. Collectively, these anticipated results would provide compelling evidence for the direct role of PAR modulation on HIRA localization and activity.

5.5 What is the Interplay between Factors that Mediate HIRA Recruitment to ALT Telomeres?

HIRA localization to ALT telomeres is not completely dependent on PAR modulation, which suggests that there might be other unknown modes of recruitment. Ray-Gallet et al. confirmed that the HIRA complex showed direct binding to DNA without any sequence specificity (291). In addition, UBN1 and CABIN1 could bind directly to DNA, unlike ASF1a. They argued that the lack of sequence specificity for DNA binding targets HIRA to destabilized nucleosomal DNA regions, where it could alter nucleosome organization as part of a gap-filling mechanism. It has been determined that the lysine residues within the 176-295 region of UBN1 contribute to its ability to non-specifically bind DNA (288). Whereas the UBN1 middle domain interacts specifically with H3.3/H4 over H2A/H2B. However, it is not involved in nucleosome binding and cannot associate with H3.3/H4 after it has been deposited onto DNA. Interestingly, DNA fragments of over 24 bp can compete with H3.3/H4 for UBN1 binding. This infers that UBN1 disassociates from DNA immediately after incorporation of H3.3/H4. We can acquire a mutant

construct of YFP-UBN1 that lacks the DNA-binding region to test whether UBN1 facilitates intermittent binding of the HIRA complex to ALT telomeres. If UBN1 can bind to ALT telomeres through its lysine-rich region, then we would expect the YFP-UBN1 DNA binding mutant to lack the ability to colocalize at ALT telomeres in the absence of PARGi. Furthermore, we can deplete these cells of UBN1, transiently transfect in YFP-UBN1 or the YFP-UBN1 DNA binding mutant, and then perform IF on endogenous HIRA localization at telomeres. The HIRA complex should still assemble with the YFP-UBN1 DNA binding mutant. However, due to lack of DNA binding, it should not localize to ALT telomeres for subsequent H3.3 deposition. It would also be interesting to test whether UBN1 DNA binding becomes dispensable with PARGi. If the same experiment is performed with PARGi, depletion of UBN1 should not affect endogenous HIRA localization to ALT telomeres. In addition, a rescue with YFP-UBN1 would not enhance HIRA recruitment to telomeres, unless PARylated UBN1 has additional roles. These set of experiments would elucidate whether UBN1 ensures that the HIRA complex is in close proximity to ALT telomeres.

Another hypothesis is that HIRA can be partially recruited to ALT telomeres by interacting with RPA. Zhang et al. showed that HIRA may bind to RPA-coated R-loops that form at gene regulatory units in the G1 phase (301). RPA is also involved during ALT, where it may coat resected telomeric ends for the RAD51-dependent pathway or bind to the ssDNA loop of TERRA-generated R-loops. Similar to the UBN1 experiments, we can knock down RPA and look at HIRA localization to ALT telomeres in the absence of PARGi. Likewise, if RPA is required, we would expect a decrease in HIRA localization to these telomeres. Our unpublished work shows that accumulation of PAR displaces RPA from telomeric oligos and abolishes RPA recruitment to U2OS TRF1-FokI telomeres. This is supported by data from Illuzzi et al. showing that excessive PAR prevents binding of RPA onto chromatin in HU-treated cells (302). This implicates an early

role of RPA in keeping the HIRA complex proximal to ALT telomeres. However, once the complex is recruited, RPA quickly disassociates to allow H3.3 deposition by HIRA.

It would be valuable to expound on the intricacy of PAR modulation in regulating the outcome of HIRA complex assembly at ALT telomeres. A simple scenario would be that PAR modulation of HIRA recruits the entire complex to incorporate H3.3 at ALT telomeres undergoing HDR-mediated DNA synthesis. A more intricate model would suggest that UBN1 and CABIN1 are not solely part of the complex for stability and H3.3 deposition. As suggested by our Af1521 PAR proteomics, both subunits could be PARylated or bind to PAR to propagate a positive feedback loop that generates a permissive chromatin environment for recombination. Thus, to confirm their regulation by PAR, we can perform *in vitro* PARylation, *in vitro* PAR-binding, and *in vivo* PARylation assays.

If UBN1 and CABIN1 are indeed modulated by PAR, it begs the question of whether their PAR regulation is necessary for HIRA complex recruitment or function. An approach we can take is to generate non-PARylatable constructs of UBN1 and CABIN1 and test their capacity for PAR-binding or PARylation. Initially, we would create truncated mutants to determine what region of the subunits are PAR-binding or PARylated. After we acquire our non-PAR-binding or non-PARylatable UBN1 and CABIN1 constructs, we could test their ability for complex assembly, recruitment at ALT telomeres, and efficiency of H3.3 deposition in the context of UBN1, CABIN1, or HIRA depletion. The data regarding these mutant UBN1 and CABIN1 constructs would be compared to our data with the YFP-HIRA B-domain mutant, as well as repeated with the YFP-HIRA RRR (458-460) mutant construct that was previously described in 5.4. In an ideal situation, we would find non-PAR-binding or non-PARylatable UBN1 and CABIN1 constructs, together with the previous YFP-HIRA RRR (458-460) mutants, that could still form a stable HIRA

complex, but has disrupted recruitment and/or activity at ALT telomeres. This would provide greater insight into whether PAR regulation signals the assembly of the complex or its recruitment to ALT telomeres.

5.6 What is the Role of PAR-mediated HIRA Chromatin Assembly at ALT Telomeres?

5.6.1 Does PAR modulation of HIRA disrupt de novo H3.3 synthesis at ALT telomeres?

Although the role of HIRA has been characterized in the context of transcription recovery and nucleosome gap-filling, its function and dependency on PAR at ALT telomeres has only been explored in this thesis dissertation (226,291). We demonstrated that HIRA and its PAR modulation is necessary to facilitate the HDR mechanisms that direct ALT telomere maintenance. The HIRA complex deposits the variant H3.3, which is constitutively expressed throughout the cell-cycle (277). Interestingly, Kraushaar et al. showed that there is differential H3.3 deposition kinetics in mouse embryonic fibroblasts (MEFs) (324). H3.3 incorporation is rapid and robust at promoters, enhancers, and gene bodies. The slowest incorporation of H3.3 occurs at heterochromatic regions, such as telomeres while no turnover is observed at pericentromeric regions. Slow H3.3 turnover at telomeres represents a continuous exchange of nucleosomes that is required for telomere maintenance. This implies that there are distinct mechanisms of nucleosome assembly, stability, and eviction at different regions of the genome to mediate transcription and chromatin integrity (324). Indeed, the ATRX/DAXX complex deposits H3.3 at telomeres and pericentric heterochromatin while HIRA incorporates H3.3 at actively transcribed regions (275). ATRX/DAXX loss of function mutations are prevalent in ALT cancers (325,326). This means that

H3.3 deposition in ALT is solely dependent on the HIRA complex, as we show for the first time in this thesis. Thus, it is possible that HIRA's function in H3.3 incorporation can extend beyond its known role to support telomere maintenance in ALT. Based on this speculation, the next question to ask is whether PAR modulation of HIRA alters H3.3 deposition at ALT telomeres and whether this uncouples ALT HDR-coupled nucleosome assembly.

Histone management shapes the chromatin landscape and orchestrates the fate of DNA repair. It has been shown that parental H3.3 recycling is independent of new H3.3 deposition at UVC-damaged sites (327). Adam et al. demonstrated that parental H3.3 redistribution precedes incorporation of newly synthesized H3.3. While parental H3.3 rapidly distributes within minutes of UVC irradiation, new H3.3 accumulation is detected starting at 30 minutes after damage. HIRA does not function to facilitate parental H3.3 dynamics in response to UV irradiation. Rather, HIRA mediates H3.3 de novo deposition throughout the cell cycle, but is excluded from replication sites in S-phase. However, H3.3 can be incorporated at replication sites when H3.1 incorporation is impaired due to CAF1 depletion, which only interacts with the replisome to deposit H3.1/H4 onto newly synthesized DNA in S-phase (291,328). This highlights the notion that HIRA can be a compensatory mechanism to manage chromatin assembly defects. Notably, Orsi et al. showed that HU treatment and ASF1a depletion impairs the recycling of parental H3.1 and H3.3 histones and their nuclear distribution (329). ASF1 depletion leads to recycling of parental H3.3 at sites distant from their initial location during mid/late S-phase. They hypothesized that parental histones that are not properly secured during replication fork progression are recognized as new histones and deposited to distant regions by HIRA or ATRX/DAXX. It has also been shown that the added stress caused by ASF1 depletion could compound on the replicative challenges at telomeres to trigger the ALT pathway (243). Taken together, these studies emphasize the importance of histone

management at homeostatic levels. Thus, a parsimonious model to explain the relevance of HIRA at ALT telomeres is that HIRA-mediated H3.3 deposition is coupled to DNA synthesis in ALT during G2-BIR, where CAF1 does not deposit H3.1/H4 and ATRX/DAXX is not available to incorporate H3.3/H4. HIRA simply acts as a safeguard mechanism to ensure that replication stress levels at ALT telomeres does not surpass a threshold that would be detrimental to survival.

An important future direction to pursue is characterization of HIRA-mediated newly synthesized H3.3 during HDR-mediated DNA synthesis at ALT telomeres. We can visualize newly synthesized H3.3 and parental H3.3 at replication sites in U2OS cells that stably express the SNAP-tag labelling system with depletion of HIRA (329) (Figure 35). The SNAP-tag technology allows the distinction between old and newly deposited histones. The SNAP-tag is an engineered version of the DNA repair protein O6-alkylguanine-DNA alkyl transferase. It covalently and irreversibly binds to O6-benzylguanine (BG) that is coupled to the fluorophore tetramethylrhodamine (TMR). The SNAP-tag also reacts with the optically inert group bromothenylpteridine (BTP), which is referred to as the "Block". Our methodology would involve the "quench-chase-pulse" labelling of G2 arrested H3.3-SNAP U2OS cells that are depleted of HIRA or expressing the various HIRA mutants. During the "Quench" step, all pre-existing histones are bound to the "Block". The "Chase" step enables new H3.3 to be deposited at telomeric DNA. During this step, we would also add EdU to mark sites of replication. The "Pulse" phase includes the addition of TMR to label all SNAP-H3.3. Using IF, we can stain for TRF2 and quantify the colocalization between SNAP-H3.3, EdU, and TRF2. This would represent incorporation of newly synthesized H3.3 at replicating telomeres in G2-phase, allowing us to validate that HIRA is responsible for H3.3 deposition at ALT telomeres.

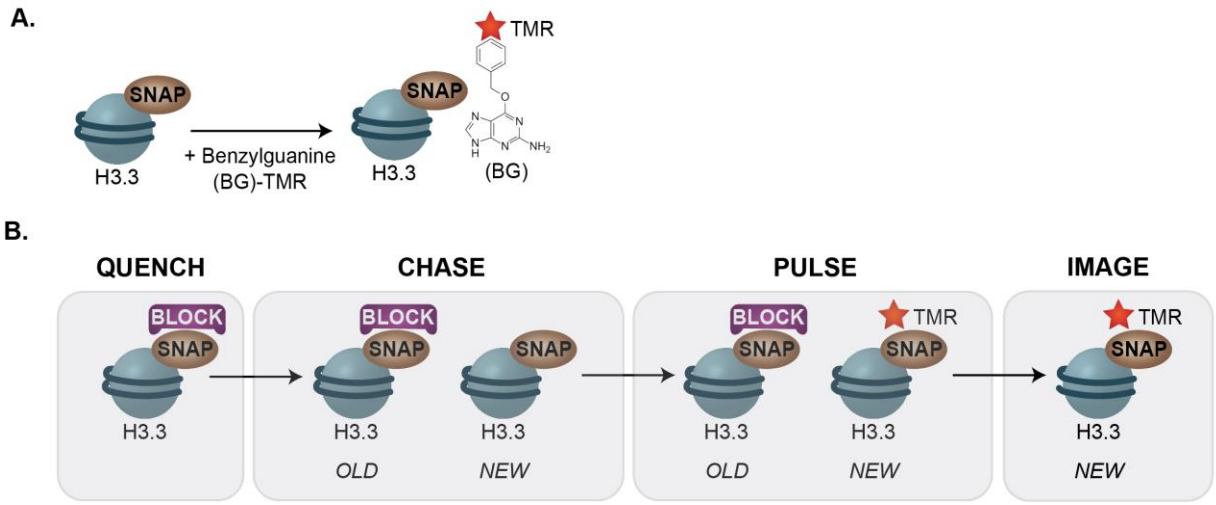

Figure 35. H3.3 SNAP-TAG system to observe histone dynamics. H3.3 is fused to SNAP-TAG, which reacts covalently with benzylguanine derivatives that are labelled with fluorescent TMR. B) Schematic for labelling new histones. The Quench step involves the addition of the "Block", an optically inert molecule, that binds to old H3.3. At the Chase phase, newly synthesized H3.3-SNAP is not bound by the Block. During the Pulse step, addition of TMR leads to a covalent, non-reversible interaction with H3.3-SNAP. Newly synthesized H3.3 bound to fluorescent TMR can be visualized after Triton-X extraction to remove soluble histone pools. Adapted from Torne J. et al., Histone Variants, 2018 (329) (https://link.springer.com/protocol/10.1007%2F978-1-4939-8663-7_11).

Based on the proposed model, we would expect that depletion of HIRA will impede H3.3 incorporation at telomeres during G2-BIR because there is no other histone chaperone to compensate for its activity. This is supported by Ray-Gallet et al. who showed that H3.3 can substitute for impairment in H3.1 deposition at replication sites, but H3.1 cannot replace the loss of H3.3 incorporation outside of S-phase (291). To confirm this in our system, we could also perform the same experimental scheme, but with depletion of CAF1, to which we should not see an effect on newly synthesized H3.3 at ALT telomeres. It would also be informative to generate WT TRF1-FokI cells with the SNAP-H3.3 tag, especially since we observe decreased nascent telomere synthesis with the absence of HIRA in WT TRF1-FokI cells. Taken together, it is

tempting to envisage a model where replication stress can subject ALT telomeres to HDR-coupled DNA synthesis that would require HIRA-mediated H3.3 deposition to maintain chromatin integrity at the moving D-loop.

PAR modulation poses an additional layer to control HIRA recruitment and activity at ALT telomeres that are primed for HDR-mediated DNA synthesis. To tease out the role of PAR regulation in HIRA-dependent H3.3 incorporation in ALT, we can deplete endogenous HIRA in the U2OS SNAP-tag cells and reintroduce WT-HIRA, as well as the varying HIRA mutant constructs mentioned previously (homotrimerization, I461D ASF1 binding, ΔB-domain, and RRR). If HIRA's PAR modulation is essential for its sequestration at ALT telomeres, then we would not expect the defective PAR-modulated HIRA mutants to rescue H3.3 incorporation at ALT telomeres. Both the ΔB-domain and RRR mutants contain the regions necessary for interaction with ASF1a. A viable model would be that PAR regulation precedes ASF1a binding by recruiting HIRA to ALT telomeres. Since PAR turnover is rapid, removal of PAR likely allows for ASF1a binding to HIRA. Retention of PAR at HIRA within the B-domain would actually block the HIRA-ASF1a contact and subsequent deposition of H3.3 at ALT telomeres. Thus, we should see impaired H3.3 incorporation if we simply treat the U2OS SNAP-tag cells with PARGi. This means that PAR regulation of HIRA can provide immediate and localized restoration of chromatin at HDR intermediates in ALT.

5.6.2 How does HIRA-mediated H3.3 deposition couple with HDR mechanisms in ALT?

It is possible that PAR modulation facilitates ASF1a's regulation of H3.3 biogenesis and usage during HDR in ALT. Perhaps ALT cells employ a similar mechanism observed during the tight coordination of histone buffering during S-phase. Groth et al. proposed that inhibition of

DNA replication triggers the shuttling of ASF1a from a histone-free form to an active multichaperone complex in order to counteract low histone biogenesis (330). These S-phase histones become readily available to enable CAF1-mediated histone loading for recovery and repair. We can speculate the importance of a parallel mechanism in G2-BIR to relieve the replicative burden that naturally occurs at ALT telomeres. In ALT, ASF1a shuttling of H3.3 for the HIRA complex during G2 could play an important role because of the lack of redundancy in histone chaperones during this phase. CAF1 only acts in S-phase and H3.1 cannot replace H3.3 incorporation throughout the cell-cycle. ATRX/DAXX is not present in most ALT cancers to compensate for loss of H3.3 incorporation. To address this idea, we can follow the pool of soluble H3.3 throughout the cell-cycle in ALT cells. This will be done using stable expression of C-terminal FLAG-and HA-epitope tagged H3.1 and H3.3 by retroviral transduction (273). Cells will be collected in S-phase or G2-phase after a double thymidine block. In control samples, we should see the increased pool of soluble H3.1 in S-phase, but not H3.3 since H3.3 supports chromatin assembly uncoupled from DNA replication. The opposite results should be seen in G2-phase, which would promote G2-BIR in ALT cells. Immunoprecipitation of these extracts should show higher proportion of endogenous ASF1a and HIRA bound to H3.3 if HIRA and ASF1 are required for H3.3 coupled G2-BIR.

The presence of mutant H3.3 has been shown to alter epigenetic marks near genes involved in cancer processes and brain function (331). Frey et al. observed that a mutation of H3.3K27, a residue whose trimethylation is associated with polycomb target gene silencing, also exhibits similar sensitivity to the knockout of H3.3 (332,333). The histone H3.3K27 mutation has been reported in 60% of pediatric brain cancers (121). To add on, H3.3 G34R/V mutations also contribute to gliomagenesis and is hypothesized to activate the oncogene MYCN in pediatric

gliomas (334). This is of particular importance because ALT has a high prevalence in pediatric high-grade gliomas, with 44% of pediatric glioblastoma (GBM) demonstrating ALT activity (335). In fact, it was recently shown that the presence of H3.3-ATRX/DAXX- P53 mutations is a strong driver of ALT (336,337). The prevalence of H3.3 mutations in the pediatric cancer setting clearly raises the importance of chaperones, histone-modifying enzymes and factors that feed into H3.3 function. Given the importance of H3.3 mutations in ALT, it would be worthwhile to test if this correlates to elevated levels of HIRA protein expression or transcription of mRNA in ALT+ and TEL+ cancers. A cycloheximide (CHX) chase experiment, through pulse labelling of newly synthesized proteins with 35S-methionine and cysteine, would further address HIRA protein stability (28). This will shed light on the tight regulation of HIRA, either through post-transcriptional or post-translational mechanisms, that is necessary to mediate H3.3 incorporation in ALT.

ALT cancer cells must maintain a balance between pro- and anti-recombinogenic signals. A shift from this equilibrium poses rampant replicative stress that leads to unproductive ALT activity. It is plausible to assume a mode of G2-BIR coupled nucleosome assembly to protect the integrity of advancing forks. Several studies have reported the impact of histone dynamics on replication fork progression and stability (338–342). Nucleosomes are a physical barrier for the replication machinery. During S-phase, histones are evicted ahead of the fork while de novo histones are synthesized behind the fork (343). CAF1 is the most well-characterized replication-coupled chromatin assembly factor (299). CAF1 associates with the replication fork through its interaction with PCNA and collaborates with ASF1, which has the capacity to bind to RFC as seen in budding yeast (344,345). The obligate coupling of chromatin remodeling and DNA synthesis is underscored by the fact that depletion of CAF1 or ASF1 evokes stalled replication forks and

inhibits S-phase progression (299,346,347). Intriguingly, MCM2, a component of the replicative helicase, can bind to either a H3-H4 tetramer or dimer (348,349). The latter involves initial capture of parental H3-H4 by MCM2 at the proximity of the fork, which is disrupted by ASF1 to mediate redeposition of H3-H4 dimers and free the MCM complex so it can progress with the fork (350). In budding yeast, BIR has been documented to require all essential DNA replication factors, including the MCM complex (351).

It would be incredibly valuable to assess whether the HIRA complex is part of the G2-BIR replisome to facilitate ALT telomere maintenance. *In situ* analysis of protein interactions at DNA replication forks (SIRF) can be employed to quantify protein associations with nascent DNA at active and stalled replication forks (Figure 36). SIRF is a robust and sensitive combination of the isolation of proteins on nascent DNA (iPOND) and proximity ligation (PLA) assay (352,353). In WT TRF1-FokI U2OS cells that are arrested in G2, newly synthesized DNA is labeled with EdU and then biotinylated by click chemistry. Primary antibodies are added against biotin and HIRA or ASF1a. Cells are then incubated with secondary antibodies conjugated with oligonucleotides that serve as proximity probes. Secondary antibodies that are within 40 nm in proximity will allow for the oligomers to anneal and form a nicked circular DNA molecule, which become a template for rolling circle amplification. A telomere sequence-specific fluorescence DNA probe is annealed to these amplified DNA circles and the signal intensity is then quantified. This is a powerful tool that has the potential to capture the HIRA-mediated replisome specifically in ALT cells during G2.

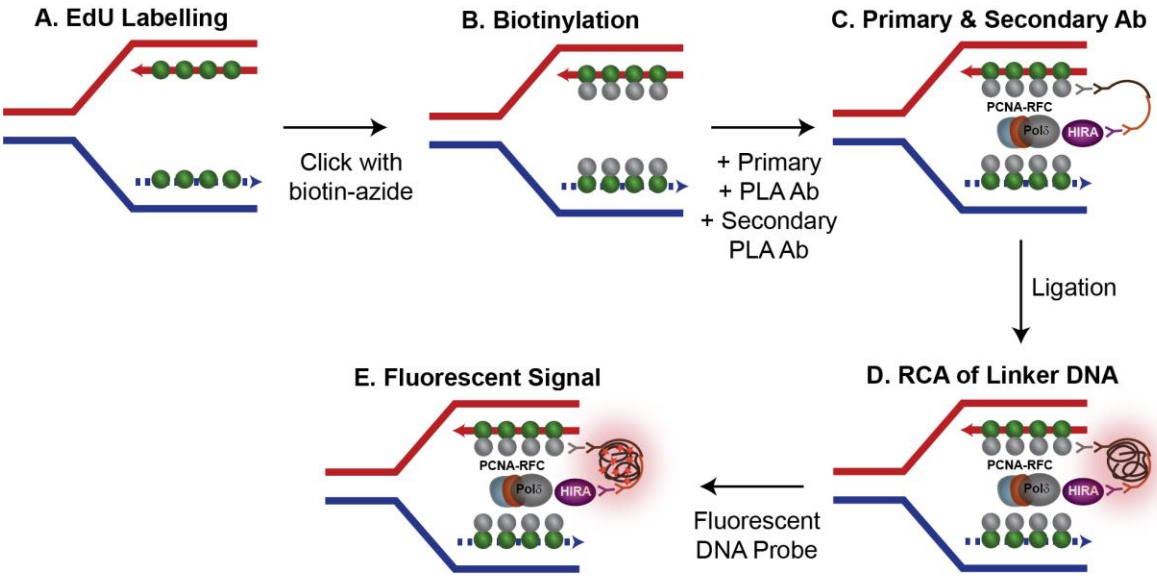

Figure 36. Schematic of SIRF method. A) Cells are pulsed with EdU. B) EdU is biotinylated by click chemistry. C) Primary antibody against protein of interest and biotin are added to slides. Slides are then incubated with secondary PLA antibodies containing DNA-oligomers. D) Upon association, DNA oligomers ligate and enable rolling circle amplifcation. E) Fluoresent DNA probe anneals to the sequence. Adapted from Roy S et al., JCB, 2018 (https://rupress.org/jcb/article-lookup/doi/10.1083/jcb.201709121).

DNA synthesis and histone deposition also partner during DNA repair and oncogenesis. CAF1 is known to promote Recombination-Dependent-Replication (RDR) in fission yeast. It was observed that RDR-coupled histone deposition stabilizes D-loop intermediates and counteracts the activity of Rqh1, the fission yeast orthologue of human RecQ1. Thus, histone deposition ensures continuous chromatin assembly upon damaged lesions induced by Hydroxyurea and Camptothecin (354). In chicken DT40 cells, loss of H3.3 leads to defective fork progression on UV-damaged DNA (333). Intriguingly, replication stress has been shown to perturb H3.3 epigenetic stability by interfering with pre-deposition marking and histone recycling. Jasencakova et al. observed that replication stress traps new and old H3.3 at ASF1, both of which can be incorporated at unscheduled sites upon fork restart (355). In particular, there was mainly the accumulation of

H3K9me1 at ASF1 complexes. H3K9me1 can be a precursor of H3K9me3, which poses a hazard for unscheduled silencing and challenges the integrity of the epigenome (355–357). ALT cancers likely use the previously mentioned mechanisms to manage recurrent cycles of replication stress to generate DSBs for HDR mechanisms. Loss of the HIRA complex simply unleashes unwarranted telomeric defects that are not resolved by DNA repair and eventually become hazardous to cells. As a consequence, either absence of HIRA or loss of its activity will lead to replication defects, such as telomere fragility, inefficient replication, or delay into mitosis. These examples illustrate how distinct chromatin reorganization could mediate the intricate balance between genome instability and survival.

5.6.3 Why is H3.3 incorporation necessary at ALT telomeres?

If the above speculations are true, then it raises the question of why the histone variant H3.3 is particularly important in ALT. There are seven human H3 variants in the H3 family: two canonical H3.1 and H3.2, replication-independent H3.3, centromere protein A (CENP-A), testis-specific histone H3t and the primate specific H3.X and H3.Y (358). Although H3.3 only differs from its canonical counterparts by 4-5 amino acids, this confers distinct epigenetic patterns and chromatin regulation that lead to diverse biological outcomes (359). Canonical H3.1 and H3.2 do not contain introns, are organized in multi-clusters, and the mRNA is not polyadenylated. On the other hand, H3.3 is redundantly encoded from two intron-containing *H3F3A* and *H3F3B* genes (359,360). Nucleosomes that contain H3.3 are intrinsically unstable and are even less stable with the combination of H3.3 and H2A.Z, a noncanonical H2A histone (361). These unstable histone variants could possibly be more easily displaced by transcription factors at active gene bodies. They can also serve as temporary placeholders to prevent the binding of stable, canonical histones

or leave the region vacant for non-specific association of chromatin-binding factors. This implies a dynamic cycling of histone occupancy at different regions in the genome (362). Therefore, narrow windows exist where chromatin is bound or free during these exchanges.

The high level of amino acid homology between H3 variants means that the same PTMs can decorate shared residues. However, each histone variant carries a characteristic histone signature and occupies different regions of the genome, which confers distinct function (324). H3.3 is enriched with post-translational modifications (PTMs) associated with active chromatin (362–364). Tvardovskiy et al. employed a quantitative middle-down proteomics approach to determine the dynamic changes in the H3.3 PTM landscape across the lifespan of mice from 3-24 months (365). They report that H3.3 accumulates in somatic issues with increasing age. Unexpectedly, they found that individual and combinatorial H3 methyl PTMs exhibit stable enrichment on H3.3. These PTM signatures may allow cells to rapidly turn on or off specific genes in response to specific stimuli. Despite H3.3 being correlated with gene activation, a study showed its underappreciated role in the establishment of the bivalent chromatin landscape at developmental genes that exhibit low expression in embryonic stem cells (ESCs) (289). Thus, HIRA-dependent H3.3 deposition is essential to maintain accurate gene expression upon differentiation. This is an important feature because some cancers, including gliomas, are speculated to arise from regression to a less differentiated state or initial failure to establish differentiation (366–368). Thus, the unique properties of H3.3 might be beneficial to accommodate the dynamic chromatin landscape of ALT.

Given the importance of H3.3 and its PTMs, we need to conduct experiments to validate that the specific loss of H3.3 perturbs telomeric chromatin in a manner that impairs HDR at ALT. Depletion of H3.3 should mimic the phenotypes seen with loss of HIRA, if HIRA-mediated H3.3 incorporation is indeed important for ALT activity. Furthermore, depletion of HIRA or H3.3

possibly leads to a more permanent, open chromatin environment that is permissive to cleavage by the SLX-MUS endonuclease to generate more DSBs. We can use the micrococcal nuclease (MNase) digestion to determine chromatin accessibility in response to absence of HIRA or H3.3 (369). Cell lysates are incubated in MNase, which cleaves at nucleosome linker regions. The DNA can be fractionated by agarose gel electrophoresis and subjected to southern blotting with a radioactive telomeric probe. The blot will reveal a ladder of bands that correspond to the size of the nucleosome core and linker (~200 base pairs). Greater distance between the bands represents nucleosome-free regions. With loss of H3.3 or HIRA, we expect de-condensation of the chromatin, which will be represented by the increased distance in the ladder of bands in the MNase digestion.

We reason that tight regulation of H3.3 incorporation is necessary to maintain the proper chromatin dynamics that facilitates ALT. H3.3 PTMs at ALT telomeres could serve as an additional layer for fine-tune control. Similar to the approach taken by Tvardovskiy et al., we could utilize a MS-based middle-down proteomics approach to measure H3.3 proteoforms in ALT+ and TEL+ isogenic cell lines, ALT+ cancers in each cell cycle, and WT TRF1-FokI U2OS cells (365). We expect the H3.3 PTM profiles to be distinct between ALT+ and TEL+ cancers as well as throughout the cell cycle. WT TRF1-FokI U2OS cells will likely have a similar pattern to that of U2OS cells arrested in G2-phase, which supports the notion that TRF1-FokI telomeric DSBs induces DNA synthesis in G2/M. It would be reaffirming to observe specific PTMs at H3.3K27 and H3.3 G34R/V across all ALT+ cancers, especially since these H3.3 mutants are common in pediatric brain tumors. This strategy has the potential to uncover novel H3.3 PTMs that could be driver mutations or biomarkers of ALT.

5.6.4 Is there a crosstalk between PAR and H3.3 post-translational modifications?

The crosstalk between these epigenetic marks at H3.3 and PARylation merits further exploration because it potentially orchestrates localized action at ALT telomeres. As discussed in prior chapters, PARylation has broad effects on chromatin configuration to enable the plasticity for DNA repair. PARylation has been shown to restrain the enzymatic activity of SIRT1, a NAD+-dependent deacetylase (370). Thus, PARylation cooperates with histone acetylation to maintain accessible chromatin and transcription. While acetylation is attributed to active transcription at any modified residue, the outcome of methylation varies depending on the degree of methylation (mono-, di-, or tri-) and the modified lysine residue. PARylation of EZH2 histone methyltransferase, a member of the polycomb repressive complex 2 (PRC2) leads to decreased levels of H3K27me3. It was also reported that PARP1 can PARylate H3 and disrupt the affinity of EZH2 to its substrate (371). These factors work in concert to enhance chromatin decondensation and prevent EZH2 from repressing genes involved in DNA repair. Interestingly, chromatin remodeler CHD2 is recruited to DSBs in a PARP1-dependent manner to incorporate H3.3 at these sites and promote repair by cNHEJ (204). NHEJ and HR compete for DSBs as a substrate so it would be interesting to uncover whether PTMs at H3.3 could alter pathway choice outside of S-phase (372). This is certainly relevant in the context of G2-BIR processes that occur in ALT cancers. It is plausible that the interplay between PAR and PTMs at H3.3 create a unique barcode in ALT that shunts NHEJ repair to productive HDR mechanisms.

This opens a vast area of exploration into how PAR and different PTMs modulate the optimal balance of genome stability at ALT telomeres. If the previously described MS-approach to analyze H3.3 PTMs works, then we can add PARGi to the same conditions to determine if retention of PAR alters the profile of H3.3 PTMs. This is informative because it further elucidates

the exact outcomes of PARylation on ALT chromatin. We can envision a possibility where PARylation will abolish H3.3 PTMs that promote chromatin decondensation or DNA repair factors at ALT telomeres. In an ideal situation, it would be useful to see if PARylation directly disrupts the enzymes that catalyze H3.3 PTMs, such as Histone acetyltransferases (HATs) and DNA methyltransferases (DMNTs). However, these enzymes have broad, genome-wide roles so it would be challenging to tease out whether the observed effects are due to PARGi.

5.6.5 Does HIRA contribute to TERRA function at ALT telomeres?

Another avenue to pursue is whether the RPA-HIRA-H3.3 axis that regulates transcription could have a non-canonical role at RNA-DNA hybrids in ALT. RNA-DNA hybrid structures (R-loops) are frequently detected at gene regulatory elements (373). These structures comprise of a displaced ssDNA filament that is likely coated by RPA. R-loops are required for H3.3 deposition at promoters and enhancers since overexpression of RNase1 H1, which cleaves the RNA region, lowers the levels of H3.3 incorporation. This RPA and R-loop association promotes the recruitment of HIRA to these regions to regulate the directionality of transcription (301) (Figure 37). There is mounting evidence that confirms the upregulation of recombinogenic long noncoding telomeric RNA TERRA at ALT telomeres, which forms RNA-DNA hybrids with the telomeric C-rich strand (105,240,374,375). We can envision the resemblance of this structure to R-loops formed at active gene bodies. Thus, HIRA can be recruited to RPA-bound telomeric R-loops.

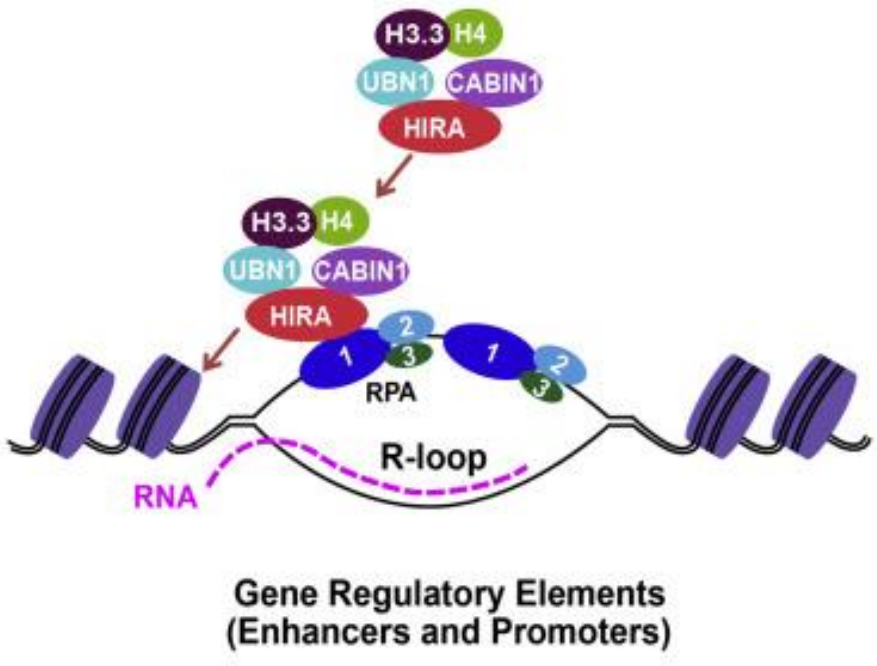

Figure 37. RPA-HIRA-H3.3 complex at R-loops. RPA co-localizes with HIRA and H3.3 at R-loops within gene regulatory elements. This regulates transcriptional directionality at promoters. Adapted from Zhang et al., Mol Cell, 2017 (301) (https://www.sciencedirect.com/science/article/pii/S1097276516307754?via%3Dihub).

An attractive possibility would be that HIRA functions to relieve telomere instability related to TERRA-telomeric hybrids. Long stretches of ssDNA in telomeric R-loops are prone to breakage, which can be DSB substrates for HR and subsequently promote ALT activity. Nguyen DT et al. proposed that ATRX normally plays a role in processing R-loops or preventing their formation at G-rich regions (303). It is speculated that ATRX could recruit other enzymes that degrade R-loops to sustain genome stability. In ALT cells that lack functional ATRX/DAXX, HIRA is likely present at telomeric R-loops to re-establish a normal chromatin structure during telomere synthesis. However, it remains unknown whether HIRA's recruitment to telomeric R-loops is sufficient to signal other factors to resolve these structural impediments. This could include RNaseH1, which has been shown to inhibit hybrid formation and the recombinogenic

potential of ALT telomeres (105). Thus, HIRA can either fully or partially restrain unwarranted R-loop formation to maintain HR without compromising telomere integrity too severely.

TERRA is also implicated in telomeric heterochromatin assembly through H3 trimethylation marks, which was previously attributed to downregulation by PARylation. It was reported that TERRA directly associates with the PRC2 complex components EZH2 and SUZ12, which establishes H3K9me3, H4K20me3, H327me3, and HP1 at telomeres (376). A genome-wide analysis revealed that the targeting and function of PRC2 is dependent on ATRX at Xist RNA and polycomb targets (377). ALT cancers that lack ATRX must then rely on elevated TERRA levels to compensate for PRC2 recruitment. It was also reported that SET Domain Bifurcated 1 (SETDB1) histone methyltransferase governs H3K9me3 deposition, a signature mark for heterochromatin, at ALT telomeres (378). Thus, ALT cells exhibit atypical heterochromatinization that can drive TERRA transcription at telomeres and other ALT features. This heterochromatin mark is necessary for ATRX localization to telomeres and suppression of ALT activity. Taken together, there appears to be a complex epigenetic landscape that is conducive for HIRA activity during TERRA transcription.

Based on these speculations, we could envision that loss of HIRA permits excessive levels of TERRA-telomeric loops that would unleash telomere instability and lead to unproductive ALT. Initially, we can perform a TERRA RNA-pulldown in ALT+ cancer cells to determine whether HIRA interacts with TERRA. Biotinylated RNA oligonucleotides containing UUAGGG repeats are incubated with nuclear abstracts from ALT+ cells (240). Streptavidin pulldown of TERRA can be performed and HIRA interaction can be detected using gel electrophoresis. We then need to investigate whether HIRA can promote telomere RNA-DNA hybrids. RT-PCR and Northern blotting can quantify the amount of detectable TERRA transcript in HIRA KD cells (240,379).

Both techniques use primers that amplify the subtelomeric portions of TERRA, which originate from chromosomes 1 and 21, or chromosomes 2, 10, and 13. RNA-FISH would show TERRA localization to APBs in ALT cells (105). We would measure the formation between TERRA and the telomeric C-strand through co-immunocytochemistry with antibodies to TRF1 and purified S9.6 monoclonal antibodies, which specifically detects RNA-DNA hybrids in a sequence-dependent manner. If HIRA antagonizes TERRA formation in ALT cells, then we would expect its loss to contribute to downstream telomeric replication defects that eventually become unmanageable for ALT telomere maintenance.

5.6.6 What is the role of HIRA in ALT cell survival by autophagy?

HIRA's implicated role in innate immune defense could aid the autophagic pathway that confers ALT cell survival. In Hela cells, HIRA-mediated H3.3 incorporation at the host's chromatin facilitates transcription of Herpes simplex virus type 1 (HSV-1) upon the early lytic stage of infection (380). It appears that HSV-1 manipulates the distinct features of H3.3 to increase viral transcription. H3.3 at actively transcribed genes can allow them to be accessible and primed for transcription. H3.3 is enriched at active chromatin marks, which could accommodate the rapid recruitment of cellular and viral transcription factors. In contrast to these findings, Rai TS et al. reported that HIRA recognizes naked viral DNA and suppresses viral gene expression, virus replication and lytic infection in an array of primary cell lines (298). In primary cells, HIRA responds to anti-viral interferons (IFNs) and localizes to PML nuclear bodies (PML-NBs), which are thought to be sites of anti-viral activity. Ultimately, this induces heterochromatinization and silencing of foreign viral DNA (298,381). This is an important anti-viral response because many viruses have evolved antagonizing strategies, such as expression of ICP0 (RING-finger ubiquitin

ligase with SUMO-Targeting Ubiquitin Ligase (STUbL) properties), to disrupt HIRA targeting to infecting viral genomes and PML-NBs (382,383). They reconciled these observed differences by suggesting that the anti-viral function of HIRA may be cell-type dependent since some cancer cell have evolved distinct mechanisms to counteract this response. To confirm this hypothesis, they showed that Hela cells and other transformed human cell lines do not display HIRA localization to PML-NBs upon IFN treatment.

Although there have been several studies that implicate HIRA in anti-viral intrinsic immunity, there has been no evidence that link this to ALT oncogenesis. Given the propensity for HIRA to deposit H3.3 at naked DNA through its gap-filling function, it is possible that HIRA could recognize extrachromosomal telomere repeat DNA within APBs or freely in the nucleus. In human fibroblasts with a STING-cGAS axis, ECTRs that are detected in the cytoplasm activate IFN and cytokine signaling, resulting in proliferation defects (321). ATRX/DAXX have been shown to restrict viral infection through epigenetic silencing or entrapment mechanisms (381,384). Simultaneous re-expression of STING and ATRX in ALT cancers restores the STING-mediated cytosolic DNA-sensing pathway (321). Taking these findings into consideration, HIRA could be an additional safeguard mechanism to sequester and resolve high levels of ECTRs in ALT cells.

Nassour et al. showed that activation of autophagy is an integral tumor suppression mechanism (322). Telomere dysfunction in epithelial and fibroblast cells during crisis generates cytosolic telomeric DNA fragments that activate the cGAS-STING pathway. It was also reported that inhibition of ALT telomere maintenance in ALT cancers lead to the release of cytosolic telomeric fragments that are recognized by cGAS and removed through AMPK-ULK1 (AMP-Activated Protein Kinas-Unc-51 Like Autophagy Activating Kinase)- and ATG7 (Autophagy Related 7)-mediated autophagosome biogenesis (28,321). ALT cancers do not exhibit an

alternative autophagy pathway that involves the cGAS-STING axis because STING expression is barely detectable in these cancers (28). Studies have shown that cells with impaired autophagy exhibit reduction in DNA damage repair capacity, such as HR and NHEJ (385). The synthetic lethal relationship between autophagy and HDR holds promise to exploit the vulnerabilities of ALT cancers. Indeed, Barroso-Gonzalez et al. showed that RAD51AP1 knockout ALT cells were more sensitive to autophagic inhibition (28). We can envisage a scenario where HIRA's regulatory role in innate immunity could converge with this pathway to remove cytosolic telomeric DNA and manage genome stability in ALT cancers.

To shed light on this, we can examine HIRA's role in autophagy as a chronic survival mechanism to offset telomere instability in ALT. First of all, we should confirm whether HIRA depletion leads to increased frequency of micronuclei, which are fragments of damaged DNA expelled into the cytoplasm, or elevated c-circle levels (72,386). We would expect that HIRA depletion can potentiate the presence of these extrachromosomal DNA species. However, HIRA KD cells likely fail to mitigate these detrimental events and telomere dysfunction ensues, leading to apoptotic death instead of pro-survival autophagy. We would expect that HIRA KD cells would be committed to apoptosis, which can be quantified through the cleavage of Caspase-3 or detection of Annexin V by flow cytometry (387).

Thus, absence of HIRA may impair ALT cell viability by autophagy survival mechanisms and activate apoptotic cell death to eliminate cells with aberrant DNA species. We can measure the levels of autophagic markers in siRNA knockdown of HIRA in ALT+ cells through western blotting. Light chain 3 protein A (LC3A) and its lipidated B-form (LC3B) are required for autophagosome biogenesis. An increase in lysosomal-associated membrane protein 1(LAMP1) and degradation of the autophagy receptor protein p62 (SQSTM1) correlates with autophagic

maturation and autophagic flux (388). To monitor autophagic flux, we can employ a tandem mCherry-GFP-tagged LC3B pH-based autophagy reporter strategy, which labels autophagosomes in yellow (mCherry and GFP) and acidic autolysosomes in red (mCherry) (389). When the double positive mCherry and GFP LC3 become acidified in mature autolysosomes, this quenches the GFP signal and leaves an mCherry positive autolysosome. We can also observe whether HIRA also contributes to the AMPK-ULK1 autophagy pathway (390). This will involve measuring phosphorylation of AMPK, ULK1, and Beclin1. We would expect a decrease in all these autophagic markers if HIRA does govern nuclear events leading to autophagy-mediated survival in ALT+ cancers.

5.7 How does ATRX Deficiency Contribute to Dependency on HIRA in ALT Cancers?

Drug-driven synthetic lethality is a promising strategy to take advantage of the distinct survival mechanisms employed by ALT. Synthetic lethality occurs when the combinatorial loss of two genes results in cell death, but the deficiency in one alone does not. A recent study conducted a genome-wide CRISPR-Cas9 screen to select for sensitivities in ATRX-generated knockout hepatocellular carcinoma cell lines, which are wild-type for the gene (391). Under stringent analysis, they identified 58 genes to be potential synthetic partners for ATRX. These genes were involved in mRNA processing, mitosis, chromatin organization, and cell cycle regulation. They pursued the G2/M checkpoint regulator Wee1 since it is the only target with a small molecule inhibitor designed and tested in clinical trials (392,393). ATRX KO cells are selectively killed by the Wee1 inhibitor due to DSBs generated by replication fork collapse and S-phase arrest. Wee1 inhibition also impairs growth of ATRX-deficient cell lines from glioma patients. Aside from

Wee1, they also found two components of the HIRA complex: ASF1a and CABIN1, which they speculated to compensate for H3.3 deposition pathways in certain contexts (391). However, they did not provide further detail about the mechanism or importance in ATRX KO cell lines or ATRX-deficient ALT cancers.

This finding corroborates the entire premise of chapter 4 in this thesis dissertation. We have essentially shown the first epigenetic synthetic lethality that is exclusive to ALT cancers. To current knowledge, the HIRA complex is the only histone chaperone that could function in place of ATRX throughout the cell cycle. H3K9me3 acts as a docking site for ATRX at telomeres to maintain heterochromatic assembly (394). ATRX can also be recruited by G4 DNA at telomeres and it can resolve these structures (283,395). It is speculated that ATRX recruitment loads H3.3 at nucleosomal free telomeric regions that arise during stalled replication or disrupted transcription. In agreement with this, the *Drosophila* ATRX homolog, *Xnp,* guides H3.3 loading to nucleosome-depleted chromatin gaps at active transcription sites (396).

HIRA and ATRX appear to share similar stimuli, epigenetic marks, and role in mitigating DNA damage. As discussed in previous chapters, the H3K9me3 mark is associated with ASF1 and TERRA, and HIRA carries a nucleosome-gap filling function (291,376). The ATRX-DAXX-H3.3 complex has been shown to promote HR at genomic DSBs (282). ATRX provides topological stability to the moving D-loop through the coordination of histone disassembly ahead and reassembly behind it. It seems counterintuitive that HR is upregulated at telomeres in ALT+ cancers with an ATRX deficiency. This alludes to a fundamental difference between non-telomeric and telomeric DSBs, in which telomeric DSBs engage in a distinct HIRA-mediated HDR pathway choice that is more prone to replication stress. However, HIRA is not completely redundant for ATRX since it has not been shown to resolve G4 structures. This is an important feature because

it allows HIRA to moderate replication stress, but still provides the chromatin environment that is conducive to ALT telomere maintenance.

Another key question relates to whether HIRA's elevated role in ALT is solely dependent upon the lack of ATRX/DAXX in ALT+ cancers. Our cell survival assays demonstrate that ALT+ cells are more sensitive to loss of HIRA in comparison to TEL+ cancers, which have ATRX/DAXXX activity. So far, we have not validated that the phenotypes seen are due to direct loss of HIRA. Conventional CRISPR-Cas9 knockout of HIRA is virtually impossible to conduct since ALT+ U2OS cells are completely inviable after prolonged loss of HIRA (unpublished data). To circumvent this issue, we can employ the CRISPR-FLIP strategy to create bi-allelic conditional knockouts of HIRA in ALT+ cells (397) (Figure 38). This involves fusing an invertible intronic cassette (FLIP) to Cas9-assisted gene editing. The non-mutagenic orientation of the FLIP cassette enables the selection of the correct nuclease-assisted targeting into the exon of one allele and the simultaneous accumulation of cells that inactivate the second allele by nuclease-mediated NHEJ. With the addition of Cre recombinase, the FLIP cassette becomes inverted and triggers a cryptic splice acceptor and polyadenylation signal (pA), which is mutagenic because it terminates transcription and results in the complete loss of gene function. This approach will allow us temporarily deplete HIRA and then rescue the phenotype with re-expression of HIRA upon release of Cre recombinase.

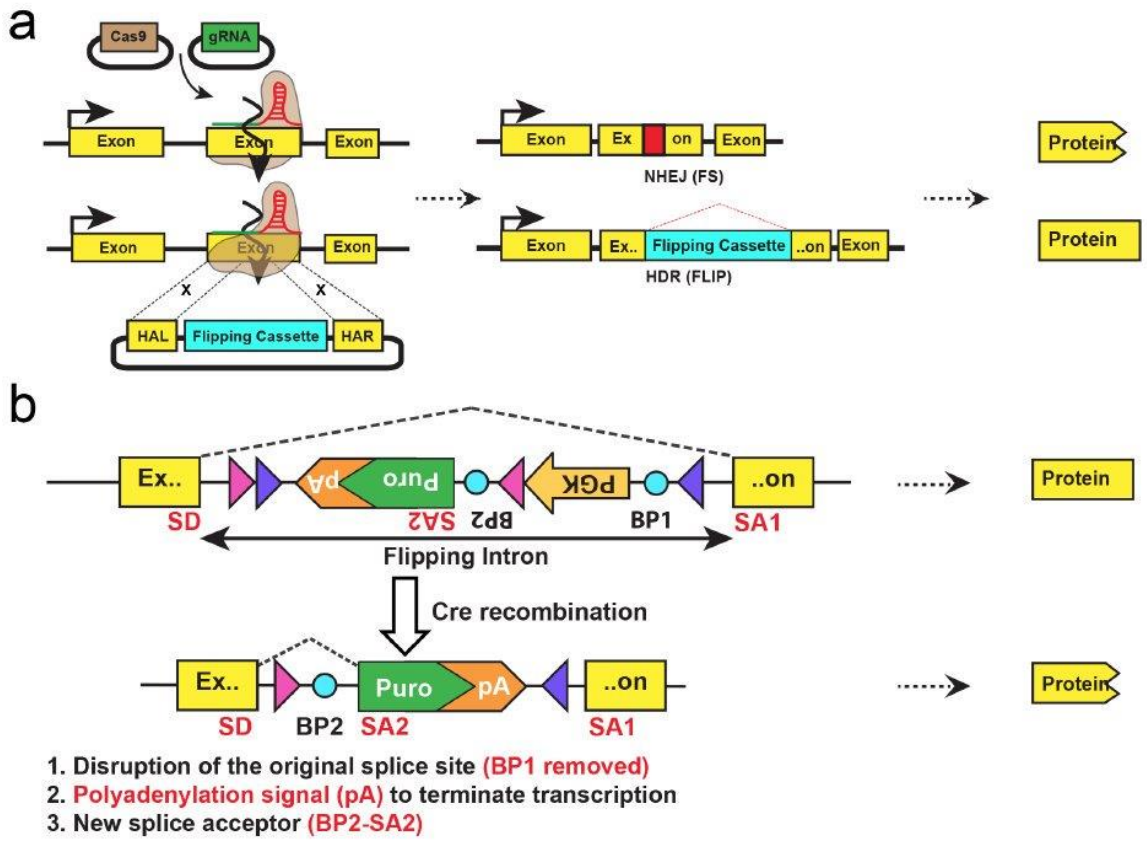

Figure 38. CRISPR-FLIP strategy for bi-allelic conditional gene modification. Schematic for the CRISPR-FLIP approach. B) Design of the FLIP cassette. SD: Splice donor, SA1 and SA2: Splice acceptor, purple triangles: LoxP1 sites, pink triangles: Lox5171 sites, blue circles: BP1 and BP2, branching point, and pA: polyadenylation signal. Adapted from Andersson-Rolf A et al., Nat Methods, 2017 (397) (https://www.nature.com/articles/nmeth.4156).

Studies have already documented that the depletion of ATRX is not sufficient to induce ALT, which implies that several factors work in conjunction to create the pro-ALT environment (42). Additionally, our clonogenic assays fail to address whether loss of ATRX directly attributes to the sensitivity of ALT+ cancers to HIRA depletion. We could still attempt to simultaneously deplete TEL+ cells of ATRX and HIRA using shRNA knockdown. If this combinatorial depletion impedes cell survival in TEL+ cells, then it would further affirm the importance of H3.3 deposition via ATRX or HIRA in cancer cells. This would support the effectiveness of targeting the synthetic

lethality of ATRX and HIRA in ALT+ cancers that already have a deficiency in ATRX. As we've shown in chapter 4, reconstitution of ATRX in U2OS cells prevents HIRA localization to ALT telomeres. This suggests that ATRX seems to be the preferred histone chaperone at telomeres and directly competes with HIRA in ALT. To explore the functional consequence of this, we could determine whether re-expression of ATRX in HIRA-depleted U2OS cells would rescue proliferation. Additionally, we can examine whether depletion of HIRA inhibits growth in patient-derived primary cell lines from ALT+ tumors, such as gliomas and osteosarcomas. This would raise the significance of our findings because it validates that this reliance on HIRA can be exploited to treat aggressive ALT+ tumors. Collectively, these studies will confirm the unique role of HIRA at ALT telomeres for compensation of ATRX deficiency (Figure 39).

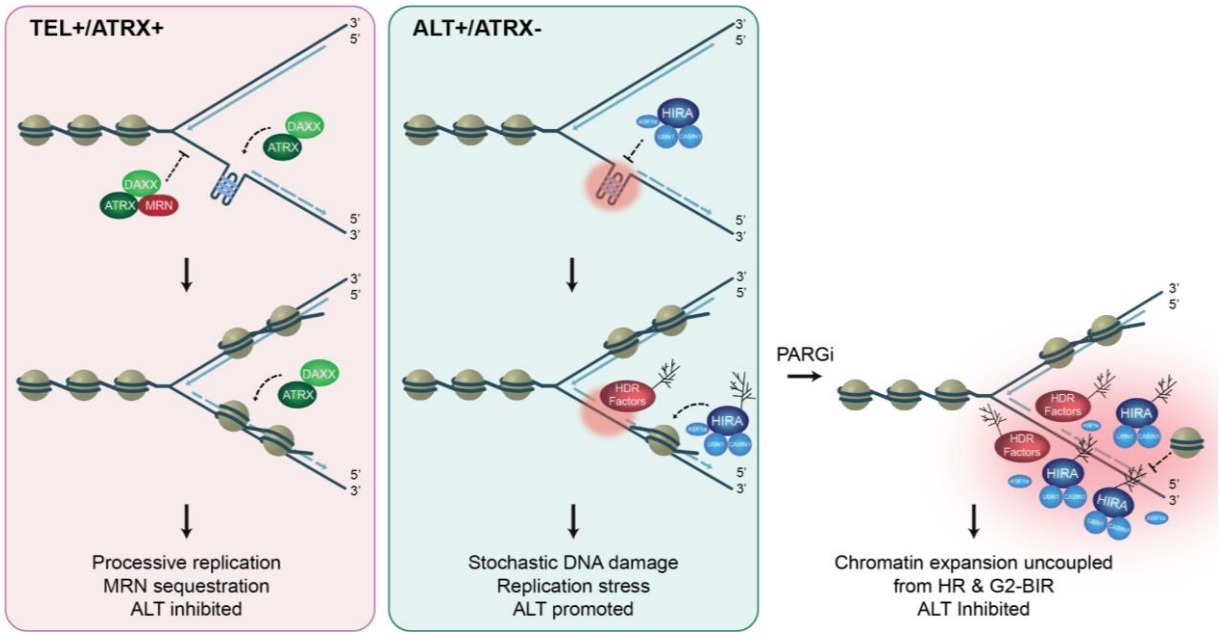

Figure 39. Proposed model of PAR-modulated HIRA at ALT telomeres. Tel+ cancers rely on ATRX/DAXX to resolve G4 structures during replication. ATRX/DAXX also sequesters the MRN complex and inhibits HDR at replication forks, allowing for normal replication to ensue. ALT+ cancers, which lack functional ATRX/DAXX, have an elevated reliance on the HIRA complex for H3.3 deposition during HDR-coupled replication. The HIRA complex is regulated by PAR to ensure localization to damaged telomeric lesions. However, persistence of PAR interferes with chromatin expansion associated with HR and G2-BIR, leading to ALT inhibition.

5.8 Can HIRA be Therapeutically Targeted to Specifically Kill ALT Cancer Cells?

We still need to decipher the HIRA protein interactions at ALT telomeres in order to fully understand the outcomes of HIRA inhibition. There are no current studies that have characterized the HIRA interactome or even explored the role of HIRA in ALT. ATRX-deficiency in ALT cancers may have driven an adaptation for HIRA-mediated H3.3 incorporation, which should extensively reshape the telomeric landscape in ALT. Using proximity-dependent biotinylation

(BioID), we can fuse HIRA to promiscuous BirA and trace transient and temporal proteins that are proximal to HIRA in ALT+ U2OS cells (398). This will be compared to a pre-existing dataset that characterized the ALT+ U2OS telomere-associated and proximal proteins (87). By looking at the overlap between the two datasets, we can identify ALT+ telomeric proteins that interact with HIRA. This will lead to greater insight into a complex HIRA-telomere network, where we can begin to dissect for the development of more selective and impactful therapies against ALT, as previously discussed.

Therapeutic strategies that target HIRA will tip the delicate balance between replication stress and ALT cancer survival. There are no known drugs that are designed against HIRA, especially since there are not many studies that directly implicate HIRA in cancer progression. A recent study connected the dynamics of histone variants to tumor progression and metastasis formation (399). Gomes et al. reported that suppression of CAF1 is required for metastatic colonization in breast cancers. Low levels of H3.1/H3.2 essentially leaves the space for nucleosome gap-filling by HIRA-dependent H3.3 deposition at the promoter of EMT (epithelial to mesenchymal transition) and pro-metastasis transcription factors. This is the first study to directly implicate HIRA with acquisition of aggressive traits in tumorigenesis. This is relevant to the field of ALT because ALT+ cancers are known to be highly aggressive and lead to poor patient outcomes (31,400). Cumulatively, these findings and our results support the notion for development of a small-molecule inhibitor of HIRA to target ALT tumors. This will make a huge impact since it has the potential to impair the initiation and progression of ALT cancers through deregulation of ALT telomere maintenance and restraint of metastasis.

Specific small-molecule inhibitors can be designed against HIRA to target its complex assembly or protein-protein interactions. Based on our findings and structural studies, the B-

domain is an appealing region to perturb because it would disrupt ASF1a binding and subsequent H3.3 deposition at ALT telomeres. As discussed in chapter 4, the B-domain is key to the HIRA-ASF1a interface, where it forms a β-hairpin that associates with the β-sandwich structure of the ASF1a N-terminal core domain through β-sheet, salt bridge and van der Waals interactions (Figure 40A-B) (286). The minimum HIRA fragment that binds to ASF1a spans residues 421–729. The binding site forms a shallow hydrophobic pocket that is lined by the residues Val60, Val62, Val65, Pro66, Phe72, and Phe74 from the β5–β6 region and residue Phe28 and Leu38 from the β3 and β4 strands of ASF1 to residues Ile461, Pro463 and Leu464 of the HIRA B-domain (Figure 40A). A cluster of salt bridges is seen between the acidic residues Asp37, Glu39, and Asp58 and of ASF1a and the basic residues Arg458, Arg459 and Arg460 of HIRA (Figure 40B).

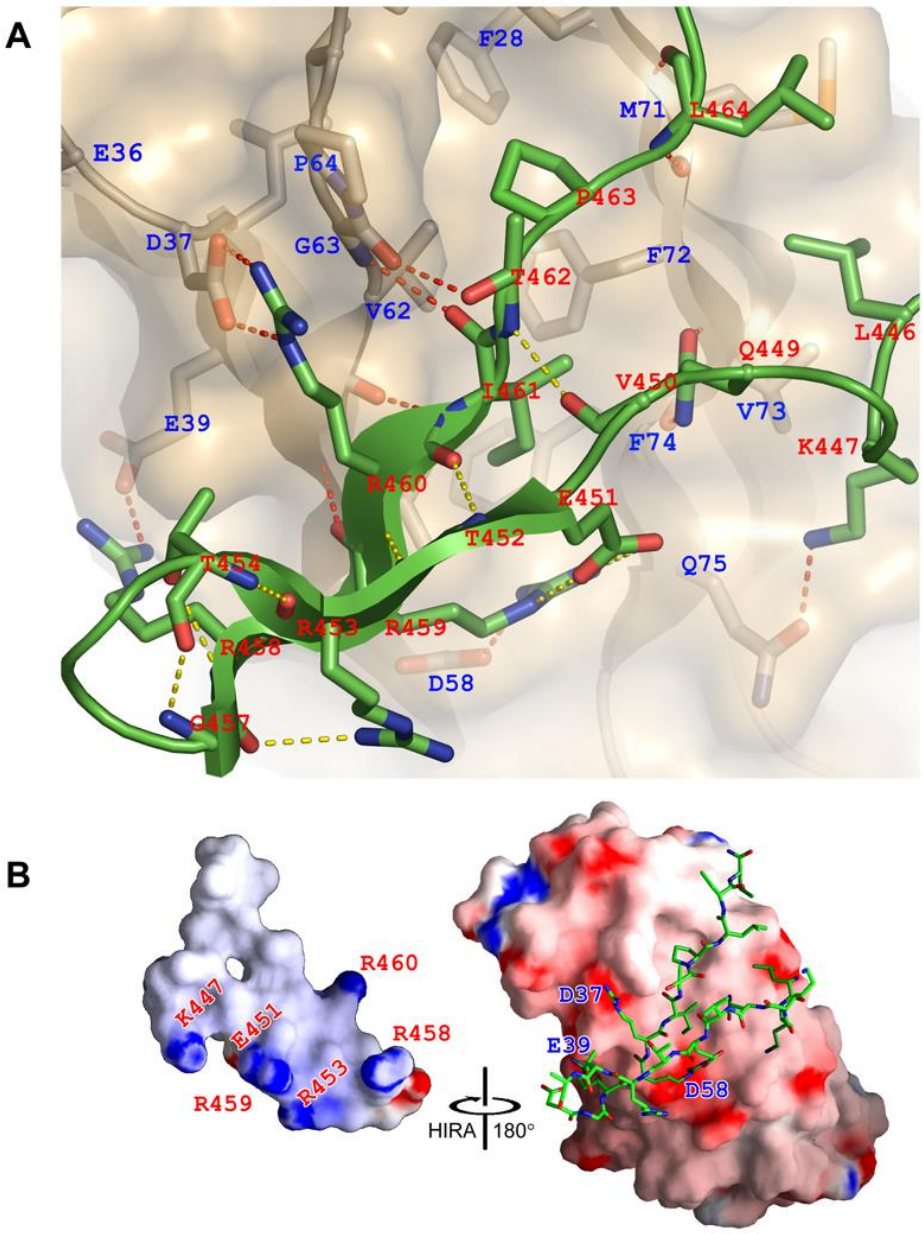

Figure 40. HIRA and ASF1a interface. A) HIRA is represented as a green ribbon. ASF1a is shown as a gold ribbon with a semi-transparent surface representation. Residues involved with hydrophobic interactions, hydrogen bonds, and salt bridge formation, are represented as sticks with CPK coloring. Hydrogen bonds: dashed lines, yellow: intra-molecular, and red: inter-molecular. B) Surface electrostatic representation of ASF1a and HIRA association. *Left:* HIRA surface shown in an open-book format. Critical residues that mediate salt-bridge formation is revealed on the surface. *Right:* HIRA fragment shown as sticks with CPK coloring within the complex. Adapted from Tang Y. et al., Nat Struct Mol Biol, 2006 (286) (https://www.nature.com/articles/nsmb1147).

Most of these residues are conserved in both ASF1 and HIRA, which emphasizes the importance of this interaction. Thus, we could envision peptide-like inhibitors with primary epitopes that could mimic short linear peptides, such as ASF1's acidic residues or secondary structural epitopes that could disrupt the β-sheet interface. To date, the B-domain has not been widely reported outside of the HIRA family, with the exception of some shared homology with the p60 subunit of CAF1 (286,401). Although the HIRA B-domain and the B-domain-like motifs of CAF1 p60 bind to ASF1a in similar manner, a striking difference is CAF1's lack of conservation of the three arginine residues 458-460 in HIRA. This brings forth the possibility for targeting this region to selectively uncouple HIRA-ASF1a activity.

Another attractive option is to disrupt HIRA homotrimerization, which is a prerequisite for CABIN1 binding and efficient H3.3 deposition at UV-enriched sites (227). The crystal structure of the HIRA C-domain reveals that the β-strand region is essential for homotrimerization and β-loop region mediates direct interaction with CABIN1 (Figure 41A-D). The residues Tryp799 and/or Asp800, which are located within the β2 strand, are critical for HIRA homooligomerization (Figure 41B). Asp800 does not associate with an adjacent HIRA subunit, but Trp799 forms a hydrophobic patch with Ile771 and Val806, which then interacts with Leu 851 and Thr853 of an adjacent HIRA subunit (Figure 41C). Mutations of Asp800 and Trp799 are sufficient to abolish HIRA complex assembly and function. We can imagine a small molecule inhibitor that could wedge within this hydrophobic pocket and block the association between adjacent HIRA subunits. Collectively, inhibition of HIRA represents a suitable therapeutic target against ALT+ cancers.

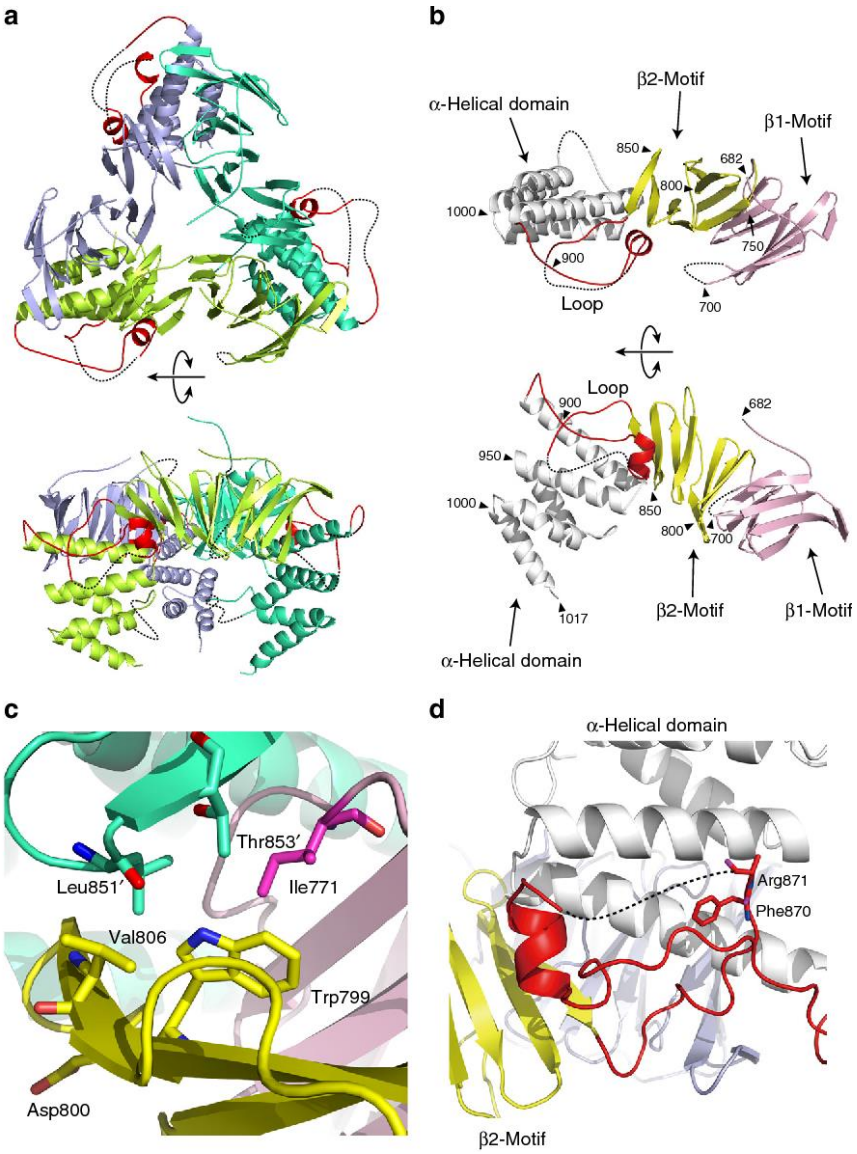

Figure 41. HIRA crystal structure reveals homotrimerization. Structure of homotrimeric HIRA (644-1017). Subunits A, B, and C are represented in light green, emerald green, and blue, respectively. Loop regions (860-907) shown in red. B) Structure of the HIRA monomer. The β1 and β2 motifs are represented as pink and yellow, respectively. The α-helical domain and the loop region are represented as white and red, respectively. The black triangles indicate critical residues of HIRA for homotrimerization. C) Trp799 is located at the interface between HIRA subunits A and B (yellow and emerald green). D) HIRA homotrimerization is required for CABIN1 binding to HIRA. The CABIN-binding loop is shown in red, highlighting residues Phe870 and Arg871. The α-helical domain of HIRA is shown in white. Adapted from Ray-Gallet et al., Nat Comm, 2018 (227) (https://www.nature.com/articles/s41467-018-05581-y).

5.9 Concluding Remarks

This thesis establishes a fundamental role of PARylation in the tight regulation of early factors that mediate ALT telomere maintenance. We have identified the first epigenetic synthetic lethality between ATRX and HIRA in ALT+ cancers. We envision a model where PAR-modulation of HIRA relieves chronic replication stress at ALT telomeres. The absence of HIRA leads to irreversibly stalled forks at telomeric DNA, which collapse into DSBs that remain unresolved. The saturation of DNA damage overwhelms the repair machinery and uncouples productive ALT activity. There are still plenty of questions regarding the mechanistic details that govern the initiation and progression of ALT. It is our hope that the findings and models in this dissertation shed light into one critical aspect of the ALT pathway that could be targeted to treat ALT+ tumors.

Appendix A

A.1 Chapter 2 Supplemental Material

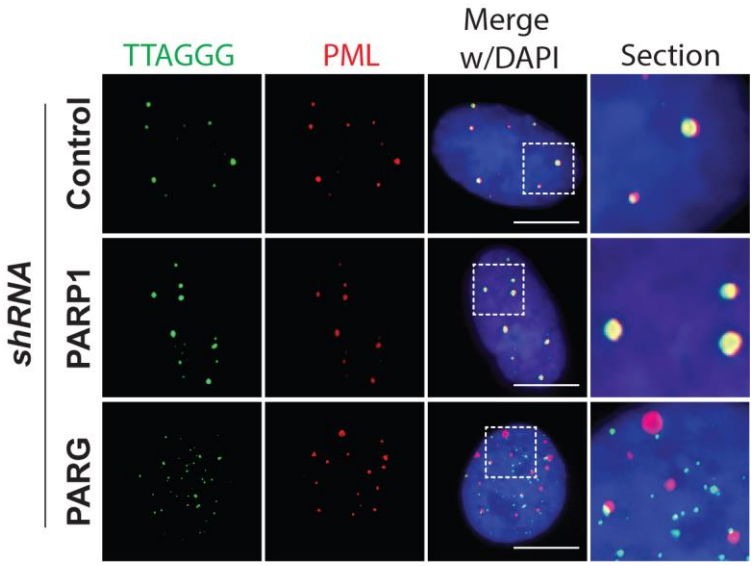

Figure 42. PARP and PARG depletion induces opposing effects on frequency of APBs. Representative immunofluorescence images of APBs (PML-TTAGGG) in U2OS cells expressing shControl, shPARP1 or shPARG.

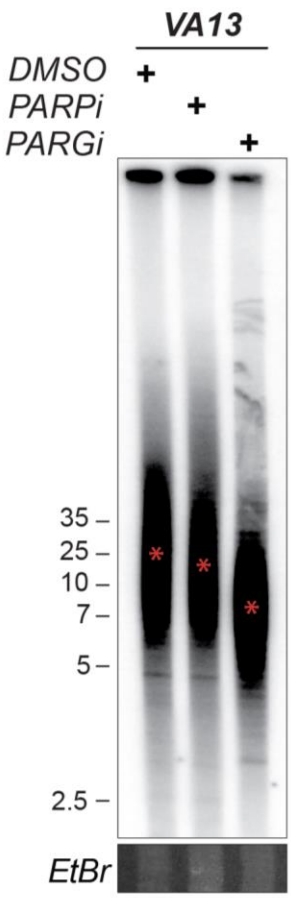

Figure 43. PARGi decreases telomere length in VA13 cells. PFGE of DMSO, PARPi (100nM) or PARGi (1μM) treated VA13 cells. The mean telomere length (kb) was calculating using TeloTool and is indicated by the red dot.

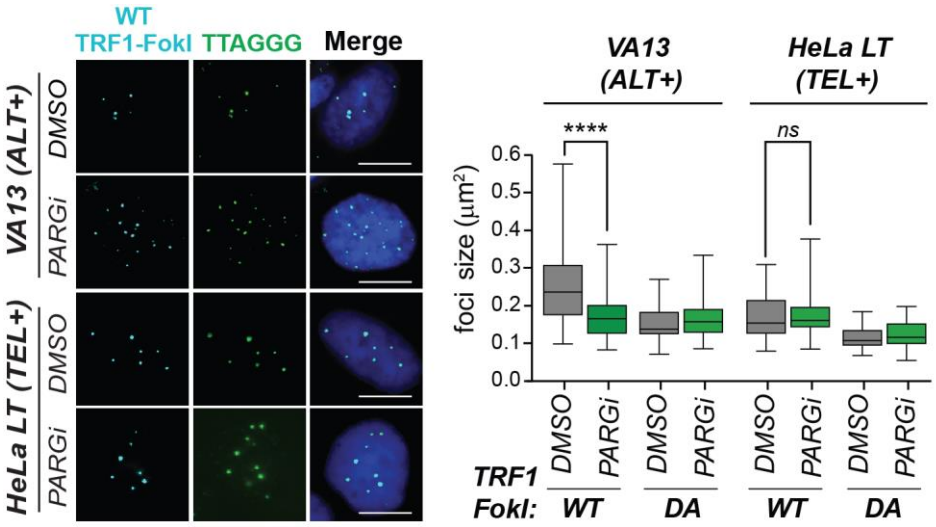

Figure 44. PARGi diminishes telomere clustering in ALT+ VA13 cells and not TEL+ Hela LT cells. *Left:* Representative IF images of VA13 and Hela LT cells transfected with WT TRF1-FokI. *Right:* TRF1-FokI foci size observed in each condition, including DA TRF1-FokI cells (images not shown). All graphed data in the figure are mean ± SEM, n=150 cells. Statistical significance was determined using one-way ANOVA. *P≤ 0.05, **P≤ 0.001, ***P≤ 0.001, ****P< 0.001.

Appendix B

B.1 Chapter 3 Supplemental Material

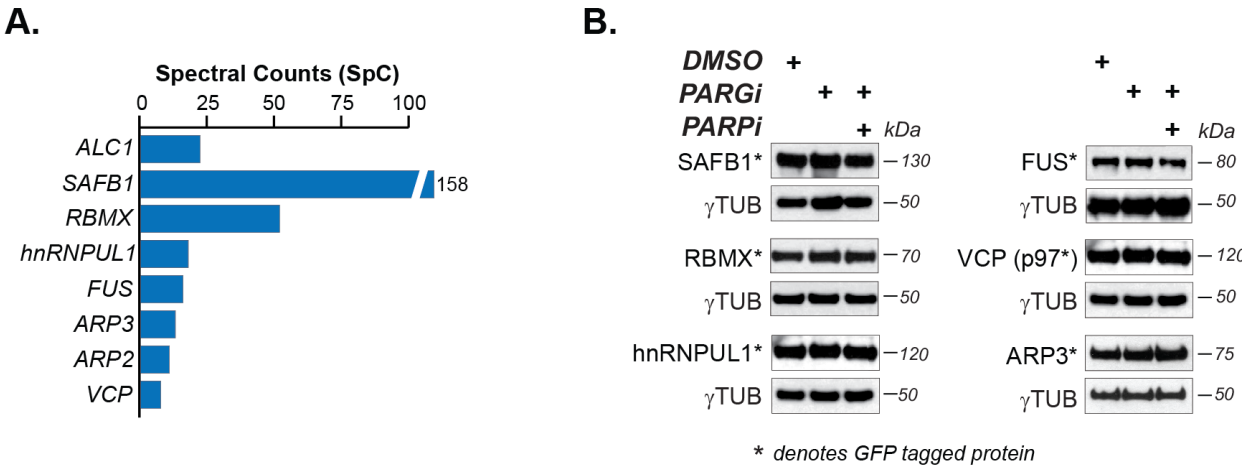

Figure 45. PAR-dependent recruitment of factors to ALT telomeric DSBs. A) Spectral counts for the indicated proteins that were identified by Af1521-PAR proteomics. B) Western blot analysis illustrating the expression of GFP fusion proteins in U2OS cells. GFP antibody was used to blot for protein expression in each treatment.

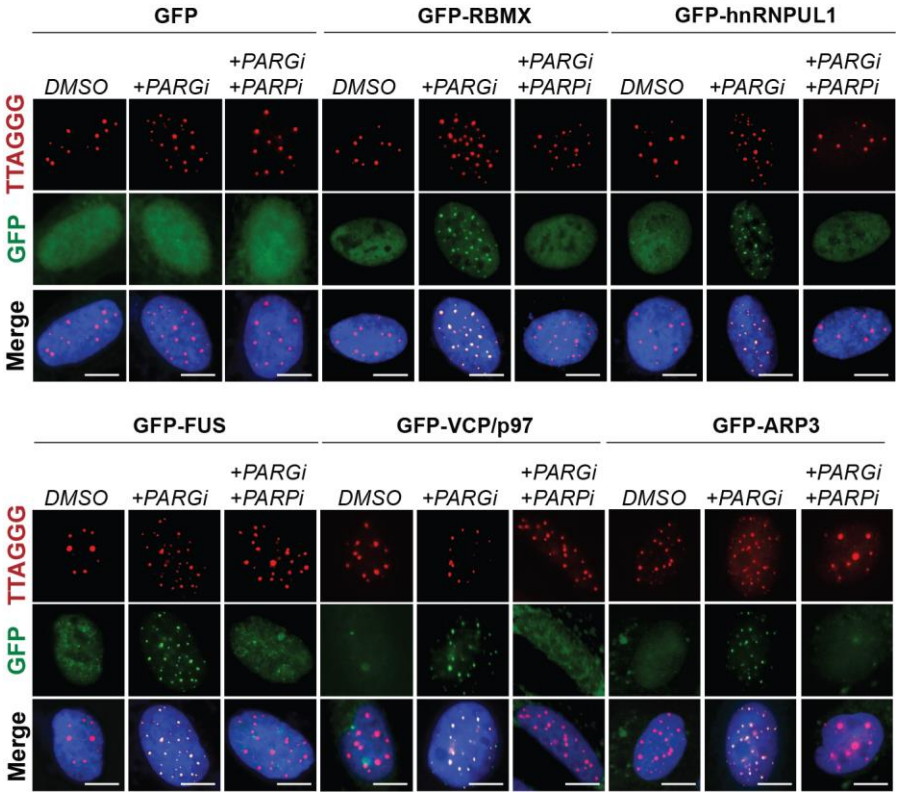

Figure 46. PAR-regulated factors localize to ALT telomeres. Representative IF images showing the localization of the indicated GFP fusion proteins in WT TRF1-FokI U2OS cells following treatment with DMSO, PARPi (5μM) and combined PARGi/PARPi (both 5μM).

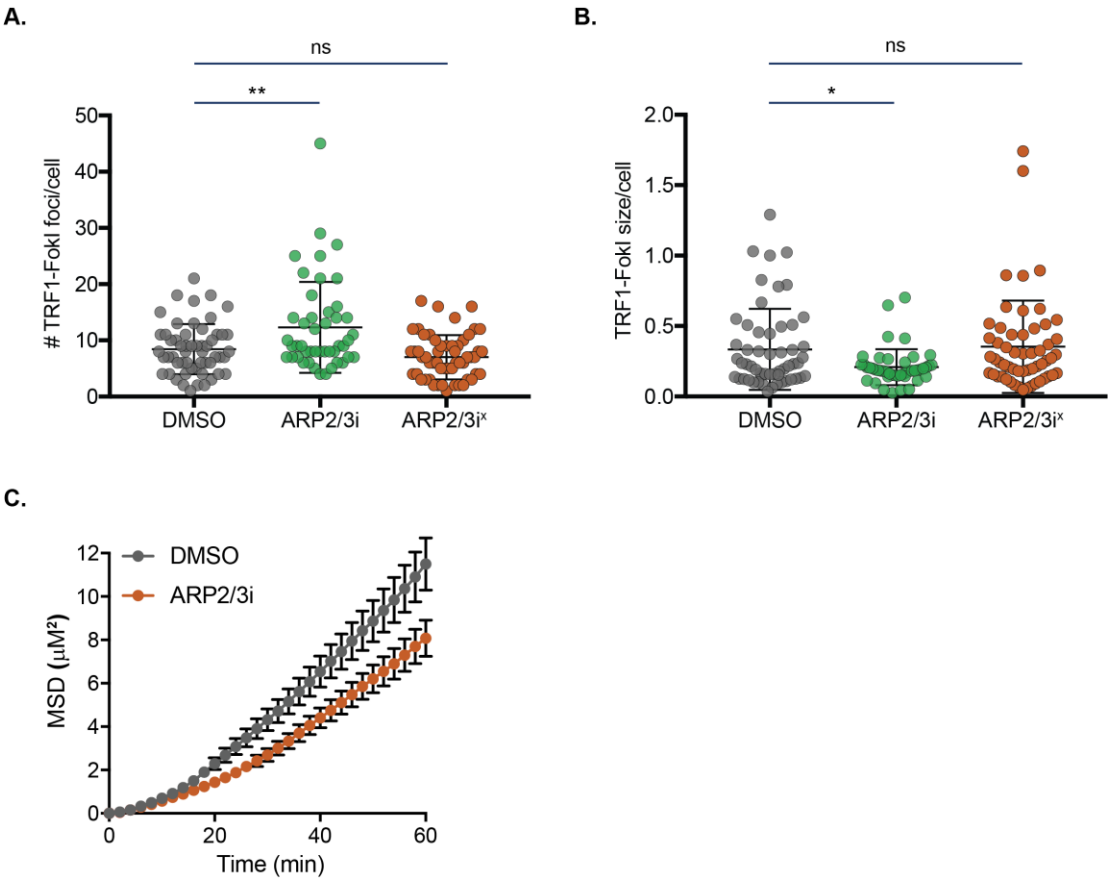

Figure 47. Inhibition of ARP2/3 impairs HDR in ALT. Quantification of TRF1-FokI telomeric foci A) number and B) size in WT cells treated with ARP2/3 inhibitor (ARP2/3) and ARP2/3 inactive inhibitor (ARP2/3i^{x}). C) Tracked telomere (eGFP-TRF1) movement in U2OS cells treated with ARP2/3i. Graph displays the cumulative Mean Squared Displacement (MSD) of telomeres imaged and analyzed, n=100 telomeres. Inhibitors used at 1μM. All graphed data in the figure are mean ± SEM. A) and B) n=150 cells and C) n=10 cells. Statistical significance was determined using one-way ANOVA. *P≤ 0.05, **P≤ 0.001, ***P≤ 0.001, ****P< 0.001.

Appendix C

C.1 Chapter 4 Supplemental Material

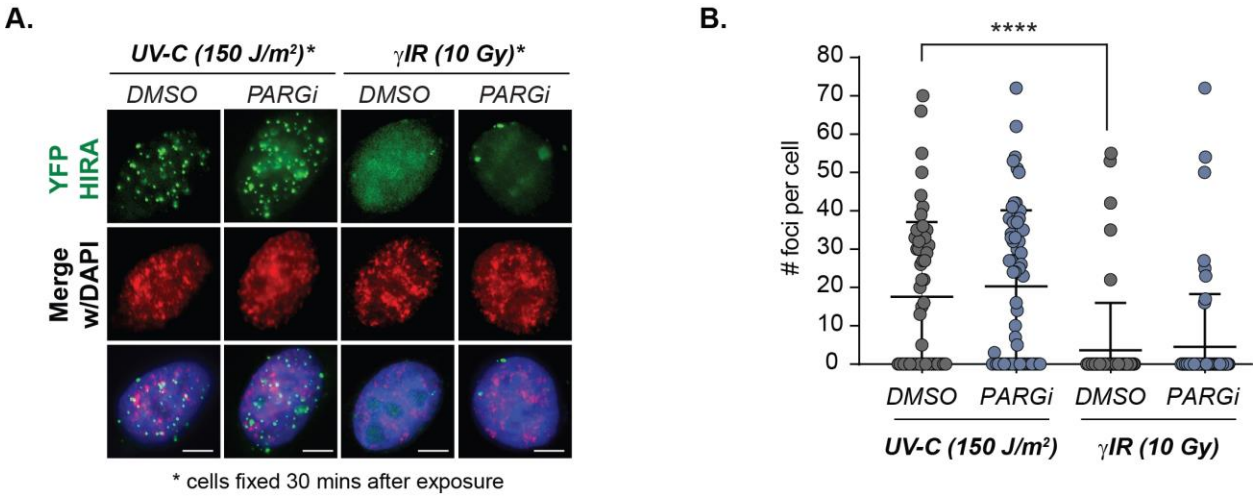

Figure 48. Selectivity of HIRA localization for UV-C damage. Representative IF images of YFP-HIRA localization in U2OS cells after exposure to 150 J/m^2 ultra-violet C (UV-C) and 10Gy ionizing irradiation (γIR). B) Quantification of YFP-HIRA foci in U2OS cells treated as indicated above. All graphed data in the figure are mean ± SEM, n=50 cells. Statistical significance was determined using one-way ANOVA. *P≤ 0.05, **P≤ 0.001, ***P≤ 0.001, ****P< 0.001.

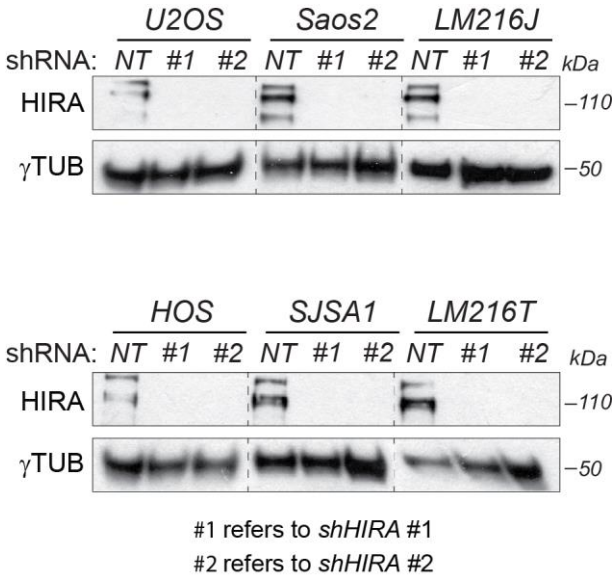

Figure 49. WB of HIRA KD using shRNA. Western blot validation of HIRA knockdown using two independent shRNAs (HIRA#1 and HIRA #2). γTUB images were cropped from the original.

Appendix D

D.1 *Af1521* PAR proteomics

Table 1. *Af1521* Mass Spectrometry Hits

Protein ID	Fold Change Average	Av. Spectral Counts
CHD1L	20.57	23.6
CABIN1	13.36	20.2
HIRA	8.69	12
CHD7	8.64	93.8
UBN1	8.52	15
XRCC1	7.58	24.2
PCNA	7.39	6.2
HUWE1	7.26	16.4
MLL2	7.24	21.8
UBN2	6.44	10
VCP	5.8	6.8
WDR1	5.68	11.4
AKAP2	4.74	7.4
SIPA1	4.53	10.2

Table 1 continued.

KIAA1671	4.05	11.2
SPECC1	4.03	6.6
SPTAN1	4.02	273
CASC3	3.93	6.4
UNC45A	3.92	12.2
TGM2	3.86	4.4
CORO1C	3.77	114.8
SALL1	3.75	4.4
TFAM	3.67	5
UACA	3.65	31.4
CFL2	3.59	6.2
PPP1CB	3.57	10.4
SPTBN1	3.56	298.4
SYNPO	3.4	28.4
AMOTL1	3.35	3.4
NFATC1	3.32	4
LIG3	3.27	59.8
MYLK	3.13	4
BAZ2B	3.08	14
NEXN	3.04	30.4
ARPC2	3.04	9.6
ZNF185	3.04	5

Table 1 continued.

CASZ1	3.04	2.6
GNB2	3.02	8.4
SATB2	2.98	5
NFAT5	2.93	6.2
TWF1	2.92	8.8
CORO1B	2.91	3
LIMA1	2.85	92.6
FN1	2.79	48
YES1	2.78	7.6
ITPR3	2.73	3.6
HNRNPA2B1	2.71	74.8
ZFHX4	2.71	38
PARP2	2.71	13.6
PARP1	2.68	288.2
TNKS	2.63	2
CBFB	2.6	3.2
MYO18A	2.59	87.6
RAD50	2.58	2.6
LMO7	2.57	142
GLDC	2.57	1.4
TMOD3	2.56	9.6
LZTS2	2.56	2.8

Table 1 continued.

CTTN	2.55	16.8
UTRN	2.55	3.2
TRPS1	2.52	11
SSH1	2.52	3.6
GAPDHS	2.51	3.8
POTE2B	2.48	3.4
HNRNPH3	2.47	3.6
H2BFS	2.46	2
HNRNPA1	2.44	45.6
DBN1	2.41	82.8
PABPC4	2.4	7.8
MGA	2.39	6.6
COL1A1	2.37	2.2
HNRNPD	2.36	10
YLPM1	2.34	40.2
ACTR3	2.33	12.6
DAPK3	2.28	2.8
CALD1	2.26	5.4
SPRR3	2.24	1.8
AMOTL2	2.2	1.6
PPP1R12A	2.19	98.2
LRRC59	2.18	2.6

Table 1 continued.

PAWR	2.17	2.4
CHAF1A	2.16	4.6
CAV1	2.15	10.8
ILF2	2.15	2.8
ACTR2	2.14	9.2
RPL9	2.13	12.2
KPNA2	2.13	6
DST	2.11	322.2
CD59	2.11	9.4
ARPC3	2.11	7.8
LRRFIP2	2.11	4.2

Appendix E

E.1 Plasmids, siRNAs, shRNAs, and Antibodies

Table 2. Plasmids

Name	Source
GFP-PARG-FL	Dr. Dea Slade (Max Perutz Lab, Vienna)
GFP-PARG-Q76A-K409A	Dr. Dea Slade (Max Perutz Lab, Vienna)
GFP-SAFB1	Dr. Steffi Oesterreich (University of Pittsburgh)
GFP-RBMX	Dr. Kyle Miller (University of Texas at Austin)
GFP-hnRNPUL1	Dr. Sophie Polo (Université Paris Diderot)
GFP-FUS1	Dr. Matthias Altmeyer (University of Zurich)
GFP-EWS1	Dr. Matthias Altmeyer (University of Zurich)
GFP-TAF15	Dr. Matthias Altmeyer (University of Zurich)
GFP-VCP/p97	Dr. Nico Dantuma (Addgene, #23971)
GFP-ARP3	Dr. Matthew Welch (Addgene, #8462)
YFP-HIRA	Dr. Geneviève Almouzni (Institut Curie)
YFP-HIRA-799-800	Dr. Geneviève Almouzni (Institut Curie)
YFP-HIRA-I461D	Dr. Geneviève Almouzni (Institut Curie)
YFP-HIRA-ΔB	This study

Table 2 continued.

GFP-Histone H3.3	Dr. Geneviève Almouzni (Institut Curie)

Table 3. siRNAs

Name	**Description/Cat#**
HIRA	5'-GAUGACGACAGUGUUAUCCUU-3'
HIRA 3'UTR	5'-UUUACAUAGGUCUUAGGUCUU-3'
CABIN1	Dharmacon SMARTpool, #J-012454-09
UBN1	Dharmacon SMARTpool, #J-014195-05
SAFB1	5'-UCAAUUUCGUCAGGAUUACUU-3'
RBMX	Dharmacon SMARTpool, #J-011691-09
hnRNPUL1	Dharmacon SMARTpool, #J-004132005
FUS	Dharmacon SMARTpool, #J-009497-07
VCP/p97	Dharmacon SMARTpool, #J-008727-09
ARP2	Dharmacon SMARTpool, #L-012076-02
ARP3	Dharmacon SMARTpool, #L-012076-02

Table 4. shRNAs

Name	Description/Cat#
HIRA #1	Sigma/ TRCN0000020515 Target Sequence: CGTGGATAACACTGTCGTCAT
HIRA #2	Sigma/TRCN0000020517 Target Sequence: GCTTGGTCAAAGGGTTGACAT
PARG	Dr. Robert W. Sobol (University of South Alabama)
PARP1	Dr. Robert W. Sobol (University of South Alabama)

Table 5. IF antibodies

Target	Source/Cat#	Dilution
PCNA	Cell Signaling, #2586	1:2500
Poly (ADP-ribose)	Millipore, #MABC547, clone [10H]	1:400
POLD3	Abnova, #H00010714-M01	1:500
PML	Santa Cruz, #sc-377390	1:200
FLAG	Cell Signaling, #14793	1:1000

Table 6. WB antibodies

Target	Source/Cat#	Dilution
PCNA	Cell Signaling, #2586	1:2000
RPA2	Abcam, #ab2175	1:1000
Poly (ADP-ribose)	Millipore, #MABC547	1:400
PARP1	Active Motif, #39559	1:5000
PARG	Cell Signaling, #66564	1:1000
ALC1 (CHD1L)	Bethyl, #A303-342A	1:2000
TRF1	Dr. Jan Karlseder (Salk Institute, CA)	1:1000
TRF2	Novus, #NB110-57130	1:1000
POLD3	Abnova, #H00010714-M01	1:1000
RECQ1	Bethyl, #A300-447A	1:1000
NFκB/p65	Santa-Cruz c-20	1:250
Histone H2AX S139	Millipore, #05-635	1:1000
CHK2 T68	Cell Signaling, #2197	1:1000
SAFB1	Bethyl, #A300-812A	1:1000
FUS	Bethyl, #A300-292A	1:200
hnRNPUL1	Bethyl, #A300-862A	1:1000
HIRA	Active Motif, #39557	1:200
CABIN1	Abcam, #ab3349	1:1000
UBN1	Abcam, #ab101282	1:2000

Appendix F

F.1 List of Abbreviations

ADPr: ADP-ribose

ALC1: Amplified in Liver Cancer 1

alt-NHEJ: Alternative Non-Homologous End-Joining

APBs: ALT-associated PML bodies

ARP 2/3: Actin-Related Proteins 2 and 3

ASF1a: Anti-Silencing Function 1A Histone Chaperone

ATM: Ataxia-Telangiectasia-Mutated

ATR: Ataxia-Rad3-related

ATRX: Alpha-thalassemia/Mental Retardation Syndrome, X-linked

BARD1: BRCA1-Associated RING Domain Protein 1

BIR: Break-Induced Replication

BLM: Bloom Helicase

BRCA1: Breast Cancer Gene 1

BRCA2: Breast Cancer Gene 2

BTR Complex: BLM-TOP3A-RMI1-2 complex

CABIN1: Calcineurin Binding Protein 1

CAF1: Chromatin Assembly Factor

cGAS: Cyclin GMP-AMP Synthase

CHD2: Chromatin Remodeler Chromodomain Helicase DNA-binding Protein 2

c-NHEJ: Classical Non-Homologous End-Joining

CO-FISH: Chromosome-orientation Fluorescent in situ Hybridization

DAXX: Death Domain Associated Protein

DNMT: DNA methyltransferase 1

DSB: Double-stranded Break

ECTR: Extrachromosomal Telomeric Repeat

EWS: Ewing Sarcoma

EZH2: Enhancer of Zeste 2

FANCM: Fanconi Anemia Complementation Goup M

FUS: Fused in Liposarcoma

G2-BIR: G2-Break Induced Repair

gH2AX: Gamma-H2A Histone Family Member X

HDR: Homology-Directed Repair

HIRA: Histone Regulator A

hnRNPUL1: heterogenous nuclear ribonucleoprotein U-like 1

HOP2: Homologous Pairing Protein 2

HSV-1: Herpes simplex virus type 1

IDH1: Isocitrate Dehydrogenase

IF-FISH: Immunofluorescence-Fluorescence in situ Hybridization

IFN: Interferon

MARylation: Mono(ADP-ribosyl)ation

MiDAS: Spontaneous Mitotic DNA synthesis

MND1: Meiotic Nuclear Division Protein 1

Mre11: Meiotic Recombination 11 Homolog 1

NBS1: Nijmegen Breakage Syndrome Protein 1

NER: Nucleotide Excision Repair

NuRD Complex: Nucleosome Modeling and Histone Deacetylation

PanNET: Pancreatic Neuroendocrine Tumor

PARG: Poly(ADP-ribose) Glycohydrolase

PARP1: Poly(ADP-ribose) Polymerase 1

PARylation: Poly(ADP-ribosyl)ation

PBM: PAR-Binding Motif

PBZ: PAR-Binding Zinc Finger

PCNA: Proliferating Cellular Nuclear Antigen

POT1: Protection of Telomere 1

Rad50: ATP-binding Cassette-ATPase

RAP1: Repressor/Activator Protein 1

RBMX: RNA-Binding Motif Protein X-Linked

RFC: Replication Factor C

RPA: Replication Protein A

RRM: RNA Recognition Motif

SAFB1: Scaffold Attachment Factor B1

SETD2: SET domain containing 2

SIM: SUMO-interacting motif

SMARCAL1: SWI/SNF-related, Matrix-associated, Actin-dependent Regulator of Chromatin, Subfamily A-like 1

SMC4/6: Structural Maintenance of Chromosomes Protein 5/6

SMX Complex: SLX1-SLX4, MUS81-EME1, and XPF-ERCC1

SSA: Single-strand Annealing

SSB: Single-stranded Break

STING: Stimulator of Interferon Genes

SUMO: Small Ubiquitin-like Modifiers (SUMO)

TAF15: TATA-box Binding Protein Associated Factor 15

TIN2: TRF1-and TRF2-Interacting Nuclear Protein 2

TNKS: Tankyrase

TPP1: Adrenocortical Dysplasia Homolog (ACD)

TRF1: Telomere Repeat Binding Factor 1

TRF2: Telomere Repeat Binding Factor 2

T-SCE: Telomere Sister Chromatid Exchange

UBN1: Ubinuclein 1

VCP/p97: Vasolin-Containing Protein

53BP1: p53-Binding Protein 1

Bibliography

1. Neumann AA, Reddel RR. Telomere maintenance and cancer -- look, no telomerase. Nat Rev Cancer. 2002 Nov;2(11):879–884.
2. Griffith JD, Comeau L, Rosenfield S, Stansel RM, Bianchi A, Moss H, et al. Mammalian telomeres end in a large duplex loop. Cell. 1999 May 14;97(4):503–514.
3. Van Ly D, Low RRJ, Frölich S, Bartolec TK, Kafer GR, Pickett HA, et al. Telomere loop dynamics in chromosome end protection. Mol Cell. 2018 Aug 16;71(4):510–525.e6.
4. Doksani Y, Wu JY, de Lange T, Zhuang X. Super-resolution fluorescence imaging of telomeres reveals TRF2-dependent T-loop formation. Cell. 2013 Oct 10;155(2):345–356.
5. de Lange T. Shelterin-Mediated Telomere Protection. Annu Rev Genet. 2018 Nov 23;52:223–247.
6. Webb CJ, Wu Y, Zakian VA. DNA repair at telomeres: keeping the ends intact. Cold Spring Harb Perspect Biol. 2013 Jun 1;5(6).
7. Wellinger RJ. In the end, what's the problem? Mol Cell. 2014 Mar 20;53(6):855–856.
8. Victorelli S, Passos JF. Telomeres and Cell Senescence - Size Matters Not. EBioMedicine. 2017 Jul;21:14–20.
9. Davoli T, Denchi EL, de Lange T. Persistent telomere damage induces bypass of mitosis and tetraploidy. Cell. 2010 Apr 2;141(1):81–93.
10. Qian Y, Chen X. Senescence regulation by the p53 protein family. Methods Mol Biol. 2013;965:37–61.

11. Chicas A, Wang X, Zhang C, McCurrach M, Zhao Z, Mert O, et al. Dissecting the unique role of the retinoblastoma tumor suppressor during cellular senescence. Cancer Cell. 2010 Apr 13;17(4):376–387.

12. Maciejowski J, de Lange T. Telomeres in cancer: tumour suppression and genome instability. Nat Rev Mol Cell Biol. 2017 Jan 18;18(3):175–186.

13. Maciejowski J, Li Y, Bosco N, Campbell PJ, de Lange T. Chromothripsis and kataegis induced by telomere crisis. Cell. 2015 Dec 17;163(7):1641–1654.

14. Reddel RR. Telomere maintenance mechanisms in cancer: clinical implications. Curr Pharm Des. 2014;20(41):6361–6374.

15. Kim NW, Piatyszek MA, Prowse KR, Harley CB, West MD, Ho PL, et al. Specific association of human telomerase activity with immortal cells and cancer. Science. 1994 Dec 23;266(5193):2011–2015.

16. Yuan X, Larsson C, Xu D. Mechanisms underlying the activation of TERT transcription and telomerase activity in human cancer: old actors and new players. Oncogene. 2019 Aug;38(34):6172–6183.

17. Leão R, Apolónio JD, Lee D, Figueiredo A, Tabori U, Castelo-Branco P. Mechanisms of human telomerase reverse transcriptase (hTERT) regulation: clinical impacts in cancer. J Biomed Sci. 2018 Mar 12;25(1):22.

18. Cristofari G, Lingner J. Telomere length homeostasis requires that telomerase levels are limiting. EMBO J. 2006 Feb 8;25(3):565–574.

19. Liu T, Yuan X, Xu D. Cancer-Specific Telomerase Reverse Transcriptase (TERT) Promoter Mutations: Biological and Clinical Implications. Genes (Basel). 2016 Jul 18;7(7).

20. Chiba K, Lorbeer FK, Shain AH, McSwiggen DT, Schruf E, Oh A, et al. Mutations in the promoter of the telomerase gene TERT contribute to tumorigenesis by a two-step mechanism. Science. 2017 Sep 29;357(6358):1416–1420.

21. Akıncılar SC, Khattar E, Boon PLS, Unal B, Fullwood MJ, Tergaonkar V. Long-Range Chromatin Interactions Drive Mutant TERT Promoter Activation. Cancer Discov. 2016 Sep 20;6(11):1276–1291.

22. Horn S, Figl A, Rachakonda PS, Fischer C, Sucker A, Gast A, et al. TERT promoter mutations in familial and sporadic melanoma. Science. 2013 Feb 22;339(6122):959–961.

23. Vinagre J, Almeida A, Pópulo H, Batista R, Lyra J, Pinto V, et al. Frequency of TERT promoter mutations in human cancers. Nat Commun. 2013;4:2185.

24. Bryan TM, Englezou A, Dalla-Pozza L, Dunham MA, Reddel RR. Evidence for an alternative mechanism for maintaining telomere length in human tumors and tumor-derived cell lines. Nat Med. 1997 Nov;3(11):1271–1274.

25. Henson JD, Neumann AA, Yeager TR, Reddel RR. Alternative lengthening of telomeres in mammalian cells. Oncogene. 2002 Jan 21;21(4):598–610.

26. Sobinoff AP, Pickett HA. Alternative lengthening of telomeres: DNA repair pathways converge. Trends Genet. 2017 Sep 29;33(12):921–932.

27. Pan X, Drosopoulos WC, Sethi L, Madireddy A, Schildkraut CL, Zhang D. FANCM, BRCA1, and BLM cooperatively resolve the replication stress at the ALT telomeres. Proc Natl Acad Sci USA. 2017 Jul 18;114(29):E5940–E5949.

28. Barroso-González J, García-Expósito L, Hoang SM, Lynskey ML, Roncaioli JL, Ghosh A, et al. RAD51AP1 is an essential mediator of alternative lengthening of telomeres. Mol Cell. 2019 Oct 3;76(1):11–26.e7.

29. Cox KE, Maréchal A, Flynn RL. SMARCAL1 resolves replication stress at ALT telomeres. Cell Rep. 2016 Feb 9;14(5):1032–1040.

30. Silva B, Pentz R, Figueira AM, Arora R, Lee YW, Hodson C, et al. FANCM limits ALT activity by restricting telomeric replication stress induced by deregulated BLM and R-loops. Nat Commun. 2019 May 28;10(1):2253.

31. Muntoni A, Reddel RR. The first molecular details of ALT in human tumor cells. Hum Mol Genet. 2005 Oct 15;14 Spec No. 2:R191–6.

32. Alternative Lengthening of Telomeres in Human Cells on JSTOR [Internet]. [cited 2019 Oct 3]. Available from: https://www.jstor.org/stable/3580402?seq=1#metadata_info_tab_contents

33. Dilley RL, Greenberg RA. Alternative telomere maintenance and cancer. Trends Cancer. 2015 Oct 1;1(2):145–156.

34. Henson JD, Hannay JA, McCarthy SW, Royds JA, Yeager TR, Robinson RA, et al. A robust assay for alternative lengthening of telomeres in tumors shows the significance of alternative lengthening of telomeres in sarcomas and astrocytomas. Clin Cancer Res. 2005 Jan 1;11(1):217–225.

35. Hakin-Smith V, Jellinek DA, Levy D, Carroll T, Teo M, Timperley WR, et al. Alternative lengthening of telomeres and survival in patients with glioblastoma multiforme. Lancet. 2003 Mar 8;361(9360):836–838.

36. De Vitis M, Berardinelli F, Sgura A. Telomere Length Maintenance in Cancer: At the Crossroad between Telomerase and Alternative Lengthening of Telomeres (ALT). Int J Mol Sci. 2018 Feb 18;19(2).

37. Serakinci N, Hoare SF, Kassem M, Atkinson SP, Keith WN. Telomerase promoter reprogramming and interaction with general transcription factors in the human mesenchymal stem cell. Regen Med. 2006 Jan;1(1):125–131.

38. Koelsche C, Renner M, Hartmann W, Brandt R, Lehner B, Waldburger N, et al. TERT promoter hotspot mutations are recurrent in myxoid liposarcomas but rare in other soft tissue sarcoma entities. J Exp Clin Cancer Res. 2014 Apr 11;33:33.

39. Grobelny JV, Kulp-McEliece M, Broccoli D. Effects of reconstitution of telomerase activity on telomere maintenance by the alternative lengthening of telomeres (ALT) pathway. Hum Mol Genet. 2001 Sep 1;10(18):1953–1961.

40. Ford LP, Zou Y, Pongracz K, Gryaznov SM, Shay JW, Wright WE. Telomerase can inhibit the recombination-based pathway of telomere maintenance in human cells. J Biol Chem. 2001 Aug 24;276(34):32198–32203.

41. Heaphy CM, de Wilde RF, Jiao Y, Klein AP, Edil BH, Shi C, et al. Altered telomeres in tumors with ATRX and DAXX mutations. Science. 2011 Jul 22;333(6041):425.

42. Lovejoy CA, Li W, Reisenweber S, Thongthip S, Bruno J, de Lange T, et al. Loss of ATRX, genome instability, and an altered DNA damage response are hallmarks of the alternative lengthening of telomeres pathway. PLoS Genet. 2012 Jul 19;8(7):e1002772.

43. Mason-Osann E, Dai A, Floro J, Lock YJ, Reiss M, Gali H, et al. Identification of a novel gene fusion in ALT positive osteosarcoma. Oncotarget. 2018 Aug 28;9(67):32868–32880.

44. Singhi AD, Liu T-C, Roncaioli JL, Cao D, Zeh HJ, Zureikat AH, et al. Alternative Lengthening of Telomeres and Loss of DAXX/ATRX Expression Predicts Metastatic Disease and Poor Survival in Patients with Pancreatic Neuroendocrine Tumors. Clin Cancer Res. 2017 Jan 15;23(2):600–609.

45. Napier CE, Huschtscha LI, Harvey A, Bower K, Noble JR, Hendrickson EA, et al. ATRX represses alternative lengthening of telomeres. Oncotarget. 2015 Jun 30;6(18):16543–16558.

46. Sadikovic B, Al-Romaih K, Squire JA, Zielenska M. Cause and consequences of genetic and epigenetic alterations in human cancer. Curr Genomics. 2008 Sep;9(6):394–408.

47. Núñez FJ, Mendez FM, Kadiyala P, Alghamri MS, Savelieff MG, Garcia-Fabiani MB, et al. IDH1-R132H acts as a tumor suppressor in glioma via epigenetic up-regulation of the DNA damage response. Sci Transl Med. 2019 Feb 13;11(479).

48. Dang L, White DW, Gross S, Bennett BD, Bittinger MA, Driggers EM, et al. Cancer-associated IDH1 mutations produce 2-hydroxyglutarate. Nature. 2009 Dec 10;462(7274):739–744.

49. Yeager TR, Neumann AA, Englezou A, Huschtscha LI, Noble JR, Reddel RR. Telomerase-negative immortalized human cells contain a novel type of promyelocytic leukemia (PML) body. Cancer Res. 1999 Sep 1;59(17):4175–4179.

50. Cesare AJ, Heaphy CM, O'Sullivan RJ. Visualization of telomere integrity and function in vitro and in vivo using immunofluorescence techniques. Curr Protoc Cytom. 2015 Jul 1;73:12.40.1–31.

51. Venturini L, Erdas R, Costa A, Gronchi A, Pilotti S, Zaffaroni N, et al. ALT-associated promyelocytic leukaemia body (APB) detection as a reproducible tool to assess alternative lengthening of telomere stability in liposarcomas. J Pathol. 2008 Mar;214(4):410–414.

52. Grobelny JV, Godwin AK, Broccoli D. ALT-associated PML bodies are present in viable cells and are enriched in cells in the G(2)/M phase of the cell cycle. J Cell Sci. 2000 Dec;113 Pt 24:4577–4585.

53. Nabetani A, Yokoyama O, Ishikawa F. Localization of hRad9, hHus1, hRad1, and hRad17 and caffeine-sensitive DNA replication at the alternative lengthening of telomeres-associated promyelocytic leukemia body. J Biol Chem. 2004 Jun 11;279(24):25849–25857.

54. Zhong Z-H, Jiang W-Q, Cesare AJ, Neumann AA, Wadhwa R, Reddel RR. Disruption of telomere maintenance by depletion of the MRE11/RAD50/NBS1 complex in cells that use alternative lengthening of telomeres. J Biol Chem. 2007 Oct 5;282(40):29314–29322.

55. Potts PR, Yu H. The SMC5/6 complex maintains telomere length in ALT cancer cells through SUMOylation of telomere-binding proteins. Nat Struct Mol Biol. 2007 Jul;14(7):581–590.

56. Chung I, Osterwald S, Deeg KI, Rippe K. PML body meets telomere: the beginning of an ALTernate ending? Nucleus. 2012 Jun;3(3):263–275.

57. Wang Y, Dasso M. SUMOylation and deSUMOylation at a glance. J Cell Sci. 2009 Dec 1;122(Pt 23):4249–4252.

58. Chung I, Leonhardt H, Rippe K. De novo assembly of a PML nuclear subcompartment occurs through multiple pathways and induces telomere elongation. J Cell Sci. 2011 Nov 1;124(Pt 21):3603–3618.

59. Banani SF, Rice AM, Peeples WB, Lin Y, Jain S, Parker R, et al. Compositional Control of Phase-Separated Cellular Bodies. Cell. 2016 Jul 28;166(3):651–663.

60. Wu G, Jiang X, Lee W-H, Chen P-L. Assembly of functional ALT-associated promyelocytic leukemia bodies requires Nijmegen Breakage Syndrome 1. Cancer Res. 2003 May 15;63(10):2589–2595.

61. Jiang W-Q, Zhong Z-H, Henson JD, Neumann AA, Chang AC-M, Reddel RR. Suppression of alternative lengthening of telomeres by Sp100-mediated sequestration of the MRE11/RAD50/NBS1 complex. Mol Cell Biol. 2005 Apr;25(7):2708–2721.

62. Perrem K, Colgin LM, Neumann AA, Yeager TR, Reddel RR. Coexistence of alternative lengthening of telomeres and telomerase in hTERT-transfected GM847 cells. Mol Cell Biol. 2001 Jun;21(12):3862–3875.

63. Draskovic I, Arnoult N, Steiner V, Bacchetti S, Lomonte P, Londoño-Vallejo A. Probing PML body function in ALT cells reveals spatiotemporal requirements for telomere recombination. Proc Natl Acad Sci USA. 2009 Sep 15;106(37):15726–15731.

64. Zhang J-M, Yadav T, Ouyang J, Lan L, Zou L. Alternative Lengthening of Telomeres through Two Distinct Break-Induced Replication Pathways. Cell Rep. 2019 Jan 22;26(4):955–968.e3.

65. Cesare AJ, Griffith JD. Telomeric DNA in ALT cells is characterized by free telomeric circles and heterogeneous t-loops. Mol Cell Biol. 2004 Nov;24(22):9948–9957.

66. Nabetani A, Ishikawa F. Unusual telomeric DNAs in human telomerase-negative immortalized cells. Mol Cell Biol. 2009 Feb;29(3):703–713.

67. Cesare AJ, Reddel RR. Alternative Lengthening of Telomeres in Mammalian Cells - Madame Curie Bioscience Database - NCBI Bookshelf. 2013;

68. Tokutake Y, Matsumoto T, Watanabe T, Maeda S, Tahara H, Sakamoto S, et al. Extra-chromosomal telomere repeat DNA in telomerase-negative immortalized cell lines. Biochem Biophys Res Commun. 1998 Jun 29;247(3):765–772.

69. Henson JD, Cao Y, Huschtscha LI, Chang AC, Au AYM, Pickett HA, et al. DNA C-circles are specific and quantifiable markers of alternative-lengthening-of-telomeres activity. Nat Biotechnol. 2009 Dec;27(12):1181–1185.

70. Zhang T, Zhang Z, Shengzhao G, Li X, Liu H, Zhao Y. Strand break-induced replication fork collapse leads to C-circles, C-overhangs and telomeric recombination. PLoS Genet. 2019 Feb 4;15(2):e1007925.

71. Plantinga MJ, Pascarelli KM, Merkel AS, Lazar AJ, von Mehren M, Lev D, et al. Telomerase suppresses formation of ALT-associated single-stranded telomeric C-circles. Mol Cancer Res. 2013 Jun;11(6):557–567.

72. Henson JD, Lau LM, Koch S, Martin La Rotta N, Dagg RA, Reddel RR. The C-Circle Assay for alternative-lengthening-of-telomeres activity. Methods. 2017 Feb 1;114:74–84.

73. Tomaska L, Nosek J, Kramara J, Griffith JD. Telomeric circles: universal players in telomere maintenance? Nat Struct Mol Biol. 2009 Oct 6;16(10):1010–1015.

74. Pickett HA, Cesare AJ, Johnston RL, Neumann AA, Reddel RR. Control of telomere length by a trimming mechanism that involves generation of t-circles. EMBO J. 2009 Apr 8;28(7):799–809.

75. Pickett HA, Henson JD, Au AYM, Neumann AA, Reddel RR. Normal mammalian cells negatively regulate telomere length by telomere trimming. Hum Mol Genet. 2011 Dec 1;20(23):4684–4692.

76. Brault ME, Autexier C. Telomeric recombination induced by dysfunctional telomeres. Mol Biol Cell. 2011 Jan 15;22(2):179–188.

77. Londoño-Vallejo JA, Der-Sarkissian H, Cazes L, Bacchetti S, Reddel RR. Alternative lengthening of telomeres is characterized by high rates of telomeric exchange. Cancer Res. 2004 Apr 1;64(7):2324–2327.

78. Bailey SM, Brenneman MA, Goodwin EH. Frequent recombination in telomeric DNA may extend the proliferative life of telomerase-negative cells. Nucleic Acids Res. 2004 Jul 16;32(12):3743–3751.

79. Nabetani A, Ishikawa F. Alternative lengthening of telomeres pathway: recombination-mediated telomere maintenance mechanism in human cells. J Biochem. 2011 Jan;149(1):5–14.

80. Claussin C, Chang M. The many facets of homologous recombination at telomeres. Microb Cell. 2015 Jul 30;2(9):308–321.

81. Sobinoff AP, Allen JA, Neumann AA, Yang SF, Walsh ME, Henson JD, et al. BLM and SLX4 play opposing roles in recombination-dependent replication at human telomeres. EMBO J. 2017 Oct 2;36(19):2907–2919.

82. Lundblad V, Blackburn EH. An alternative pathway for yeast telomere maintenance rescues est1- senescence. Cell. 1993 Apr 23;73(2):347–360.

83. Chen Q, Ijpma A, Greider CW. Two survivor pathways that allow growth in the absence of telomerase are generated by distinct telomere recombination events. Mol Cell Biol. 2001 Mar;21(5):1819–1827.

84. Lydeard JR, Jain S, Yamaguchi M, Haber JE. Break-induced replication and telomerase-independent telomere maintenance require Pol32. Nature. 2007 Aug 16;448(7155):820–823.

85. Grandin N, Charbonneau M. Telomerase- and Rad52-independent immortalization of budding yeast by an inherited-long-telomere pathway of telomeric repeat amplification. Mol Cell Biol. 2009 Feb;29(4):965–985.

86. Larrivée M, Wellinger RJ. Telomerase- and capping-independent yeast survivors with alternate telomere states. Nat Cell Biol. 2006 Jul;8(7):741–747.

87. Garcia-Exposito L, Bournique E, Bergoglio V, Bose A, Barroso-Gonzalez J, Zhang S, et al. Proteomic profiling reveals a specific role for translesion DNA polymerase η in the alternative lengthening of telomeres. Cell Rep. 2016 Nov 8;17(7):1858–1871.

88. Banumathy G, Somaiah N, Zhang R, Tang Y, Hoffmann J, Andrake M, et al. Human UBN1 is an ortholog of yeast Hpc2p and has an essential role in the HIRA/ASF1a chromatin-remodeling pathway in senescent cells. Mol Cell Biol. 2009 Feb;29(3):758–770.

89. Déjardin J, Kingston RE. Purification of proteins associated with specific genomic Loci. Cell. 2009 Jan 9;136(1):175–186.

90. Grolimund L, Aeby E, Hamelin R, Armand F, Chiappe D, Moniatte M, et al. A quantitative telomeric chromatin isolation protocol identifies different telomeric states. Nat Commun. 2013;4:2848.

91. Acharya S, Kaul Z, Gocha AS, Martinez AR, Harris J, Parvin JD, et al. Association of BLM and BRCA1 during Telomere Maintenance in ALT Cells. PLoS One. 2014 Aug 1;9(8):e103819.

92. Grudic A, Jul-Larsen A, Haring SJ, Wold MS, Lønning PE, Bjerkvig R, et al. Replication protein A prevents accumulation of single-stranded telomeric DNA in cells that use alternative lengthening of telomeres. Nucleic Acids Res. 2007 Oct 24;35(21):7267–7278.

93. Min J, Wright WE, Shay JW. Alternative Lengthening of Telomeres Mediated by Mitotic DNA Synthesis Engages Break-Induced Replication Processes. Mol Cell Biol. 2017 Oct 15;37(20).

94. Verma P, Dilley RL, Zhang T, Gyparaki MT, Li Y, Greenberg RA. RAD52 and SLX4 act nonepistatically to ensure telomere stability during alternative telomere lengthening. Genes Dev. 2019 Feb 1;33(3-4):221–235.

95. Dunham MA, Neumann AA, Fasching CL, Reddel RR. Telomere maintenance by recombination in human cells. Nat Genet. 2000 Dec;26(4):447–450.

96. Cho NW, Dilley RL, Lampson MA, Greenberg RA. Interchromosomal homology searches drive directional ALT telomere movement and synapsis. Cell. 2014 Sep 25;159(1):108–121.

97. Roumelioti F-M, Sotiriou SK, Katsini V, Chiourea M, Halazonetis TD, Gagos S. Alternative lengthening of human telomeres is a conservative DNA replication process with features of break-induced replication. EMBO Rep. 2016 Oct 19;17(12):1731–1737.

98. Dilley RL, Verma P, Cho NW, Winters HD, Wondisford AR, Greenberg RA. Break-induced telomere synthesis underlies alternative telomere maintenance. Nature. 2016 Nov 3;539(7627):54–58.

99. Temime-Smaali N, Guittat L, Sidibe A, Shin-ya K, Trentesaux C, Riou J-F. The G-quadruplex ligand telomestatin impairs binding of topoisomerase IIIalpha to G-quadruplex-forming oligonucleotides and uncaps telomeres in ALT cells. PLoS One. 2009 Sep 9;4(9):e6919.

100. Wang Q, Liu J, Chen Z, Zheng K, Chen C, Hao Y-H, et al. G-quadruplex formation at the 3’ end of telomere DNA inhibits its extension by telomerase, polymerase and unwinding by helicase. Nucleic Acids Res. 2011 Aug;39(14):6229–6237.

101. Couch FB, Bansbach CE, Driscoll R, Luzwick JW, Glick GG, Bétous R, et al. ATR phosphorylates SMARCAL1 to prevent replication fork collapse. Genes Dev. 2013 Jul 15;27(14):1610–1623.

102. Alexander JL, Orr-Weaver TL. Replication fork instability and the consequences of fork collisions from rereplication. Genes Dev. 2016 Oct 15;30(20):2241–2252.

103. Cortez D. Preventing replication fork collapse to maintain genome integrity. DNA Repair (Amst). 2015 Aug;32:149–157.

104. Lu R, O’Rourke JJ, Sobinoff AP, Allen JAM, Nelson CB, Tomlinson CG, et al. The FANCM-BLM-TOP3A-RMI complex suppresses alternative lengthening of telomeres (ALT). Nat Commun. 2019 May 28;10(1):2252.

105. Arora R, Lee Y, Wischnewski H, Brun CM, Schwarz T, Azzalin CM. RNaseH1 regulates TERRA-telomeric DNA hybrids and telomere maintenance in ALT tumour cells. Nat Commun. 2014 Oct 21;5:5220.

106. Schrank BR, Aparicio T, Li Y, Chang W, Chait BT, Gundersen GG, et al. Nuclear ARP2/3 drives DNA break clustering for homology-directed repair. Nature. 2018 Jun 20;559(7712):61–66.

107. Bhattacharyya S, Keirsey J, Russell B, Kavecansky J, Lillard-Wetherell K, Tahmaseb K, et al. Telomerase-associated protein 1, HSP90, and topoisomerase IIalpha associate directly with the BLM helicase in immortalized cells using ALT and modulate its helicase activity using telomeric DNA substrates. J Biol Chem. 2009 May 29;284(22):14966–14977.

108. Bizard AH, Hickson ID. The dissolution of double Holliday junctions. Cold Spring Harb Perspect Biol. 2014 Jul 1;6(7):a016477.

109. Özer Ö, Bhowmick R, Liu Y, Hickson ID. Human cancer cells utilize mitotic DNA synthesis to resist replication stress at telomeres regardless of their telomere maintenance mechanism. Oncotarget. 2018 Mar 23;9(22):15836–15846.

110. Bhowmick R, Minocherhomji S, Hickson ID. RAD52 facilitates mitotic DNA synthesis following replication stress. Mol Cell. 2016 Dec 15;64(6):1117–1126.

111. Sotiriou SK, Kamileri I, Lugli N, Evangelou K, Da-Ré C, Huber F, et al. Mammalian RAD52 Functions in Break-Induced Replication Repair of Collapsed DNA Replication Forks. Mol Cell. 2016 Dec 15;64(6):1127–1134.

112. Panier S, Maric M, Hewitt G, Mason-Osann E, Gali H, Dai A, et al. SLX4IP Antagonizes Promiscuous BLM Activity during ALT Maintenance. Mol Cell. 2019 Oct 3;76(1):27–43.e11.

113. Wan B, Yin J, Horvath K, Sarkar J, Chen Y, Wu J, et al. SLX4 assembles a telomere maintenance toolkit by bridging multiple endonucleases with telomeres. Cell Rep. 2013 Sep 12;4(5):861–869.

114. Sarkar J, Wan B, Yin J, Vallabhaneni H, Horvath K, Kulikowicz T, et al. SLX4 contributes to telomere preservation and regulated processing of telomeric joint molecule intermediates. Nucleic Acids Res. 2015 Jul 13;43(12):5912–5923.

115. Conomos D, Stutz MD, Hills M, Neumann AA, Bryan TM, Reddel RR, et al. Variant repeats are interspersed throughout the telomeres and recruit nuclear receptors in ALT cells. J Cell Biol. 2012 Dec 10;199(6):893–906.

116. Conomos D, Reddel RR, Pickett HA. NuRD-ZNF827 recruitment to telomeres creates a molecular scaffold for homologous recombination. Nat Struct Mol Biol. 2014 Sep;21(9):760–770.

117. Conomos D, Pickett HA, Reddel RR. Alternative lengthening of telomeres: remodeling the telomere architecture. Front Oncol. 2013 Feb 20;3:27.

118. Lewis PW, Elsaesser SJ, Noh K-M, Stadler SC, Allis CD. Daxx is an H3.3-specific histone chaperone and cooperates with ATRX in replication-independent chromatin assembly at telomeres. Proc Natl Acad Sci USA. 2010 Aug 10;107(32):14075–14080.

119. Linger JG, Tyler JK. Chromatin disassembly and reassembly during DNA repair. Mutat Res. 2007 May 1;618(1-2):52–64.

120. Law MJ, Lower KM, Voon HPJ, Hughes JR, Garrick D, Viprakasit V, et al. ATR-X syndrome protein targets tandem repeats and influences allele-specific expression in a size-dependent manner. Cell. 2010 Oct 29;143(3):367–378.

121. Chan K-M, Fang D, Gan H, Hashizume R, Yu C, Schroeder M, et al. The histone H3.3K27M mutation in pediatric glioma reprograms H3K27 methylation and gene expression. Genes Dev. 2013 May 1;27(9):985–990.

122. Khuong-Quang D-A, Buczkowicz P, Rakopoulos P, Liu X-Y, Fontebasso AM, Bouffet E, et al. K27M mutation in histone H3.3 defines clinically and biologically distinct subgroups of pediatric diffuse intrinsic pontine gliomas. Acta Neuropathol. 2012 Sep;124(3):439–447.

123. Gupte R, Liu Z, Kraus WL. PARPs and ADP-ribosylation: recent advances linking molecular functions to biological outcomes. Genes Dev. 2017 Jan 15;31(2):101–126.

124. Oei SL, Keil C, Ziegler M. Poly(ADP-ribosylation) and genomic stability. Biochem Cell Biol. 2005 Jun;83(3):263–269.

125. Schreiber V, Dantzer F, Ame J-C, de Murcia G. Poly(ADP-ribose): novel functions for an old molecule. Nat Rev Mol Cell Biol. 2006 Jul;7(7):517–528.

126. Morales J, Li L, Fattah FJ, Dong Y, Bey EA, Patel M, et al. Review of poly (ADP-ribose) polymerase (PARP) mechanisms of action and rationale for targeting in cancer and other diseases. Crit Rev Eukaryot Gene Expr. 2014;24(1):15–28.

127. Vyas S, Matic I, Uchima L, Rood J, Zaja R, Hay RT, et al. Family-wide analysis of poly(ADP-ribose) polymerase activity. Nat Commun. 2014 Jul 21;5:4426.

128. Ray Chaudhuri A, Nussenzweig A. The multifaceted roles of PARP1 in DNA repair and chromatin remodelling. Nat Rev Mol Cell Biol. 2017 Oct;18(10):610–621.

129. Gibson BA, Kraus WL. New insights into the molecular and cellular functions of poly(ADP-ribose) and PARPs. Nat Rev Mol Cell Biol. 2012 Jun 20;13(7):411–424.

130. Beck C, Robert I, Reina-San-Martin B, Schreiber V, Dantzer F. Poly(ADP-ribose) polymerases in double-strand break repair: focus on PARP1, PARP2 and PARP3. Exp Cell Res. 2014 Nov 15;329(1):18–25.

131. Alemasova EE, Lavrik OI. Poly(ADP-ribosyl)ation by PARP1: reaction mechanism and regulatory proteins. Nucleic Acids Res. 2019 May 7;47(8):3811–3827.

132. Krishnakumar R, Kraus WL. The PARP side of the nucleus: molecular actions, physiological outcomes, and clinical targets. Mol Cell. 2010 Jul 9;39(1):8–24.

133. Schreiber V, Ricoul M, Amé J-C, Dantzer F, Meder V, Spenlehauer C, et al. PARP-2: Structure-Function Relationship. Poly(ADP-Ribosyl)ation. Boston, MA: Springer US; 2006. p. 13–31.

134. Yélamos J, Schreiber V, Dantzer F. Toward specific functions of poly(ADP-ribose) polymerase-2. Trends Mol Med. 2008 Apr;14(4):169–178.

135. Beck C, Boehler C, Guirouilh Barbat J, Bonnet M-E, Illuzzi G, Ronde P, et al. PARP3 affects the relative contribution of homologous recombination and nonhomologous end-joining pathways. Nucleic Acids Res. 2014 May;42(9):5616–5632.

136. Boehler C, Gauthier LR, Mortusewicz O, Biard DS, Saliou J-M, Bresson A, et al. Poly(ADP-ribose) polymerase 3 (PARP3), a newcomer in cellular response to DNA damage and mitotic progression. Proc Natl Acad Sci USA. 2011 Feb 15;108(7):2783–2788.

137. Chiang YJ, Hsiao SJ, Yver D, Cushman SW, Tessarollo L, Smith S, et al. Tankyrase 1 and tankyrase 2 are essential but redundant for mouse embryonic development. PLoS One. 2008 Jul 9;3(7):e2639.

138. Kim MK. Novel insight into the function of tankyrase. Oncol Lett. 2018 Dec;16(6):6895–6902.

139. MacPherson L, Tamblyn L, Rajendra S, Bralha F, McPherson JP, Matthews J. 2,3,7,8-Tetrachlorodibenzo-p-dioxin poly(ADP-ribose) polymerase (TiPARP, ARTD14) is a mono-ADP-ribosyltransferase and repressor of aryl hydrocarbon receptor transactivation. Nucleic Acids Res. 2013 Feb 1;41(3):1604–1621.

140. Atasheva S, Akhrymuk M, Frolova EI, Frolov I. New PARP gene with an anti-alphavirus function. J Virol. 2012 Aug;86(15):8147–8160.

141. Gao G, Guo X, Goff SP. Inhibition of retroviral RNA production by ZAP, a CCCH-type zinc finger protein. Science. 2002 Sep 6;297(5587):1703–1706.

142. Daugherty MD, Young JM, Kerns JA, Malik HS. Rapid evolution of PARP genes suggests a broad role for ADP-ribosylation in host-virus conflicts. PLoS Genet. 2014 May 29;10(5):e1004403.

143. Li N, Chen J. ADP-ribosylation: activation, recognition, and removal. Mol Cells. 2014 Jan 27;37(1):9–16.

144. Luo X, Kraus WL. On PAR with PARP: cellular stress signaling through poly(ADP-ribose) and PARP-1. Genes Dev. 2012 Mar 1;26(5):417–432.

145. Mendoza-Alvarez H, Alvarez-Gonzalez R. Poly(ADP-ribose) polymerase is a catalytic dimer and the automodification reaction is intermolecular. J Biol Chem. 1993 Oct 25;268(30):22575–22580.

146. Alvarez-Gonzalez R. 3'-Deoxy-NAD+ as a substrate for poly(ADP-ribose)polymerase and the reaction mechanism of poly(ADP-ribose) elongation. J Biol Chem. 1988 Nov 25;263(33):17690–17696.

147. Althaus FR, Kleczowska HE, Malanga M, Müntener CR, Pleschke JM, Ebner M, et al. Poly ADP-ribosylation: A DNA break signal mechanism. Mol Cell Biochem.

148. Dawicki-McKenna JM, Langelier M-F, DeNizio JE, Riccio AA, Cao CD, Karch KR, et al. PARP-1 Activation Requires Local Unfolding of an Autoinhibitory Domain. Mol Cell. 2015 Dec 3;60(5):755–768.

149. Eustermann S, Wu W-F, Langelier M-F, Yang J-C, Easton LE, Riccio AA, et al. Structural Basis of Detection and Signaling of DNA Single-Strand Breaks by Human PARP-1. Mol Cell. 2015 Dec 3;60(5):742–754.

150. Liu L, Kong M, Gassman NR, Freudenthal BD, Prasad R, Zhen S, et al. PARP1 changes from three-dimensional DNA damage searching to one-dimensional diffusion after auto-PARylation or in the presence of APE1. Nucleic Acids Res. 2017 Dec 15;45(22):12834–12847.

151. Ji Y, Tulin AV. The roles of PARP1 in gene control and cell differentiation. Curr Opin Genet Dev. 2010 Oct;20(5):512–518.

152. Kraus WL. Transcriptional control by PARP-1: chromatin modulation, enhancer-binding, coregulation, and insulation. Curr Opin Cell Biol. 2008 Jun;20(3):294–302.

153. Gagné J-P, Isabelle M, Lo KS, Bourassa S, Hendzel MJ, Dawson VL, et al. Proteome-wide identification of poly(ADP-ribose) binding proteins and poly(ADP-ribose)-associated protein complexes. Nucleic Acids Res. 2008 Dec;36(22):6959–6976.

154. Teloni F, Altmeyer M. Readers of poly(ADP-ribose): designed to be fit for purpose. Nucleic Acids Res. 2016 Feb 18;44(3):993–1006.

155. Yelamos J, Farres J, Llacuna L, Ampurdanes C, Martin-Caballero J. PARP-1 and PARP-2: New players in tumour development. Am J Cancer Res. 2011 Jan 8;1(3):328–346.

156. Boehler C, Gauthier L, Yelamos J, Noll A, Schreiber V, Dantzer F. Phenotypic characterization of Parp-1 and Parp-2 deficient mice and cells. Methods Mol Biol. 2011;780:313–336.

157. Ménissier de Murcia J, Ricoul M, Tartier L, Niedergang C, Huber A, Dantzer F, et al. Functional interaction between PARP-1 and PARP-2 in chromosome stability and embryonic development in mouse. EMBO J. 2003 May 1;22(9):2255–2263.

158. Pascal JM, Ellenberger T. The rise and fall of poly(ADP-ribose): An enzymatic perspective. DNA Repair (Amst). 2015 Aug;32:10–16.

159. David KK, Andrabi SA, Dawson TM, Dawson VL. Parthanatos, a messenger of death. Front Biosci (Landmark Ed). 2009 Jan 1;14:1116–1128.

160. Yu S-W, Andrabi SA, Wang H, Kim NS, Poirier GG, Dawson TM, et al. Apoptosis-inducing factor mediates poly(ADP-ribose) (PAR) polymer-induced cell death. Proc Natl Acad Sci USA. 2006 Nov 28;103(48):18314–18319.

161. Andrabi SA, Kim NS, Yu S-W, Wang H, Koh DW, Sasaki M, et al. Poly(ADP-ribose) (PAR) polymer is a death signal. Proc Natl Acad Sci USA. 2006 Nov 28;103(48):18308–18313.

162. Yu S-W, Wang H, Poitras MF, Coombs C, Bowers WJ, Federoff HJ, et al. Mediation of poly(ADP-ribose) polymerase-1-dependent cell death by apoptosis-inducing factor. Science. 2002 Jul 12;297(5579):259–263.

163. Moubarak RS, Yuste VJ, Artus C, Bouharrour A, Greer PA, Menissier-de Murcia J, et al. Sequential activation of poly(ADP-ribose) polymerase 1, calpains, and Bax is essential in apoptosis-inducing factor-mediated programmed necrosis. Mol Cell Biol. 2007 Jul;27(13):4844–4862.

164. Zaja R, Mikoč A, Barkauskaite E, Ahel I. Molecular Insights into Poly(ADP-ribose) Recognition and Processing. Biomolecules. 2012 Dec 21;3(1):1–17.

165. Barkauskaite E, Brassington A, Tan ES, Warwicker J, Dunstan MS, Banos B, et al. Visualization of poly(ADP-ribose) bound to PARG reveals inherent balance between exo- and endo-glycohydrolase activities. Nat Commun. 2013;4:2164.

166. Liu C, Vyas A, Kassab MA, Singh AK, Yu X. The role of poly ADP-ribosylation in the first wave of DNA damage response. Nucleic Acids Res. 2017 Aug 21;45(14):8129–8141.

167. Oka S, Kato J, Moss J. Identification and characterization of a mammalian 39-kDa poly(ADP-ribose) glycohydrolase. J Biol Chem. 2006 Jan 13;281(2):705–713.

168. Sharifi R, Morra R, Appel CD, Tallis M, Chioza B, Jankevicius G, et al. Deficiency of terminal ADP-ribose protein glycohydrolase TARG1/C6orf130 in neurodegenerative disease. EMBO J. 2013 May 2;32(9):1225–1237.

169. Palazzo L, Thomas B, Jemth A-S, Colby T, Leidecker O, Feijs KLH, et al. Processing of protein ADP-ribosylation by Nudix hydrolases. Biochem J. 2015 Jun 1;468(2):293–301.

170. Lin S, Gasmi L, Xie Y, Ying K, Gu S, Wang Z, et al. Cloning, expression and characterisation of a human Nudix hydrolase specific for adenosine 5′-diphosphoribose (ADP-ribose). Biochimica et Biophysica Acta (BBA) - Protein Structure and Molecular Enzymology. 2002 Jan;1594(1):127–135.

171. Min W, Cortes U, Herceg Z, Tong W-M, Wang Z-Q. Deletion of the nuclear isoform of poly(ADP-ribose) glycohydrolase (PARG) reveals its function in DNA repair, genomic stability and tumorigenesis. Carcinogenesis. 2010 Dec;31(12):2058–2065.

172. Meyer RG, Meyer-Ficca ML, Whatcott CJ, Jacobson EL, Jacobson MK. Two small enzyme isoforms mediate mammalian mitochondrial poly(ADP-ribose) glycohydrolase (PARG) activity. Exp Cell Res. 2007 Aug 1;313(13):2920–2936.

173. Meyer-Ficca ML, Meyer RG, Coyle DL, Jacobson EL, Jacobson MK. Human poly(ADP-ribose) glycohydrolase is expressed in alternative splice variants yielding isoforms that localize to different cell compartments. Exp Cell Res. 2004 Jul 15;297(2):521–532.

174. Slade D, Dunstan MS, Barkauskaite E, Weston R, Lafite P, Dixon N, et al. The structure and catalytic mechanism of a poly(ADP-ribose) glycohydrolase. Nature. 2011 Sep 4;477(7366):616–620.

175. Till S, Ladurner AG. Sensing NAD metabolites through macro domains. Front Biosci (Landmark Ed). 2009 Jan 1;14:3246–3258.

176. Karras GI, Kustatscher G, Buhecha HR, Allen MD, Pugieux C, Sait F, et al. The macro domain is an ADP-ribose binding module. EMBO J. 2005 Jun 1;24(11):1911–1920.

177. Kaufmann T, Grishkovskaya I, Polyansky AA, Kostrhon S, Kukolj E, Olek KM, et al. A novel non-canonical PIP-box mediates PARG interaction with PCNA. Nucleic Acids Res. 2017 Sep 19;45(16):9741–9759.

178. Mortusewicz O, Fouquerel E, Amé J-C, Leonhardt H, Schreiber V. PARG is recruited to DNA damage sites through poly(ADP-ribose)- and PCNA-dependent mechanisms. Nucleic Acids Res. 2011 Jul;39(12):5045–5056.

179. Hanzlikova H, Kalasova I, Demin AA, Pennicott LE, Cihlarova Z, Caldecott KW. The Importance of Poly(ADP-Ribose) Polymerase as a Sensor of Unligated Okazaki Fragments during DNA Replication. Mol Cell. 2018 Jul 19;71(2):319–331.e3.

180. Koh DW, Lawler AM, Poitras MF, Sasaki M, Wattler S, Nehls MC, et al. Failure to degrade poly(ADP-ribose) causes increased sensitivity to cytotoxicity and early embryonic lethality. Proc Natl Acad Sci USA. 2004 Dec 21;101(51):17699–17704.

181. Cortes U, Tong W-M, Coyle DL, Meyer-Ficca ML, Meyer RG, Petrilli V, et al. Depletion of the 110-kilodalton isoform of poly(ADP-ribose) glycohydrolase increases sensitivity to genotoxic and endotoxic stress in mice. Mol Cell Biol. 2004 Aug;24(16):7163–7178.

182. Ray Chaudhuri A, Ahuja AK, Herrador R, Lopes M. Poly(ADP-ribosyl) glycohydrolase prevents the accumulation of unusual replication structures during unperturbed S phase. Mol Cell Biol. 2015 Mar;35(5):856–865.

183. Yang G, Liu C, Chen S-H, Kassab MA, Hoff JD, Walter NG, et al. Super-resolution imaging identifies PARP1 and the Ku complex acting as DNA double-strand break sensors. Nucleic Acids Res. 2018 Apr 20;46(7):3446–3457.

184. Haince J-F, Kozlov S, Dawson VL, Dawson TM, Hendzel MJ, Lavin MF, et al. Ataxia telangiectasia mutated (ATM) signaling network is modulated by a novel poly(ADP-ribose)-dependent pathway in the early response to DNA-damaging agents. J Biol Chem. 2007 Jun 1;282(22):16441–16453.

185. Aguilar-Quesada R, Muñoz-Gámez JA, Martín-Oliva D, Peralta A, Valenzuela MT, Matínez-Romero R, et al. Interaction between ATM and PARP-1 in response to DNA damage and sensitization of ATM deficient cells through PARP inhibition. BMC Mol Biol. 2007 Apr 25;8:29.

186. Haince J-F, McDonald D, Rodrigue A, Déry U, Masson J-Y, Hendzel MJ, et al. PARP1-dependent kinetics of recruitment of MRE11 and NBS1 proteins to multiple DNA damage sites. J Biol Chem. 2008 Jan 11;283(2):1197–1208.

187. Li M, Yu X. Function of BRCA1 in the DNA damage response is mediated by ADP-ribosylation. Cancer Cell. 2013 May 13;23(5):693–704.

188. Schwertman P, Bekker-Jensen S, Mailand N. Regulation of DNA double-strand break repair by ubiquitin and ubiquitin-like modifiers. Nat Rev Mol Cell Biol. 2016 May 23;17(6):379–394.

189. Claybon A, Karia B, Bruce C, Bishop AJR. PARP1 suppresses homologous recombination events in mice in vivo. Nucleic Acids Res. 2010 Nov;38(21):7538–7545.

190. Schultz N, Lopez E, Saleh-Gohari N, Helleday T. Poly(ADP-ribose) polymerase (PARP-1) has a controlling role in homologous recombination. Nucleic Acids Res. 2003 Sep 1;31(17):4959–4964.

191. Farmer H, McCabe N, Lord CJ, Tutt ANJ, Johnson DA, Richardson TB, et al. Targeting the DNA repair defect in BRCA mutant cells as a therapeutic strategy. Nature. 2005 Apr 14;434(7035):917–921.

192. Bryant HE, Schultz N, Thomas HD, Parker KM, Flower D, Lopez E, et al. Specific killing of BRCA2-deficient tumours with inhibitors of poly(ADP-ribose) polymerase. Nature. 2005 Apr 14;434(7035):913–917.

193. Chiruvella KK, Liang Z, Wilson TE. Repair of double-strand breaks by end joining. Cold Spring Harb Perspect Biol. 2013 May 1;5(5):a012757.

194. Iliakis G, Murmann T, Soni A. Alternative end-joining repair pathways are the ultimate backup for abrogated classical non-homologous end-joining and homologous recombination repair: Implications for the formation of chromosome translocations. Mutat Res Genet Toxicol Environ Mutagen. 2015 Nov;793:166–175.

195. Doksani Y, de Lange T. Telomere-Internal Double-Strand Breaks Are Repaired by Homologous Recombination and PARP1/Lig3-Dependent End-Joining. Cell Rep. 2016 Nov 1;17(6):1646–1656.

196. Petermann E, Orta ML, Issaeva N, Schultz N, Helleday T. Hydroxyurea-stalled replication forks become progressively inactivated and require two different RAD51-mediated pathways for restart and repair. Mol Cell. 2010 Feb 26;37(4):492–502.

197. Berti M, Ray Chaudhuri A, Thangavel S, Gomathinayagam S, Kenig S, Vujanovic M, et al. Human RECQ1 promotes restart of replication forks reversed by DNA topoisomerase I inhibition. Nat Struct Mol Biol. 2013 Mar;20(3):347–354.

198. Maya-Mendoza A, Moudry P, Merchut-Maya JM, Lee M, Strauss R, Bartek J. High speed of fork progression induces DNA replication stress and genomic instability. Nature. 2018 Jun 27;559(7713):279–284.

199. Ciccarone F, Zampieri M, Caiafa P. PARP1 orchestrates epigenetic events setting up chromatin domains. Semin Cell Dev Biol. 2017;63:123–134.

200. Poirier GG, de Murcia G, Jongstra-Bilen J, Niedergang C, Mandel P. Poly(ADP-ribosyl)ation of polynucleosomes causes relaxation of chromatin structure. Proc Natl Acad Sci USA. 1982 Jun;79(11):3423–3427.

201. Messner S, Altmeyer M, Zhao H, Pozivil A, Roschitzki B, Gehrig P, et al. PARP1 ADP-ribosylates lysine residues of the core histone tails. Nucleic Acids Res. 2010 Oct;38(19):6350–6362.

202. Ahel D, Horejsí Z, Wiechens N, Polo SE, Garcia-Wilson E, Ahel I, et al. Poly(ADP-ribose)-dependent regulation of DNA repair by the chromatin remodeling enzyme ALC1. Science. 2009 Sep 4;325(5945):1240–1243.

203. Singh HR, Nardozza AP, Möller IR, Knobloch G, Kistemaker HAV, Hassler M, et al. A Poly-ADP-Ribose Trigger Releases the Auto-Inhibition of a Chromatin Remodeling Oncogene. Mol Cell. 2017 Dec 7;68(5):860–871.e7.

204. Luijsterburg MS, de Krijger I, Wiegant WW, Shah RG, Smeenk G, de Groot AJL, et al. PARP1 Links CHD2-Mediated Chromatin Expansion and H3.3 Deposition to DNA Repair by Non-homologous End-Joining. Mol Cell. 2016 Feb 18;61(4):547–562.

205. Smeenk G, Wiegant WW, Marteijn JA, Luijsterburg MS, Sroczynski N, Costelloe T, et al. Poly(ADP-ribosyl)ation links the chromatin remodeler SMARCA5/SNF2H to RNF168-dependent DNA damage signaling. J Cell Sci. 2013 Feb 15;126(Pt 4):889–903.

206. Dziadkowiec KN, Gąsiorowska E, Nowak-Markwitz E, Jankowska A. PARP inhibitors: review of mechanisms of action and BRCA1/2 mutation targeting. Prz Menopauzalny. 2016 Dec;15(4):215–219.

207. Murai J, Huang SN, Das BB, Renaud A, Zhang Y, Doroshow JH, et al. Trapping of PARP1 and PARP2 by clinical PARP inhibitors. Cancer Res. 2012 Nov 1;72(21):5588–5599.

208. Ringley JT, Moore DC, Patel J, Rose MS. Poly (ADP-ribose) Polymerase Inhibitors in the Management of Ovarian Cancer: A Drug Class Review. P T. 2018 Sep;43(9):549–556.

209. Franzese E, Centonze S, Diana A, Carlino F, Guerrera LP, Di Napoli M, et al. PARP inhibitors in ovarian cancer. Cancer Treat Rev. 2019 Feb;73:1–9.

210. Jiang X, Li W, Li X, Bai H, Zhang Z. Current status and future prospects of PARP inhibitor clinical trials in ovarian cancer. Cancer Manag Res. 2019 May 10;11:4371–4390.

211. Blenn C, Wyrsch P, Althaus FR. The ups and downs of tannins as inhibitors of poly(ADP-ribose)glycohydrolase. Molecules. 2011 Feb 22;16(2):1854–1877.

212. Slama JT, Aboul-Ela N, Goli DM, Cheesman BV, Simmons AM, Jacobson MK. Specific inhibition of poly(ADP-ribose) glycohydrolase by adenosine diphosphate (hydroxymethyl)pyrrolidinediol. J Med Chem. 1995 Jan 20;38(2):389–393.

213. Slama JT, Aboul-Ela N, Jacobson MK. Mechanism of inhibition of poly(ADP-ribose) glycohydrolase by adenosine diphosphate (hydroxymethyl)pyrrolidinediol. J Med Chem. 1995 Oct 13;38(21):4332–4336.

214. Finch KE, Knezevic CE, Nottbohm AC, Partlow KC, Hergenrother PJ. Selective small molecule inhibition of poly(ADP-ribose) glycohydrolase (PARG). ACS Chem Biol. 2012 Mar 16;7(3):563–570.

215. Formentini L, Arapistas P, Pittelli M, Jacomelli M, Pitozzi V, Menichetti S, et al. Mono-galloyl glucose derivatives are potent poly(ADP-ribose) glycohydrolase (PARG) inhibitors and partially reduce PARP-1-dependent cell death. Br J Pharmacol. 2008 Dec;155(8):1235–1249.

216. Steffen JD, Coyle DL, Damodaran K, Beroza P, Jacobson MK. Discovery and structure-activity relationships of modified salicylanilides as cell permeable inhibitors of poly(ADP-ribose) glycohydrolase (PARG). J Med Chem. 2011 Aug 11;54(15):5403–5413.

217. James DI, Smith KM, Jordan AM, Fairweather EE, Griffiths LA, Hamilton NS, et al. First-in-Class Chemical Probes against Poly(ADP-ribose) Glycohydrolase (PARG) Inhibit DNA Repair with Differential Pharmacology to Olaparib. ACS Chem Biol. 2016 Nov 18;11(11):3179–3190.

218. James DI, Durant S, Eckersley K, Fairweather E, Griffiths LA, Hamilton N, et al. An assay to measure poly(ADP ribose) glycohydrolase (PARG) activity in cells. [version 2; peer review: 2 approved]. F1000Res. 2016 Apr 25;5:736.

219. Shen Y, Aoyagi-Scharber M, Wang B. Trapping Poly(ADP-Ribose) Polymerase. J Pharmacol Exp Ther. 2015 Jun;353(3):446–457.

220. Hopkins TA, Ainsworth WB, Ellis PA, Donawho CK, DiGiammarino EL, Panchal SC, et al. PARP1 trapping by PARP inhibitors drives cytotoxicity in both cancer cells and healthy bone marrow. Mol Cancer Res. 2019;17(2):409–419.

221. Sun K, Mikule K, Wang Z, Poon G, Vaidyanathan A, Smith G, et al. A comparative pharmacokinetic study of PARP inhibitors demonstrates favorable properties for niraparib efficacy in preclinical tumor models. Oncotarget. 2018 Dec 14;9(98):37080–37096.

222. Tucker JA, Bennett N, Brassington C, Durant ST, Hassall G, Holdgate G, et al. Structures of the human poly (ADP-ribose) glycohydrolase catalytic domain confirm catalytic mechanism and explain inhibition by ADP-HPD derivatives. PLoS One. 2012 Dec 10;7(12):e50889.

223. Jungmichel S, Rosenthal F, Altmeyer M, Lukas J, Hottiger MO, Nielsen ML. Proteome-wide identification of poly(ADP-Ribosyl)ation targets in different genotoxic stress responses. Mol Cell. 2013 Oct 24;52(2):272–285.

224. Altmeyer M, Neelsen KJ, Teloni F, Pozdnyakova I, Pellegrino S, Grøfte M, et al. Liquid demixing of intrinsically disordered proteins is seeded by poly(ADP-ribose). Nat Commun. 2015 Aug 19;6:8088.

225. Zhang H, Liu M, Dilley R, Chenoweth DM, Greenberg RA, Lampson MA. Liquid condensation drives telomere clustering during ALT. BioRxiv. 2019 May 9;

226. Adam S, Polo SE, Almouzni G. Transcription recovery after DNA damage requires chromatin priming by the H3.3 histone chaperone HIRA. Cell. 2013 Sep 26;155(1):94–106.

227. Ray-Gallet D, Ricketts MD, Sato Y, Gupta K, Boyarchuk E, Senda T, et al. Functional activity of the H3.3 histone chaperone complex HIRA requires trimerization of the HIRA subunit. Nat Commun. 2018 Aug 6;9(1):3103.

228. Clynes D, Jelinska C, Xella B, Ayyub H, Scott C, Mitson M, et al. Suppression of the alternative lengthening of telomere pathway by the chromatin remodelling factor ATRX. Nat Commun. 2015 Jul 6;6:7538.

229. Gomez M, Wu J, Schreiber V, Dunlap J, Dantzer F, Wang Y, et al. PARP1 Is a TRF2-associated poly(ADP-ribose)polymerase and protects eroded telomeres. Mol Biol Cell. 2006 Apr;17(4):1686–1696.

230. Palm W, de Lange T. How shelterin protects mammalian telomeres. Annu Rev Genet. 2008;42:301–334.

231. Schmutz I, Timashev L, Xie W, Patel DJ, de Lange T. TRF2 binds branched DNA to safeguard telomere integrity. Nat Struct Mol Biol. 2017 Sep;24(9):734–742.

232. Mateos-Gomez PA, Gong F, Nair N, Miller KM, Lazzerini-Denchi E, Sfeir A. Mammalian polymerase θ promotes alternative NHEJ and suppresses recombination. Nature. 2015 Feb 12;518(7538):254–257.

233. Margalef P, Kotsantis P, Borel V, Bellelli R, Panier S, Boulton SJ. Stabilization of reversed replication forks by telomerase drives telomere catastrophe. Cell. 2018 Jan 25;172(3):439–453.e14.

234. Amé J-C, Fouquerel E, Gauthier LR, Biard D, Boussin FD, Dantzer F, et al. Radiation-induced mitotic catastrophe in PARG-deficient cells. J Cell Sci. 2009 Jun 15;122(Pt 12):1990–2002.

235. Skowron P, Kaczorowski T, Tucholski J, Podhajska AJ. Atypical DNA-binding properties of class-IIS restriction endonucleases: evidence for recognition of the cognate sequence by a FokI monomer. Gene. 1993 Mar 15;125(1):1–10.

236. Catto LE, Ganguly S, Milsom SE, Welsh AJ, Halford SE. Protein assembly and DNA looping by the FokI restriction endonuclease. Nucleic Acids Res. 2006 Mar 23;34(6):1711–1720.

237. Bitinaite J, Wah DA, Aggarwal AK, Schildkraut I. FokI dimerization is required for DNA cleavage. Proc Natl Acad Sci USA. 1998 Sep 1;95(18):10570–10575.

238. Turk AA, Wisinski KB. PARP inhibitors in breast cancer: Bringing synthetic lethality to the bedside. Cancer. 2018 Jun 15;124(12):2498–2506.

239. Hu J, Hwang SS, Liesa M, Gan B, Sahin E, Jaskelioff M, et al. Antitelomerase therapy provokes ALT and mitochondrial adaptive mechanisms in cancer. Cell. 2012 Feb 17;148(4):651–663.

240. Petti E, Buemi V, Zappone A, Schillaci O, Broccia PV, Dinami R, et al. SFPQ and NONO suppress RNA:DNA-hybrid-related telomere instability. Nat Commun. 2019 Mar 1;10(1):1001.

241. Sfeir A, Kosiyatrakul ST, Hockemeyer D, MacRae SL, Karlseder J, Schildkraut CL, et al. Mammalian telomeres resemble fragile sites and require TRF1 for efficient replication. Cell. 2009 Jul 10;138(1):90–103.

242. Episkopou H, Draskovic I, Van Beneden A, Tilman G, Mattiussi M, Gobin M, et al. Alternative Lengthening of Telomeres is characterized by reduced compaction of telomeric chromatin. Nucleic Acids Res. 2014 Apr;42(7):4391–4405.

243. O'Sullivan RJ, Arnoult N, Lackner DH, Oganesian L, Haggblom C, Corpet A, et al. Rapid induction of alternative lengthening of telomeres by depletion of the histone chaperone ASF1. Nat Struct Mol Biol. 2014 Feb;21(2):167–174.

244. Min J, Wright WE, Shay JW. Clustered telomeres in phase-separated nuclear condensates engage mitotic DNA synthesis through BLM and RAD52. Genes Dev. 2019 Jul 1;33(13-14):814–827.

245. González-Prieto R, Cuijpers SAG, Luijsterburg MS, van Attikum H, Vertegaal ACO. SUMOylation and PARylation cooperate to recruit and stabilize SLX4 at DNA damage sites. EMBO Rep. 2015 Apr;16(4):512–519.

246. Murnane JP, Sabatier L, Marder BA, Morgan WF. Telomere dynamics in an immortal human cell line. EMBO J. 1994 Oct 17;13(20):4953–4962.

247. Molenaar C, Wiesmeijer K, Verwoerd NP, Khazen S, Eils R, Tanke HJ, et al. Visualizing telomere dynamics in living mammalian cells using PNA probes. EMBO J. 2003 Dec 15;22(24):6631–6641.

248. Gagné J-P, Pic E, Isabelle M, Krietsch J, Ethier C, Paquet E, et al. Quantitative proteomics profiling of the poly(ADP-ribose)-related response to genotoxic stress. Nucleic Acids Res. 2012 Sep;40(16):7788–7805.

249. Letunic I, Copley RR, Schmidt S, Ciccarelli FD, Doerks T, Schultz J, et al. SMART 4.0: towards genomic data integration. Nucleic Acids Res. 2004 Jan 1;32(Database issue):D142–4.

250. Krastev DB, Pettitt SJ, Campbell J, Song F, Tanos BE, Stoynov SS, et al. Coupling bimolecular PARylation biosensors with genetic screens to identify PARylation targets. Nat Commun. 2018 May 22;9(1):2016.

251. Dani N, Stilla A, Marchegiani A, Tamburro A, Till S, Ladurner AG, et al. Combining affinity purification by ADP-ribose-binding macro domains with mass spectrometry to define the mammalian ADP-ribosyl proteome. Proc Natl Acad Sci USA. 2009 Mar 17;106(11):4243–4248.

252. Alvarez-Gonzalez R, Althaus FR. Poly(ADP-ribose) catabolism in mammalian cells exposed to DNA-damaging agents. Mutation Research/DNA Repair. 1989 Sep;218(2):67–74.

253. Acs K, Luijsterburg MS, Ackermann L, Salomons FA, Hoppe T, Dantuma NP. The AAA-ATPase VCP/p97 promotes 53BP1 recruitment by removing L3MBTL1 from DNA double-strand breaks. Nat Struct Mol Biol. 2011 Nov 27;18(12):1345–1350.

254. Altmeyer M, Toledo L, Gudjonsson T, Grøfte M, Rask M-B, Lukas C, et al. The chromatin scaffold protein SAFB1 renders chromatin permissive for DNA damage signaling. Mol Cell. 2013 Oct 24;52(2):206–220.

255. Townson SM, Sullivan T, Zhang Q, Clark GM, Osborne CK, Lee AV, et al. HET/SAF-B overexpression causes growth arrest and multinuclearity and is associated with aneuploidy in human breast cancer. Clin Cancer Res. 2000 Sep;6(9):3788–3796.

256. Flynn RL, Centore RC, O'Sullivan RJ, Rai R, Tse A, Songyang Z, et al. TERRA and hnRNPA1 orchestrate an RPA-to-POT1 switch on telomeric single-stranded DNA. Nature. 2011 Mar 24;471(7339):532–536.

257. Polo SE, Blackford AN, Chapman JR, Baskcomb L, Gravel S, Rusch A, et al. Regulation of DNA-end resection by hnRNPU-like proteins promotes DNA double-strand break signaling and repair. Mol Cell. 2012 Feb 24;45(4):505–516.

258. Adamson B, Smogorzewska A, Sigoillot FD, King RW, Elledge SJ. A genome-wide homologous recombination screen identifies the RNA-binding protein RBMX as a component of the DNA-damage response. Nat Cell Biol. 2012 Mar 1;14(3):318–328.

259. Altmeyer M, Lukas J. To spread or not to spread--chromatin modifications in response to DNA damage. Curr Opin Genet Dev. 2013 Apr;23(2):156–165.

260. Das BB, Huang SN, Murai J, Rehman I, Amé J-C, Sengupta S, et al. PARP1-TDP1 coupling for the repair of topoisomerase I-induced DNA damage. Nucleic Acids Res. 2014 Apr;42(7):4435–4449.

261. Pellegrino S, Altmeyer M. Interplay between Ubiquitin, SUMO, and Poly(ADP-Ribose) in the Cellular Response to Genotoxic Stress. Front Genet. 2016 Apr 19;7:63.

262. Galanty Y, Belotserkovskaya R, Coates J, Polo S, Miller KM, Jackson SP. Mammalian SUMO E3-ligases PIAS1 and PIAS4 promote responses to DNA double-strand breaks. Nature. 2009 Dec 17;462(7275):935–939.

263. Galanty Y, Belotserkovskaya R, Coates J, Jackson SP. RNF4, a SUMO-targeted ubiquitin E3 ligase, promotes DNA double-strand break repair. Genes Dev. 2012 Jun 1;26(11):1179–1195.

264. Yin Y, Seifert A, Chua JS, Maure J-F, Golebiowski F, Hay RT. SUMO-targeted ubiquitin E3 ligase RNF4 is required for the response of human cells to DNA damage. Genes Dev. 2012 Jun 1;26(11):1196–1208.

265. Smeenk G, Wiegant WW, Vrolijk H, Solari AP, Pastink A, van Attikum H. The NuRD chromatin-remodeling complex regulates signaling and repair of DNA damage. J Cell Biol. 2010 Sep 6;190(5):741–749.

266. Chou DM, Adamson B, Dephoure NE, Tan X, Nottke AC, Hurov KE, et al. A chromatin localization screen reveals poly (ADP ribose)-regulated recruitment of the repressive polycomb and NuRD complexes to sites of DNA damage. Proc Natl Acad Sci USA. 2010 Oct 26;107(43):18475–18480.

267. Gudjonsson T, Altmeyer M, Savic V, Toledo L, Dinant C, Grøfte M, et al. TRIP12 and UBR5 suppress spreading of chromatin ubiquitylation at damaged chromosomes. Cell. 2012 Aug 17;150(4):697–709.

268. Singatulina AS, Hamon L, Sukhanova MV, Desforges B, Joshi V, Bouhss A, et al. PARP-1 Activation Directs FUS to DNA Damage Sites to Form PARG-Reversible Compartments Enriched in Damaged DNA. Cell Rep. 2019 May 7;27(6):1809–1821.e5.

269. Nomura T, Watanabe S, Kaneko K, Yamanaka K, Nukina N, Furukawa Y. Intranuclear aggregation of mutant FUS/TLS as a molecular pathomechanism of amyotrophic lateral sclerosis. J Biol Chem. 2014 Jan 10;289(2):1192–1202.

270. Hong Z, Jiang J, Ma J, Dai S, Xu T, Li H, et al. The role of hnRPUL1 involved in DNA damage response is related to PARP1. PLoS One. 2013 Apr 5;8(4):e60208.

271. Sfeir A, Symington LS. Microhomology-Mediated End Joining: A Back-up Survival Mechanism or Dedicated Pathway? Trends Biochem Sci. 2015 Nov;40(11):701–714.

272. Ryan DP, Owen-Hughes T. Snf2-family proteins: chromatin remodellers for any occasion. Curr Opin Chem Biol. 2011 Oct 1;15(5):649–656.

273. Tagami H, Ray-Gallet D, Almouzni G, Nakatani Y. Histone H3.1 and H3.3 complexes mediate nucleosome assembly pathways dependent or independent of DNA synthesis. Cell. 2004 Jan 9;116(1):51–61.

274. Cacchione S, Biroccio A, Rizzo A. Emerging roles of telomeric chromatin alterations in cancer. J Exp Clin Cancer Res. 2019 Jan 17;38(1):21.

275. Goldberg AD, Banaszynski LA, Noh K-M, Lewis PW, Elsaesser SJ, Stadler S, et al. Distinct factors control histone variant H3.3 localization at specific genomic regions. Cell. 2010 Mar 5;140(5):678–691.

276. Wirbelauer C, Bell O, Schübeler D. Variant histone H3.3 is deposited at sites of nucleosomal displacement throughout transcribed genes while active histone modifications show a promoter-proximal bias. Genes Dev. 2005 Aug 1;19(15):1761–1766.

277. Ahmad K, Henikoff S. The histone variant H3.3 marks active chromatin by replication-independent nucleosome assembly. Mol Cell. 2002 Jun;9(6):1191–1200.

278. Drané P, Ouararhni K, Depaux A, Shuaib M, Hamiche A. The death-associated protein DAXX is a novel histone chaperone involved in the replication-independent deposition of H3.3. Genes Dev. 2010 Jun 15;24(12):1253–1265.

279. Wong LH, McGhie JD, Sim M, Anderson MA, Ahn S, Hannan RD, et al. ATRX interacts with H3.3 in maintaining telomere structural integrity in pluripotent embryonic stem cells. Genome Res. 2010 Mar;20(3):351–360.

280. Hake SB, Garcia BA, Kauer M, Baker SP, Shabanowitz J, Hunt DF, et al. Serine 31 phosphorylation of histone variant H3.3 is specific to regions bordering centromeres in metaphase chromosomes. Proc Natl Acad Sci USA. 2005 May 3;102(18):6344–6349.

281. Ghosal G, Muniyappa K. Saccharomyces cerevisiae Mre11 is a high-affinity G4 DNA-binding protein and a G-rich DNA-specific endonuclease: implications for replication of telomeric DNA. Nucleic Acids Res. 2005 Aug 22;33(15):4692–4703.

282. Juhász S, Elbakry A, Mathes A, Löbrich M. ATRX Promotes DNA Repair Synthesis and Sister Chromatid Exchange during Homologous Recombination. Mol Cell. 2018 Jul 5;71(1):11–24.e7.

283. Wang Y, Yang J, Wild AT, Wu WH, Shah R, Danussi C, et al. G-quadruplex DNA drives genomic instability and represents a targetable molecular abnormality in ATRX-deficient malignant glioma. Nat Commun. 2019 Feb 26;10(1):943.

284. Rai TS, Puri A, McBryan T, Hoffman J, Tang Y, Pchelintsev NA, et al. Human CABIN1 is a functional member of the human HIRA/UBN1/ASF1a histone H3.3 chaperone complex. Mol Cell Biol. 2011 Oct;31(19):4107–4118.

285. Tang Y, Puri A, Ricketts MD, Rai TS, Hoffmann J, Hoi E, et al. Identification of an ubinuclein 1 region required for stability and function of the human

HIRA/UBN1/CABIN1/ASF1a histone H3.3 chaperone complex. Biochemistry. 2012 Mar 27;51(12):2366–2377.

286. Tang Y, Poustovoitov MV, Zhao K, Garfinkel M, Canutescu A, Dunbrack R, et al. Structure of a human ASF1a-HIRA complex and insights into specificity of histone chaperone complex assembly. Nat Struct Mol Biol. 2006 Oct;13(10):921–929.

287. Ricketts MD, Marmorstein R. A Molecular Prospective for HIRA Complex Assembly and H3.3-Specific Histone Chaperone Function. J Mol Biol. 2017 Jun 30;429(13):1924–1933.

288. Ricketts MD, Frederick B, Hoff H, Tang Y, Schultz DC, Singh Rai T, et al. Ubinuclein-1 confers histone H3.3-specific-binding by the HIRA histone chaperone complex. Nat Commun. 2015 Jul 10;6:7711.

289. Banaszynski LA, Wen D, Dewell S, Whitcomb SJ, Lin M, Diaz N, et al. Hira-dependent histone H3.3 deposition facilitates PRC2 recruitment at developmental loci in ES cells. Cell. 2013 Sep 26;155(1):107–120.

290. Pchelintsev NA, McBryan T, Rai TS, van Tuyn J, Ray-Gallet D, Almouzni G, et al. Placing the HIRA histone chaperone complex in the chromatin landscape. Cell Rep. 2013 Apr 25;3(4):1012–1019.

291. Ray-Gallet D, Woolfe A, Vassias I, Pellentz C, Lacoste N, Puri A, et al. Dynamics of histone H3 deposition in vivo reveal a nucleosome gap-filling mechanism for H3.3 to maintain chromatin integrity. Mol Cell. 2011 Dec 23;44(6):928–941.

292. Loppin B, Bonnefoy E, Anselme C, Laurençon A, Karr TL, Couble P. The histone H3.3 chaperone HIRA is essential for chromatin assembly in the male pronucleus. Nature. 2005 Oct 27;437(7063):1386–1390.

293. Roberts C, Sutherland HF, Farmer H, Kimber W, Halford S, Carey A, et al. Targeted mutagenesis of the Hira gene results in gastrulation defects and patterning abnormalities of mesoendodermal derivatives prior to early embryonic lethality. Mol Cell Biol. 2002 Apr;22(7):2318–2328.

294. Sherwood PW, Tsang SV, Osley MA. Characterization of HIR1 and HIR2, two genes required for regulation of histone gene transcription in Saccharomyces cerevisiae. Mol Cell Biol. 1993 Jan;13(1):28–38.

295. Szenker E, Lacoste N, Almouzni G. A developmental requirement for HIRA-dependent H3.3 deposition revealed at gastrulation in Xenopus. Cell Rep. 2012 Jun 28;1(6):730–740.

296. Rai TS, Cole JJ, Nelson DM, Dikovskaya D, Faller WJ, Vizioli MG, et al. HIRA orchestrates a dynamic chromatin landscape in senescence and is required for suppression of neoplasia. Genes Dev. 2014 Dec 15;28(24):2712–2725.

297. Zhang R, Poustovoitov MV, Ye X, Santos HA, Chen W, Daganzo SM, et al. Formation of MacroH2A-containing senescence-associated heterochromatin foci and senescence driven by ASF1a and HIRA. Dev Cell. 2005 Jan;8(1):19–30.

298. Rai TS, Glass M, Cole JJ, Rather MI, Marsden M, Neilson M, et al. Histone chaperone HIRA deposits histone H3.3 onto foreign viral DNA and contributes to anti-viral intrinsic immunity. Nucleic Acids Res. 2017 Nov 16;45(20):11673–11683.

299. Hoek M, Stillman B. Chromatin assembly factor 1 is essential and couples chromatin assembly to DNA replication in vivo. Proc Natl Acad Sci USA. 2003 Oct 14;100(21):12183–12188.

300. O'Sullivan RJ, Almouzni G. Assembly of telomeric chromatin to create ALTernative endings. Trends Cell Biol. 2014 Nov;24(11):675–685.

301. Zhang H, Gan H, Wang Z, Lee J-H, Zhou H, Ordog T, et al. RPA Interacts with HIRA and Regulates H3.3 Deposition at Gene Regulatory Elements in Mammalian Cells. Mol Cell. 2017 Jan 19;65(2):272–284.

302. Illuzzi G, Fouquerel E, Amé J-C, Noll A, Rehmet K, Nasheuer H-P, et al. PARG is dispensable for recovery from transient replicative stress but required to prevent detrimental accumulation of poly(ADP-ribose) upon prolonged replicative stress. Nucleic Acids Res. 2014 Jul;42(12):7776–7792.

303. Nguyen DT, Voon HPJ, Xella B, Scott C, Clynes D, Babbs C, et al. The chromatin remodelling factor ATRX suppresses R-loops in transcribed telomeric repeats. EMBO Rep. 2017 May 9;18(6):914–928.

304. Berger NA. Poly(ADP-ribose) in the cellular response to DNA damage. Radiat Res. 1985 Jan;101(1):4–15.

305. D'Amours D, Desnoyers S, D'Silva I, Poirier GG. Poly(ADP-ribosyl)ation reactions in the regulation of nuclear functions. Biochem J. 1999 Sep 1;342 (Pt 2):249–268.

306. Goodwin PM, Lewis PJ, Davies MI, Skidmore CJ, Shall S. The effect of gamma radiation and neocarzinostatin of NAD and ATP levels in mouse leukaemia cells. Biochimica et Biophysica Acta (BBA) - General Subjects. 1978 Nov;543(4):576–582.

307. Skidmore CJ, Davies MI, Goodwin PM, Halldorsson H, Lewis PJ, Shall S, et al. The involvement of poly(ADP-ribose) polymerase in the degradation of NAD caused by gamma-radiation and N-methyl-N-nitrosourea. Eur J Biochem. 1979 Nov 1;101(1):135–142.

308. Fakouri NB, Durhuus JA, Regnell CE, Angleys M, Desler C, Hasan-Olive MM, et al. Rev1 contributes to proper mitochondrial function via the PARP-NAD+-SIRT1-PGC1α axis. Sci Rep. 2017 Oct 2;7(1):12480.

309. Yang Y, Mohammed FS, Zhang N, Sauve AA. Dihydronicotinamide riboside is a potent NAD+ concentration enhancer in vitro and in vivo. J Biol Chem. 2019 Jun 7;294(23):9295–9307.

310. Uchida M, Hanai S, Uematsu N, Sawamoto K, Okano H, Miwa M, et al. Overexpression of poly(ADP-ribose) polymerase disrupts organization of cytoskeletal F-actin and tissue polarity in Drosophila. J Biol Chem. 2002 Feb 22;277(8):6696–6702.

311. Lang AE, Schmidt G, Schlosser A, Hey TD, Larrinua IM, Sheets JJ, et al. Photorhabdus luminescens toxins ADP-ribosylate actin and RhoA to force actin clustering. Science. 2010 Feb 26;327(5969):1139–1142.

312. Wang M, Wu W, Wu W, Rosidi B, Zhang L, Wang H, et al. PARP-1 and Ku compete for repair of DNA double strand breaks by distinct NHEJ pathways. Nucleic Acids Res. 2006 Nov 6;34(21):6170–6182.

313. Gogola E, Duarte AA, de Ruiter JR, Wiegant WW, Schmid JA, de Bruijn R, et al. Selective Loss of PARG Restores PARylation and Counteracts PARP Inhibitor-Mediated Synthetic Lethality. Cancer Cell. 2018 Jun 11;33(6):1078–1093.e12.

314. Gravells P, Neale J, Grant E, Nathubhai A, Smith KM, James DI, et al. Radiosensitization with an inhibitor of poly(ADP-ribose) glycohydrolase: A comparison with the PARP1/2/3 inhibitor olaparib. DNA Repair (Amst). 2018;61:25–36.

315. Pillay N, Tighe A, Nelson L, Littler S, Coulson-Gilmer C, Bah N, et al. DNA Replication Vulnerabilities Render Ovarian Cancer Cells Sensitive to Poly(ADP-Ribose) Glycohydrolase Inhibitors. Cancer Cell. 2019 Mar 18;35(3):519–533.e8.

316. Deeg KI, Chung I, Bauer C, Rippe K. Cancer Cells with Alternative Lengthening of Telomeres Do Not Display a General Hypersensitivity to ATR Inhibition. Front Oncol. 2016 Aug 23;6:186.

317. Flynn RL, Cox KE, Jeitany M, Wakimoto H, Bryll AR, Ganem NJ, et al. Alternative lengthening of telomeres renders cancer cells hypersensitive to ATR inhibitors. Science. 2015 Jan 16;347(6219):273–277.

318. Tan Z, Tang J, Kan Z-Y, Hao Y-H. Telomere G-Quadruplex as a Potential Target to Accelerate Telomere Shortening by Expanding the Incomplete End-Replication of Telomere DNA. Curr Top Med Chem. 2015;15(19):1940–1946.

319. Han M, Napier CE, Frölich S, Teber E, Wong T, Noble JR, et al. Synthetic lethality of cytolytic HSV-1 in cancer cells with ATRX and PML deficiency. J Cell Sci. 2019 Mar 14;132(5).

320. Episkopou H, Diman A, Claude E, Viceconte N, Decottignies A. TSPYL5 Depletion Induces Specific Death of ALT Cells through USP7-Dependent Proteasomal Degradation of POT1. Mol Cell. 2019 Aug 8;75(3):469–482.e6.

321. Chen Y-A, Shen Y-L, Hsia H-Y, Tiang Y-P, Sung T-L, Chen L-Y. Extrachromosomal telomere repeat DNA is linked to ALT development via cGAS-STING DNA sensing pathway. Nat Struct Mol Biol. 2017 Dec;24(12):1124–1131.

322. Nassour J, Radford R, Correia A, Fusté JM, Schoell B, Jauch A, et al. Autophagic cell death restricts chromosomal instability during replicative crisis. Nature. 2019 Jan 23;565(7741):659–663.

323. Barretina J, Caponigro G, Stransky N, Venkatesan K, Margolin AA, Kim S, et al. The Cancer Cell Line Encyclopedia enables predictive modelling of anticancer drug sensitivity. Nature. 2012 Mar 28;483(7391):603–607.

324. Kraushaar DC, Jin W, Maunakea A, Abraham B, Ha M, Zhao K. Genome-wide incorporation dynamics reveal distinct categories of turnover for the histone variant H3.3. Genome Biol. 2013;14(10):R121.

325. Amorim JP, Santos G, Vinagre J, Soares P. The role of ATRX in the alternative lengthening of telomeres (ALT) phenotype. Genes (Basel). 2016 Sep 19;7(9).

326. Dyer MA, Qadeer ZA, Valle-Garcia D, Bernstein E. ATRX and DAXX: mechanisms and mutations. Cold Spring Harb Perspect Med. 2017 Mar 1;7(3).

327. Adam S, Dabin J, Chevallier O, Leroy O, Baldeyron C, Corpet A, et al. Real-Time Tracking of Parental Histones Reveals Their Contribution to Chromatin Integrity Following DNA Damage. Mol Cell. 2016 Oct 6;64(1):65–78.

328. Sauer PV, Gu Y, Liu WH, Mattiroli F, Panne D, Luger K, et al. Mechanistic insights into histone deposition and nucleosome assembly by the chromatin assembly factor-1. Nucleic Acids Res. 2018 Nov 2;46(19):9907–9917.

329. Torné J, Orsi GA, Ray-Gallet D, Almouzni G. Imaging Newly Synthesized and Old Histone Variant Dynamics Dependent on Chaperones Using the SNAP-Tag System. Methods Mol Biol. 2018;1832:207–221.

330. Groth A, Ray-Gallet D, Quivy J-P, Lukas J, Bartek J, Almouzni G. Human Asf1 regulates the flow of S phase histones during replicational stress. Mol Cell. 2005 Jan 21;17(2):301–311.

331. Yuen BTK, Knoepfler PS. Histone H3.3 mutations: a variant path to cancer. Cancer Cell. 2013 Nov 11;24(5):567–574.

332. Leatham-Jensen M, Uyehara CM, Strahl BD, Matera AG, Duronio RJ, McKay DJ. Lysine 27 of replication-independent histone H3.3 is required for Polycomb target gene silencing but not for gene activation. PLoS Genet. 2019 Jan 30;15(1):e1007932.

333. Frey A, Listovsky T, Guilbaud G, Sarkies P, Sale JE. Histone H3.3 is required to maintain replication fork progression after UV damage. Curr Biol. 2014 Sep 22;24(18):2195–2201.

334. Bjerke L, Mackay A, Nandhabalan M, Burford A, Jury A, Popov S, et al. Histone H3.3. mutations drive pediatric glioblastoma through upregulation of MYCN. Cancer Discov. 2013 May;3(5):512–519.

335. Dorris K, Sobo M, Onar-Thomas A, Panditharatna E, Stevenson CB, Gardner SL, et al. Prognostic significance of telomere maintenance mechanisms in pediatric high-grade gliomas. J Neurooncol. 2014 Mar;117(1):67–76.

336. Schwartzentruber J, Korshunov A, Liu X-Y, Jones DTW, Pfaff E, Jacob K, et al. Driver mutations in histone H3.3 and chromatin remodelling genes in paediatric glioblastoma. Nature. 2012 Jan 29;482(7384):226–231.

337. Sturm D, Witt H, Hovestadt V, Khuong-Quang D-A, Jones DTW, Konermann C, et al. Hotspot mutations in H3F3A and IDH1 define distinct epigenetic and biological subgroups of glioblastoma. Cancer Cell. 2012 Oct 16;22(4):425–437.

338. Annunziato AT. The fork in the road: histone partitioning during DNA replication. Genes (Basel). 2015 Jun 23;6(2):353–371.

339. Krude T, Keller C. Chromatin assembly during S phase: contributions from histone deposition, DNA replication and the cell division cycle. Cell Mol Life Sci. 2001 May;58(5-6):665–672.

340. Prado F, Maya D. Regulation of replication fork advance and stability by nucleosome assembly. Genes (Basel). 2017 Jan 24;8(2).

341. Mousson F, Ochsenbein F, Mann C. The histone chaperone Asf1 at the crossroads of chromatin and DNA checkpoint pathways. Chromosoma. 2007 Apr;116(2):79–93.

342. Groth A, Corpet A, Cook AJL, Roche D, Bartek J, Lukas J, et al. Regulation of replication fork progression through histone supply and demand. Science. 2007 Dec 21;318(5858):1928–1931.

343. Ransom M, Dennehey BK, Tyler JK. Chaperoning histones during DNA replication and repair. Cell. 2010 Jan 22;140(2):183–195.

344. Franco AA, Lam WM, Burgers PM, Kaufman PD. Histone deposition protein Asf1 maintains DNA replisome integrity and interacts with replication factor C. Genes Dev. 2005 Jun 1;19(11):1365–1375.

345. Moggs JG, Grandi P, Quivy JP, Jónsson ZO, Hübscher U, Becker PB, et al. A CAF-1-PCNA-mediated chromatin assembly pathway triggered by sensing DNA damage. Mol Cell Biol. 2000 Feb;20(4):1206–1218.

346. Sanematsu F, Takami Y, Barman HK, Fukagawa T, Ono T, Shibahara K-I, et al. Asf1 is required for viability and chromatin assembly during DNA replication in vertebrate cells. J Biol Chem. 2006 May 12;281(19):13817–13827.

347. Ye X, Franco AA, Santos H, Nelson DM, Kaufman PD, Adams PD. Defective S phase chromatin assembly causes DNA damage, activation of the S phase checkpoint, and S phase arrest. Mol Cell. 2003 Feb;11(2):341–351.

348. Huang H, Strømme CB, Saredi G, Hödl M, Strandsby A, González-Aguilera C, et al. A unique binding mode enables MCM2 to chaperone histones H3-H4 at replication forks. Nat Struct Mol Biol. 2015 Aug;22(8):618–626.

349. Richet N, Liu D, Legrand P, Velours C, Corpet A, Gaubert A, et al. Structural insight into how the human helicase subunit MCM2 may act as a histone chaperone together with ASF1 at the replication fork. Nucleic Acids Res. 2015 Feb 18;43(3):1905–1917.

350. Clément C, Almouzni G. MCM2 binding to histones H3-H4 and ASF1 supports a tetramer-to-dimer model for histone inheritance at the replication fork. Nat Struct Mol Biol. 2015 Aug;22(8):587–589.

351. Lydeard JR, Lipkin-Moore Z, Sheu Y-J, Stillman B, Burgers PM, Haber JE. Break-induced replication requires all essential DNA replication factors except those specific for pre-RC assembly. Genes Dev. 2010 Jun 1;24(11):1133–1144.

352. Jalili R, Horecka J, Swartz JR, Davis RW, Persson HHJ. Streamlined circular proximity ligation assay provides high stringency and compatibility with low-affinity antibodies. Proc Natl Acad Sci USA. 2018 Jan 30;115(5):E925–E933.

353. Sirbu BM, McDonald WH, Dungrawala H, Badu-Nkansah A, Kavanaugh GM, Chen Y, et al. Identification of proteins at active, stalled, and collapsed replication forks using isolation of proteins on nascent DNA (iPOND) coupled with mass spectrometry. J Biol Chem. 2013 Nov 1;288(44):31458–31467.

354. Hardy J, Dai D, Ait Saada A, Teixeira-Silva A, Dupoiron L, Mojallali F, et al. Histone deposition promotes recombination-dependent replication at arrested forks. PLoS Genet. 2019 Oct 4;15(10):e1008441.

355. Jasencakova Z, Scharf AND, Ask K, Corpet A, Imhof A, Almouzni G, et al. Replication stress interferes with histone recycling and predeposition marking of new histones. Mol Cell. 2010 Mar 12;37(5):736–743.

356. Pinheiro I, Margueron R, Shukeir N, Eisold M, Fritzsch C, Richter FM, et al. Prdm3 and Prdm16 are H3K9me1 methyltransferases required for mammalian heterochromatin integrity. Cell. 2012 Aug 31;150(5):948–960.

357. Veiseth SV, Rahman MA, Yap KL, Fischer A, Egge-Jacobsen W, Reuter G, et al. The SUVR4 histone lysine methyltransferase binds ubiquitin and converts H3K9me1 to H3K9me3 on transposon chromatin in Arabidopsis. PLoS Genet. 2011 Mar 10;7(3):e1001325.

358. Szenker E, Ray-Gallet D, Almouzni G. The double face of the histone variant H3.3. Cell Res. 2011 Mar;21(3):421–434.

359. Bano D, Piazzesi A, Salomoni P, Nicotera P. The histone variant H3.3 claims its place in the crowded scene of epigenetics. Aging (Albany, NY). 2017 Mar 10;9(3):602–614.

360. Mendiratta S, Gatto A, Almouzni G. Histone supply: Multitiered regulation ensures chromatin dynamics throughout the cell cycle. J Cell Biol. 2019 Jan 7;218(1):39–54.

361. Jin C, Felsenfeld G. Nucleosome stability mediated by histone variants H3.3 and H2A.Z. Genes Dev. 2007 Jun 15;21(12):1519–1529.

362. Jin C, Zang C, Wei G, Cui K, Peng W, Zhao K, et al. H3.3/H2A.Z double variant-containing nucleosomes mark “nucleosome-free regions” of active promoters and other regulatory regions. Nat Genet. 2009 Aug;41(8):941–945.

363. McKittrick E, Gafken PR, Ahmad K, Henikoff S. Histone H3.3 is enriched in covalent modifications associated with active chromatin. Proc Natl Acad Sci USA. 2004 Feb 10;101(6):1525–1530.

364. Chen P, Zhao J, Wang Y, Wang M, Long H, Liang D, et al. H3.3 actively marks enhancers and primes gene transcription via opening higher-ordered chromatin. Genes Dev. 2013 Oct 1;27(19):2109–2124.

365. Tvardovskiy A, Schwämmle V, Kempf SJ, Rogowska-Wrzesinska A, Jensen ON. Accumulation of histone variant H3.3 with age is associated with profound changes in the histone methylation landscape. Nucleic Acids Res. 2017 Sep 19;45(16):9272–9289.

366. Menendez JA, Alarcón T. Metabostemness: a new cancer hallmark. Front Oncol. 2014 Sep 29;4:262.

367. Enane FO, Saunthararajah Y, Korc M. Differentiation therapy and the mechanisms that terminate cancer cell proliferation without harming normal cells. Cell Death Dis. 2018 Sep 6;9(9):912.

368. Swartling FJ, Čančer M, Frantz A, Weishaupt H, Persson AI. Deregulated proliferation and differentiation in brain tumors. Cell Tissue Res. 2015 Jan;359(1):225–254.

369. Micrococcal nuclease–Southern blot assay. Nat Methods. 2005 Sep;2(9):719–720.

370. Cantó C, Sauve AA, Bai P. Crosstalk between poly(ADP-ribose) polymerase and sirtuin enzymes. Mol Aspects Med. 2013 Dec;34(6):1168–1201.

371. Caruso LB, Martin KA, Lauretti E, Hulse M, Siciliano M, Lupey-Green LN, et al. Poly(ADP-ribose) Polymerase 1, PARP1, modifies EZH2 and inhibits EZH2 histone methyltransferase activity after DNA damage. Oncotarget. 2018 Feb 13;9(12):10585–10605.

372. Kass EM, Jasin M. Collaboration and competition between DNA double-strand break repair pathways. FEBS Lett. 2010 Sep 10;584(17):3703–3708.

373. Sanz LA, Hartono SR, Lim YW, Steyaert S, Rajpurkar A, Ginno PA, et al. Prevalent, Dynamic, and Conserved R-Loop Structures Associate with Specific Epigenomic Signatures in Mammals. Mol Cell. 2016 Jul 7;63(1):167–178.

374. Arora R, Azzalin CM. Telomere elongation chooses TERRA ALTernatives. RNA Biol. 2015;12(9):938–941.

375. Bettin N, Oss Pegorar C, Cusanelli E. The emerging roles of TERRA in telomere maintenance and genome stability. Cells. 2019 Mar 15;8(3).

376. Montero JJ, López-Silanes I, Megías D, F Fraga M, Castells-García Á, Blasco MA. TERRA recruitment of polycomb to telomeres is essential for histone trymethylation marks at telomeric heterochromatin. Nat Commun. 2018 Apr 18;9(1):1548.

377. Sarma K, Cifuentes-Rojas C, Ergun A, Del Rosario A, Jeon Y, White F, et al. ATRX directs binding of PRC2 to Xist RNA and Polycomb targets. Cell. 2014 Nov 6;159(4):869–883.

378. Gauchier M, Kan S, Barral A, Sauzet S, Agirre E, Bonnell E, et al. SETDB1-dependent heterochromatin stimulates alternative lengthening of telomeres. Sci Adv. 2019 May 8;5(5):eaav3673.

379. Feretzaki M, Lingner J. A practical qPCR approach to detect TERRA, the elusive telomeric repeat-containing RNA. Methods. 2017 Feb 1;114:39–45.

380. Placek BJ, Huang J, Kent JR, Dorsey J, Rice L, Fraser NW, et al. The histone variant H3.3 regulates gene expression during lytic infection with herpes simplex virus type 1. J Virol. 2009 Feb;83(3):1416–1421.

381. Cohen C, Corpet A, Roubille S, Maroui MA, Poccardi N, Rousseau A, et al. Promyelocytic leukemia (PML) nuclear bodies (NBs) induce latent/quiescent HSV-1 genomes chromatinization through a PML NB/Histone H3.3/H3.3 Chaperone Axis. PLoS Pathog. 2018 Sep 20;14(9):e1007313.

382. Boutell C, Cuchet-Lourenço D, Vanni E, Orr A, Glass M, McFarlane S, et al. A viral ubiquitin ligase has substrate preferential SUMO targeted ubiquitin ligase activity that counteracts intrinsic antiviral defence. PLoS Pathog. 2011 Sep 15;7(9):e1002245.

383. Cuchet-Lourenço D, Vanni E, Glass M, Orr A, Everett RD. Herpes simplex virus 1 ubiquitin ligase ICP0 interacts with PML isoform I and induces its SUMO-independent degradation. J Virol. 2012 Oct;86(20):11209–11222.

384. Lukashchuk V, Everett RD. Regulation of ICP0-null mutant herpes simplex virus type 1 infection by ND10 components ATRX and hDaxx. J Virol. 2010 Apr;84(8):4026–4040.

385. Hewitt G, Korolchuk VI. Repair, reuse, recycle: the expanding role of autophagy in genome maintenance. Trends Cell Biol. 2017;27(5):340–351.

386. Mackenzie KJ, Carroll P, Martin C-A, Murina O, Fluteau A, Simpson DJ, et al. cGAS surveillance of micronuclei links genome instability to innate immunity. Nature. 2017 Aug 24;548(7668):461–465.

387. Banfalvi G. Methods to detect apoptotic cell death. Apoptosis. 2017 Feb;22(2):306–323.

388. Levine B, Kroemer G. Biological functions of autophagy genes: A disease perspective. Cell. 2019 Jan 10;176(1-2):11–42.

389. N'Diaye E-N, Kajihara KK, Hsieh I, Morisaki H, Debnath J, Brown EJ. PLIC proteins or ubiquilins regulate autophagy-dependent cell survival during nutrient starvation. EMBO Rep. 2009 Feb;10(2):173–179.

390. Egan DF, Chun MGH, Vamos M, Zou H, Rong J, Miller CJ, et al. Small molecule inhibition of the autophagy kinase ULK1 and identification of ULK1 substrates. Mol Cell. 2015 Jul 16;59(2):285–297.

391. Liang J, Zhao H, Diplas BH, Liu S, Liu J, Wang D, et al. Genome-wide CRISPR-Cas9 screen reveals selective vulnerability of ATRX-mutant cancers to WEE1 inhibition. Cancer Res. 2019 Sep 24;

392. Fu S, Wang Y, Keyomarsi K, Meric-Bernstam F, Meric-Bernstein F. Strategic development of AZD1775, a Wee1 kinase inhibitor, for cancer therapy. Expert Opin Investig Drugs. 2018 Aug 21;27(9):741–751.

393. Matheson CJ, Backos DS, Reigan P. Targeting WEE1 kinase in cancer. Trends Pharmacol Sci. 2016 Jul 14;37(10):872–881.

394. Udugama M, M Chang FT, Chan FL, Tang MC, Pickett HA, R McGhie JD, et al. Histone variant H3.3 provides the heterochromatic H3 lysine 9 tri-methylation mark at telomeres. Nucleic Acids Res. 2015 Dec 2;43(21):10227–10237.

395. Clynes D, Higgs DR, Gibbons RJ. The chromatin remodeller ATRX: a repeat offender in human disease. Trends Biochem Sci. 2013 Sep;38(9):461–466.

396. Schneiderman JI, Orsi GA, Hughes KT, Loppin B, Ahmad K. Nucleosome-depleted chromatin gaps recruit assembly factors for the H3.3 histone variant. Proc Natl Acad Sci USA. 2012 Nov 27;109(48):19721–19726.

397. Andersson-Rolf A, Mustata RC, Merenda A, Kim J, Perera S, Grego T, et al. One-step generation of conditional and reversible gene knockouts. Nat Methods. 2017 Jan 30;14(3):287–289.

398. Roux KJ, Kim DI, Burke B. BioID: a screen for protein-protein interactions. Curr Protoc Protein Sci. 2013 Nov 5;74:Unit 19.23.

399. Gomes AP, Ilter D, Low V, Rosenzweig A, Shen Z-J, Schild T, et al. Dynamic Incorporation of Histone H3 Variants into Chromatin Is Essential for Acquisition of Aggressive Traits and Metastatic Colonization. Cancer Cell. 2019 Oct 14;36(4):402–417.e13.

400. Kim JY, Brosnan-Cashman JA, An S, Kim SJ, Song KB, Kim M-S, et al. Alternative lengthening of telomeres in primary pancreatic neuroendocrine neoplasms is associated with aggressive clinical behavior and poor survival. Clin Cancer Res. 2016 Sep 23;

401. Tyler JK, Collins KA, Prasad-Sinha J, Amiott E, Bulger M, Harte PJ, et al. Interaction between the Drosophila CAF-1 and ASF1 chromatin assembly factors. Mol Cell Biol. 2001 Oct;21(19):6574–6584.